INVESTIGATIONS ON MOLECULAR PRE-ORGANIZATION AND INTERMOLECULAR ACYL TRANSFER REACTIVITY IN CRYSTALLINE INOSITOL DERIVATIVES

THESIS SUBMITTED TO THE
UNIVERSITY OF PUNE

FOR THE DEGREE OF
DOCTOR OF PHILOSOPHY
IN
CHEMISTRY

BY

SHOBHANA KRISHNASWAMY

RESEARCH SUPERVISOR
DR. MOHAN M. BHADBHADE

CENTER FOR MATERIALS CHARACTERIZATION
NATIONAL CHEMICAL LABORATORY
PUNE 411 008, INDIA

MAY 2011

Investigations on molecular pre-organization and intermolecular acyl transfer reactivity in crystalline inositol derivatives

A thesis

submitted to the

UNIVERSITY OF PUNE

for the degree of

DOCTOR OF PHILOSOPHY

in

CHEMISTRY

by

SHOBHANA KRISHNASWAMY

Center for Materials Characterization
National Chemical Laboratory
Pune 411008

May 2011

DECLARATION

I hereby declare that the thesis entitled **"Investigations on molecular pre-organization and intermolecular acyl transfer reactivity in crystalline inositol derivatives"** submitted for Ph. D. degree to the University of Pune has not been submitted by me for a degree to any other University.

Date: **SHOBHANA KRISHNASWAMY**

Center for Materials Characterization
National Chemical Laboratory
Pune 411008, India

Acknowledgements

This thesis is the compilation of five years of work that was carried out in the Center for Materials Characterization (CMC) and Division of Organic Synthesis (DOC) of the National Chemical Laboratory. I wish to thank the people who encouraged and supported me through this journey.

At the outset, I would like to thank my research supervisor ***Dr. Mohan M. Bhadbhade****, for introducing me to the fascinating world of X-ray crystallography and organic solid-state reactions. His suggestions, enthusiasm, patience, and words of encouragement helped me immensely during the period of research and thesis writing. I would also like express my gratitude towards my research co-guide* ***Dr. M. S. Shashidhar*** *who gave me an interesting research problem in the field of inositol chemistry and also wore the mantle of research guide when the occasion demanded it. He impressed upon me the importance of being meticulous and accurate with my work. His wide knowledge and logical way of thinking have been of great value for me.*

I am grateful to Dr. Sourav Pal, (head, CMC and Director, NCL) for his support and encouragement besides providing the infrastructure to carry out this work and access to all divisional facilities. I thank Dr. Ganesh Pandey (head, DOC) for giving me an opportunity to work in the organic chemistry division and providing the necessary facilities. I thank Dr. N. N. Joshi, Dr. Avinash Kumbhar and Dr. Sandhya Rane (members of my PhD committee) for insightful comments, discussions and advice. I also thank Prof. G. R. Desiraju, Prof. T. N. Guru Row, Dr. E. Suresh, Dr. C. R. Rajan and Dr. Rahul Banerjee for words of wisdom and encouragement.

I am grateful to CSIR for award of a research fellowship and for supporting my active participation in the 21st IUCr Congress.

I wish to express my sincere gratitude towards Dr. Rajesh Gonnade, who taught me the basics of X-ray crystallography, structure solution and data analysis. I also thank Dr. (Mrs.) Vedavati G. Puranik for constant encouragement, care and advice in matters within and outside the laboratory. I am grateful to Dr. Smita Mule for providing almost all of the DSC data in this thesis and fruitful discussions, Mrs. Sunita Sawant and Mrs. Chitra Sanas for microanalysis data, and current and ex-members of the NMR group, Hilda, Deepak and Shrikant. I thank BRUKER engineers, especially Noel and Mantri for their timely help with maintenance of the X-ray diffractometer.

I would like to thank my senior colleagues, Dr. Manash, Dr. Devaraj, Dr. Shailesh, Dr. Gaurav, Dr. Manoj, Dr. Murali and Dr. Rajendra for their advice and help and my lab-mates Madhuri, Bharat, Alson, Majid, Richa, Rupesh, Omkar, Archana and Pranaya for maintaining a

cheerful atmosphere during the long hours in the lab. I also thank Moreji for lab maintenance. I specially thank Bharat, Madhuri and Richa for the proofreading of this thesis.

I thank Dr. (Mrs.) Ranjana Bhadbhade, Dr. (Mrs.) Vidya Shashidhar, Mrs. Vaishali Gonnade and Mrs. Nandini Dixit, for care and constant encouragement.

I am grateful to my M.Sc project advisor Dr. A. Sudalai and co-guide Dr. T. Shivakumar, and my teachers Prof. D. D. Dhavale, Prof. M. S. Wadia, Prof. B. S. M. Rao, Dr. (Mrs.) R. S. Kusurkar, Dr. M. G. Kulkarni, Prof. S. R. Gadre, Prof. S. P. Gejji, (M.Sc., University of Pune), Late Prof. S. Khasgiwale, Dr. V. M. Sholapurkar and Dr. Modak (B.Sc., Sir Parashurambhau College) for their guidance and encouragement.

I also thank my friends and colleagues Archana, Bhakti, Kumar, Mira, Neena & Kunal, Santosh, Yogesh, Snehal, Bhakti, Vaishali & Nikhilesh, Arundhati Annegiri, Prashant, Nayana, Kavita, Sapna, Sayali, Deepti, Pooja, Tanwir, Victor, Arun, Pandurang, Prasad, Sanjay, Kishor, Megha, Amit, Puspesh, Indresh, Abhishek, Yogesh, Prince, Nagarajan, Manish, Trupti, Seema, Sachin, Anjan, Reema, Divya, Pradnya and Manaswini for their help, pleasant company and support through the ups and downs in this journey.

I wish to express my gratitude towards my parents and all family members for their never-ending support, affection, care and encouragement and dedicate this thesis to them.

May 2011 *Shobhana Krishnaswamy*

Contents

Abbreviations

Ac	Acetyl
All	Allyl
Anhy.	Anhydrous
Aq.	Aqueous
Bz	Benzoyl
Calcd.	Calculated
DCM	Dichloromethane
D_2O	Deuterium oxide
DMF	*N, N*-Dimethylformamide
DMSO	Dimethyl sulphoxide
El	Electrophile
Eq.	Equivalent
Et_3N	Triethyl amine
g	Gram
h	Hour(s)
Hz	Hertz
IR	Infrared
M.p.	Melting point
MeOH	Methanol
Me	Methyl
mL	millilitre
mmol	millimole
NLO	Non-linear optics
NMR	Nuclear magnetic resonance
Nu	Nucleophile
ORTEP	Oak Ridge Thermal Ellipsoid Plot
Ph	Phenyl
Rac-	racemic
RT	Room temperature 22 – 30°C
THF	Tetrahydrofuran
TLC	Thin layer chromatography

Synopsis of the thesis

The thesis entitled **"Investigations on molecular pre-organization and intermolecular acyl transfer reactivity in crystalline inositol derivatives"** comprises of five chapters and deals with the design, synthesis, characterization and the investigation of the solid-state acyl group transfer reactivity of several crystalline *myo*-inositol derivatives. The aim of the present work was to design molecules that would yield crystals that have the required organization of molecules for facile acyl transfer in the solid state. The first chapter presents an illustrative review of the literature in the general area of chemical reactions in molecular crystals and a brief introduction to inositols including reports of solid-state reactivity in *myo*-inositol derivatives. The second chapter describes the molecular design, synthesis and characterization of *myo*-inositol orthoester derivatives investigated in this work. The third chapter presents and discusses the crystal structures of some di-*O*-acylated *myo*-inositol orthoester derivatives in the context of acyl transfer reactivity in the solid-state. Chapter 4 is divided into 2 sections; Section 4A examines the effect of polymorphism and phase transitions on the solid-state reactivity of racemic 2,6-di-*O*-benzoyl-*myo*-inositol 1,3,5,-orthobenzoate and racemic 2,6-di-*O*-(4-halobenzoyl)-*myo*-inositol 1,3,5-orthoformates and correlation between their crystal structures. Section 4B is a correlation of the structures and solid-state reactivity of some mono-acylated *myo*-inositol orthoester derivatives. Chapter 5 summarizes the criteria necessary for facile solid-state reactivity in crystals and analyses literature reports of solid-state acyl transfer reactions (in compounds other than inositol derivatives) in the light of our observations; directions for future work are also presented.

Chapter 1: A literature review of organic solid state reactions and acyl transfer in molecular crystals of cyclitol derivatives

Organic reactions in the solid-state have been attracting the attention of chemists in recent times because of the product selectivity (due to the fixed orientation and minimum movement of molecules in the crystal lattice), which is often different from that observed in the solution state. The reactions in the solid state can be regarded as environment friendly green reactions. Techniques such as X-ray crystallography, solid-state NMR spectroscopy[1] and electron microscopy[2] have

emerged as tools that provide information about the reaction centers and mechanism of reactions that proceed in the solid state. Amongst the earliest reported and well-studied solid-state reactions are photochemical addition reactions of olefinic double bonds (C=C).[3] A variety of other reactions such as pinacol coupling, Beckmann rearrangement, Chapman rearrangement, Michael addition, Grignard, Reformatsky and Luche reactions, Wittig reactions, sodium borohydride reduction, group transfer reactions (methyl, aryl and acyl groups), *cis-trans* isomerization, and epimerization are known to proceed in the solid-state or under solvent free conditions.[4]

Nucleophilic addition to carbonyl groups is one of the most frequently encountered reactions in organic chemistry. Often, the tetrahedral intermediate generated in such an addition reaction undergoes elimination to regenerate the carbonyl group in a new product, as in reactions of carboxylic acids and their derivatives. Although addition – elimination reactions in solution phase are ubiquitous, documentation of their occurrence in the condensed phases (solvent less) is scarce. Facile benzoyl group migration in the solid-state in di-*O*-acylated *myo*-inositol orthoester derivatives was reported from our laboratory (Scheme 1, Fig. 1).[5] The subsequent chapters describe our attempt to further probe and understand and broaden the scope of these acyl transfer reactions.

Scheme 1

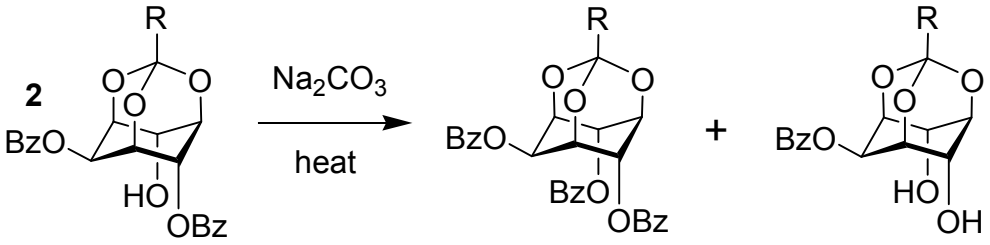

R	R	R
1 H ($P2_1/c$ crystals)	**4** H (47%)	**7** H (49%)
2 Me (Form I; $P2_1/n$ crystals)	**5** Me (19%)	**8** Me (21%)
Me (Form II; $C2/c$ crystals)	Me (42%)	Me (42%)
3 Ph ($P2_1/c$ crystals)	**6** Ph (49%)	**9** Ph (48%)
1·**2** (*Cc* co-crystals)	**4** + **5** (41%)	**7** + **8** (35%)

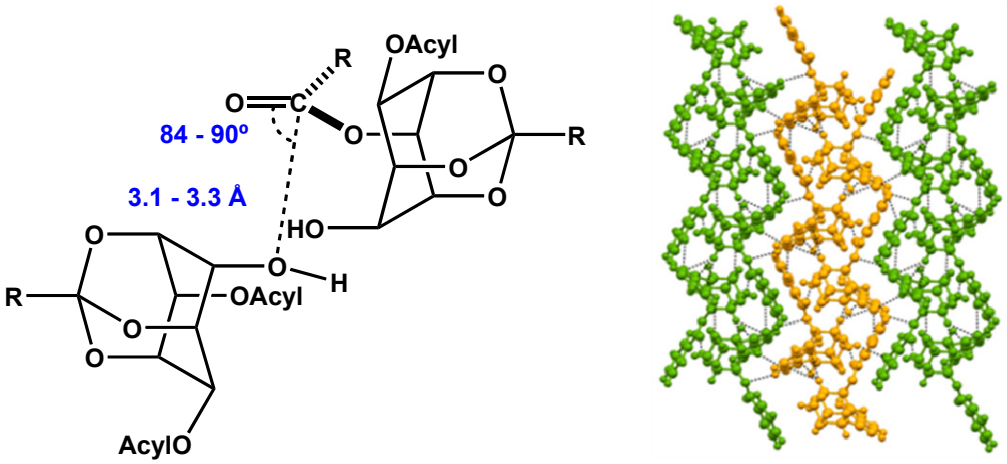

(a) **(b)**

Figure 1. (a) Relative orientation of the closely interacting molecules (electrophile-C=O, nucleophile-OH) poised for the acyl transfer reaction (R = H, Me, Ph; acyl = benzoyl) and (b) helices which serve as reaction tunnels in crystals of the reactive diesters shown in scheme 1.

Chapter 2: The molecular design, synthesis and characterization of *myo*-inositol derivatives

Earlier work in our laboratory investigated the effect of substitution of the hydrogen atom at the bridgehead carbon (in **1**, Scheme 1) with methyl and phenyl groups. The effect of substitution of the ester groups at other positions in *myo*-inositol orthoformate on molecular organization and reactivity in the crystalline state has now

been studied by synthesizing esters other than benzoates at C-6 and C-2 positions. This chapter presents the synthesis and characterization of derivatives **2.1 – 2.9** shown in Scheme 2.

Scheme 2

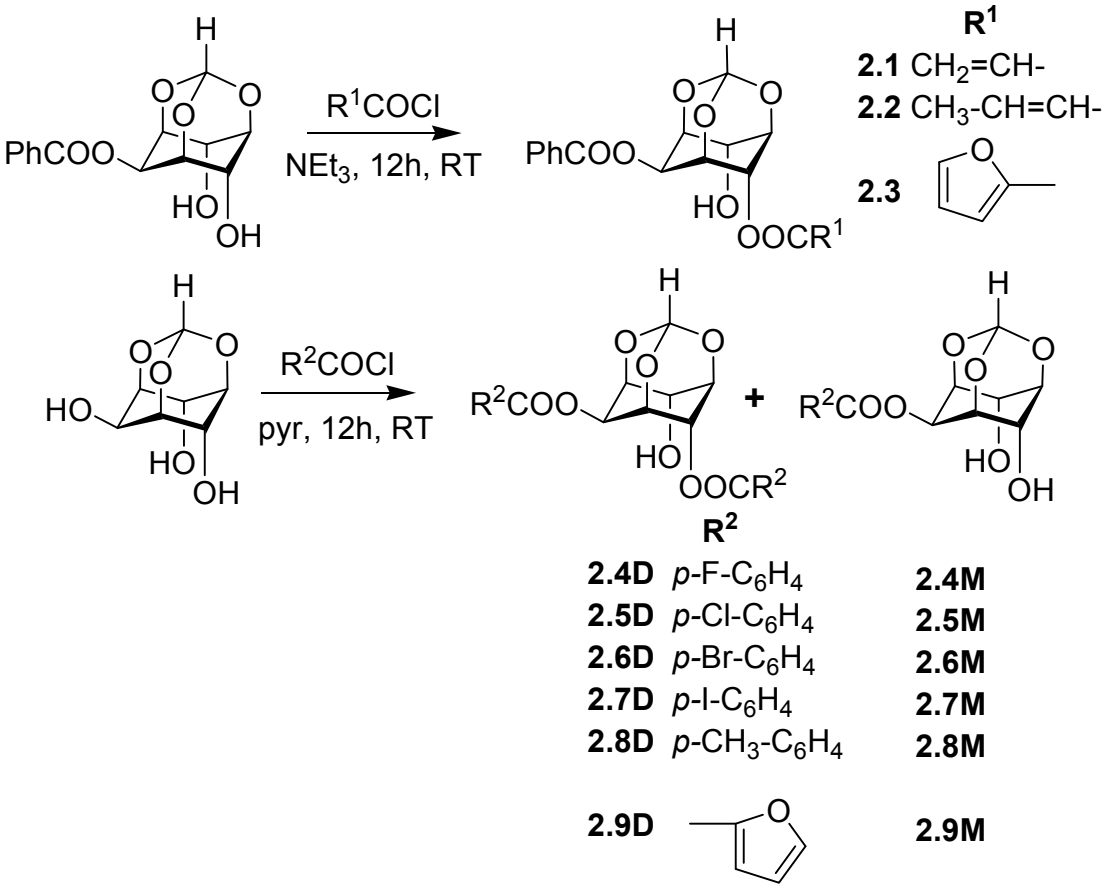

Chapter 3: Crystallization and reactivity of di-*O*-acylated *myo*-inositol derivatives

The diesters **2.1** - **2.3** (Scheme 2) were prepared in order to study the effect of replacing the benzoyl group at the C-6 position by ester groups containing either a double bond or other aromatic rings on the molecular organization. Compound **2.1** yielded conformational dimorphs [triclinic - form I and monoclinic – form II] at room temperature, separately or concomitantly, depending on the solvent of crystallization. DSC curves and hot stage microscopy of the Form II crystals suggested a phase transition which was confirmed by X-ray crystallographic studies (by determining unit cell parameters) as the irreversible transition *via* melt crystallization of Form II to Form I crystals.[6] However, neither of the dimorphs possessed the proper molecular pre-organization for acyl transfer (Form I, Fig. 2a); this was confirmed by studying

the solid-state reactivity of form I crystals which yielded a mixture of products. Compound **2.2**, failed to yield suitable crystals for single crystal X-ray diffraction studies. Compound **2.3** crystallized as rectangular plates from dichloromethane. The crystal structure revealed an assembly of glide-related molecules linked through hydrogen bonding between the hydroxyl group and the furanyl oxygen, supported by stacking interactions of furan rings.

Compound **2.8D** could be crystallized from different solvents (ethyl acetate, acetone, methanol, acetonitrile, dioxane, dichloromethane), yielding needles. Compound **2.9D**, when crystallized from common organic solvents yielded triclinic rectangular plates. Packing of molecules (Fig. 2b, 2c) in crystals of these compounds was not conducive for the acyl transfer reaction. Heating of these crystals with sodium carbonate did not bring about facile acyl transfer reaction as expected from their crystal structure.

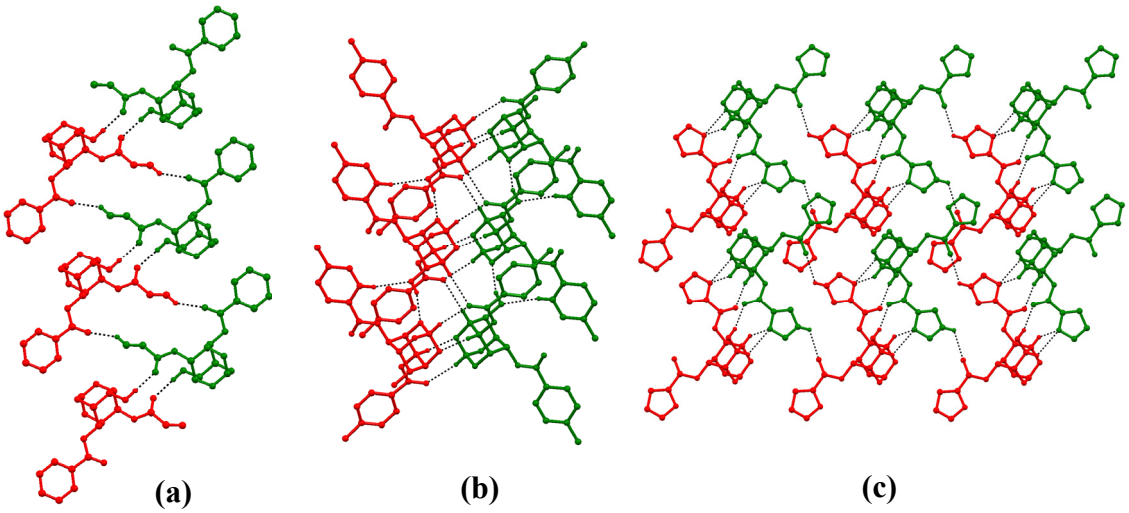

Figure 2. Molecular organization in crystals of (a) racemic **2.1** (Form I, *P*-1) (b) racemic **2.8D** (*P*-1) and (b) racemic **2.9D** (*P*-1). Red and green molecules indicate the two enantiomers. Dotted lines represent O-H…O and C-H…O interactions.

Chapter 4: Creating helical assemblies of *myo*-inositol derivatives for acyl transfer reactivity in their crystals

Section A: Polymorphism and reactivity

Polymorphism, the existence of molecules in more than one crystalline arrangement, has implications on the solid-state physical and chemical properties of a compound. Since the crystalline-state properties of a compound are determined by the molecular arrangement and weak non-covalent intermolecular interactions of constituent molecules in crystals, it is plausible that polymorphs can exhibit differential solid-state reactivity. As a corollary, the facility of solid-state reactions of organic compounds can be controlled by studying their polymorphic behaviour and growing crystals of the desired polymorph for chemical reaction. Further, the crystalline state properties and reactivity of a compound can also be tuned by co-crystallizing it with one or more solid components[5] or by introducing guest molecules in the lattice, creating solvates or hydrates. Compounds **2.4D** - **2.7D** were synthesized to explore the effect of replacing the benzoyl groups in **1** with *p*-halobenzoyl groups on molecular organization and solid-state reactivity.

2.4D gave solvent free monoclinic crystals from methanol, monoclinic solvates from chloroform, DCM, THF, dichloroethane, nitromethane, *etc*. and it yielded triclinic solvates from benzene, toluene and *o*-xylene. Crystal structure solution revealed that solvent free crystals and the triclinic solvates formed molecular strings *via* O-H...O hydrogen bonding, which are linked by C-H...O interactions to form bilayers. In the solvent free form, the bilayers are stitched together by weak C-H...F and C-H...π interactions, whereas in the solvates, the solvent molecules inhabit the space between the bilayers linking them by C-H...O, C-H...F and C-H...π contacts. The halo benzoates **2.5D** and **2.6D** when crystallized from methanol and ethyl acetate, each produced triclinic solvent free dimorphs which exhibited a one-dimensional isostructurality in their crystals.[7] When crystallized from other organic solvents, **2.5D** and **2.6D** yielded isostructural monoclinic solvates. The monoclinic solvates of **2.4D** - **2.6D** exhibited a uniform helical self-assembly of host molecules through O-H...O hydrogen bonding similar to that observed in the reactive diesters **1-3** (Fig. 3a). In compounds **1-3**, the neighbouring helices are linked together by C-H...O interactions, in the helical solvates of **2.4D** they are connected by C-H...O and C-H...F contacts and in **2.5D** and **2.6D** by C-H...X (X=Cl, Br), C-X...O (X = Cl, Br) and Cl...Cl contacts.[8]

The DSC and hot stage polarizing microscopic studies revealed conversion of the solvated crystals into the Form I crystals which further undergo a single crystal-to-single crystal transformation to the Form II crystals. The solvates of **2.4D** also showed escape of solvent from the lattice followed by transition to an as yet unidentified crystalline modification. Therefore the solid-state reactivity of these solvated crystals was studied at temperatures below the escape of solvent from the lattice.

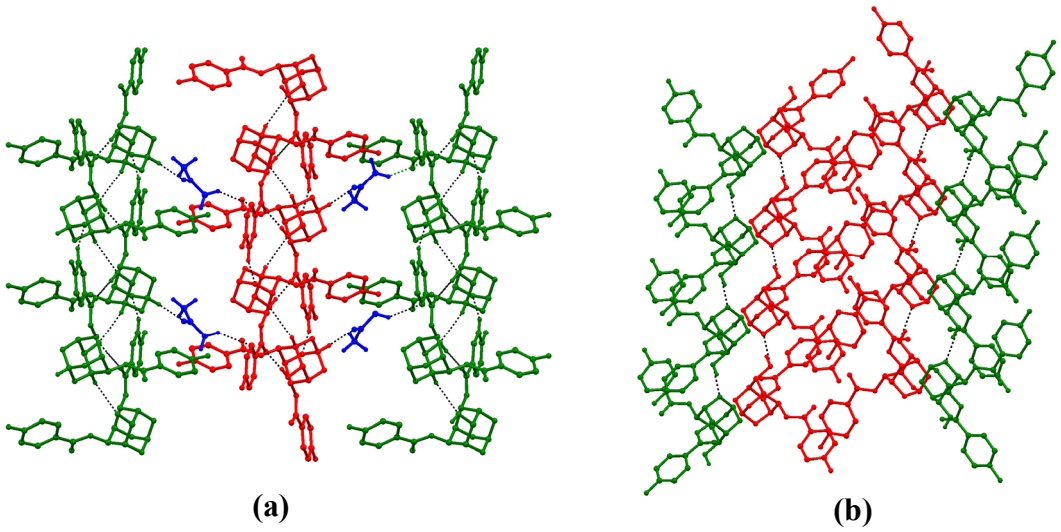

Figure 3. Molecular organization in (a) monoclinic solvated crystals and (b) solvent free crystals of racemic **2.4D**. Red and green molecules indicate the two enantiomers, blue molecules represent the entrapped solvent. In the solvated crystals, each helix is comprised of a single enantiomer, whereas in the solvent free crystal each enantiomer forms molecular strings that are linked to form bilayers. Dotted lines represent O-H…O and C-H…O interactions.

The solvates of **2.5D** and **2.6D** when heated with activated sodium carbonate at a temperature below which the solvent escaped, showed transesterification as revealed by TLC, but the extent of acyl transfer could not be quantified. The acyl transfer reactivity in solvates of the fluoro derivative **2.4D** was estimated using fluorine-19 NMR spectroscopy. The low yield in these reactions could be attributed to the parallel physical change (phase transition) occurring in these crystals along with a chemical change (acyl transfer reaction). On the other hand, heating the solvent free crystals of **2.4D** with sodium carbonate yielded a mixture of several products, including the triester and the diol. The dissimilar reactivity patterns of the solvent free and the solvated form, by virtue of the difference in molecular organization (Fig. 3),

underscores the importance of molecular orientation in crystals for solid-state transesterification reaction.

Racemic **3** when crystallized from ethyl acetate, chloroform, methanol, acetone, dichloromethane, etc. yielded monoclinic crystals (form I, $P2_1/c$)[9] but crystallization from benzene, toluene and 2-propanol gave thin whisker like solvates (Form II, *P*-1) concomitantly with plates of form I. DSC curves and hot stage microscopy suggested a phase transition that was confirmed by X-ray crystallographic studies (by determining unit cell parameters) as the conversion of these thin Form II crystals into the Form I crystals *via* melt crystallization. The 2-propanol and toluene solvates of **3**, did not show any acyl transfer activity below the phase transition temperature, but instead showed transesterification activity when heated with sodium carbonate at (or above) the transition temperature (135 °C). Molecules in Form II crystals are organized differently as compared to the Form I crystals (Fig. 4). Such an arrangement of molecules does not place the electrophile and the nucleophile in proper orientation for the acyl transfer reaction in form II crystals. However, when Form II crystals are heated to the transition temperature of 135 ºC in the presence of solid sodium carbonate, *in situ* melt crystallization occurs, and the unreactive Form II crystals are slowly transformed into the reactive Form I crystals which react to give the products **6** and **9** (Scheme 1). However, the extent of conversion of **3** (about 50%) to products in Form II crystals is not as good as that observed in Form I crystals (>90%).

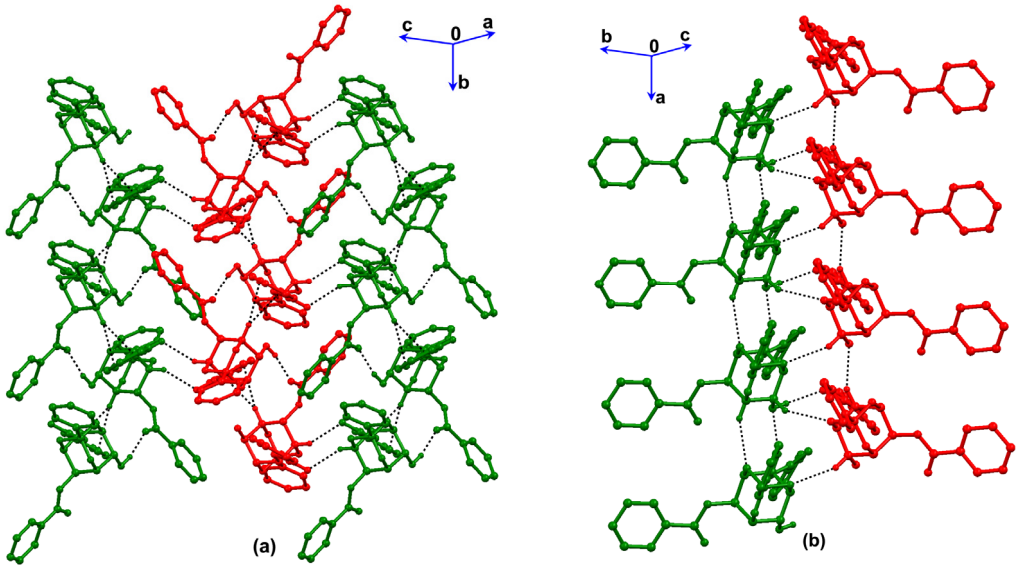

Figure 4 Molecular organization in (a) Form I ($P2_1/c$) and (b) Form II (*P*-1) crystals of racemic **3**. Red and green molecules indicate the two enantiomers. In Form I each

helix is comprised of a single enantiomer, whereas in form II they form homochiral chains.

Heating the Form I crystals with sodium carbonate brings in only a chemical change, but heating of Form II crystals with sodium carbonate activates parallel phase changes and chemical changes in the solid reaction mixture at the transition temperature. This differentiation could also contribute to the observed difference in the extent of conversion of **3** to products in the polymorphs.[10] Thus, as can be inferred from the systems studied above, it is possible to tune the reactivity of small molecules in their crystals by understanding their polymorphic behaviour.

Section B: Structures and reactivities of some mono-acylated *myo*-inositol derivatives

Intramolecular acyl migration in racemic 4-*O*-acyl *myo*-inositol-1,3,5-orthoesters, in the presence of sodium hydride, to the corresponding 2-*O*-acyl derivatives is very fast and facile in solution[11] but the reaction is irreversible.

Scheme 3

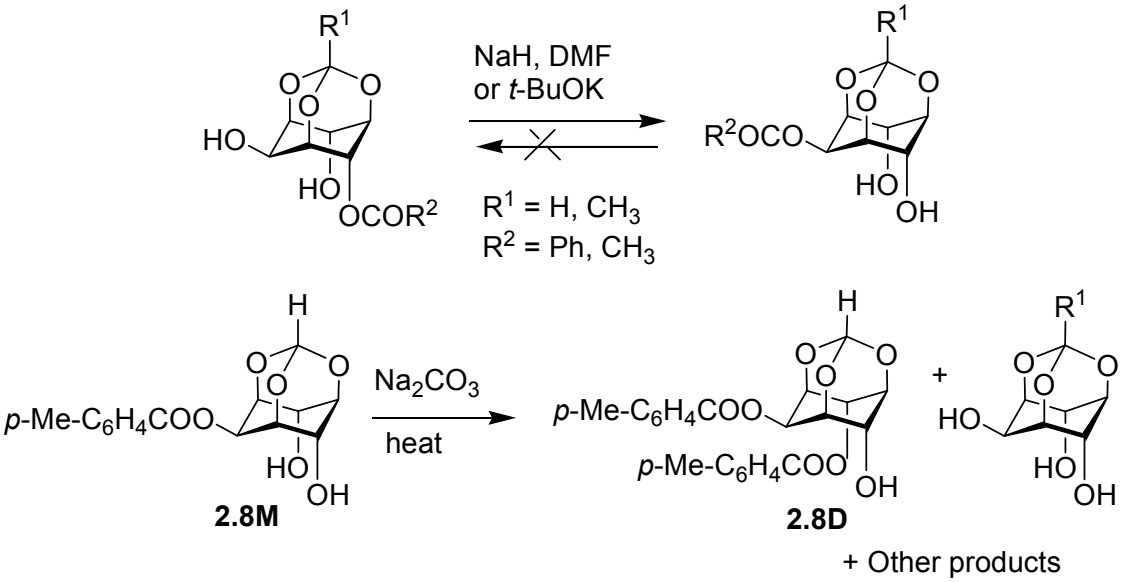

Analysis of the crystal structures of 2-*O*-benzoyl-*myo*-inositol-1,3,5-orthoesters revealed a relative orientation of molecules that appeared conducive for exhibiting the solid state acyl transfer reactivity although not with great facility (Scheme 3).

Reaction of the monobenzoate **7** in its crystals yielded a mixture of products including the racemic C4-benzoate. It is fascinating to observe that although these mono-benzoates failed to undergo transesterification in solution, they reacted in the crystalline state due to the relatively rigid assembly of molecules in the lattice.[9] Hence we sought to explore the crystal structures of some mono-acylated *myo*-inositol-1,3,5-orthoesters in our quest for molecules with the reactive pre-organization. Crystals of the monoesters **2.5M** and **2.6M** are isostructural which reveal molecular strings formed *via* hydrogen bonding linked by halogen...halogen interactions. The geometry of the molecules in these crystals is not conducive for facile transesterification which was confirmed by testing the solid-state reactivity of **2.6M**, which yielded a mixture of several products. The toluate **2.8M**, crystallised as hexagonal plates, wherein the *n* glide related molecules are associated through O-H...O hydrogen bonding between the hydroxyl group and the orthoester oxygen atom. The pattern of association is similar to that observed in racemic **7**. The solid-state reactivity of **2.8M** was determined by heating crystals ground with sodium carbonate at 126 °C for 20 h. The major products obtained were the diester **2.8D** (29%) and *myo*-inositol 1,3,5-orthoformate (39%, Scheme 3). The same reaction when carried out for a longer period of time or at lower temperatures resulted in the formation of several products.

On the other hand 2-*O*-acetyl-*myo*-inositol 1,3,5-orthoformate,[11] when dissolved in acetone, crystallized in the chiral orthorhombic space group $P2_12_12_1$ with two independent molecules in the asymmetric unit along with a molecule of water. Crystallization from various solvents neither yielded any different crystalline forms nor inclusion of other solvents. The formation of chiral crystals of a *meso* (or achiral) compound, besides aiding in understanding the process of crystallization,[12] has application in areas of asymmetric autocatalysis[13] and NLO materials.[14]

Chapter 5: Acyl group migration in crystals: scrutiny of literature reports and conclusions

A comprehensive study of the crystal structures and the geometry of the reacting molecules leads us to conclude that a facile intermolecular acyl transfer occurs in crystals which have pre-organization of molecules that (a) brings an electrophile (C=O) and the nucleophile (OH) in favourable geometry,[15] (b) favours supporting weak interactions[16] which stabilize the migrating benzoyl group in proper

orientation for the nucleophilic attack, and (c) function as reaction channels and facilitate a domino type of reaction to ensure high convertibility of reactants to products.[9] The angle of approach of the electrophile (El) towards the nucleophile (Nu) and the distance between them in the reactive crystals of inositol orthoester derivatives lies in the range of 84 – 90º and 3.1 – 3.3 Å respectively.[5] In the case of the pseudopolymorphic helices of the halobenzoates, which exhibit mild acyl transfer reactivity the El...Nu distance varies from 3.31 - 4.47 Å and the angle of approach shows a large variation from 40 - 87º. It is interesting to note that in the reactive crystals where the distance between the reaction centers is lesser than the sum of their van der Waals radii, the El and Nu groups are poised for reaction at an angle of ~ 90º. Hence, a survey of the Cambridge Structure Database (v5.31, November 2009) was undertaken for structures containing electrophiles (C=O group, ester or carboxylic acid) and nucleophiles (alcohols and amines). Analysis of the results as scatter plots showed that when the distance between potential pairs of electrophiles and nucleophiles was lesser than the sum of van der Waals radii, the angle between them (O=C···O/N) approaches 90° or is clustered between 80 and 100°.

In the light of these observations, we have also examined some of the solid-state acyl group migrations and nucleophilic additions reported in literature in greater detail, notably the acyl migration in acylsalicylamides,[17] imide formation in co-crystals of amine- anhydride[18], cyclization of *o*-acetamidobenzamide[19] and intermediate co-crystals formed during the solvent-free benzoylation of naphthalenediol.[20] Details of this analysis and some directions for the future course of research pertaining to acyl transfer reactions in the solid state are presented in this chapter.

References:

1. (a) A. B. Fernandez, I. Lezcano-Gonzalez, M. Boronat, T. Blasco and A. Corma, *Phys. Chem. Chem. Phys.*, **2009**, *11*, 5134-5141; (b) M. Khan, G. Brunklaus, V. Enkelmann and H-W. Spiess, *J. Am. Chem. Soc.*, **2008**, *130*, 1741-1748.
2. G. Kaupp, *Curr. Opin. Solid State Mater. Sci.,* **2002**, *6*, 131-138.
3. (a) M. D. Cohen, and G. M. J. Schmidt, *J. Chem. Soc.* **1964**, 1996-2000; (b) M. D. Cohen, G. M. J. Schmidt and F. I. Sonntag, *J. Chem. Soc.* **1964**, 2000-

2014; (c) G. M. J. Schmidt, *J. Chem. Soc.* **1964**, 2014-2021; (d) J. Bregman, K. Osaki, G. M. J. Schmidt and F. I. Sonntag, *J. Chem. Soc.* **1964**, 2021-2030.

4. K. Tanaka and F. Toda, *Chem. Rev.*, **2000**, *100*, 1025-1074.
5. C. Murali, M. S. Shashidhar, R. G. Gonnade and M. M. Bhadbhade, *Chem. Eur. J.* **2009**, *15*, 261-269 and references cited therein.
6. S. Krishnaswamy, R. G. Gonnade, M. M. Bhadbhade and M. S. Shashidhar, *Acta Cryst*. **2009**, *C65*, o54–o57.
7. R. G. Gonnade, M. M. Bhadbhade and M. S. Shashidhar, *CrystEngComm* **2008**, *10*, 288- 296.
8. S. Krishnaswamy, R. G. Gonnade, M. S. Shashidhar, and M. M. Bhadbhade, *CrystEngComm*. DOI: 10.1039/B924482D
9. C. Murali, M. S. Shashidhar, R. G. Gonnade, and M. M. Bhadbhade, *Eur. J. Org. Chem.* **2007**, 1153-1159.
10. S. Krishnaswamy, M. S. Shashidhar and M. M. Bhadbhade, *CrystEngComm*, communicated.
11. K. M. Sureshan and M. S. Shashidhar, *Tetrahedron Lett.* **2000**, *41*, 4185-4188.
12. R. G. Gonnade, M. S. Shashidhar, M. M. Bhadbhade, *Chem. Commun.* **2004**, 2530-2531.
13. (a) T. Kawasaki, K. Jo, H. Igarashi, I. Sato, M. Nagano, H. Koshima and K. Soai, *Angew. Chem. Int. Ed*., **2005**, *44*, 2774-2777; (b) T. Kawasaki, K. Suzuki, K. Hatase, M. Otsuka, H. Koshima and K. Soai, *Chem. Commun*., **2006**, 1869-1871; (c) M. Sakamoto, S. Kobaru, T. Mino and T. Fujita, *Chem. Commun*., **2004**, 1002 -1003.
14. (a) R. D. Wampler, N. J. Begue and G. J. Simpson, *Cryst. Growth Des.*, **2008**, *8*, 2589-2594; (b) H. Koshima, Y. Wang and T. Matsuura, *Mol. Cryst. Liq. Cryst.*, **1996**, *277*, 63-71.
15. (*a*) H. B. Bürgi, J. D. Dunitz and E. Shefter, *J. Am. Chem. Soc.* **1973**, *95*, 5065-5067; (*b*) H. B. Bürgi, J. D. Dunitz and E. Shefter, *Acta Crystallogr. Sect. B,* **1974**, *30*, 1517-1527; (*c*) H. B. Bürgi, J.-M. Lehn and G. J. Wipff, *J. Am. Chem. Soc*., **1974**, *96*, 1956-1957; (*d*) H. B. Bürgi, J. D. Dunitz, J. M. Lehn and G. J. Wipff, *Tetrahedron*, **1974**, *30*, 1563-1572; (*e*) H. B. Bürgi and J. D. Dunitz, *Acc. Chem. Res.* **1983**, *16*, 153-161.
16. O. Takahashi, Y. Kohno, and M. Nishio, *Chem. Rev*. ASAP article, DOI**:**10.1021/cr100072x.

17. K. Vyas, H. Manohar and K. Venkatesan, *J. Phys. Chem.* **1990**, *94,* 6069-6073.
18. M. L. Cheney, G. J. McManus, J. A. Perman, Z. Wang and M. J. Zaworotko, *Cryst. Growth Des.* **2007**, *7,* 616-617.
19. M. C. Etter, *J. Chem. Soc., Perkin Trans. 2,* **1983**, 115-121.
20. S. Nakamatsu, K. Yoshizawa, S. Toyota, F. Toda and I. Matijasic, *Org. Biomol. Chem.*, **2003**, *1*, 2231-2234.

Note: Compound numbers in the synopsis are different from those in the thesis and references are included separately for each chapter.

List of publications

1. 'Two modes of O-H…O hydrogen bonding utilized in dimorphs of racemic 6-*O*-acryloyl-2-*O*-benzoyl-*myo*-inositol-1,3,5-orthoformate'
   S. Krishnaswamy, R. G. Gonnade, M. M. Bhadbhade and M. S. Shashidhar, *Acta Cryst*. **2009**, *C65*, o54-o57.
2. 'Helical self-assembly of molecules in pseudopolymorphs of racemic 2,6-di-*O*-(4-halobenzoyl)-*myo*-inositol 1,3,5-orthoformates: Clues for the construction of molecular assemblies for intermolecular acyl transfer reaction'
   S. Krishnaswamy, R. G. Gonnade, M. S. Shashidhar, and M. M. Bhadbhade, *CrystEngComm*. **2010**, *12*, 4184-4197.
3. 'Intermolecular benzoyl group transfer reactivity in crystals of racemic 2,6-di-O-benzoyl-myo-inositol 1,3,5-orthobenzoate: Controlling reactivity by solvate (pseudopolymorph) formation'
   S. Krishnaswamy, M. S. Shashidhar and M. M. Bhadbhade, *CrystEngComm*, **2011**, *13*, 3258-3264.

Poster presentations

1. 'Correlating Molecular Organization with Solid State Acyl Transfer: Concomitant dimorphs of racemic 2-*O*-benzoyl-4-*O*-acryloyl *myo*-inositol 1, 3, 5-orthoformate and Phase Transition of Form I to Form II Crystals'.
   S. Krishnaswamy, R. G. Gonnade, M. M. Bhadbhade & M. S. Shashidhar *Presented at the 36th National Seminar on Crystallography held at the University of Madras, Chennai, India, 22-24 January **2007**.*
2. 'Solvent inclusion induces helical molecular assembly in crystals of halobenzoates of *myo*-inositol'.
   S. Krishnaswamy, R. G. Gonnade, M. M. Bhadbhade & M. S. Shashidhar
   *Presented at the 21st Congress and General Assembly of the International Union of Crystallography held at Grand Cube, Osaka, Japan, 23-31 August **2008**.*
3. 'Different patterns of molecular association in crystals of racemic 2,6-di-*O*-(*p*-halo benzoyl) *myo*-inositol 1,3,5-orthoformates'.
   S. Krishnaswamy, R. G. Gonnade, M. M. Bhadbhade & M. S. Shashidhar
   *Presented at the 38th National Seminar on Crystallography held at University of Mysore, Mysore, India, 11-13 February **2009**.*

Chapter 1

A literature review of organic solid-state reactions and acyl transfer in molecular crystals of cyclitol derivatives

Organic chemistry just now is enough to drive one mad. It gives me the impression of a primeval forest full of the most remarkable things, a monstrous and boundless thicket, with no way of escape, into which one may well dread to enter.

-Friedrich Wöhler

1.1 Introduction

From its beginnings in the early 19th century, knowledge in the area of organic chemistry has mostly been accumulated through the study of reactions in solution. The earliest chemists were probably prejudiced by the Greek philosopher Aristotle's reflection '*No coopora nisi fluida*' or 'No reaction occurs in the absence of solvent', in the times when philosophy and religion had a major influence on science. However, today there are many examples of reactions known to proceed in the absence of solvent or in the crystalline state, with many reviews[1] and a few books[2] dealing with the subject. Solid-state reactions can be developed as green reactions on account of their solvent-free nature and simplicity in workup and purification.[3] While spectroscopic methods have been used for understanding solution-state phenomena, techniques developed to study solid-state reactions include single crystal and powder X-ray diffraction, differential scanning calorimetry, electron microscopy,[4] infrared and solid-state nuclear magnetic resonance spectroscopy.[5]

Reactions in crystals often occur with facility and high selectivity because of the topochemical control exerted by the crystal lattice. Reactivity in crystalline state largely depends on the packing of molecules in the crystal through weak interactions and proximity of reactive groups, whereas reactivity in solution is dictated by electronic properties of molecules. In the solid state, the crystal lattice serves to predispose the reactants in a favorable orientation for the reaction and thwart changes in their relative orientation with respect to the neighboring molecules, as opposed to the gaseous and solution states, where molecules are free to constantly reorient with respect to each other. Pre-organization of the reacting groups provided by the crystal lattice is a factor responsible for the enhanced rate and / or the stereochemistry of the product obtained in reactions that proceed in crystals. Crystal packing forces can lower the entropy of activation of a reaction by constraining the molecular conformation leading to an intra-molecular reaction or fixing the relative orientation of the sites in the crystal lattice facilitating intermolecular processes. However, numerous other interactions (like hydrogen bonding, halogen bonding, electrophile – nucleophile interactions, etc.) in the crystal lattice can prevent potentially reactive groups from existing in reactive organisations. Hence, unlike solution state reactions, reactions in crystals often exhibit extreme behavior, *viz*., they can be very facile and selective (*stereo*-, *regio*- *etc*.) or may not proceed at all relative to the corresponding solution state reactions. In contrast, solution state reactions may not be highly

selective, but often provide required products in isolable quantities. Since relative orientation of the neighboring molecules is a major factor deciding the facility of the reactions in crystals, unlike in solution state reactions, electronic factors may not contribute much to the facility of the reactions.

Amongst the earliest known and well studied solid-state reactions are addition to C=C bonds. Photodimerization of cinnamic acid (Scheme 1.1) was studied by Schmidt and Cohen,[6] which led to the reiteration of Kohlschutter's postulate that '*reaction in the solid state occurs with a minimum amount of atomic or molecular movement*'.

Photochemical reactivity in crystals of *trans*-cinnamic acid[6]

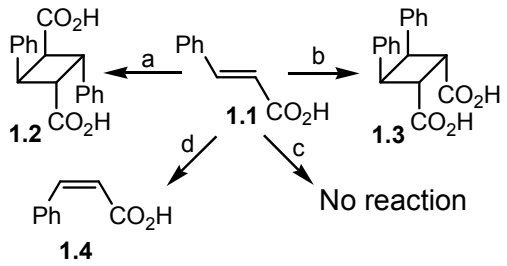

Scheme 1.1 (a) hν, α form (b) hν, β form (c) hν, γ form (d) hν, solution

However, this postulate could not be applied to gas-solid and solid-solid reactions wherein the crystal structures of the reactant and product vary greatly.[1i,1j] Kaupp and co-workers used atomic force microscopy to study the crystal surfaces in such reaction processes and demonstrated that molecules could migrate to great distance within the crystals, often resulting in destruction of the reactant crystal. They concluded that in a solid-state reaction, three processes must occur: namely molecules must be able to migrate within the crystal, the product phase must form at a reasonable rate and the crystal must disintegrate for the generation of a new surface.[4] Additionally, a mechanochemical inter-solid reaction may involve phenomena such as local melting and formation of intermediate eutectic phases resulting in formation of the product in a liquid phase followed by solidification with recrystallization yielding the product crystal lattice.[1j, 7]

Photochemically induced reactions in organic crystals have been reported and reviewed in recent times[1h,8] and current research includes the design and creation of templates, host-guest systems and novel substrates for control of reactivity.[9] Solid-state polymerizations also belong to a well-documented class of reactions.[10] Paul, Curtin and co-workers examined thermally induced organic reactions and rearrangements in the solid-state.[11] Toda and Tanaka were among the first chemists to

comprehensively study organic non-photochemical solid-state and solvent free organic reactions[1f,1i] with more examples emerging in recent times, including Baeyer-Villiger oxidation,[12] hydride reduction,[13] halogenation,[14] Michael addition,[15] aldol addition,[16] aldol condensation,[17] Dieckmann condensation,[18] Wittig-Horner reaction,[19] Grignard reaction,[20] Reformatsky and Luche reaction,[21] ylide reaction,[22] oxidative coupling of alcohols with ferric chloride,[23] Meyer-Schuster rearrangement,[24] pinacol rearrangement,[25] Glaser and Eglinton coupling of acetylinic compounds,[26] benzilic acid rearrangement,[27] Beckmann rearrangement[28] and Chapman rearrangement.[29] Kaupp and co-workers reported gas-solid and solid-solid reactions which yielded a single product nearly quantitatively. They also studied reactions in crystals using atomic force microscopy (AFM) and scanning near-field optical microscopy (SNOM) to prove that (as opposed to Schmidt's postulate[6]) molecules could migrate to great distances within the crystal as a precondition for reactivity.[3d,4,30] Byrn and co-workers studied the mechanisms of solid-state reactions in pharmaceutical compounds.[31] Braga and Grepioni investigated the preparation of crystals (inclusion and metal-ligand complexes) from crystalline reactants using solvent-free and mechanochemical reactions.[1j,1k,32] A few instances of thermally, as well as photochemically induced *cis-trans*[33] and *E-Z* isomerization[34] in crystals have also been reported. Solid-state epimerization though rare has also been documented.[35] Phenomena such as racemization or loss of optical activity[36] and thermally induced resolution in the solid state[37] have been observed. Reactions in chiral crystals of an achiral compound have been known to yield optically active products.[38-40] The following sections review types of organic solid-state reactions involving atom/group transfer, with a section devoted to acyl group transfer reactions in crystals leading to the present work.

1.2 Atom migrations in the solid state

A number of examples of atom migration in the solid-state involving movement of protons and hydrides, and halogens are reported. The most common examples of proton transfer in the solid state are related to the thermally or photochemically motivated keto-enol tautomerism of thermochromic compounds. Well studied systems include salicylideneanilines,[41] pyrazoles[42] and nitrobenzyl pyridines.[43] Examples from each class are represented in Scheme 1.2. Proton transfer has also been observed in crystalline complexes of quinone-hydroquinones.[44]

(i) Solid-state proton migration in salicylideneanilines[41]

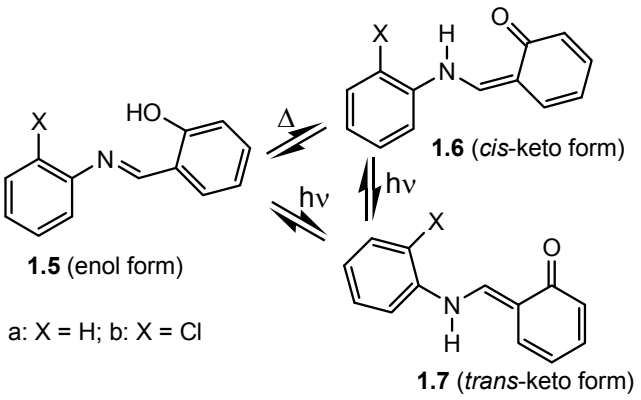

(ii) Solid-state proton migration in pyrazoles[42]

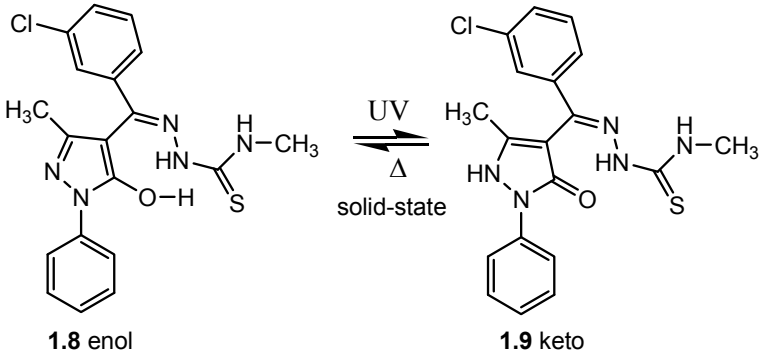

(iii) Solid-state proton migration in nitrobenzylpyridines[43]

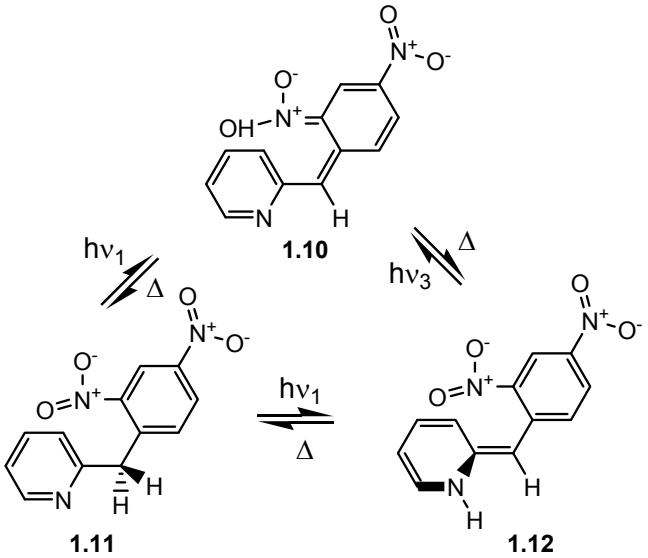

Scheme 1.2 Solid-state proton migration.

Hydride transfer has been observed in the solid-state sodium borohydride reduction of cage diketones[45] and regioselective reductive opening of epoxides by lithium borohydride.[46] Reduction of substrates included within cyclodextrins has yielded products with interesting *regio*- and *stereo*-selectivities.[47]

(i) Chlorine migration during solid-state Orton rearrangement[48]

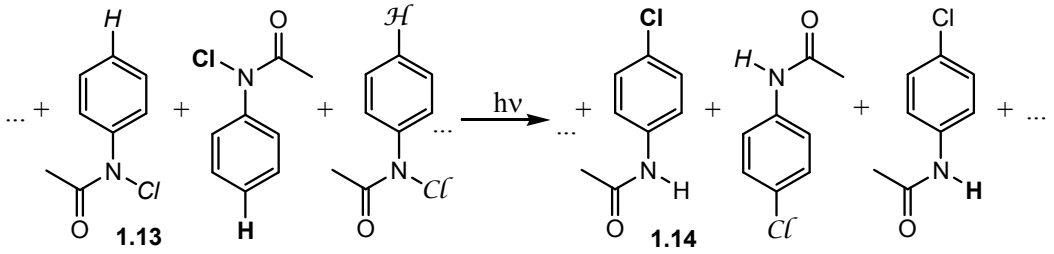

(ii) Chlorine and fluorine migration in enones[49]

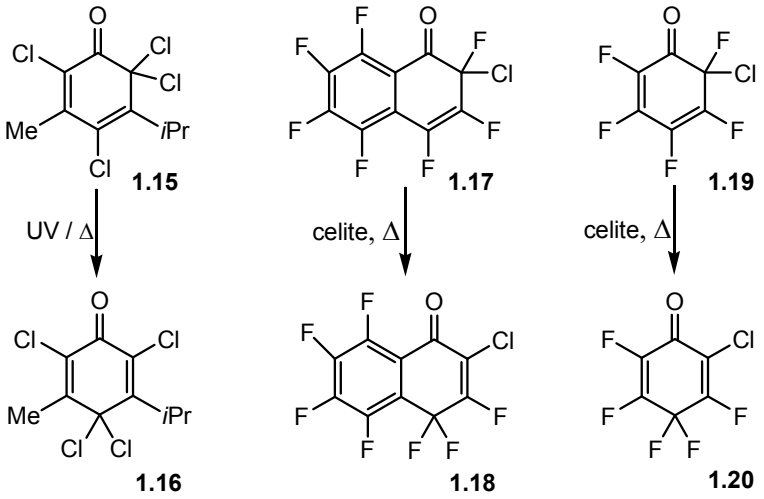

Scheme 1.3 Halogen migration in the solid-state. Labels of the reactive atoms originating from the same molecule in (i) are represented in the same font.

Halogen atom migration, though rare, has been documented in the photo-induced single-crystal-to-single-crystal Orton rearrangement (Scheme 1.3, i) of *N*-chloro-*N*-acetylaminobenzene (**1.13**) to *p*-chloroacetanilide (**1.14**).[48] Substituted cyclohexadienones also exhibit halogen migration at ambient temperature or under thermal / UV irradiation conditions (Scheme 1.3, ii). The reaction mechanism was concluded to be homogeneous[1c] (a topotactic reaction, where the crystal structure of the product is related to the crystal structure of the reactant) by microscopic observations of heated and irradiated single crystals.[49] Bromine migration was seen in the spontaneous rearrangement of *o*-quinobromides to *p*-quinobromides[50] and during the bromination of 3,4-dimethylphenol.[51]

1.3 Alkyl / aryl migrations in the solid state

This section is divided into three parts, describing thermally and photochemically induced alkyl / aryl group transfer, and migration of bulky groups in the solid state.

1.3.1 Thermally induced alkyl / aryl migration in the solid-state

The earliest known example of methyl migration in the crystalline state is the thermally initiated conversion of tetramethyl glycine ester into sarcosyltriglycine and other side products.[52] The reaction possibly consists of two major parts: one being a single phase reaction up to about 25% conversion and the other a heterophase reaction to about 30-35% conversion.[53]

Another well examined reaction is the thermal conversion (Scheme 1.4, i) of methyl *p*-dimethylaminobenzenesulfonate (**1.21**) into *p*-trimethylammoniumbenzenesulfonate (**1.22**).[54] While the reaction occurs in melt as well as in solution, it proceeds at a remarkably faster rate in the crystal, because the packing of the molecules in the crystal is such that ester methyl group of one molecule is transferred to the dimethyl amino group of the adjacent molecule, presumably as a chain process.[55] The exothermic nature of the reaction is due to the difference in the lattice energies of the crystals.[56]

A third instance of methyl group rearrangement is the Chapman-like thermal rearrangement (Scheme 1.4, ii) of imino ethers (**1.23**-**1.26**) to *N*-alkyl amides (**1.27**-**1.30**), involving O $\rightarrow$ N methyl group migration.[57] That the reaction is much faster in the solid state than in the melt was observed and explained by the favourable packing of molecules in the crystal and evidence from theoretical calculations.[58]

An interesting S_N2 reaction featuring O $\rightarrow$ N methyl migration (Scheme 1.4, iii) was observed during the aminolysis of a 1,1-binaphthyl ester (**1.31**) in the crystalline state. X-ray analysis revealed that the NH_2 group and migrating CH_3 of adjacent homochiral molecules lie in close proximity and hence the reaction occurs between homochiral molecules, rigorous proof for which was obtained by double isotopic labeling experiments.[59]

Thermal rearrangement of 4-alkyl 4*H*-1,2,4-triazoles to the corresponding 1-alkyl triazoles (Scheme 1.4, iv) was found to occur in the solid as well as molten state *via* a nucleophilic group transfer mechanism. The methyl substituted triazole (**1.33**) reacted faster than the corresponding ethyl derivative (**1.34**) and the reactivity could be correlated with the orientation and proximity of the reacting centres, which resulted in lowering of the entropy of activation of the reaction.[60]

(i) Methyl transfer in crystals of methyl *p*-dimethylaminobenzenesulfonate[54-56]

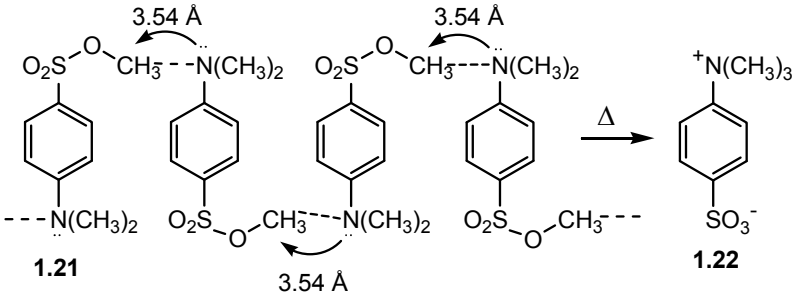

1.21 **1.22**

(ii) Thermal rearrangement of imino ethers to *N*-alkyl amides[57-58]

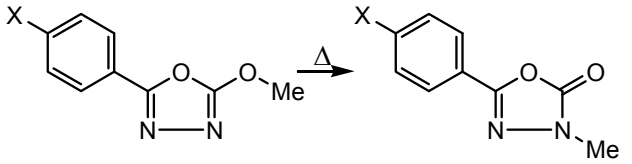

1.23 X = H
1.24 X = Cl
1.25 X = OMe
1.26 X = NO_2

1.27 X = H; 0%
1.28 X = Cl; 85%
1.29 X = OMe; 90%
1.30 X = NO_2; 9.5%

(iii) Solid-state S_N2 reaction : methyl migration[59]

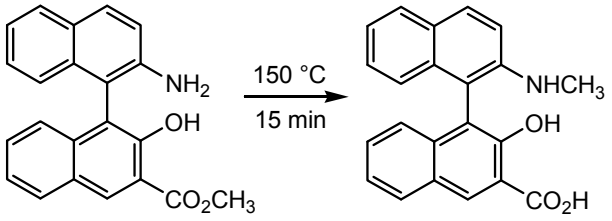

1.31 **1.32**

(iv) Alkyl migration in triazoles[60]

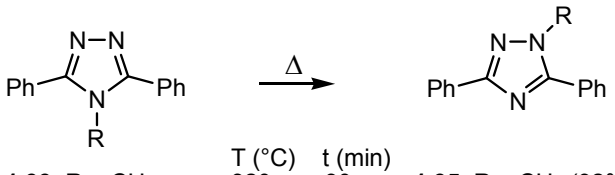

		T (°C)	t (min)	
1.33	R = CH_3	320	30	**1.35** R = CH_3 (92%)
1.34	R = CH_2CH_3	335	30	**1.36** R = CH_2CH_3 (85%)

Scheme 1.4 Thermally induced alkyl migration in the solid-state.

Benzisoxazole and naphthisoxazolequinones undergo thermal rearrangement in the solid-state with O → N methyl transfer yielding the corresponding N-methylbenzisoxazolonequinones.[61]

O → N and O → S methyl migrations in the solid-state were observed under thermal conditions and at room temperature respectively in methyl cyanurates and thiocyanurates.[62] Kinetic studies showed that the reaction is intermolecular and proceeds faster in the melt or in the solid compared to solution.

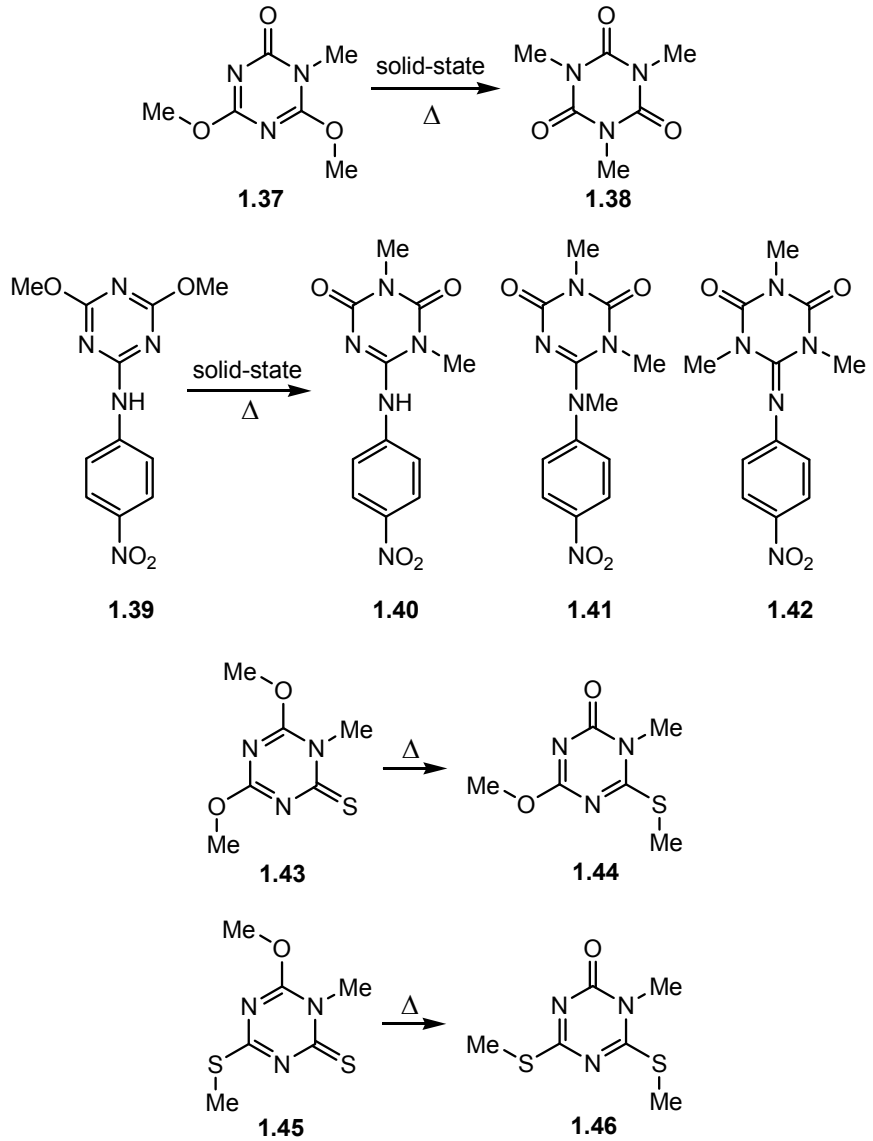

Scheme 1.5 Thermal methyl migration in crystals of methoxy triazines and methyl-thio triazines.

Kaftory and co-workers analysed the crystal structures of methoxy-triazines and methylthio-triazines and hence rationalised the formation of possible intermediates and products in the solid and molten states (Scheme 1.5). Information on the thermal processes was also gathered from HTXRD and DSC data.[63] Replacement of methyl groups by ethyl groups was done to examine the possibility of rearrangement of bulkier alkyl groups. While some rearrangements proceeded in solution, a few occurred in the solid and molten states. They concluded that rearrangement occurs in the liquid state whenever the melting temperature of the compound is low compared to the temperature where the rearrangement reaction starts. When packing forces are

strong and the melting temperature is higher than rearrangement temperature then the reaction occurs in the solid-state.[64] O → S topochemically controlled methyl migration in the analogous thiocyanurates was also investigated by crystal structure analysis, DSC and theoretical molecular energy calculations.[65]

(i) Methyl migration in crystalline CPTTOR[66]

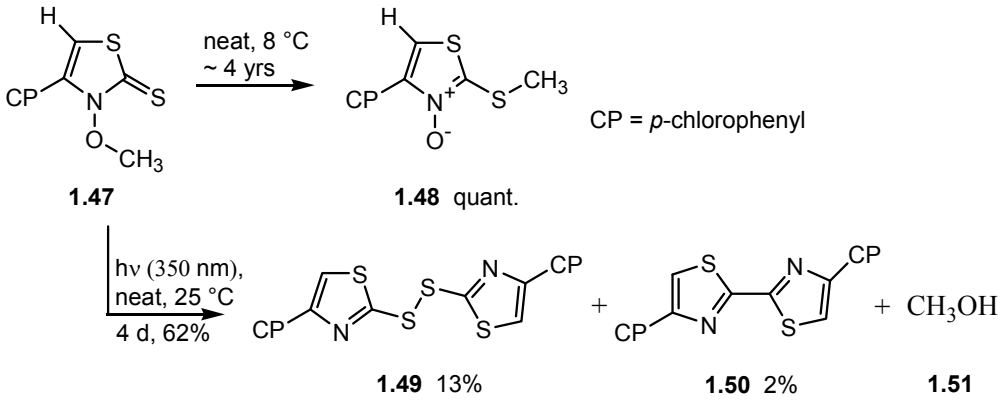

(ii) Thermal allyl migration[68]

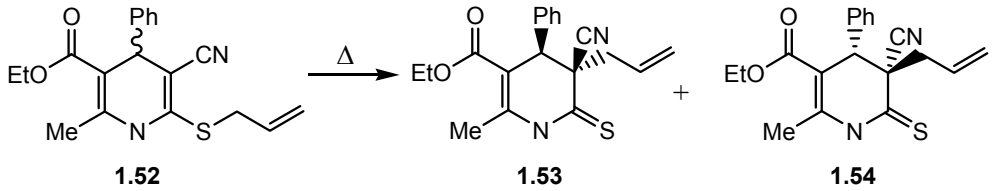

(iii) Thermal demethylation in tin complexes[69]

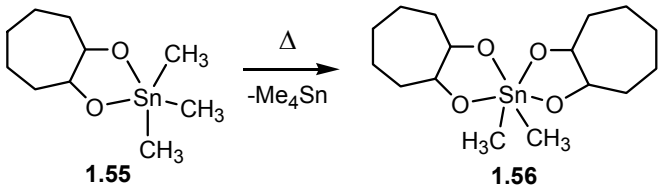

(iv) Conversion of thieranium ion to thietanium ion[70]

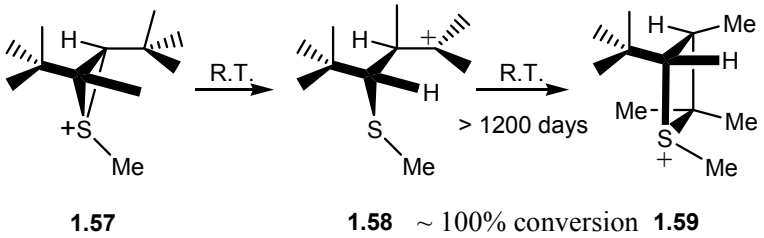

Scheme 1.6 Methyl migration and demethylation in the solid-state.

3-Alkoxy-4-(*p*-chlorophenyl)-1,3-thiazole-2(3*H*)-thiones (CPTTORs) are colorless solids, stored and used as reagents for alkoxyl radical generation in the absence of strong oxidant and metal ions at neutral pH. However, 3-methoxy-4-(*p*-chlorophenyl)-

1,3-thiazole-2(3*H*)-thione (Scheme 1.6, i, **1.47**) unexpectedly exhibited an O → S methyl transfer upon storage at 8 °C for ~ 4 years resulting in nearly quantitative conversion to the *S*-methylated product (**1.48**), verified by spectroscopic methods and X-ray diffraction analysis. Attempts to accelerate the conversion at elevated temperatures resulted in decomposition of the substrate while photoactivation of the substrate provided the disulfide **1.49**, the bithiazyl **1.50** and methanol.[66]

A thermally induced non-topochemical solid-state O → S methyl transfer was reported to occur in methyl 2-(methylthio) benzenesulfonate yielding a zwitterionic species. The crystal packing is unfavourable for intermolecular methyl transfer and the reaction possibly proceeds at defects in the ordered crystal.[67]

An uncommon example of thermally induced solid-state allyl group migration (Scheme 1.6, ii) was observed by Bürgi and co-workers,[68] in the crystals of ethyl 5-cyano-1,4-dihydro-2-methyl-4-phenyl-6-allylthio-3-pyridinecarboxylate (**1.52**). The molecular structure and crystal packing indicate that the rearrangement proceeds through either (a) an intramolecular Cope rearrangement or (b) an intermolecular transfer.

A rare example of thermally induced solid-state methyl migration in organometallic compounds was reported by Deák and co-workers in tin complexes. Single crystals of tetrameric $[Me_3Sn(PhN_2O_2)]_4$ and $Me_3Sn(trop)$ (**1.55**) demethylate upon heating into single crystals of $[Me_2Sn(PhN_2O_2)_2]_2$ and $Me_2Sn(trop)_2$ (**1.56**) respectively along with volatile Me_4Sn (Scheme 1.6, iii). While the demethylation of $[Me_3Sn(PhN_2O_2)]_4$ proceeded faster in the melt than in the solid, complex **1.55** appears to rearrange faster in the solid and liquid than in $CDCl_3$ solution.[69]

Single-crystal-to-single-crystal transformation at room temperature of a thiiranium ion (Scheme 1.6, **1.57**), by ring expansion, upto 100% conversion in ~ 1200 days into thietanium ion (**1.58**), and its kinetic behaviour was investigated by Destro and co-workers (Scheme 1.6, iv).[70] Intermediate stages were characterised by the site occupancy factor of the episulfonium ion and changes in unit cell volume, which indicated multi-step kinetics. *Ab initio* calculation in the gas phase suggested a spontaneous reaction with overall decrease of entropy.

Aryl migration in the solid state was observed during Beckmann-Chapman rearrangement of oxime picryl ethers (Scheme 1.7, i).[28a] Picryl ethers of benzophenone oxime (**1.60**) and its *p*-bromo derivatives (*syn* and *anti*, **1.61**-**1.62**)

underwent a thermal rearrangement involving migration of the aromatic ring *trans* to the picryloxy group of the reactant, yielding the corresponding *N*-picrylbenzanilides (**1.64**-**1.66**).

(i) Beckman-Chapman rearrangement of oxime picryl ethers[28a]

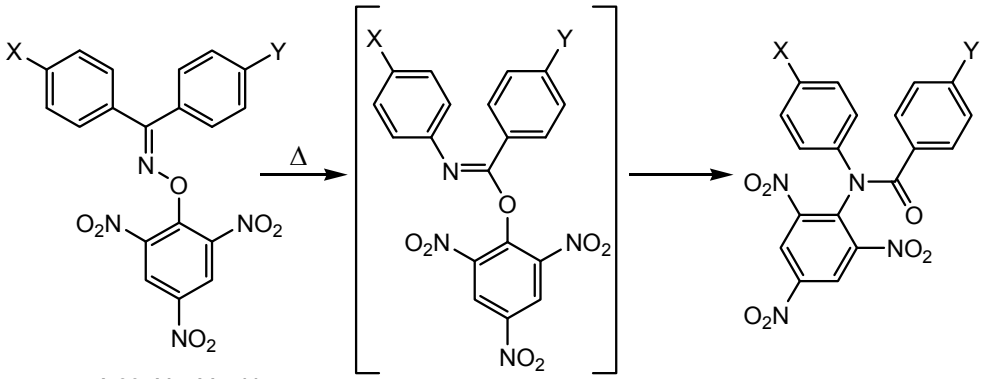

1.60 X = Y = H
1.61 X = H; Y = Br
1.62 X = Br; Y = H

1.63

1.64 X = Y = H
1.65 X = H; Y = Br
1.66 X = Br; Y = H

(ii) Solid-state aryl migration in a betaine[71]

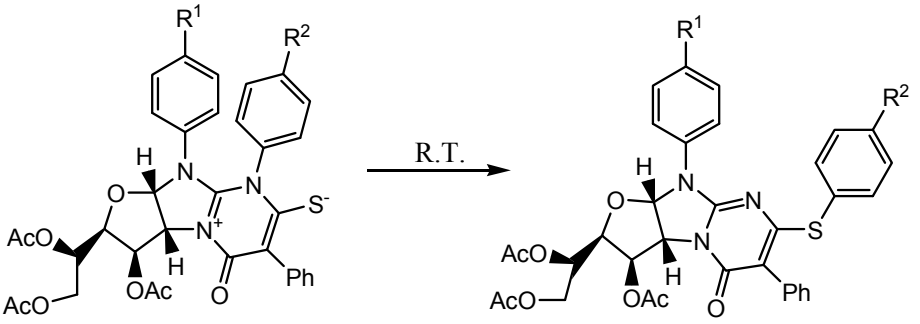

1.67 $R^1 = R^2 = NO_2$
1.68 $R^1 = NO_2$; $R^2 = OCH_3$
1.69 $R^1 = NO_2$; $R^2 = H$
1.70 $R^1 = H$; $R^2 = OCH_3$
1.71 $R^1 = OCH_3$; $R^2 = OCH_3$

1.72 $R^1 = R^2 = NO_2$ (78%)
1.73 $R^1 = NO_2$; $R^2 = OCH_3$ (No reaction)
1.74 $R^1 = NO_2$; $R^2 = H$ (No reaction)
1.75 $R^1 = H$; $R^2 = OCH_3$ (No reaction)
1.76 $R^1 = OCH_3$; $R^2 = OCH_3$ (No reaction)

(iii) Solid-state nucleophilic aromatic substitution[72]

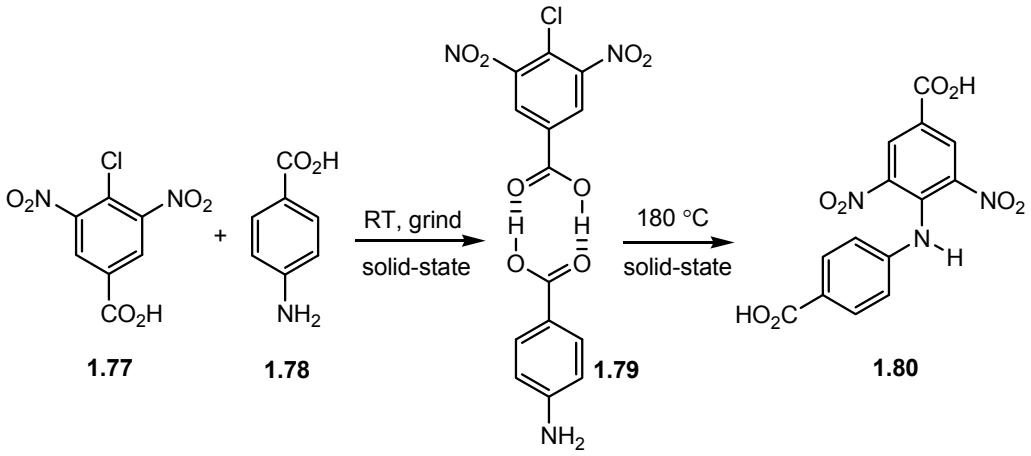

1.77 **1.78** **1.79** **1.80**

Scheme 1.7 Aryl migration in the solid-state.

Spontaneous intramolecular aryl migration was reported in a mesomeric betaine (**1.67**) in the solid state (Scheme 1.7, ii), proceeding *via* an S_NAr mechanism in which the thiolate group displaces the pyrimidinium ion of the nearest 4-nitrophenyl ring. Theoretical studies indicated a concerted pathway for the reaction which results in changes in optical and spectroscopic properties.[71]

A 1:1 co-crystal (**1.79**) of 4-chloro-3,5-dinitrobenzoic acid (Scheme 1.7, iii, **1.77**) and 4-aminobenzoic acid (**1.78**), prepared by grinding the two components together, underwent nucleophilic aromatic substitution yielding the amine **1.80**. The reaction occurs at high temperatures where large molecular motions, diffusion and reorientation are possible.[72]

1.3.2 Photochemically induced alkyl / aryl migration in the solid-state

Photochemically induced phenyl migrations in the solid-state are relatively more common compared to similar thermal processes. Although xylenes undergo photo induced isomerisation in solution as well as in their inclusion complex with deoxycholic acid, the number of by-products in the solid state isomerisation is much less than that in solution.[73]

cis-1,2-Dibenzoylalkene **1.81** exhibits a C → O photo phenyl migration (Scheme 1.8, i) characterized by the formation of a ketene intermediate **1.82** when irradiated in the solid-state. Irradiation in solution yielded a mixture of products. Intermolecular hydrogen bonding and steric interactions play a role in controlling the reactivity by preventing bond rotation and constraining the molecular conformation in the solid-state.[74]

An interesting photo phenyl migration accompanied by cyclization in chiral crystals of achiral *S*-(*o*-tolyl) *o*-benzoylbenzothioate (Scheme 1.8, ii, **1.84**) resulted in an optically active phthalide **1.86**. That the reaction proceeds *via* phenyl migration (**1.85**) and not *via* the radical pair intermediate was confirmed on the basis of the absolute configuration of the reactant and product.[75] The generality of this reaction was established by the solid-state photoreactivity of various thioester analogues **1.87**-**1.92**. The observed enantioselectivities (for **1.84**, **1.87** and **1.88**) were dependent on the conversion and reaction temperature.[76]

(i) Phenyl migration in *cis*-1,2-dibenzoylalkenes[74]

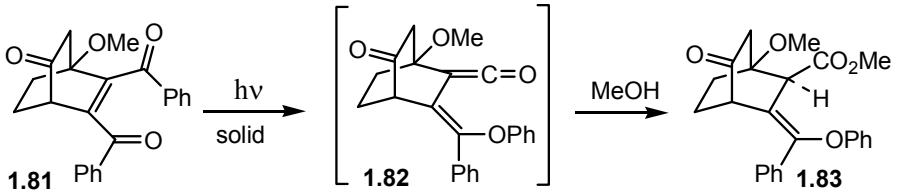

(ii) Phenyl migration in achiral *S*-(*o*-tolyl) *o*-benzoylbenzothioate[75]

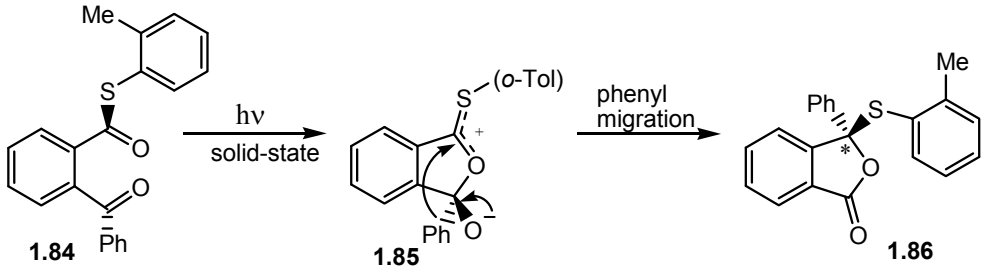

(iii) Aryl migration in aryl thioesters[76]

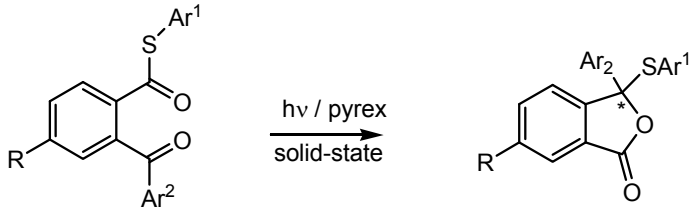

1.87	R = H, Ar^1 = Ph, Ar^2 = Ph	$P2_12_12_1$	**1.93** R = H, Ar^1 = Ph, Ar^2 = Ph
1.88	R = H, Ar^1 = (*m*-tol), Ar^2 = Ph	$P2_12_12_1$	**1.94** R = H, Ar^1 = (*m*-tol), Ar^2 = Ph
1.89	R = H, Ar^1 = (*p*-tol), Ar^2 = Ph	$P2_1/c$	**1.95** R = H, Ar^1 = (*p*-tol), Ar^2 = Ph
1.90	R = Me, Ar^1 = Ph, Ar^2 = Ph	*P*-1	**1.96** R = Me, Ar^1 = Ph, Ar^2 = Ph
1.91	R = H, Ar^1 = Ph, Ar^2 = (*p*-tol)	*P*-1	**1.97** R = H, Ar^1 = Ph, Ar^2 = (*p*-tol)
1.92	R = H, Ar^1 = Ph, Ar^2 = (*p*-ClPh)	*P*-1	**1.98** R = H, Ar^1 = Ph, Ar^2 = (*p*-ClPh)

(iv) Cyclization of *N, N*-disubstituted 2-benzoylbenzamides[77]

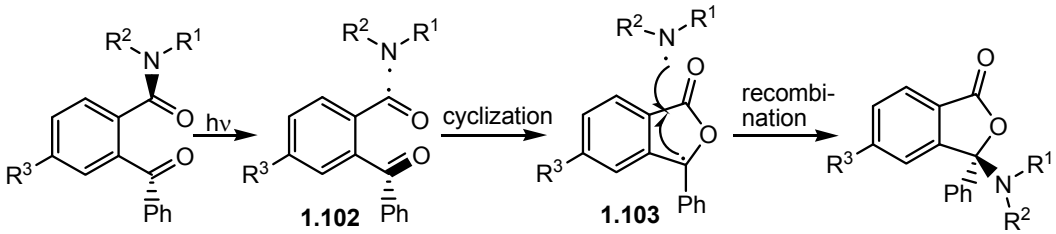

1.99	R^1 = R^2 = Me, R^3 = H	**1.104**	R^1 = R^2 = Me, R^3 = H, 0%
1.100	R^1 = Me, R^2 = Ph, R^3 = H	**1.105**	R^1 = Me, R^2 = Ph, R^3 = H 99%
1.101	R^1 = Me, R^2 = Ph, R^3 = Me	**1.106**	R^1 = Me, R^2 = Ph, R^3 = Me 99%

Scheme 1.8 Photo induced aryl migration.

The crystal structures and solid-state photoreactions of the structurally related amide derivatives were studied to explore the generality and utilization of the aryl migration pathway for asymmetric synthesis. The amides crystallised in chiral space groups and upon irradiation in solid-state afforded the corresponding phthalides (*via* a radical pair

intermediate) with good enantioselectivity. The unreactive nature of the aliphatic amide **1.99** in comparison with the aromatic amides was attributed to the unfavorable cleavage of C(=O)-N bond because of the differing stabilities of the amino radicals.[77]

Preferential photo induced aryl migration was also observed in a cyanoenone (Scheme 1.9, i, **1.107**) which crystallised in two different modifications (type A - $P2_1/c$ and type B - $C2/c$). Irradiation of type A crystals led to predominant migration of the *p*-cyanophenyl group (**1.108**) while irradiation of type B crystals led to the predominant migration of the phenyl group (**1.109**). In the B type crystals, up to 15% conversion resulted in only phenyl migration and beyond this 1:1 phenyl and cyanophenyl migration occurred. Similar results were obtained in the case of the type A crystals. Such behaviour was explained on the basis of crystal disorder.[78a] Photoreaction in benzene solution gave a mixture of two products (**1.108** and **1.109**) resulting from the migration of both phenyl groups, but *p*-cyanophenyl migration was preferred.[78b]

Solution state photolysis of 2-methyl-4,4-diphenylcyclohex-2-enone (Scheme 1.9, ii, **1.110**) yielded the bicyclic ketone **1.111** while solid-state photolysis yielded two products (**1.111** and **1.112**) in a 1:1 ratio up to 10% conversion, beyond which **1.111** was obtained exclusively. The 5-membered ketone **1.112** underwent secondary conversion to the 6-membered ketone **1.111**.

In the case of 4,5,5-triphenylcyclohex-2-enone (**1.113**) solution state and solid-state photolysis yielded different products (Scheme 1.9, iii). In the solid-state up to 12% conversion bicyclic ketone **1.116** (with phenyl migration) was the sole product and beyond 12% another bicyclic ketone **1.117** was obtained as the major product. The switch between the two stages in the solid-state reactions at 10-12% was explained on the basis of reacting clusters of molecules. A cluster consists of a central reactive molecule surrounded by other molecules which affect each other's reactivity. The stage at 10% conversion corresponds to the point at which a few molecules in the cluster have reacted and the rest react at a slower pace.[78c]

(i) Photolysis of cyanoenone[78a,78b]

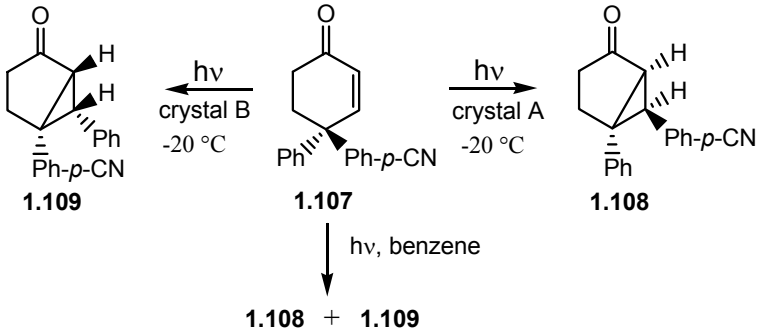

1.109 **1.107** **1.108**

1.108 + **1.109**

(ii) Photolysis of 2-methyl-4,4-diphenylcyclohex-2-enone[78c]

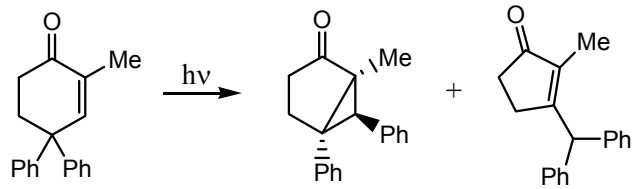

1.110 **1.111** **1.112**

Solution	1.0	0
Solid-state stage 1 (upto 10%)	1.0	1.0
Solid-state stage 2 (above 10%)	1.0	0

(iii) Photolysis of 4,5,5-triphenylcyclohex-2-enone[78c]

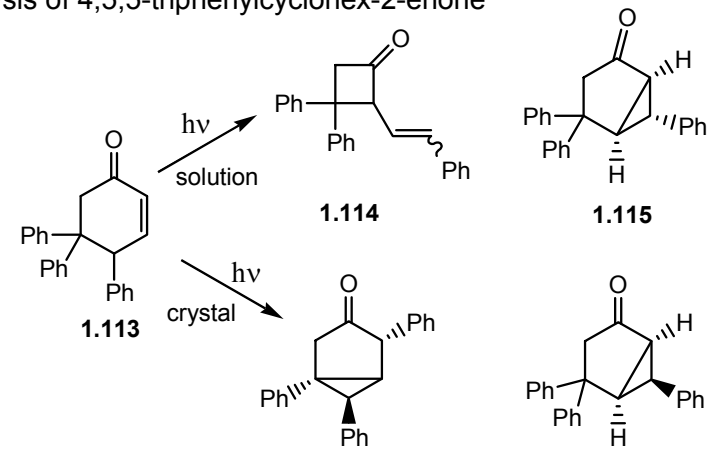

1.113 **1.114** **1.115**

1.116 **1.117**

Solid-state stage 1 (upto 12%)	1.0	0
Solid-state stage 2 (above 12%)	1.0	6.0

Scheme 1.9 Solution and solid-state photolyses of enones.

1.3.3 Migration of bulky groups in the solid-state

Thermally induced vinylogous pinacol rearrangement involving intramolecular 1,4-migration of a bulky thienothienyl substituent (Scheme 1.10, i) was observed in *trans*-9,10-dihydroxy-9,10-bis(thieno[3,2-*b*]thienyl)-9,10-dihydroanthracene (**1.118T**), resulting in quantitative formation of 10,10-bis(thieno[3,2-*b*]thienyl) anthrone (**1.119**).[79] The reactant underwent colour change without melting, along with elimination of water. The *trans* diol **1.118T** isomerized to the *cis* isomer (**1.118C**) and then rearranged to the product (**1.119**). A mixed crystal's (**1.118T•1.120T**) thermally induced reaction yielded two anthrones (**1.119** and **1.121**) that were attributable to intra-molecular migration but afforded no anthrone derivative having the two substituents possible for the intermolecular combination. These results, along with the X-ray crystal structure of the mixed crystal, demonstrate that the rearrangement in the solid-state proceeds intramolecularly.

A novel thermally induced rearrangement (Scheme 1.10, ii) of propargylallenes (**1.122-1.125**) to furofuran derivatives (**1.126-1.129**) in the solid-state was reported by Tanaka and co-workers.[80] The solid-to-solid reaction occurs without any detectable melting prior to rearrangement, with exothermic peaks appearing in the DSC curves well before melting. The reaction proceeds intra-molecularly in the crystals through the formation of a symmetrical diallene intermediate **1.130**.

Topochemical transketalization (Scheme 1.10, iii) involving thermal migration of a ketal in the solid-state was detected in the crystals of racemic 1,2:3,4-di-*O*-isopropylidene-*myo*-inositol (**1.131**).[81] Heating the crystals at 110 °C for 10 min effects a 92-95% isomerization with transketalization, occurring without any acidic catalyst. Interestingly, equilibrating DMF or benzene solution of the substrate with *p*-TsOH resulted in the formation of a mixture of four ketals (**1.131**, **1.132**, racemic 1,2:4,5-di-*O*-isopropylidene-*myo*-inositol, racemic 1,2-*O*-isopropylidene-*myo*-inositol). Crystal structure analysis of **1.131** revealed that strong intermolecular hydrogen bonding helps in orienting the reacting groups in close proximity and at a suitable angle for the reaction. Each molecule acts as a ketal donor and acceptor at the same time, accounting for the quantitative isomerization without monoketal or triketal intermediates.

(i) Thermally induced vinylogous pinacol rearrangement[79]

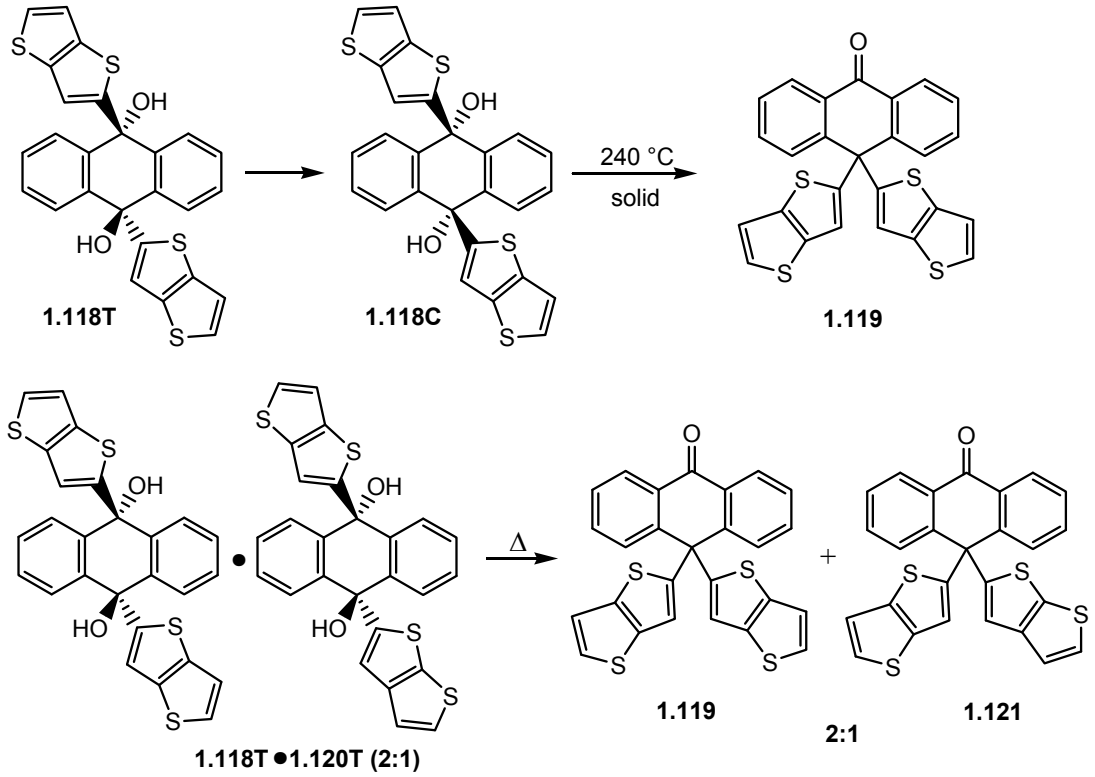

(ii) Rearrangement of a propargylallene to a furofuran[80]

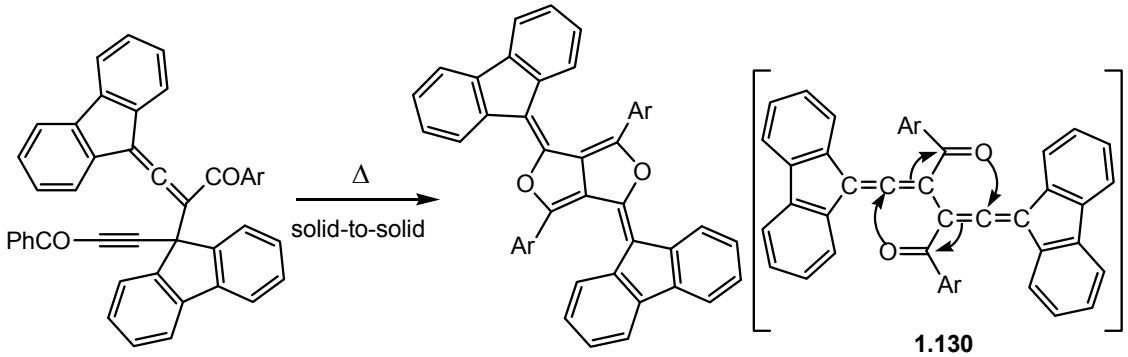

1.122 Ar = Ph
1.123 Ar = 4-MeC_6H_4
1.124 Ar = 4-ClC_6H_4
1.125 Ar = 4-$MeOC_6H_4$

1.126 Ar = Ph
1.127 Ar = 4-MeC_6H_4
1.128 Ar = 4-ClC_6H_4
1.129 Ar = 4-$MeOC_6H_4$

(iii) Topochemical thermal transketalization[81]

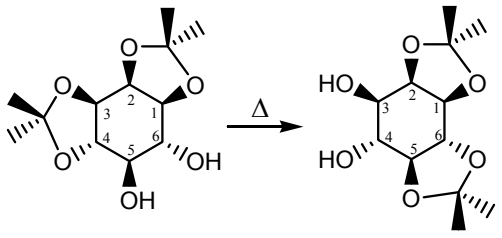

Scheme 1.10 Migration of bulky groups in solid-state.

1.4 Solid state reactions at the carbonyl center

Nucleophilic addition to carbonyl groups and transesterifications are frequently encountered reactions in solution state organic chemistry. Often, the tetrahedral intermediate generated in such an addition reaction undergoes elimination to regenerate the carbonyl group in a new product, as in reactions of carboxylic acids and their derivatives. Although addition-elimination reactions in solution phase are ubiquitous, documentation of their occurrence in the condensed phases (solvent less) is scarce.

1.4.1 Acyl migration and solid state nucleophilic reactions

Competing migration of benzoyl groups from C → O and C → N (Scheme 1.11, i) in *p*-bromobenzeneazotribenzoylmethane (**1.134**) to form α-*p*-bromobenzeneazo-β-benzoyloxybenzalacetophenone (**1.138**) and sym-benzoyl-*p*-bromophenylhydrazone (**1.136**) was studied in the solid-state and in dioxane solution by Curtin and co-workers.[11a,82] The conversion appears to involve C → O benzoyl migration, and since the reaction is faster in solution by a factor of 100-400, and the rate of the reaction in the solid state varies from one crystal to another, it was suggested that the reaction proceeds due to defects in the crystal; observation of the reaction under a microscope supported this view.

Russell and Weisleder detected a solid-state conversion (Scheme 1.11, ii) of α-phenylazo-β-benzoyloxystilbene (**1.139**) to benzil benzoylphenylhydrazone (**1.141**) involving a benzoyl migration, possibly *via* an intramolecular mechanism. The reaction also occurs in solution and is fastest in the molten state.[11b,83]

Solid phase isomerization of 1,2-diglycerides to 1,3-diglycerides from mixtures of both isomers was observed by Lutton.[84] Later Groot also reported that this solid-phase isomerization was observable in saturated and unsaturated aliphatic mixed-acid diglycerides as well as oxo acids and substituted and unsubstituted aromatic acyl groups.[85] Lok and Ward studied the macroscopic changes in the isomerization of racemic 1,2-dipalmitoylglycerol to 1,3-dipalmitoylglycerol at temperatures close to the melting points of the crystals. The intramolecular shift of an acyl group from a secondary to a primary hydroxyl was found to be a favoured process both for pure compounds and for mixtures of mono- and diacylglycerols, leading to nearly complete isomerisation.[86]

(i) Benzoyl migration in *p*-bromobenzeneazotribenzoylmethane[11a,82]

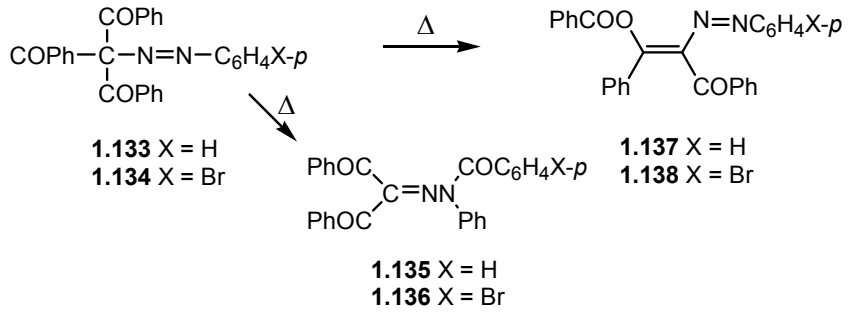

1.133 X = H
1.134 X = Br

1.137 X = H
1.138 X = Br

1.135 X = H
1.136 X = Br

(ii) Benzoyl migration in α-phenylazo-β-benzoyloxystilbene[11b,83]

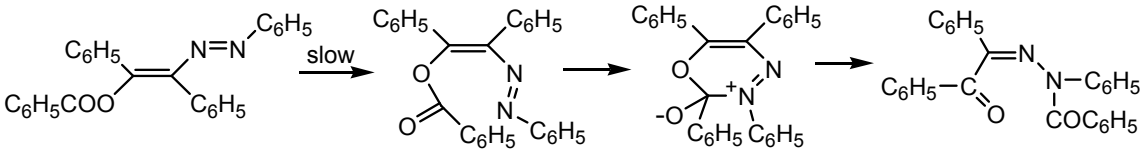

1.139 **1.140** **1.141**

(iii) Solid-state acyl migration in *O*-acylsalicylamides[87,88]

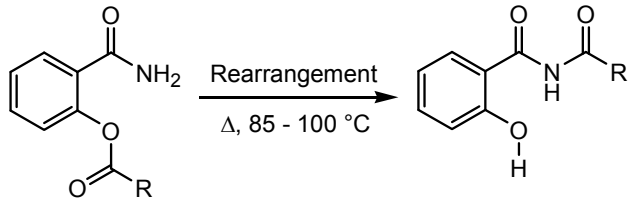

1.142 R = CH_3	100 °C	**1.145** R = CH_3
1.143 R = C_6H_5	100 °C	**1.146** R = C_6H_5
1.144 R = C_2H_5	85 °C	**1.147** R = C_2H_5

(iv) Solid-state synthesis of urea[89,90]

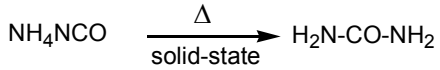

1.148 **1.149**

(v) Solid-state transacylation in drugs[91]

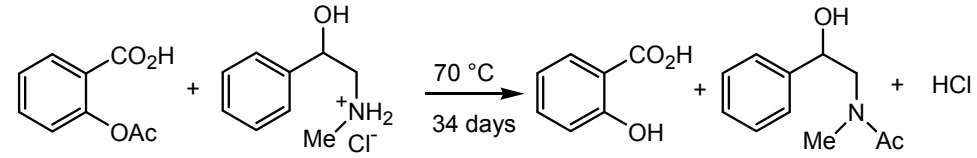

1.150 aspirin

1.151 phenylephrine hydrochloride

1.152 salicylic acid

1.153 *N*-acetyl-phenylephrine

(vi) Thermal dehydration of *o*-acetamidobenzamide[95]

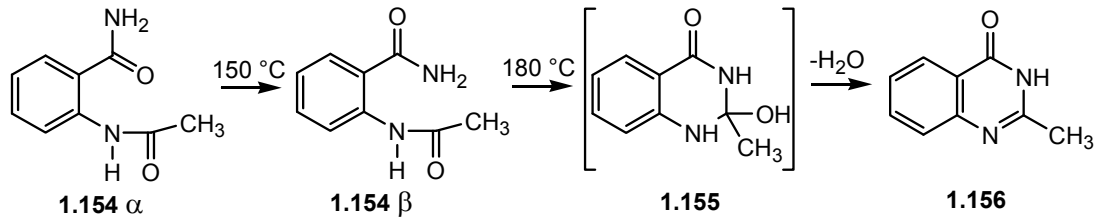

1.154 α **1.154** β **1.155** **1.156**

Scheme 1.11 Acyl migration in the solid state.

O → N acetyl migration was reported in *O*-acetylsalicylamide (Scheme 1.11, iii, **1.142**), yielding the stable *N*-acetylsalicylamide (**1.145)** on standing at room temperature, in solvents or dilute aqueous base, in the solid state below the melting point and above 100 °C in acetone (in a sealed tube).[87] The benzoyl (**1.143**) and propionyl (**1.144**) derivatives also exhibit acyl transfer in the solid-state. The crystal structures of the reactants were studied by Manohar and co-workers and an intramolecular mechanism was proposed based on the proximity and geometry of the reactive groups.[88]

The earliest known organic reaction, the Wöhler synthesis of urea, was re-examined by solid-state chemists after a lapse of about 100 years. The transformation of ammonium cyanate (**1.148**) into urea (**1.149**) occurs in both solution and solid-state (Scheme 1.11, iv) and its mechanism has been extensively studied.[89] The crystal structure of ammonium cyanate was solved recently by neutron powder diffraction data, which suggested that the N atom of ammonium ion forms N-H···N bonds with cyanate N atoms at the four corners of a distorted cube.[90] The solid state transformation to urea is presumably triggered by transfer of H^+ from NH_4^+ to NCO^- *via* a proton jump along one of the N-H···N hydrogen bonds to form H-NCO and NH_3 in close vicinity to one another in the crystal, followed by nucleophilic attack of NH_3 on the carbon atom.

Transacylation was also observed in tablet mixtures of aspirin and drugs with easily acylated functionalities (Scheme 1.11, v). Acetyl group migration was observed in a reaction between acetylsalicylic acid (**1.150**) and phenylephrine hydrochloride (**1.151**), yielding salicylic acid (**1.152**) and *N*-acetyl-phenylephrine (**1.153**).[91] Similar acyl migrations were observed in tablets containing aspirin and codeine or acetaminophen.[92]

The reactions of amides and acylanilines with various acids and anhydrides in the presence and absence of catalysts was studied in molten reaction mixtures. The reaction with monocarboxylic acids was reversible and with dicarboxylic acids yielded the corresponding cyclic imide. Transacylation with anhydrides occurred only in the presence of acid catalysts.[93] Molten state transacylation reactions of carbamates and diacylanilines with carboxylic acids and anhydrides were also investigated.[94]

o-Acetamidobenzamide (**1.154**) crystallizes in at least two different forms (α, β) which underwent thermal solid-state transformations resulting in the formation of

anhydrous 2-methylquinazol-4-one (Scheme 1.11, vi). The α polymorph can be thermally converted to the β form at 150 °C. Detailed investigation of this process revealed that the β form undergoes nucleophilic addition of the amide nitrogen to the acetyl carbonyl group to form a tetrahedral intermediate **1.155**, which underwent dehydration to give methylquinazol-4-one **1.156**.[95]

A solid-state reaction involving presumably nucleophilic attack on a thiocarbonyl group (Scheme 1.12, i) was observed when thiocarbonyldiimidazole (**1.158**) was ground together with alcohol (**1.157**) yielding the corresponding thiocarbonylimidazolides (**1.159**).[96]

(i) Solid-state synthesis of thiocarbonylimidazolides[96]

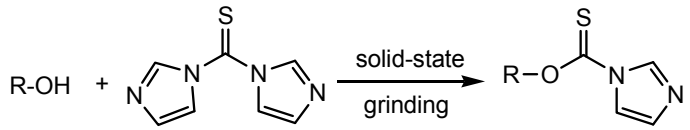

1.157 **1.158** **1.159**

(ii) Solvent free acylation of phenols and naphthols[98]

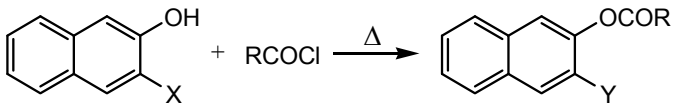

1.160 X = H; R = *p*-$CH_3C_6H_4$
1.161 X = OH; R = *p*-$CH_3C_6H_4$

1.162 Y = H; R = *p*-$CH_3C_6H_4$
1.163 Y = $OCOC_6H_4CH_3$-*p*; R = *p*-$CH_3C_6H_4$

(iii) Solid-state synthesis of imides[99]

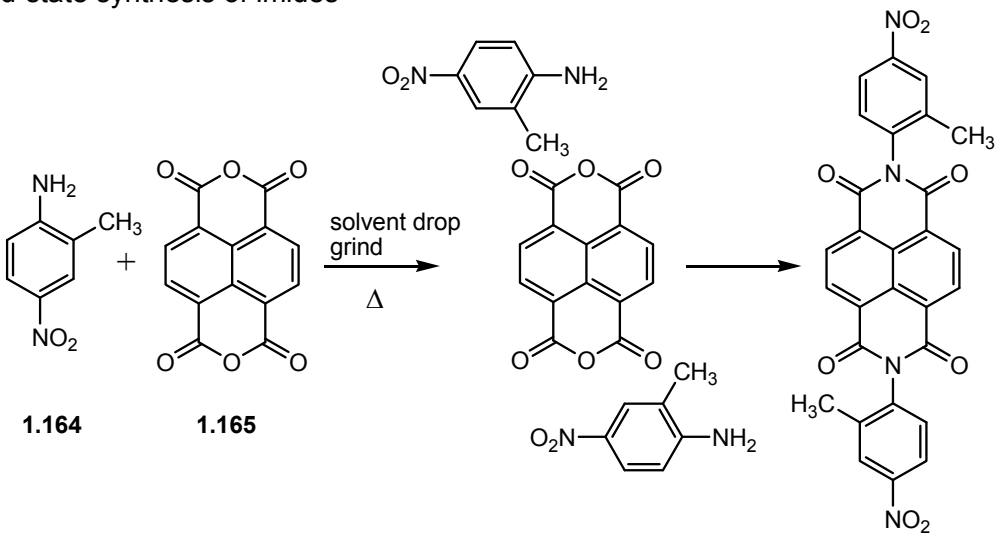

1.164 **1.165**

1.166 (2:1 co-crystal) **1.167**

Scheme 1.12 Solid-state syntheses of organic compounds.

A series of solid-state reactions was reported wherein gaseous or solid amines reacted with aldehydes giving imines, with solid anhydrides giving amides or amidic carboxylic salts or imides, with solid imides giving diamides, with solid lactones or carbonates giving carbamic esters, and with solid isothiocyanates giving thioureas.[97] Most of the reactions were quantitative and proceeded without the formation of a liquid phase.

Toda and co-workers reported[98] the efficient solvent-free benzoylation of phenols and naphthols by heating them with benzoyl chloride (Scheme 1.12, ii). Continuous monitoring of the reactions by IR spectroscopy revealed the involvement of an inclusion complex of naphthol with its benzoate.

The condensation reaction between acid anhydrides and primary amines to yield the imide *via* intermediate co-crystal formation was investigated by Zaworotko and co-workers[99] (Scheme 1.12, iii). 1,4,5,8-naphthalenetetracarboxylic dianhydride (NTCDA, **1.165**) and 2-methyl-4-nitroaniline (MNA, **1.164**) formed a 1:2 cocrystal **1.166**, which converted cleanly to diimide **1.167**, when heated at 180 °C for 3 h. NTCDA and 3-aminobenzoic acid (ABA) also formed a purple co-crystal *via* solvent-drop grinding with DMF. However, the co-crystal underwent condensation to the corresponding diimide under ambient conditions.

An unstable imine was produced in a single-crystal-to-single-crystal fashion by the condensation of the amino group of 1-aminotriphenylene with acetaldehyde in the pores of a porous co-ordination network. The aromatic amines were incorporated in the columnar array of aromatic ligands of a synthesized porous network complex. The amino group oriented toward the pore was allowed to react with acetaldehyde that was introduced into the pore of a crystal by diffusion.[100]

1.4.2 Acyl migration in inositols

Inositols are cyclohexanehexols (Scheme 1.13, i) of which five isomers (*myo*-, *neo*-, *chiro*- and *scyllo*-) occur in nature while the rest (*cis*-, *epi*-, *allo*- and *muco*-) are unnatural synthetic isomers. *myo*-Inositol (**1.172**) being the most abundant, occurs widely in nature in both free and combined forms. Of the six hydroxyl groups in *myo*-inositol, one (C2-hydroxyl group) is axial and the rest are equatorial with a plane of symmetry passing through the C2 and C5 carbon atoms, hence *myo*-inositol has the *meso* configuration (Scheme 1.13, ii). According to convention anticlockwise

numbering in an asymmetrically substituted *myo*-inositol derivative gives the D-prefix and clockwise numbering an L-prefix.[101] The International Union of Biochemistry (IUB) nomenclature allows all biologically relevant *myo*-inositol derivatives to be denoted as the D-isomer. All the *myo*-inositol derivatives reported in this thesis are racemic and for the sake of clarity, they are consistently numbered in anticlockwise fashion.

(i) Isomers of inositol

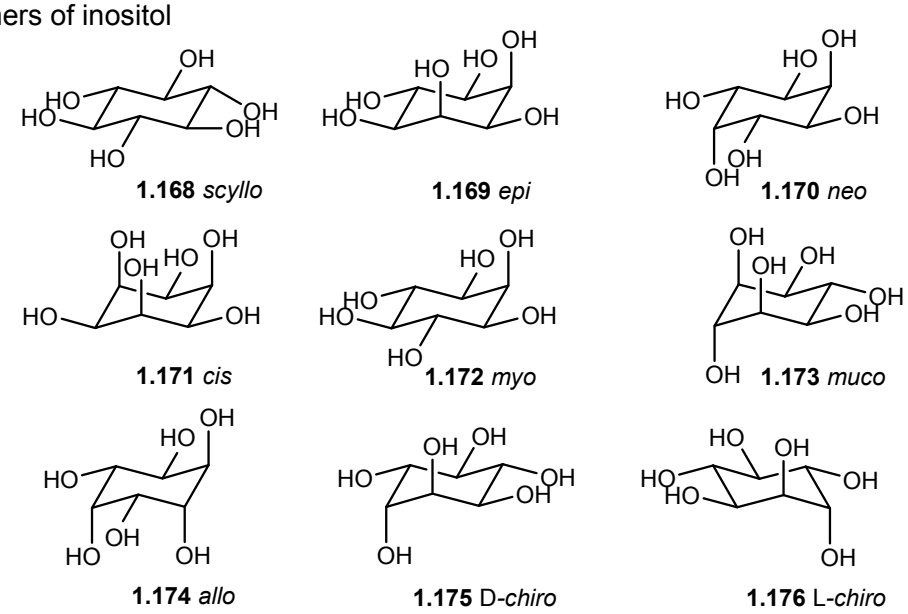

(ii) Atom numbering in *myo*-inositol

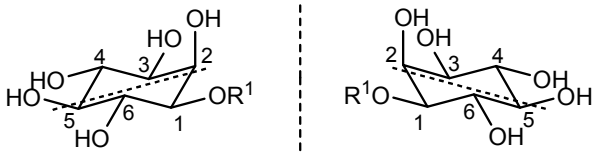

Scheme 1.13 Isomers of inositol and atom numbering in *myo*-inositol.

myo-Inositol and its phosphorylated derivatives play major roles in many cellular functions like cellular signal transduction,[102] calcium mobilization, insulin stimulation, exocytosis, cytoskeletal regulation, intracellular trafficking of vesicles and anchoring of proteins to cell membranes.[103] Revelations in biology and medicine associating the involvement of phosphoinsoitols in several biological processes in eukaryotic cells, necessitated simpler methods for the synthesis of various inositol derivatives. Synthesis of biologically relevant inositol derivatives and conversion of *myo*-inositol to other isomers involves a series of protection-deprotection reactions of

its six hydroxyl groups.[104] Adamantane-like orthoesters of *myo*-inositol, obtained by the simultaneous protection of three hydroxyl groups (C1, C3 and C5), are important intermediates for the synthesis of biologically important phosphoinositols and their derivatives, glycosyl inositols and cyclitol based metal complexing agents.

Protection of inositol hydroxyl groups as the corresponding carboxylic acid esters is frequently encountered in the literature.[105] Acyl transfer reactions, ubiquitous in natural systems,[106] have been extensively studied in the solution state.[107] Acyl transfer reactions in cyclitol derivatives have been known for decades[108] but more often than not result in the formation of a mixture of isomeric esters which are separated by HPLC. Clean migration of acyl groups in 4-O-acyl-*myo*-inositol orthoformates has been reported although the mechanism of this unusual isomerization remains unclear.[109] Hence controlled migration of the acyl groups in inositol could provide preparative routes for certain partially protected inositol derivatives useful for the synthesis of phosphoinositols.

An efficient intermolecular benzoyl group transfer reaction in the crystalline state (Scheme 1.14),[110] was observed while preparing *myo*-inositol orthoformate derivatives.[111] During its routine preparations, the racemic dibenzoate (**rac-1.177**) was always contaminated with the tribenzoate **1.180** as well as the diol **1.183** and required several crystallizations or column chromatographic separation to get rid of the contaminating benzoates. The amount of contamination increased on storage (either in solution or as a precipitate in the mother liquor or as a crude solid) in the presence of bases. Systematic experiments showed that **rac-1.177** underwent transesterification, at temperatures below its melting point with extreme ease in its crystals, in the presence of solid sodium carbonate.

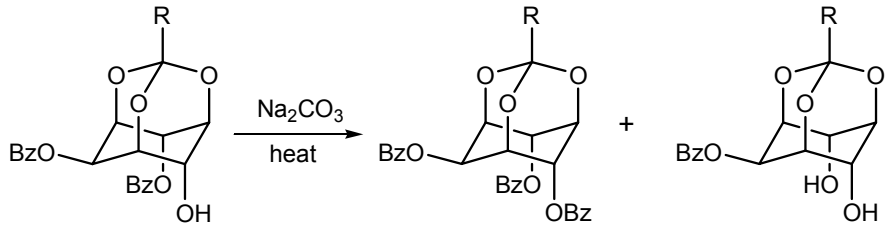

R		R		R	
1.177	H ($P2_1/c$ crystals)	**1.180**	H (47%)	**1.183**	H (49%)
1.178A	Me (Form I; $P2_1/n$ crystals)	**1.181**	Me (19%)	**1.184**	Me (21%)
1.178B	Me (Form II; $C2/c$ crystals)		Me (42%)		Me (42%)
1.179	Ph ($P2_1/c$ crystals)	**1.182**	Ph (49%)	**1.185**	Ph (48%)
1.177•1.178	(*Cc* co-crystals)	**1.180** + **1.181**	(41%)	**1.183** + **1.184**	(35%)

Scheme 1.14 Benzoyl transfer in di-*O*-benzoylated *myo*-inositol orthoesters.

Thermal data (DSC) and X-ray powder diffraction data showed that the crystals of **rac-1.177** were stable and did not undergo any phase change on heating or on mixing and grinding with sodium carbonate. Hence the crystal structure of **rac-1.177** could be correlated with its acyl transfer reactivity.

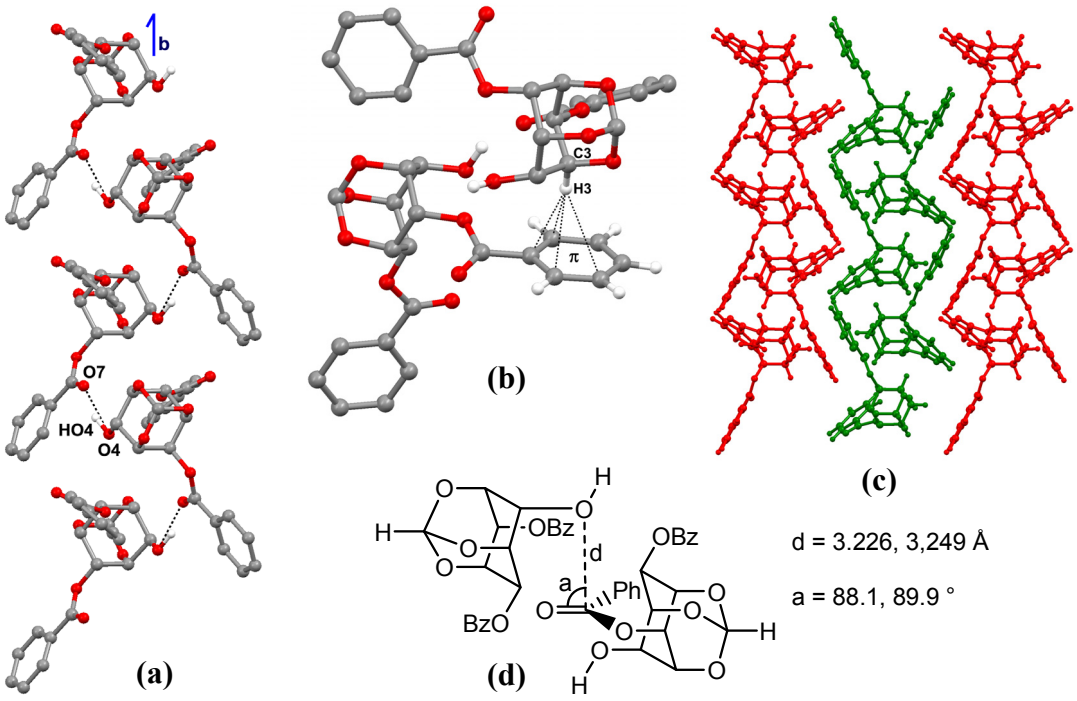

Figure 1.1 In crystals of **1.177** (a) Helix formed by O-H...O hydrogen bonding, (b) C-H···π interactions holding the migrating group in proper orientation for reaction, (c) helices which act as reaction tunnels (red and green indicate the two enantiomers) and (d) distance and angle between electrophile (C=O) and nucleophile (-OH).

Hydrogen bonding interactions between the hydroxyl group of one molecule and the carbonyl oxygen of another result in a helical molecular assembly along the 2_1-screw axis, supported by other weak interactions. Such an organization of molecules brings the electrophile (El, C=O) and nucleophile (Nu, -OH) in a favourable geometry [distance (H-O···C=O) and angle (H-O···C=O) being ~ 3.2 Å and 88-90º] for the reaction. Each helix is built up of a single enantiomer and adjacent helices contain molecules of the other enantiomer. Acyl migration is thought to occur between neighbouring molecules in a helix with the migrating group held in the proper orientation for reactivity by C-H···π interactions (Fig. 1.1). Such discretely packed

helices act as reaction tunnels in the crystal.[112] Although the crystal structure of **rac-1.177** indicated that its disproportionation in crystals is facile due to the relative orientation of the reacting molecules which brings the El and Nu in close proximity for the reaction, the reason for the more or less quantitative conversion of **rac-1.177** to the products was not clear. Hence analogous diester derivatives of *myo*-inositol orthoesters were prepared and their transesterification reactivity in crystals was investigated for better understanding of the quantitative conversion of the dibenzoates to the products along with crystal structure - reactivity correlation.[112] Also, to study the scope and utility of these acyl transfer reactions in crystals, we perturbed the structure of **rac-1.177** to generate its analogs and looked at their crystalline-state reactivity.

The modifications in the molecular structures done included substitution of the orthoester H with methyl and phenyl groups (retaining the benzoates at C2 and C6 or the equivalent C4-positions of the inositol ring). These changes gave rise to dibenzoates which exhibited varying degrees of transesterification activity depending on the crystal structure. Racemic dibenzoate **1.178** initially yielded monoclinic ($P2_1/n$) crystals (**1.178**A) which showed poor transesterification activity namely, lower yield (of the triester **1.181** and diol **1.184**) and formation of other products with longer reaction times. This was attributed to the absence of discrete packing of helices in the crystal and less than ideal geometry of C-H$\cdots\pi$ contacts holding the migrating group in the proper orientation for reaction.

In an attempt to improve the molecular organization in **rac-1.178**, it was co-crystallized with **rac-1.177**. Co-crystallization experiments involving crystallization of the mixture of varying ratios of **rac-1.177** and **rac-1.178** gave rise to a 1:1 monoclinic (*Cc*) co-crystal **1.177•1.178** which exhibited facile benzoyl transfer reaction. Molecules of **1.177** and **1.178** alternately associated through O-H$\cdots$O hydrogen bonding, and formed helices along a non-crystallographic *pseudo* two-fold axis. These hybrid crystals underwent facile transesterification, generating the corresponding tribenzoates (**1.180**+**1.181**) and diols (**1.183**+**1.184**) in good yield, which was explained based on the favourable packing of molecules and their El...Nu geometry.[112]

Racemic di-benzoate **1.179** underwent facile transesterification reaction in its crystals to yield the corresponding tri-benzoate **1.182** and the diol **1.185**, more or less

quantitatively. Its crystal structure was isomorphous with that of **rac-1.177**, with comparable El…Nu interaction.[113]

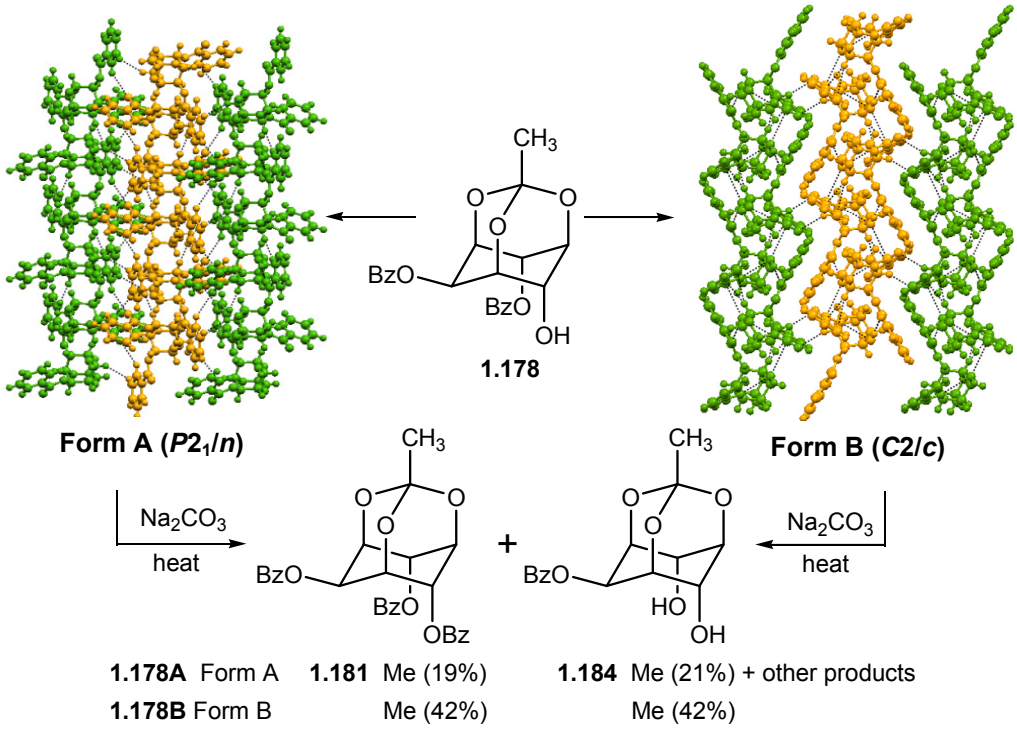

Figure 1.2 Solid-state reactivity of polymorphic crystals of **1.178**

In continuation of attempts to generate reactive packings by co-crystallization, **rac-1.178** (which exhibited poor transesterification activity) was crystallized in the presence of an enantiomer of **1.177** (***ent*-1.177**, D-2,6-di-*O*-benzoyl-*myo*-inositol-1,3,5-orthoformate). Since the helices in the reactive crystals are each composed of a single enantiomer (*R* or *S*) and benzoyl group transfer occurs between molecules of the same configuration (*R* to *R* or *S* to *S*) two outcomes were envisaged: resolution of **1.178** by formation of co-crystals consisting of one of the enantiomers in **1.178** and ***ent*-1.177** or formation of a new polymorph of **1.178**. It has been observed that additives that mimic the conformation of molecules in stable crystal structures lead to the formation of polymorphs[114] and in this case a new metastable polymorph (**1.178**B) of **1.178** was obtained. The crystals were monoclinic (*C*2/*c*) and isostructural with the co-crystal **1.177•1.178**, with favourable helical pre-organization of molecules (Fig. 1.2) and the required El...Nu geometry. As expected, they exhibited facile benzoyl transfer reactivity yielding the triester **1.181** and diol **1.184**.[115]

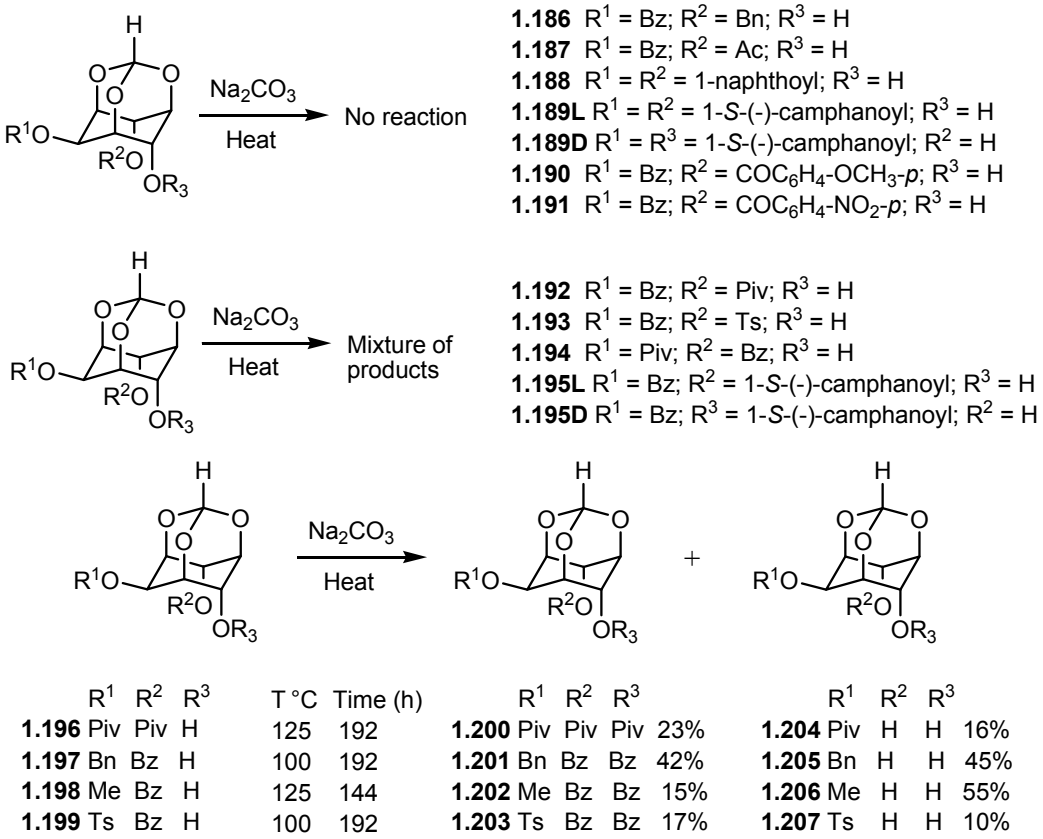

	R1	R2	R3	T °C	Time (h)
1.196	Piv	Piv	H	125	192
1.197	Bn	Bz	H	100	192
1.198	Me	Bz	H	125	144
1.199	Ts	Bz	H	100	192

	R1	R2	R3	
1.200	Piv	Piv	Piv	23%
1.201	Bn	Bz	Bz	42%
1.202	Me	Bz	Bz	15%
1.203	Ts	Bz	Bz	17%

	R1	R2	R3	
1.204	Piv	H	H	16%
1.205	Bn	H	H	45%
1.206	Me	H	H	55%
1.207	Ts	H	H	10%

Scheme 1.15 Solid-state reactivities of some di-*O*-acylated *myo*-inositol orthoformates: unreactive diesters, diesters giving a mixture of products and moderately reactive diesters.

Based on these results the ester groups at C2 and C6 (or the equivalent C4-position of the inositol ring) were modified and the solid-state reactivities of these diesters (Scheme 1.15) were examined.[116] When the axial benzoyl group was replaced by benzyl (**1.186**), acetyl (**1.187**), *p*-methoxy benzoyl (**1.190**) and *p*-nitrobenzoyl groups (**1.191**), the resulting compounds did not react in the solid-state. While racemic **1.186** did not yield suitable diffraction quality crystals for analysis, racemic **1.187** was unreactive in the solid state because it did not possess the reactive geometry of **rac-1.177**. Unlike in the solution state, the molecules of the acetate **1.187** do not have room to reorient in order to improve the El…Nu geometry. However, the acetate underwent base-catalyzed transesterification in solution. The 2,6-di-*O*-(1-naphthoyl) (**1.188**) and 2,6-di-*O*-(1-*S*-(-)-camphanoyl) *myo*-inositol orthoformates (**1.189L** and **1.189D**) were also inert in the solid-state presumably because of the larger size of the

acyl groups. However, racemic di-pivalate **1.196** underwent acyl transfer in solid-state yielding the corresponding tri-pivalate **1.200** (23%) and the diol **1.204** (61%) along with pivalic acid. Substitution of the axial benzoate groups with pivalate, tosylate and 1-S-(-)-camphanoate yielded diesters which reacted in the solid-state giving a mixture of products. Racemic **1.192** and **1.193** did not yield suitable crystals for single crystal X-ray diffraction studies and hence their reactivity could not be rationalised.

When the equatorial benzoyl group was replaced by benzyl, methyl and tosyl groups, while retaining the axial benzoate, the resulting diesters exhibited moderate solid-state reactivity.[116] Racemic **1.197** exhibited a sluggish, benzoyl transfer yielding the diester **1.201** and diol **1.205** when subjected to solid and molten state transesterification. Though the yield of the products is good, the similarity in the solid and molten state reactivity along with the absence of the requisite El...Nu geometry indicates that the reaction could be non-topochemical.

Racemic **1.198** and **1.199** when heated with solid Na_2CO_3 yielded the di-esters, **1.202** and **1.203,** and diols, **1.206** and **1.207** respectively, accompanied by decomposition and charring of the substrate, their poor reactivity attributed to the deviation from the required El...Nu geometry in crystals. Crystals of **1.194** also exhibited benzoyl transfer reactivity with low yield and in some trials mixtures of several products. Analysis of its crystal structure revealed poor El...Nu and C-H$\cdots\pi$ geometry along with absence of close packing of helices which could probably account for the observed poor reactivity.[116]

This study of the crystal structures of the diesters consistently showed that reactive crystals contained (a) good (C=O [El] and OH [Nu]) interaction; (b) favorable C-H$\cdots$O and the C-H$\cdots$ π interactions; and (c) closely packed helices constituted by the reacting molecules. Hence, Chapter 2 deals with the synthesis, characterization and crystallization of some acylated *myo*-inositol orthoformates. Chapter 3 discusses how minor modifications in the chemical structure can result in significant changes in crystal structure and molecular pre-organization and impact solid-state reactivity Chapter 4 discusses creation of helical molecular assemblies through solvent inclusion and the control of reactivity in the solid-state. Chapter 5 examines nucleophilic addition to the carbonyl group in the light of the results obtained along with examples from literature; criteria for identification of reactive crystals are also discussed.

References:

1. (*a*) I. C. Paul and D. Y. Curtin, *Acc. Chem. Res.,* **1973**, *6*, 217-225; (*b*) J. M. Thomas, *Pure Appl. Chem.,* **1979**, *51*, 1065-1082; (*c*) D. Y. Curtin, I. C. Paul, E. N. Duesler, T. W. Lewis, B. J. Mann and W. Shiau, *Mol. Cryst. Liq. Cryst.*, **1979**, *50*, 25-42; (*d*) A. Gavezzoti and M. Simonetta, *Chem. Rev.,* **1982**, *82*, 1-13; (*e*) N. B. Singh, R. J. Singh and N. P. Singh, *Tetrahedron*, **1994**, *50*, 6441-6493; (*f*) F. Toda, *Acc. Chem Res.,* **1995**, *28*, 480-486; (*g*) Y. Ohashi, *Curr. Opin. Solid State Mater. Sci.*, **1996**, *1*, 522-532; (*h*) Y. Ito, *Synthesis*, **1998**, *1*, 1-32; (*i*) K. Tanaka and F. Toda, *Chem. Rev.*, **2000**, *100*, 1025-1074; (*j*) D. Braga and F. Grepioni, *Angew. Chem. Int. Ed.*, **2004**, *43*, 4002-4011; (*k*) D. Braga and F. Grepioni, *Chem. Commun.* **2005**, 3635-3645; (*l*) G. Kaupp, *Top. Curr. Chem.*, **2005**, *254*, 95-183.
2. (*a*) G. R. Desiraju, *Organic Solid State Chemistry*, Amsterdam, Elsevier, 1987; (*b*) M. Pierrot, *Structure and Properties of Molecular Crystals*, Elsevier, 1990; (*c*) Y. Ohashi, *Reactivity in Molecular Crystals*, Weinheim-VCH, 1993; (*d*) F. Toda, *Organic Solid-State Reactions*, Kluwer Academic Publishers, 2002; (*e*) D. Braga and F. Grepioni, *Making Crystals by Design: Methods, Techniques and Applications*, Wiley-VCH, Weinheim, 2007.
3. (*a*) J. O. Metzger, *Angew. Chem. Intl. Ed.*, **1998**, *37*, 2975-2978; (*b*) A. Loupy, *Top. Curr. Chem.*, **1999**, *206*, 153-207; (*c*) G. Kaupp, J. Schmeyers and M. R. Naimi-Jamal, *Chem. Eng. Sci.*, **2002**, *57*, 763-765; (*d*) G. Kaupp, *CrystEngComm*, **2006**, *8*, 794-804; (*e*) B. Rodriguez, A. Bruckmann, T. Rantanen and C. Bolm, *Adv. Synth. Catal.*, **2007**, *349*, 2213-2233.
4. G. Kaupp, *CrystEngComm*, **2003**, *5*, 117-133.
5. (*a*) B. V. Lotsch, J. Senker and W. Schnick, *Inorg. Chem.*, **2004**, *43*, 895-904; (*b*) B. V. Lotsch, W. Schnick, E. Naumann and J. Senker, *J. Phys. Chem. B*, **2007**, *111*, 11680-11691; (*c*) M. Khan, G. Bruklaus, V. Enkelman and H.-W. Spiess, *J. Am. Chem. Soc.*, **2008**, *130*, 1741-1748.
6. (*a*) M. D. Cohen and G. M. J. Schmidt, *J. Chem. Soc*., **1964**, 1996; (*b*) M. D. Cohen, G. M. J. Schmidt and F. I. Sonntag, *J. Chem. Soc.*, **1964**, 2000; (*c*) G. M. J. Schmidt, *J. Chem. Soc.* **1964**, 2014-2021.

7. (*a*) G. Rothenberg, A. P. Downie, C. L. Raston and J. L. Scott, *J. Am. Chem. Soc.*, **2001**, *123*, 8701-8708; (*b*) O. Dolotko, J. W. Wiench, K. W. Dennis, V. K. Pecharsky and V. P. Balema, *New. J. Chem.*, **2010**, *34*, 25-28.
8. (*a*) V. Ramamurthy and K. Venkatesan, *Chem. Rev*. **1987**, *87*, 433-481; (*b*) A. E. Keating and M. A. Garcia-Garibay, *Mol. Supramol. Photochem.*, **1998**, *2*, 195-248; (*c*) I. Turowska-Tyrk, *J. Phys. Org. Chem*., **2004**, *17*, 837-847; (*d*) M. Nagarathinam, A. M. P. Peedikakkal and J. J. Vittal, *Chem. Commun*., **2008**, 5277-5288.
9. (*a*) L. R. MacGillivray, G. S. Papaefstathiou, T. Friscic, D. Varshney and T. D. Hamilton, *Top. Curr. Chem.*, **2004**, *248*, 201-221; (*b*) X. Mei, S. Liu and C. Wolf, *Org. Lett.*, **2007**, *9*, 2729-2732; (*c*) J. Yang, M. B. Dewal, S. Profeta, Jr., M. D. Smith, Y. Li and L. S. Shimizu, *J. Am. Chem. Soc.*, **2008**, *130*, 612-621; (*d*) L. R. Macgillivray, *J. Org. Chem.*, **2008**, *73*, 3311-3317; (*e*) L. R. Macgillivray, G. S. Papaefstathiou, T. Friscic, T. D. Hamilton, D.-K. Bucar, Q, Chu. D. B. Varshney and I. G. Georgiev, *Acc. Chem. Res.*, **2008**, *41*, 280-291; (*f*) M. W. Ghosn and C. Wolf, *J. Org. Chem.*, **2010**, *75*, 6653-6659; (*g*) M. H. Mir, L. L. Koh, G. K. Tan and J. J. Vittal, *Angew. Chem. Int. Ed.* **2010**, *49*, 390-393.
10. (*a*) S. Okamura, *Pure Appl. Chem.*, **1972**, *30*, 181-198; (*b*) M. Nishii, *Annu. Rev. Mater. Sci.*, **1975**, *5*, 135-149; (*c*) A. Matsumoto and T. Odani, *Macromol. Rapid Commun.*, **2001**, *22*, 1195-1215; (*d*) A. Matsumoto, D. Furukawa, Y. Mori, T. Tanaka and K. Oka, *Cryst. Growth. Des.,* **2007**, *7*, 1978-1085; (*e*) J. W. Lauher, F. W. Fowler and N. Goroff, *Acc. Chem. Res.*, **2008**, *41*, 1215-1229.
11. (*a*) R. T. Puckett, C. E. Pfluger and D. Y. Curtin, *J. Am. Chem. Soc.*, **1966**, *88*, 4637-4642; (*b*) C. S. Russell and D. Weisleder, *J. Org. Chem.*, **1967**, *32*, 2626-2627; (*c*) D. B. Pendergrass, D. Y. Curtin and I. C. Paul, *J. Am. Chem. Soc.*, **1972**, *94*, 8722-8730; (*d*) I. C. Paul and D. Y. Curtin, *Acc. Chem. Res.*, **1973**, *6*, 217-225; (*e*) S. A. Puckett, M. K. Greensley, I. C. Paul and D. Y. Curtin, *J. Chem. Soc. Perkin Trans. 2*, **1977**, 847-859.
12. H. Hagiwara, H. Nagatomo, S. Kazayama, H. Sakai. T. Hoshi, T. Suzuki and M. Ando, *J. Chem. Soc. Perkin Trans. 1*, **1999**, 457-459.
13. H. Du, K. Ding and J. Meng, *Chin. J. Chem.,* **2001**, *19*, 716-718.

14. (*a*) G. I. Nikishin, L. L. Sokova, V. D. Makhaev, L. A. Petrova, A. V. Ignatenko and N. I. Kapustina, *Russ. Chem. Bull.,* **1998**, *47*, 1353-1355; (*b*) J. A. R. P. Sarma and A. Nagaraju, *J. Chem. Soc. Perkin Trans. 2*, **2000**, 1113-1118; (*c*) I. Pravst, M. Zupan and S. Stavber, *Tetrahedron*, **2008**, *64*, 5191-5199.
15. (*a*) X. Li, Y. Wang, B. Tian, T. Matsuura and J. Meng, *J. Heterocycl. Chem.,* **1998**, *35*, 129-134; (*b*) X. Li, Y. Wang, T. Matsuura and J. Meng, *J. Heterocycl. Chem.*, **1999**, *36*, 697-701.
16. Y. Wei and R. Bakthavatchalam, *Tetrahedron Lett*., **1991**, *32*, 1535-1538.
17. Y. Li, X. Yao, X. Feng, X. Wang and J. Wang, *J. Organomet. Chem.,* **1996**, *509*, 221-224.
18. F. Toda, T. Suzuki and S. Higa, *J. Chem. Soc. Perkin Trans. 1*, **1998**, 3521-3522.
19. F. Toda and H. Akai, *J. Org. Chem.*, **1990**, *55*, 3447-3450.
20. F. Toda, H. Takumi, and H. Yamaguchi, *Chem. Exp*., **1989**, *4*, 507-510.
21. H. Tanaka, S. Kishigami, and F. Toda, *J. Org. Chem*., **1991**, *56*, 4333-4334.
22. V. P. Balema, J. W. Wiench, M. Pruski and V. K. Pecharsky, *J. Am. Chem. Soc.*, **2002**, *124*, 6244-6245.
23. (*a*) F. Toda, K. Tanaka, and S. Iwata, *J. Org. Chem.* **1989**, *54*, 3007-3009; (*b*) P. J. Wallis, K. J. Booth, A. F. Patti and J. L. Scott, *Green Chem.*, **2006**, *8*, 333-337.
24. F. Toda, H. Takumi and M. Akehi, *J. Chem. Soc. Chem. Commun.*, **1990**, 1270-1271.
25. (*a*) F. Toda and T. Shigemasa, *J. Chem. Soc. Perkin Trans. 1*, **1989**, *1*, 209-211; (*b*) P. Rashidi-Ranjbar and E. Kianmehr, *Molecules*, **2001**, *6*, 442-447.
26. (*a*) F. Toda, J. Okada and K. Mori, *Angew. Chem. Int. Ed.*, **1988**, *27*, 859-860; (*b*) F. Toda, K. Tanaka and S. Iwata, *J. Org. Chem.*, **1989**, *54*, 3007-3009; (*c*) F. Toda and Y. Tokumaru, *Chem. Lett.*, **1990**, 987-990.
27. (*a*) F. Toda, K. Tanaka,Y. Kagawa and Y. Sakaino, *Chem. Lett.*, **1990**, 373-376; (*b*) H. Yu, S. Chen, M. Tseng, S. Chen and K. Wang, *J. Chem. Res., Synop.,* **1999**, 62-63.
28. (*a*) J. D. McCullough, D. Y. Curtin and I. C. Paul, *J. Am. Chem. Soc.*, **1972**, *94*, 874-882; (*b*) S. Chandrashekhar and K. Gopalaiah, *Tetrahedron Lett.*, **2001**, *42*, 8123-8125.

29. R. Almeida, A. Gomez-Zavaglia, A. Kaczor, M. L. S. Cristiano, M. E. S. Eusebio, T. M. R. Maria and R. Fausto, *Tetrahedron*, **2008**, *64*, 3296-3305.
30. (*a*) G. Kaupp and A. Kuse, *Mol. Cryst. Liq. Cryst.*, **1998**, *313*, 361-366; (*b*) G. Kaupp, *J. Phys. Org. Chem.,* **2008**, *21*, 630-643.
31. (*a*) S. R. Byrn, *J. Pharm. Sci.*, **1976**, *65*, 1-22; (*b*) S. R. Byrn, R. R. Pfeiffer and J. G. Stowell, *Solid-State Chemistry of Drugs*, 2nd Ed, West Lafayette, Indiana, SSCI, Inc., 1999; (*c*) S. R. Byrn, W. Xu and A. W. Newman, *Adv. Drug Deliv. Rev.,* **2001**, *48*, 115-136; (*d*) X. Chen, U. J. Griesser, R. L. Te, R. R. Pfeiffer. K. R. Morris, J. G. Stowell and S. R. Byrn, *J. Pharm. Biomed. Anal.*, **2005**, *38*, 670-677; (*e*) Z. Qui, J. G. Stowell, W. Cao, K. R. Morris, S. R. Byrn and M. T. Carvajal, *J. Pharm. Sci.*, **2005**, *94*, 2568-2580.
32. D. Braga, S. L. Giaffreda, F. Grepioni, A. Pettersen, L. Maini, M. Curzi and M. Polito, *Dalton Trans.*, **2006**, 1249-1263.
33. (*a*) F. Toda, K. Tanaka, T. Tamashima and M. Kato, *Angew. Chem. Int. Ed.*, **1998**, *37*, 2724-2727; (*b*) J. N. Moorthy, P. Venkatakrishnan, G. Savitha and R. G. Weiss, *Photochem. Photobiol. Sci.*, **2006**, *5*, 903-913; (*c*) J. Saltiel, T. S. R. Krishna, S. Laohhasurayotin, K. Fort and R. J. Clark, *J. Phys. Chem A*, **2008**, *112*, 199-209; (*d*) J. Harada, M. Harakawa, S. Sugiyama and K. Ogawa, *CrystEngComm*, **2009**, *11*, 1235-1239.
34. (*a*) T. Odani, A. Matsumoto, K. Sada and M. Miyata, *Chem. Commun.*, **2001**, 2004-2005; (*b*) D. Furukawa, S. Kobatake and A. Matsumoto, *Chem. Commun.*, **2008**, 55-57.
35. (*a*) M. L. Kearley and P. M. Lahti, *Tetrahedron Lett.*, **1991**, *32*, 5869-5872; (*b*) R. Sakurai, S. Suzuki, J. Hashimoto, M. Baba, O. Itoh, A. Uchida, T. Hattori, S. Miyano and M. Yamaura, *Org. Lett.*, **2004**, *6*, 2241-2244; (*c*) R. Sakurai, O. Itoh, A. Uchida, T. Hattori, S. Miyano and M. Yamaura, *Tetrahedron*, **2004**, *60*, 10553-10557.
36. (*a*) R. E. Pincock, M. Tong and K. R. Wilson, *J. Am. Chem. Soc.*, **1971**, *93*, 1669-1672; (*b*) M. D. Lu and R. E. Pincock, *J. Org. Chem.*, **1978**, *43*, 601-604.
37. (*a*) R. E. Pincock and K. R. Wilson, *J. Am. Chem. Soc.*, **1971**, *93*, 1291-1292; (*b*) K. R. Wilson and R. E. Pincock, *J. Am. Chem. Soc.*, **1975**, *97*, 1474-1478; (*c*) R. B. Kress, E. N. Duesler, M. C. Etter, I. C. Paul and D. Y. Curtin, *J. Am. Chem. Soc.*, **1980**, *102*, 7709-7714.

38. (*a*) K. Penzien and G. M. J. Schmidt, *Angew. Chem. Int. Ed. Engl*. **1969**, *8*, 608-609; (*b*) B. S. Green and M. Lahav, *J. Mol. Evol.,* **1975**, *6*, 99-115; (*c*) S. V. Evans, M. Garcia-Gariba, N. Omkaram, J. R. Scheffer, J. Trotter and F. Wireko, *J. Am. Chem Soc.,* **1986**, *108*, 5648-5650; (*d*) G. Kaupp and M. Haak, *Angew. Chem. Int. Ed. Engl*. **1993**, *32*, 694-695; (*e*) M. Sakamoto, *Chem. Eur. J.*, **1997**, *3*, 684-689.
39. (*a*) J. N. Gamlin, R. Jones, M. Leibovitch, B. Patrick, J. R. Scheffer, J. Trotter, *Acc. Chem. Res.* **1996**, *29*, 203-209; (*b*) E. Cheung, K. Rademacher, J. R. Scheffer and J. Trotter, *Tetrahedron Lett.*, **1999**, *40,* 8733-8736; (*c*) E. Cheung, M. R. Netherton, J. R. Scheffer and J. Trotter, *Tetrahedron Lett.*, **1999**, *40*, 8737-8740; (*d*) J. R. Scheffer and W. J. Xia, *Top. Curr. Chem.* **2005**, *254*, 233-262; (*e*) E. Y. Cheung, K. D. M. Harris, T. Kang, J. R. Scheffer and J. Trotter, *J. Am. Chem. Soc.*, **2006**, *128*, 15554-15555; (*f*) C. Yang and W. Xia, *Chem. Asian J.*, **2009**, *4*, 1774-1784.
40. (*a*) K. Soai, *Top. Curr. Chem.*, **2008**, *284*, 1-33; (*b*) T. Kawasaki, M. Nakaoda, N. Kaito, T. Sasagawa and K. Soai, *Orig. Life Evol. Biosph.*, **2010**, *40*, 65-78.
41. (*a*) T. Fujiwara, J. Harada and K. Ogawa, *J. Phys. Chem. B*, **2004**, *108*, 4035-4038; (*b*) J. Harada, T. Fujiwara and K. Ogawa, *J. Am. Chem. Soc.*, **2007**, *129*, 16216-16221.
42. (*a*) J. Guo, G. Liu, D. Jia, J. Wang and X. Xie, *J. Phys. Chem. A*, **2009**, *113*, 1255-1258; (*b*) L. Liu, S. Jia, Y. Ji and K. Yu, *J. Photochem. Photobiol. A*, **2003**, *154*, 117-122; (*c*) T. Zhang, G. Liu, L. Liu, D. Jia and L. Zhang, *Chem. Phys. Lett.*, **2006**, *427*, 443-448.
43. (*a*) P. Naumov, A. Sekine, H. Uekusa and Y. Ohashi, *J. Am. Chem. Soc.*, **2002**, *124*, 8540-8541; (*b*) P. Naumov and Y. Ohashi, *Acta Crystallogr. Sect. B*, **2004**, *60*, 343-349; (*c*) P. Naumov, K. Sakurai, T. Ishikawa, J. Takahashi, S. Koshihara and Y. Ohashi, *J. Phys. Chem. A*, **2005**, *109*, 7264-7575; (*d*) P. Naumov, K. Sakurai, Y. Ohashi and S. Ng, *Chem. Mater.*, **2005**, *17*, 5394-5397.
44. A. O. Patil, D. Y. Curtin and I. C. Paul, *J. Am. Chem. Soc.*, **1984**, *106*, 4010-4015.
45. A. P. Marchand and G. M. Reddy, *Tetrahedron*, **1991**, *47*, 6571-6576.
46. K. Sugita, M. Onaka and Y. Izumi, *Tetrahedron Lett.*, **1990**, *31*, 7467-7468.

47. (*a*) K. Pitchumani, P. Velusamy and C. Srinivasan, *Tetrahedron*, **1994**, *50*, 12979-12988; (*b*) J. Doussot, A. Guy, J. Siague, C. Ferroud and A. Guieres, *Chirality*, **1999**, *11*, 541-545.
48. (*a*) C. W. Porter and P. Wilbur, *J. Am. Chem. Soc.*, **1927**, *49*, 2145-2149; (*b*) P. Naumov, K. Sakurai, M. Tanaka and H. Hara, *J. Phys. Chem. B*, **2007**, *111*, 10373-10378.
49. (*a*) J. Vicens, R. Perrin, G. Aureille-salvadori and M. Perrin, *Mol. Cryst. Liq. Cryst.*, **1983**, *96*, 45-47; (*b*) C. Decoret, G. Bertholon, C. Gaget, J. Vicens, J. Royer, M. Perrin and S. Lecocq, *Mol. Cryst. Liq, Cryst.*, **1983**, *96*, 49-55; (*c*) C. Decoret, J. Vicens and J. Royer, *J. Mol. Struc.*, **1985**, *121*, 13-22; (*d*) J. Vicens, *Tetrahedron*, **1987**, *43*, 1361-1369.
50. V. V. Ershov and A. A. Volodkin, *Russ. Chem. Bull.*, **1965**, *14*, 313-318.
51. P. B. D. de la Mare, N. S. Isaacs and P. D. McIntyre, *Tetrahedron Lett.*, **1976**, *52*, 4835-4836.
52. (*a*) L. A. Ae. Sluyterman and H. J. Veenendaal, *Rec. Trav. Chim. Pays-Bas*, **1952**, *71*, 137-152; (*b*) L. A. Ae. Sluyterman and M. Kooistra, *Rec. Trav. Chim. Pays-Bas*, **1952**, *71*, 277-284.
53. E. Y. Shalaev, S. R. Byrn and G. Zografi, *Int. J. Chem Kinet.*, **1997**, *29*, 339-348.
54. (*a*) R. Kuhn and H. W. Ruelius, *Chem. Ber.*, **1950**, *83*, 420-431; (*b*) J. C. D. Brand and A. Rutherford, *J. Chem. Soc.*, **1952**, 3927-3931.
55. (*a*) C. N. Sukenik, J. A. P. Bonapace, N. S. Mandel, R. G. Bergman, P. Lau and G. Wood, *J. Am. Chem. Soc.*, **1975**, *97*, 5290-5291; (*b*) C. N. Sukenik, J. A. P. Bonapace, N. S. Mandel, P. Lau, G. Wood and R. G. Bergman, *J. Am. Chem. Soc.*, **1977**, *99*, 851-858; (*c*) F. M. Menger, H. B. Kaiserman and L. J. Scotchie, *Tetrahedron Lett.*, **1984**, *25*, 2311-2312.
56. M. Oda and N. Sato, *Chem. Phys. Lett.*, **1997**, *275*, 40-45.
57. M. Dessolin and M. Golfier, *J. Chem. Soc. Chem. Comm.*, **1986**, 38-39.
58. M. Dessolin, O. Eisenstein, M. Golfier, T. Prange and P. Sautet, *J. Chem. Soc. Chem. Comm.*, **1992**, 132-134.
59. M. Smrcina, S. Vyskocil, V. Hanus, M. Polásek, V. Langer, B. G. M. Chew, D. B. Zax, H. Verrier, K. Harper, T. A. Claxton and P. Kocovský, *J. Am. Chem. Soc.*, **1996**, *118*, 487-488.

60. (*a*) O. R. Gautun and P. H. J. Carlsen, *Acta Chem. Scand.*, **1994**, *48*, 411-416; (*b*) P. H. J. Carlsen, K. B. Joergensen, O. R. Gautun, S. Jagner and M. Haakansson, *Acta Chem. Scand.*, **1995**, *49*, 676-682.
61. M. V. Martínez-Díaz, S. Rodríguez-Morgade, W. Schäfer and T. Torres, *Tetrahedron*, **1993**, *49*, 2261-2274.
62. (*a*) M. L. Tosato and L Soccorsi, *J. Chem. Soc. Perkin Trans. 2*, **1982**, 1321-1326; (*b*) M. L. Tosato, *J. Chem. Soc. Perkin Trans. 2*, **1984**, 1593-1599.
63. (*a*) E. Handelsman-Benory, M. Botoshansky, M. Greenberg, V. Shteiman and M. Kaftory, *Tetrahedron*, 2000, *56*, 6887-6897; (*b*) M. Kaftory and E. Handelsman-Benory, *Mol. Cryst. Liq. Cryst.*, **1994**, *240*, 241-249.
64. H. Taycher, M. Botoshansky, V. Shteiman and M. Kaftory, *Supramol. Chem.*, **2001**, *13*, 181-192.
65. M. Greenberg, V. Shteiman and M. Kaftory, *Acta Crystallogr. Sect B: Struc. Sci.*, **2001**, *57*, 428-434.
66. J. Hartung, K. Daniel, U. Bergsträßer, I. Kempter, N. Schneiders, S. Danner, P. Schmidt, I. Svoboda and H. Fuess, *Eur. J. Org. Chem.*, **2009**, 4135-4142.
67. P. Venugopalan and K. Venkatesan, *Helv. Chim. Acta*., **1991**, *74*, 662-669.
68. (*a*) V. N. Nesterov, V. E. Shklover, Yu. T. Struchkov, Yu. A. Sharanin, M. P. Goncharenko and V. D. Dyachenko, *Russ. Chem. Bull.*, **1991**, *40*, 453-454; (*b*) T. P. E. Auf der Heyde, H. B. Bürgi and V. E. Shklover, *Acta Crystallogr. Sect C*, **1991**, *47*, 566-569.
69. (*a*) A. Deák and G. Tárkányi, *Chem. Commun.*, **2005**, 4074-4076; (*b*) A. Deák, P. Király and G. Tárkányi, *Dalton Trans.,* **2007**, 234-239.
70. R. Destro, E. Ortoleva, R. Soave, L. Loconte and L. L. Presti, *Phys. Chem. Chem. Phys.*, **2009**, *11*, 7181-7188.
71. D. Cantillo, M. Avalos, R. Babiano, P. Cintas, J. L. Jimenez, M. E. Light and J. C. Palacios, *J. Org. Chem.*, **2010**, *75*, 4300-4303.
72. M. C. Etter, G. M. Frankenbach and J. Bernstein, *Tetrahedron Lett.*, **1989**, *30*, 3617-3620.
73. F. Gallese, A. Guarino and E. Possagno, *J. Incl. Phenom. Mol. Recognit.*, **1992**, *14*, 55-64.
74. D. Maji, R. Singh, G. Mostafa, S. Ray and S. Lahiri, *J. Org. Chem.*, **1996**, *61*, 5165-5168.

75. M. Sakamoto, M. Takahashi, S. Moriizumi, K. Yamaguchi, T. Fujita and S. Watanabe, *J. Am. Chem. Soc.*, **1996**, *118*, 8138-8139.
76. M. Takahashi, N. Sekine, T. Fujita, S. Watanabe, K. Yamaguchi and M. Sakamoto, *J. Am. Chem. Soc.*, **1998**, *120*, 12770-12776.
77. M. Sakamoto, N. Sekine, H. Miyoshi, T. Mino and T. Fujita, *J. Am. Chem. Soc.*, **2000**, *122*, 10210-10211.
78. (*a*) H. E. Zimmerman, I. V. Alabugin, W. Chen and Z. Zhu, *J. Am. Chem. Soc.*, **1999**, *121*, 11930-11931; (*b*) H. E. Zimmerman, R. D. Rieke and J. R. Scheffer, *J. Am. Chem. Soc.*, **1967**, *89*, 2033-2047; (*c*) H. E. Zimmerman and E. E. Nesterov, *J. Am. Chem. Soc.*, **2002**, *124*, 2818-2830.
79. R. Sekiya, K. Kiyo-oka, T. Imakubo and K. Kobayashi, *J. Am. Chem. Soc.*, **2000**, *122*, 10282-10288.
80. K. Tanaka, A. Tomomori and J. L. Scott, *Eur. J. Org. Chem.*, **2003**, 2035-2038.
81. K. M. Sureshan, T. Murakami, T. Miyasou and Y. Watanabe, *J. Am. Chem. Soc.*, **2004**, *126*, 9174-9175.
82. D. Y. Curtin, S. R. Byrn and D. B. Pendergrass, Jr., *J. Org. Chem.*, **1969**, *34*, 3345-3349.
83. C. S. Russell, *J. Solid State Chem.*, **1987**, *69*, 43-47.
84. E. S. Lutton, *J. Am. Oil Chem. Soc*., **1972**, *49*, 1-9.
85. W. Th. M. de Groot, *Lipids*, **1972**, *7*, 626-628.
86. C. M. Lok and J. P. Ward, *Chem. Phys. Lipids*, **1986**, *39*, 19-29.
87. A. J. Gordon, *Tetrahedron*, **1967**, *23*, 863-870.
88. (*a*) K. Vyas, V. Mohan Rao and H. Manohar, *Acta Crystallogr. Sect. C*, **1987**, *43*, 1197-1200; (*b*) K. Vyas, H. Manohar and K. Venkatesan, *J. Phys. Chem.*, **1990**, *94*, 6069-6073; (*c*) K. Vyas and H. Manohar, *Mol. Cryst. Liq. Cryst.*, **1986**, *137*, 37-43.
89. J. Shorter, *Chem. Soc. Rev*., **1978**, *7*, 1-14.
90. (*a*) J. D. Dunitz, K. D. M. Harris, R. L. Johnston, B. M. Kariuki, E. J. MacLean, K. Psallidas, W. B. Schweizer and R. R. Tykwinski, *J. Am. Chem. Soc.*, **1998**, *120*, 13274-13275; (*b*) E. J. MacLean, K. D. M. Harris, B. M. Kariuki, S. J. Kichin, R. R. Tykwinski, I. P. Swainson and J. D. Dunitz, *J. Am. Chem. Soc.*, **2003**, *125*, 14449-14451.
91. A. E. Troup and H. Mitchner, *J. Pharm. Sci.*, **1964**, *53*, 375-379.

92. (*a*) A. L. Jacobs, A. E. Dilatush, S. Weinstein and J. J. Windheuser, *J. Pharm. Sci.*, **1966**, *55*, 893-895; (*b*) K. T. Koshy, A. E. Troup, R. N. Duvall, R. N. Conwell and L. L. Shankle, *J. Pharm. Sci.*, **1967**, *56*, 1117-1121.
93. (*a*) M. Michman, S. Patai and I. Shenfeld, *J. Chem. Soc. C*, **1967**, 1337-1340; (*b*) M. Krasnoselsky and S. Patai, *J. Chem. Soc. B*, **1969**, 24-27.
94. (*a*) M. Michman and M. Frenkel, *J. Chem. Soc. C*, **1971**, 3856-3859; (*b*) M. Michman, S. Patai and Y. Wiesel, *J. Chem. Soc. Perkin Trans. 1*, **1977**, 1705-1710.
95. (*a*) L. A. Errede, M. C. Etter, R. C. Williams and S. M. Darnauer, *J. Chem. Soc. Perkin Trans. 2*, **1981**, 233-238; (*b*) M. C. Etter, *J. Chem. Soc. Perkin Trans. 2*, **1983**, 115-121.
96. H. Hagiwara, S. Ohtsubo and M. Kato, *Tetrahedron*, **1997**, *53*, 2415-2420.
97. G. Kaupp, J. Schemeyers and J. Boy, *Tetrahedron*, **2000**, *56*, 6899-6911.
98. S. Nakamatsu, K. Yoshizawa, S. Toyota, F. Toda and I. Matijasic, *Org. Biomol. Chem.*, **2003**, *1*, 2231-2234.
99. M. L. Cheney, G. J. McManus, J. A. Perman, Z. Wang and M. J. Zaworotko, *Cryst. Growth Des.*, **2007**, *7*, 616-617.
100. T. Haneda, M. Kawano and M. Fujita, *J. Am. Chem. Soc.*, **2008**, *130*, 1578-1579.
101. R. Parthasarathy and F. Eisenberg Jr., *Biochem J.*, **1986**, *235*, 313-322.
102. (*a*) D. C. Billington, Ed.; *The Inositol Phosphates. Chemical Synthesis and Biological Significance*, VCH: New York, 1993; (*b*) K. S. Bruzik, Ed.; *Phosphoinositides: Chemistry, Biochemistry and Biomedical Applications*, ACS Symposium Series Vol. 718, American Chemical Society, Washington D.C. USA, 1999.
103. (*a*) J. R. Thomas, R. A. Dwek and T. W. Rademacher, *Biochemistry*, **1990**, *29*, 5413-5422; (*b*) B. V. L. Potter and D. Lampe, *Angew. Chem. Int. Ed.*, **1995**, *34*, 1933-1972; (*c*) K. Hinchcliffe and R. Irvine, *Nature*, **1997**, *390*, 123-124; (*d*) M. G. Low, *Mol. Biol. Intell. Unit 7 (GPI-Anchored Membrane Proteins and Carbohydrates)*, **1999**, 1-14; (*e*) M. J. McConville and A. K. Menon, *Mol. Membr. Biol.*, **2000**, *17*, 1-16.
104. (*a*) K. M. Sureshan, M. S. Shashidhar, T. Praveen and T. Das, *Chem. Rev.*, **2003**, *103*, 4477-4503; (*b*) R. C. Jagdhane and M. S. Shashidhar, *Eur. J. Org.*

Chem., **2010**, 2945-2953; (*c*) B. Kilbas and M. Balci, *Tetrahedron,* **2011**, DOI:10.1016/j.tet.2011.01.012

105. (*a*) B. V. L. Potter, A. M. Riley and M. F. Mahon, *Angew. Chem. Int. Ed.*, **1997**, *36*, 1472-1474; (*b*) S. W. Garrett, C. Liu, A. M. Riley and B. V. L. Potter, *J. Chem. Soc. Perkin Trans. 1*, **1998**, 1367-1368; (*c*) T. Praveen, T. Das, K. M. Sureshan, M. S. Shashidhar, U. Samanta, D. Pal and P. Chakrabarti, *J. Chem. Soc. Perkin Trans. 2*, **2002**, 358-365.; (*d*) S. J. Mills, A. M. Riley, C. Liu, M. F. Mahon and B. V. L. Potter, *Chem. Eur. J.*, **2003**, *9*, 6207-6214.
106. (*a*) *Enzymes*, 3rd Ed, Ed., P. D. Boyer, Academic, New York, 1973, 8, pp 155-199; (*b*) D. Voet and J. G. Voet, *Biomolecules*, *Mechanisms of Enzyme Action and Metabolism, Biochemistry*, Vol. 1, Wiley, New York, 2003.
107. (*a*) S. Patai, *The Chemistry of Functional Groups: The Chemistry of Carboxylic Acids and Esters*, Ed., S. Patai, Wiley, New York, 1969, p. 1155; (*b*) *Transition States of Biochemical Processes*, Ed., R. D. Gandour and R. L. Schowen, Plenum, New York, pp 355-428, 1978; (*c*) A. Williams, *Acc. Chem. Res.*, **1989**, *22*, 387-392.
108. (*a*) S. J. Angyal and G. J. H. Melrose, *J. Chem. Soc.*, **1965**, 6494-6500; (*b*) S. J. Angyal, P. T. Gilham and G. J. H. Melrose, *J. Chem. Soc.*, **1965**, 5252-5255; (*c*) V. I. Shvets, *Russ. Chem. Rev.*, **1974**, *43*, 488-502; (*d*) S. Chung and Y. Chang, *J. Chem. Soc. Chem. Commun.*, **1995**, 13-14; (*e*) S. Chung, Y. Chang and Y. Ryu, *Pure Appl. Chem.*, **1996**, *68*, 931-935.
109. K. M. Sureshan, S. Devaraj and M. S. Shashidhar, *Tetrahedron,* **2009**, *65*, 2703-2710.
110. T. Praveen, U. Samanta, T. Das, M. S. Shashidhar, and P. Chakrabarti, *J. Am. Chem. Soc.* **1998**, *120,* 3842-3845.
111. (*a*) T. Das, T. Praveen, M. S. Shashidhar, *Carbohydr. Res.* **1998**, *313*, 55-59; (*b*) T. Das, M. S. Shashidhar, *Carbohydr. Res.*, **1998**, *308*, 165-168.
112. M. P. Sarmah, R. G. Gonnade, M. S. Shashidhar and M. M. Bhadbhade, *Chem. Eur. J.* **2005**, *11*, 2103-2110.
113. C. Murali, M. S. Shashidhar, R. G. Gonnade, and M. M. Bhadbhade, *Eur. J. Org. Chem.* **2007**, 1153-1159.

114. (*a*) R. J. Davey, N. Blagden, G. D. Potts and R. Docherty, *J. Am. Chem. Soc.*, **1997**, *119*, 1767-1772; (*b*) C.-H. Gu, K. Chatterjee, V. Young, Jr. and D. J. W. Grant, *J. Crystal Growth*, **2002**, *235*, 471-481.

115. C. Murali, M. S. Shashidhar, R. G. Gonnade and M. M. Bhadbhade, *Chem. Eur. J.*, **2009**, *15*, 261-269.

116. M. P. Sarmah, Ph.D Thesis, Univ. of Pune, 2005.

Chapter 2

The molecular design, synthesis and characterization of myo-inositol derivatives

Every discovery opens a new field for investigation of facts, shows us the imperfection of our theories. It has justly been said, that the greater the circle of light, the greater the boundary of darkness by which it is surrounded.

- Sir Humphry Davy

2.1 Introduction

The facility of reactions in solution may be manipulated by the use of suitably modified substrates, reagents and solvents based on their electronic and steric properties. Facile intermolecular reactions in crystals often depend on the molecular pre-organization and the interactions of the reactive groups. Hence, the key to performing solid-state intermolecular reactions is to design molecules and grow crystals in which the reactive groups are prearranged with the required geometry to facilitate the interaction between the reactant molecules without significantly disturbing the crystal lattice during new bond formation.

In the preceding chapter, the solid-state reactivities of some di-*O*-benzoylated *myo*-inositol 1,3,5-orthoesters and the associated acyl transfer mechanism was discussed based on the crystal structures of the reactants. In order to study the scope of this reaction, explore its possible synthetic utility, and examine the impact of small perturbations in chemical structure on the crystal structure and reactivity in the solid state, a series of compounds was prepared by modification of ester groups at various positions. The hydroxyl group at the C4 position was replaced by methyl and allyl groups retaining the benzoates at C2 and C6. The benzoyl group at the C6 position was replaced by acrylate, crotonate and furoate esters, to determine the effect of replacing the benzoate group (which engages in C-H$\cdots\pi$ interactions, Chapter 1, pg. 31, Fig. 1b) with olefinic esters and other aromatic esters, on the molecular structure of the reactive dibenzoate. Secondly, the benzoates at C2 and C6 were replaced by *para*-halobenzoyl (halo = fluoro, chloro, bromo, iodo) and *para*-toluoyl groups to study the effect of substitution on the aromatic ring on molecular pre-organization and electronic effects in solid-state transesterification reactions (Scheme 2.1). Finally, based on the reactivity displayed by the 2-*O*-benzoyl *myo*-inositol 1,3,5-orthoesters, some mono-acylated *myo*-inositol 1,3,5-orthoformate derivatives were also prepared and studied. The synthesis and characterization of these derivatives is described in this chapter. Crystal structures, thermal studies and reactivities of these compounds are discussed in the following chapters.

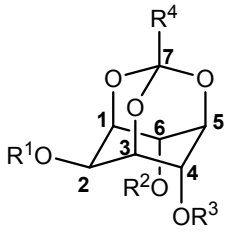

R^4 = H

	R^1	R^2	R^3
2.1	H	H	H
2.2	PhCO	PhCO	CH_3
2.3	PhCO	PhCO	CH_2-CH=CH_2
2.5	*p*-Br-C_6H_4CO	*p*-Br-C_6H_4CO	H
2.6	*p*-Br-C_6H_4CO	*p*-Br-C_6H_4CO	*p*-Br-C_6H_4CO
2.7	*p*-Cl-C_6H_4CO	*p*-Cl-C_6H_4CO	H
2.8	*p*-Cl-C_6H_4CO	*p*-Cl-C_6H_4CO	*p*-Cl-C_6H_4CO
2.9	CH_3CO	H	H
2.10	PhCO	CH_2=CHCO	H
2.11	PhCO	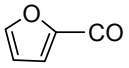	H
2.12	PhCO	CH_3CH=CHCO	H

R^4 = Ph

	R^1	R^2	R^3
2.4	H	H	H

R^4 = H

	R^1	R^2	R^3
2.13	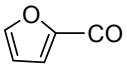	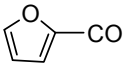	H
2.14	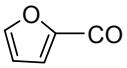	H	H
2.15	*p*-CH_3-C_6H_4CO	*p*-CH_3-C_6H_4CO	H
2.16	*p*-CH_3-C_6H_4CO	H	H
2.17	*p*-CH_3-C_6H_4CO	*p*-CH_3-C_6H_4CO	*p*-CH_3-C_6H_4CO
2.18	*p*-I-C_6H_4CO	*p*-I-C_6H_4CO	H
2.19	*p*-I-C_6H_4CO	H	H
2.20	*p*-Br-C_6H_4CO	H	H
2.21	*p*-Cl-C_6H_4CO	H	H
2.22	*p*-F-C_6H_4CO	*p*-F-C_6H_4CO	H
2.23	*p*-F-C_6H_4CO	H	H
2.24	*p*-F-C_6H_4CO	*p*-F-C_6H_4CO	*p*-F-C_6H_4CO

Scheme 2.1 *myo*-Inositol orthoester derivatives: perturbation of functional groups at C2, C4 and C6, C7.

2.2 Experimental

General: Benzoyl chloride, thionyl chloride, *p*-toluene sulfonic acid and all the solvents were purified according to the literature procedures[1] before use. Acryloyl chloride was prepared by heating acrylic acid with benzoyl chloride in the presence of hydroquinone and distillation under vacuum.[2] *p*-Toluoyl chloride and *p*-halobenzoyl chlorides were prepared by refluxing the respective acids with freshly distilled thionyl chloride for 2-3 h, followed by distillation and drying under vacuum.[3] All air or moisture sensitive reactions were conducted under argon or nitrogen atmosphere. 'Usual work up' of the residue / reaction mixture involved washing of organic layer successively with water, 2% dil. HCl solution (when acid sensitive groups were not present), water, saturated sodium bicarbonate solution and water followed by brine, drying over anhydrous sodium sulfate and evaporation of the solvent under reduced

pressure. Light petroleum refers to the 60-80º C boiling fraction of petroleum ether. Thin layer chromatography was performed on E. Merck precoated 60 F254 plates and the spots were rendered visible either by shining UV light or by charring the plates with concentrated H_2SO_4. Flash column chromatographic separations were carried out on silica gel 230-400 mesh with light petroleum-ethyl acetate mixtures, unless otherwise mentioned. Preparative TLC was carried out on Merck pre-coated 60 F254 glass plates and the spots were rendered to visible by shining UV light. The fractions were isolated by extraction of the appropriate region of the TLC plate with suitable solvents. Compounds previously reported in the literature were characterized by comparison of their melting points and / or ^{1}H NMR spectra with reported data. IR spectra were recorded either as Nujol mull or as thin film (neat) on a Shimadzu FTIR-8400 spectrophotometer. NMR spectra were recorded in deuterated solvents on Bruker AV200 (or DRX 500MHz for ^{1}H) spectrometer. Chemical shifts (δ) reported are referred to internal tetramethylsilane. ^{19}F NMR spectra were recorded on Bruker 400MHz spectrometer with C_6F_6 (hexafluorobenzene) as internal standard. Microanalytical data were obtained using a Carlo-Erba CHNS-0 EA 1108 elemental analyzer. All the melting points were recorded on a Büchi B-540 electro-thermal melting point apparatus. All the asymmetrically substituted *myo*-inositol derivatives reported are racemic; however, only one of the enantiomers is shown in all the schemes.

The following compounds were prepared as reported in the literature: *myo*-inositol 1,3,5-orthoformate[4] (**2.1**), racemic 2,6-di-*O*-benzoyl-4-*O*-methyl *myo*-inositol 1,3,5-orthoformate[5] (**2.2**), racemic 2,6-di-*O*-benzoyl-4-*O*-allyl *myo*-inositol 1,3,5-orthoformate[5] (**2.3**), 2-*O*-benzoyl *myo*-inositol 1,3,5-orthoformate[6] (**1.183**), *myo*-inositol 1,3,5-orthobenzoate[7] (**2.4**), racemic 2,6-di-*O*-benzoyl *myo*-inositol 1,3,5-orthobenzoate[8] (**1.179**), racemic 2,6-di-*O*-(4-bromobenzoyl) *myo*-inositol 1,3,5-orthoformate[9] (**2.5**), 2,4,6-tri-*O*-(4-bromobenzoyl) *myo*-inositol 1,3,5-orthoformate[10] (**2.6**), racemic 2,6-di-*O*-(4-chlorobenzoyl) *myo*-inositol 1,3,5-orthoformate[9] (**2.7**), 2,4,6-tri-*O*-(4-chlorobenzoyl) *myo*-inositol 1,3,5-orthoformate[10] (**2.8**) and 2-*O*-acetyl *myo*-inositol 1,3,5-orthoformate[11] (**2.9**).

General procedure for crystallization:

All crystallization experiments were performed under comparable conditions. A clear solution of the compound (typically 3-10 mg) in a solvent (1-2 mL depending on solubility), obtained by vigorous shaking / gentle warming was allowed to stand for 1-

6 days at ambient temperature. In some experiments (particularly those involving volatile solvents) light petroleum vapour (bp 40-60 ºC) was diffused into the solution.

Racemic 2-*O*-benzoyl-6-*O*-acryloyl *myo*-inositol 1,3,5-orthoformate (**2.10**): Freshly prepared acryloyl chloride (0.182 g, 2 mmol) was added to a cooled solution of the benzoate **1.183** (0.588 g, 2 mmol) and dry triethylamine (0.405 g, 6 mmol) in dry dimethylformamide (DMF, 12 mL) and the reaction mixture was stirred at room temperature for 12 h. The DMF was evaporated under reduced pressure, and the residue was diluted with dichloromethane and washed with water, dilute HCl, saturated sodium bicarbonate solution and brine. The organic layer was dried with anhydrous sodium sulfate and concentrated, and the product purified by column chromatography to obtain racemic **2.10**. (0.25 g, 36%).

Mp: 148-150 °C; **IR** (Nujol, cm^{-1}) ν: 3451, 1728, 1701; **^{1}H NMR** (200 MHz, $CDCl_3$): δ 2.58 (1H, d, *J* = 6.1 Hz), 4.43–4.49 (1H, m), 4.50–4.58 (2H, m), 4.63–4.74 (1H, m), 5.53 (1H, q, *J* = 1.6 Hz), 5.62 (1H, d, *J* = 1.3 Hz), 5.68 (1H, td, *J* = 3.9 and 1.6 Hz), 5.91–6.02 (1H, m), 6.07-6.24 (1H, m), 6.45-6.58 (1H, m), 7.42–7.66 (3H, m), 8.10–8.22 (2H, m) ppm; **^{13}C NMR** (125 MHz, $CDCl_3$): δ 63.4, 67.2, 68.1, 68.2, 69.2, 71.5, 102.6, 126.9, 128.2, 129.2, 129.7, 132.7, 133.3, 164.2, 165.9 ppm; **Elemental analysis:** Calcd. for $C_{17}H_{16}O_8$: C, 58.62; H, 4.63. Found: C, 58.86; H, 4.92 %.

Crystallization: Rac-2.10, upon crystallization from ethyl acetate (containing a trace of light petroleum), toluene, methanol, tetrahydrofuran, chloroform and benzene yielded exclusively plate-like crystals (form I). Crystallization from an ethyl acetate-light petroleum mixture (1:1 *v/v,* by vapour diffusion) produced needle-shaped crystals (form II), whereas crystallization from dichloromethane yielded both forms concomitantly, with the relative yield of the form I crystals consistently greater than that of form II crystals. Co-crystallization of **rac-2.10** with 2,6-di-*O*-benzoyl *myo*-inositol 1,3,5-orthoformate (**rac-1.177**) in ethyl acetate and chloroform with diffusion of light petroleum did not yield crystals.

Racemic 2-*O*-benzoyl-6-*O*-(2-furoyl) *myo*-inositol 1,3,5-orthoformate (**2.11**): 2-Furoylchloride (0.11 mL, 1.1 mmol) was added to a cooled solution of **1.183**, (0.294 g, 1 mmol) in dry pyridine (3 mL) and the reaction mixture stirred at room temperature for 12 h. Pyridine was removed by co-evaporation with toluene and the

residue was dissolved in methanol and allowed to stand. Crystals of the benzoate **1.183** appeared over a period of two days and they were filtered out. The mother liquor when allowed to stand for a further 24 h yielded crude racemic **2.11** (0.1 g, 26%) as a solid, which was extracted with dichloromethane. The residue (0.05 g) obtained from dichloromethane was purified by preparative TLC to obtain **2.11** (0.018 g). **Mp:** 185.5-187.5 ºC; **IR** (Nujol, cm^{-1}) ν: 3563, 1719, 1701; **^{1}H NMR** (200 MHz, $CDCl_3$): δ 2.92 (1H, br s) 4.49–4.53 (1H, m), 4.56-4.62 (2H, m), 4.66-4.76 (1H, m), 5.58-5.60 (1H, q, *J* = 1.6 Hz), 5.64–5.65 (1H, d, *J* = 1.3 Hz), 5.81–5.86 (1H, td, *J* = 4 and 1.7 Hz), 6.54–6.57 (1H, m), 7.30–7.32 (1H, d, *J* = 3 Hz), 7.43–7.51 (2H, m), 7.57–7.65 (2H, m), 8.13-8.19 (2H, m) ppm; **^{13}C NMR** (125 MHz, $CDCl_3$): δ 63.4, 67.7, 68.3, 68.4, 69.3, 71.9, 102.3, 112.4, 120.1, 128.5, 129.4, 130, 133.6, 143.1, 147.4, 156.3, 166.1 ppm; **Elemental analysis:** Calcd. for $C_{19}H_{16}O_9$: C, 58.77; H, 4.15. Found: C, 59.22; H, 4.39 %.

Crystallization: Rac-2.11, upon crystallization (by slow evaporation) from acetone, ethyl acetate, dichloromethane and chloroform yielded plate-like crystals.

Racemic 2-*O*-benzoyl-6-*O*-crotonoyl *myo*-inositol 1,3,5-orthoformate (**2.12**): The benzoate **1.183** (0.147 g, 0.5 mmol) was dissolved in dry DMF (3 mL) and the solution was cooled in an ice-bath. To the cooled solution, NaH (0.02 g, 0.5 mmol) was added, followed by stirring and addition of *trans*-crotonoyl chloride (0.056 mL, 0.5 mmol). The reaction mixture was stirred for 1 h, quenched with AcOH, diluted with water and extracted with ethyl acetate, washed with brine. The organic layer was dried with anhydrous Na_2SO_4, concentrated and the residue was purified by column chromatography (using gradient elution with ethyl acetate - light petroleum), yielding racemic **2.12** as a gum (0.025 g, 14%), which solidified into an amorphous powder over ~2.5 years. **Mp:** 119-124 °C; **IR** (neat, cm^{-1}) ν: 3550-3400, 1723, 1716; **^{1}H NMR** (200 MHz, $CDCl_3$): δ 1.91 (3H, dd, *J* = 7 and 1.7 Hz) 2.88 (1H, d, *J* = 5.2 Hz), 4.43-4.55 (3H, m), 4.67 (1H, br s), 5.50-5.55 (1H, m), 5.62 (1H, d, *J* = 1.3 Hz), 5.66 (1H, td, *J* = 3.9 and 1.7 Hz), 5.88 (1H, dq, *J* = 15.6 and 1.6 Hz), 7.08 (1H, dq, *J* = 15.5 and 7 Hz), 7.42–7.52 (2H, m), 7.56-7.65 (1H, m), 8.12-8.19 (2H, m) ppm; **^{13}C NMR** (125 MHz, $CDCl_3$): δ 18.3, 63.5, 67.7, 68.1, 68.3, 69.5, 71.9, 102.9, 121.2, 128.5, 129.5, 130.0, 133.6, 147.9, 164.3, 166.1 ppm; **Elemental analysis:** Calcd. for $C_{18}H_{18}O_8$: C, 59.67; H, 5.01. Found: C, 59.30; H, 4.79 %.

Crystallization: Attempts to crystallize the amorphous powder by dissolving it in chloroform or ethyl acetate resulted in the formation of a gum.

General procedure A for acylation

Freshly distilled acid chloride was added to a cooled solution of the orthoformate **2.1** in dry pyridine, with constant stirring. The reaction mixture was brought to room temperature, stirred for 18 – 20 h and quenched with ice. Pyridine was removed in *vacuo* by co-evaporation with toluene (3 × 10 mL) and the residue was diluted with ethyl acetate and worked up as usual. The residue was chromatographed on flash silica using gradient elution with light petroleum - ethyl acetate.

Racemic 2,6-di-*O*-(2-furoyl) *myo*-inositol 1,3,5-orthoformate (2.13) and 2-*O*-(2-furoyl) *myo*-inositol 1,3,5-orthoformate (2.14): Orthoformate **2.1** (0.190 g, 1 mmol) was acylated as described in general procedure A with 2-furoyl chloride (0.198 mL, 2 mmol) in dry pyridine (3 mL), yielding racemic **2.13** (0.055 g, 15%) and **2.14 (**0.060 g, 21%).

Data for **2.13**:

Mp: 181.5-183 ºC; **IR** ($CDCl_3$, cm^{-1}) ν: 3434, 1725; **^{1}H NMR** (400 MHz, $CDCl_3$): δ 2.79 (1H, d, *J* = 7.6 Hz), 4.42-4.48 (1H, m), 4.51-4.56 (2H, m), 4.64-4.70 (1H, m), 5.50-5.54 (1H, m), 5.58-5.62 (1H, m), 5.78 (1H, dt, *J* = 1.7, 5.63 Hz), 6.48-6.54 (2H, m), 7.27 (1H, d, *J* = 3.4 Hz), 7.31 (1H, d, *J* = 3.4 Hz), 7.60 (2H, d, J = 7 Hz) ppm; **^{13}C NMR** (100.6 MHz, $CDCl_3$): δ 63.5, 67.6, 68.2, 68.4, 69.3, 71.8, 102.8, 112.1, 112.4, 119.4, 120.1, 143.1, 143.8, 147.1, 147.4, 156.3, 158.1 ppm; **Elemental analysis:** Calcd. for $C_{17}H_{14}O_{10}$: C, 53.98; H, 3.73. Found: C, 54.23; H, 3.79 %.

Crystallization: Crystallization of **rac-2.13** from ethyl acetate, chloroform and dichloromethane using vapour diffusion (of light petroleum) / slow evaporation yielded rectangular plate like crystals.

Data for **2.14**:

Mp: 183-185 ºC; **IR** (Nujol, cm^{-1}) ν: 3500-3200, 1704; **^{1}H NMR** (200 MHz, CD_3SOCD_3): δ 4.26-4.32 (1H, m) 4.36–4.42 (2H, m), 4.50-4.59 (2H, m), 5.51 (1H, d, *J* = 1.1 Hz), 5.54-5.58 (1H, m), 5.71 (2H, d), 6.58 (1H, dd, *J* = 1.9 & 1.6 Hz), 7.34 (1H, d, *J* = 3 Hz, d), 7.66–7.69 (1H, m) ppm; **^{13}C NMR** (100.6 MHz, CD_3SOCD_3 +

$CDCl_3$): δ 68.7, 72.4, 73.6, 76.9, 107.1, 116.9, 123.8, 148.7, 151.7, 162.7 ppm; **Elemental analysis:** Calcd. for $C_{12}H_{12}O_8$: C, 50.71; H, 4.26. Found: C, 50.93; H, 4.12 %.

Racemic 2,6-di-*O*-(*p*-toluoyl) *myo*-inositol 1,3,5-orthoformate (2.15) and 2-*O*-(*p*-toluoyl) *myo*-inositol 1,3,5-orthoformate (2.16): Orthoformate **2.1** (0.950 g, 5 mmol) was acylated as described in general procedure A with *p*-toluoyl chloride (~ 11 mmol) in dry pyridine (12 mL), yielding a mixture which was worked up and the residue chromatographed to obtain racemic **2.15** (0.842 g, 39%) and **2.16** (0.630 g, 41%).

Data for **2.15**:

Mp: 227.3-229.3 ºC; **IR** (Nujol, cm^{-1}) ν: 3473, 1720, 1716; **^{1}H NMR** (200 MHz, $CDCl_3$): δ 2.41 (3H, s), 2.43 (3H, s) 2.59 (1H, br s), 4.46-4.53 (1H, m), 4.57-4.64 (2H, m), 4.69-4.77 (1H, m), 5.62-5.67 (2H, m), 5.83 (1H, td, J = 4 and 1.6 Hz), 7.23-7.29 (4H, m), 7.90-7.96 (2H, m), 8.01-8.08 (2H, m) ppm; **^{13}C NMR** (50.3 MHz, CD_3COCD_3): δ 21.6, 64.9, 67.9, 69.5, 70.0, 70.7, 73.0, 103.9, 127.9, 128.3, 130.0, 130.1, 130.6, 130.7, 145.1, 166.4 ppm; **Elemental analysis:** Calcd. for $C_{23}H_{22}O_8$: C, 64.78; H, 5.20. Found: C, 64.99; H, 4.80 %.

Crystallization: Rac-2.15 when crystallized from acetonitrile, acetonitrile-DCM, methanol, ethyl acetate, chloroform, dioxane and nitromethane yielded consistently thin rectangular plates. Co-crystallization of **rac-2.15** with **rac-1.177** (chloroform-light petroleum, vapor diffusion) did not yield any new crystalline forms of either compound.

Data for **2.16**

Mp: 148-150 ºC; **IR** (Nujol, cm^{-1}) ν: 3550-3350, 1703; **^{1}H NMR** (200 MHz, $CDCl_3$): δ 2.43 (3H, s), 3.60-4.42 (3H, br m), 4.44-4.50 (2H, m), 4.63-4.68 (2H, m), 5.52-5.58 (2H, m), 7.23-7.30 (2H, m), 8.00-8.06 (2H, m) ppm; **^{13}C NMR** (50.3 MHz, $CDCl_3$): δ 21.8, 63.7, 68.1, 68.6, 72.0, 102.5, 126.5, 129.3, 130.1, 144.6, 167 ppm; **Elemental analysis:** Calcd. for $C_{14}H_{16}O_7$: C, 58.44; H, 5.23. Found: C, 58.52; H, 5.20 %.

Crystallization: Rac-2.16 when crystallized from acetone, ethyl acetate, chloroform, and dichloromethane yielded hexagonal plates.

2,4,6-Tri-*O*-(*p*-toluoyl) *myo*-inositol 1,3,5-orthoformate (2.17): Orthoformate **2.1** (0.190 g, 1 mmol) was acylated as described in general procedure A with *p*-toluoyl chloride (~ 5 mmol) in dry pyridine (5 mL), yielding a mixture (consisting of **2.15**, *p*-toluic acid and **2.17**) which was worked up and the residue chromatographed to obtain **2.17** (0.140 g, 26%).

Mp: 156-158 ºC; **IR** (Nujol, cm^{-1}) ν: 1738, 1721; **^{1}H NMR** (200 MHz, $CDCl_3$): δ 2.36 (6H, s), 2.44 (3H, s), 4.64-4.69 (2H, m), 4.96-5.02 (1H, m), 5.66-5.71 (1H, m), 5.74 (1H, d, *J* = 1.3 Hz), 5.79-5.85 (2H, m), 6.98 (4H, d, *J* = 8 Hz), 7.29-7.32 (2H, m), 7.69-7.75 (4H, m), 8.03-8.09 (2H, m) ppm; **^{13}C NMR** (50.3 MHz, $CDCl_3$): δ 21.7, 63.8, 67.0, 68.3, 69.6, 103.4, 125.8, 126.6, 129.1, 129.3, 129.9, 130.0, 144.2, 144.5, 165.2, 166.3 ppm; **Elemental analysis:** Calcd. for $C_{31}H_{28}O_9$: C, 68.38; H, 5.18. Found: C, 68.07; H, 5.26 %.

Racemic 2,6-di-*O*-(4-iodobenzoyl) *myo*-inositol 1,3,5-orthoformate (2.18) and 2-*O*-(4-iodobenzoyl) *myo*-inositol 1,3,5-orthoformate (2.19): Orthoformate **2.1** (0.190 g, 1 mmol) was acylated as described in general procedure A with 4-iodobenzoyl chloride (~ 2 mmol) in dry pyridine (7 mL), yielding a mixture which was worked up and the residue chromatographed to obtain racemic **2.18** (0.150 g, 23%) and **2.19** (0.09 g, 21%).

Data for **2.18**:

Mp: 240.3-241.5 ºC; **IR** (Nujol, cm^{-1}) ν: 3468, 1716; **^{1}H NMR** (200 MHz, $CDCl_3$): δ 2.39 (1H, br s) 4.45-4.51 (1H, m), 4.55-4.65 (2H, m), 4.71-4.79 (1H, m), 5.60-5.66 (2H, m), 5.78-5.84 (1H, td, *J* = 4 and 1.7 Hz), 7.71-7.78 (2H, m), 7.80-7.88 (6H, m) ppm; **^{13}C NMR** (50.3 MHz, CD_3COCD_3 + CD_3SOCD_3): δ 65.6, 67.5, 69.8, 69.9, 70.4, 72.9, 102.2, 103.8, 130.3, 130.5, 132.2, 132.4, 138.9, 139.0, 165.6, 166.1 ppm; **Elemental analysis:** Calcd. for $C_{21}H_{16}O_8I_2$: C, 38.80; H, 2.48. Found: C, 39.03; H, 2.40 %.

Crystallization: Rac-2.18 proved to be sparingly soluble in most solvents; however crystallization from acetone, chloroform, nitromethane, 2-propanol and ethyl acetate yielded thin plate like crystals.

Data for **2.19**:

Mp: 158-161 ºC; **IR** (Nujol, cm^{-1}) ν: 3550-3300, 1724; **^{1}H NMR** (200 MHz, $CDCl_3$): δ 3.83 (2H, d, *J* = 7.2 Hz), 4.36–4.42 (1H, m), 4.44-4.49 (2H, m), 4.63-4.72 (2H, m), 5.54-5.57 (2H, m), 7.84 (4H, s) ppm; **^{13}C NMR** (50.3 MHz, CD_3COCD_3): δ 65.3, 69.1, 70.3, 73.3, 101.9, 103.6, 130.9, 132.4, 139.2, 166.2 ppm; **Elemental analysis:** Calcd. for $C_{14}H_{13}O_7I$: C, 40.02; H, 3.12. Found: C, 40.53; H, 3.11 %.

Racemic 2,6-di-*O*-(4-bromobenzoyl) *myo*-inositol 1,3,5-orthoformate (2.5) and 2-*O*-(4-bromobenzoyl) *myo*-inositol 1,3,5-orthoformate (2.20):

Orthoformate **2.1** (0.570 g, 3 mmol) was acylated as described in general procedure A with 4-bromobenzoyl chloride (~ 7.5 mmol) in dry pyridine (7 mL), yielding a mixture which was worked up and the residue chromatographed to obtain racemic **2.5** (0.236 g, 14%) and **2.20 (**0.433 g, 39%).

Data for **2.20:**

Mp: 156-157 ºC; **IR** (Nujol, cm^{-1}) ν: 3550-3250, 1716; **^{1}H NMR** (200 MHz, $CDCl_3$): δ 4.03 (2H, d, *J* = 4.8 Hz), 4.36-4.42 (1H, m), 4.46-4.50 (2H, m), 4.61-4.72 (2H, m), 5.53-5.59 (2H, m), 7.62 (2H, dt, *J* = 8.5 and 2 Hz), 8.00 (2H, dt, *J* = 8.5 and 2 Hz) ppm; **^{13}C NMR** (50.3 MHz, CD_3COCD_3): δ 69.4, 73.1, 74.3, 77.3, 107.6, 133.0, 134.5, 136.6, 137.1, 170.0 ppm; **Elemental analysis:** Calcd. for $C_{14}H_{13}O_7Br$: C, 45.06; H, 3.51. Found: C, 45.29; H, 3.61 %.

Crystallization of 2.5: Crystals of **rac-2.5** from methanol, benzene (form I) and ethyl acetate, acetonitrile (form II) were solvent free forms, whereas crystallization from acetone, chloroform, dichloromethane, nitromethane, tetrahydrofuran, dioxane, 1,2-dichloroethane and dimethyl sulphoxide yielded solvatomorphs.

Crystallization of 2.20: Crystallization of **rac-2.20** from chloroform and acetone *via* slow evaporation yielded plate-like crystals.

Racemic 2,6-di-*O*-(4-chlorobenzoyl) *myo*-inositol 1,3,5-orthoformate (2.7) and 2-*O*-(4-chlorobenzoyl) *myo*-inositol 1,3,5-orthoformate (2.21): Orthoformate **2.1** (0.760 g, 4 mmol) was acylated as described in general procedure A with 4-chlorobenzoyl chloride (~ 4 mmol) in dry pyridine (10 mL), yielding a yellow gum which was worked up and the residue chromatographed to obtain **2.7** (0.278 g, 15%) and **2.21 (**0.322 g, 25%).

Data for **2.21:**

Mp: 151-154 ºC; **IR** (Nujol, cm^{-1}) ν: 3550-3300, 1716; **^{1}H NMR** (200 MHz, $CDCl_3$): δ 4.04-4.13 (2H, m) 4.34-4.40 (1H, m), 4.42-4.47 (2H, m), 4.61-4.71 (2H, m), 5.52-5.57 (2H, m), 7.43 (2H, tt, *J* = 8.7 and 2 Hz), 8.05 (2H, tt, *J* = 8.7 and 2 Hz) ppm; **^{13}C NMR** (50.3 MHz, $CDCl_3$): δ 64.0, 68.1, 68.6, 71.9, 102.5, 127.8, 128.9, 131.4, 140.3, 165.8 ppm; **Elemental analysis:** Calcd. for $C_{14}H_{13}O_7Cl$: C, 51.16; H, 3.99. Found: C, 51.40; H, 3.82 %.

Crystallization of 2.7: Crystals of **rac-2.7** from methanol, toluene (form I) and ethyl acetate (form II) were solvent free forms, whereas crystallization from acetone, chloroform, dichloromethane, nitromethane, tetrahydrofuran, dioxane, 1,2-dichloroethane, dimethyl sulphoxide, *p*-xylene, acetonitrile and benzene yielded solvatomorphs.

The guest selectivities among the solvents, which produced inclusion crystals of **rac-2.7**, were further investigated using 1:1 mixtures of solvents. For example, crystallization from acetone-THF, 1,2-dichloroethane-THF and acetonitrile-THF mixtures resulted in the inclusion of THF. Crystallization of **rac-2.7** from a mixture of dichloromethane–acetone revealed preference for acetone inclusion. When crystallized from dioxane–THF, acetone–dioxane, nitromethane–dioxane mixtures, the host molecules uniformly favoured inclusion of dioxane. All these experiments suggest that during crystal formation, inclusion of solvent molecules containing oxygen is favoured over others, and amongst these dioxane enjoys greater preference.

Crystallization of 2.21: Crystallization of **rac-2.21** from chloroform, acetone and ethyl acetate *via* slow evaporation yielded plate-like crystals.

Racemic 2,6-di-*O*-(4-fluorobenzoyl) *myo*-inositol 1,3,5-orthoformate (2.22) and 2-*O*-(4-fluorobenzoyl) *myo*-inositol 1,3,5-orthoformate (2.23): Orthoformate **2.1** (0.760 g, 4 mmol) was acylated as described in general procedure A with 4-fluorobenzoyl chloride (~ 8.4 mmol) in dry pyridine (12 mL), yielding a golden yellow gum which was worked up and the residue chromatographed to obtain racemic **2.22** (1.104 g, 63%) and **2.23 (**0.150 g, 9%).

Data for **2.22**:

Mp: 176.5-178.5 ºC; **IR** (Nujol, cm^{-1}) ν: 3446, 1730, 1721; **^{1}H NMR** (200 MHz, CD_3COCD_3): δ 3.66-3.72 (1H, m), 3.80-3.97 (3H, m), 4.42 (1H, d, *J* = 4 Hz), 4.89-

5.00 (3H, m), 6.47–6.63 (4H, m), 7.34-7.48 (4H, m) ppm; **^{13}C NMR** (50.3 MHz, CD_3COCD_3): δ 65.3, 67.8, 69.7, 69.8, 70.5, 72.9, 103.8, 116.5 (d, $^2J_{C\text{-}F}$ = 22 Hz), 127.2 (d, $^4J_{C\text{-}F}$ = 3 Hz), 127.4 (d, $^4J_{C\text{-}F}$ = 3 Hz), 133.4 (t, $^3J_{C\text{-}F}$ = 9 Hz), 164.9, 165.5, 166.8 (d, $^1J_{C\text{-}F}$ = 252 Hz) ppm; **^{19}F NMR** (376.5 MHz, $CDCl_3$): -104.8 (1F, s), -104.3 (1F, s), -162.1 (C_6F_6) ppm; **Elemental analysis:** Calcd. for $C_{21}H_{16}O_8F_2$: C, 58.07; H, 3.71. Found: C, 57.81; H, 3.52 %.

Crystallization of 2.22: Crystals of **rac-2.22** obtained from methanol and ethyl acetate (form I) were solvent free forms, whereas crystallization from acetone, chloroform, dichloromethane, nitromethane, tetrahydrofuran, 1,2-dichloroethane, dimethyl sulphoxide, *p*-xylene, acetonitrile, benzene, toluene and *o*-xylene yielded solvatomorphs.

Data for **2.23**:

Mp: 174-176 ºC; **IR** (Nujol, cm^{-1}) ν: 3520-3350, 1704; **^{1}H NMR** (400 MHz, CD_3SOCD_3): δ 4.18-4.23 (1H, m), 4.24-4.31 (2H, m), 4.38-4.44 (2H, m), 5.45-6.05 (4H, m), 7.37 (2H, t, *J* = 8 Hz), 8.06-8.14 (2H, m) ppm; **^{13}C NMR** (100.6 MHz, CD_3SOCD_3): δ 64.5, 67.5, 70.0, 72.2, 102.2, 116.5 (d, $^2J_{C\text{-}F}$ = 22 Hz), 126.5 (d, $^4J_{C\text{-}F}$ = 2 Hz), 132.8 (d, $^3J_{C\text{-}F}$ = 9 Hz), 164.7, 165.8 (d, $^1J_{C\text{-}F}$ = 252 Hz) ppm; **^{19}F NMR** (376.5 MHz, CD_3SOCD_3): -106.1 (1F, s), -163.5 (C_6F_6) ppm; **Elemental analysis:** Calcd. for $C_{14}H_{13}O_7F$: C, 53.85; H, 4.20. Found: C, 53.94; H, 4.05 %.

Crystallization of 2.23: Crystallization of **rac-2.23** from ethyl acetate and acetone yielded thin plate-like crystals.

2,4,6-tri-*O*-(4-fluorobenzoyl) *myo*-inositol 1,3,5-orthoformate (2.24):

Orthoformate **2.1** (0.950 g, 5 mmol) was acylated as described in general procedure A with 4-fluorobenzoyl chloride (~ 11 mmol) in dry pyridine (12 mL), yielding a golden yellow gum which was worked up and the residue chromatographed to obtain racemic **2.22** (1.05 g, 48%) and **2.24 (**0.080 g, 3%).

Data for **2.24**:

Mp: 201-204 ºC; **IR** (Nujol, cm^{-1}) ν: 1732, 1716; **^{1}H NMR** (400 MHz, $CDCl_3$): δ 4.67-4.72 (2H, m) 5.01–5.06 (1H, m), 5.69-5.72 (1H, m), 5.74-5.77 (1H, m), 5.83-5.87 (2H, m), 6.93 (4H, t, *J* = 8.5 Hz), 7.19 (2H, t, *J* = 8.5 Hz), 7.86–7.93 (4H, m), 8.19-8.25 (2H, m) ppm; **^{13}C NMR** (50.3 MHz, $CDCl_3$): δ 63.9, 66.8, 68.6, 69.3,

103.3, 115.7 (d, $^{2}J_{C\text{-}F}$ = 22 Hz), 115.9 (d, $^{2}J_{C\text{-}F}$ = 22 Hz), 124.8 (d, $^{4}J_{C\text{-}F}$ = 3 Hz), 125.5 (d, $^{4}J_{C\text{-}F}$ = 2.5 Hz), 132.6 (t, $^{3}J_{C\text{-}F}$ = 9.9 Hz), 164.0, 165.3, 166.0 (d, $^{1}J_{C\text{-}F}$ = 256 Hz) ppm; **^{19}F NMR** (376.5 MHz, $CDCl_3$): -104.5 (1F, s), -104.0 (2F, s), -162.3 (C_6F_6) ppm; **Elemental analysis:** Calcd. for $C_{28}H_{19}O_9F_3$: C, 60.44; H, 3.44. Found: C, 60.43; H, 3.07 %.

Crystallization of 2.24: Crystallization of **rac-2.24** from ethyl acetate, acetone, chloroform and dichloromethane yielded rectangular plates.

Crystallization experiments of previously reported compounds:

Racemic 2,6-di-*O*-benzoyl-4-*O*-methyl *myo*-inositol 1,3,5-orthoformate (rac-2.2): When **rac-2.2** was crystallized from DCM-light petroleum (vapour diffusion), ethyl acetate-light petroleum (vapour diffusion), nitromethane, methanol, chloroform and acetone, square crystalline plates were obtained.

Racemic 2,6-di-*O*-benzoyl-4-*O*-allyl *myo*-inositol 1,3,5-orthoformate (rac-2.3): Crystallization of **rac-2.3** from nitromethane, ethyl acetate, acetone and chloroform yielded plate-like crystals.

Racemic 2,6-di-*O*-benzoyl *myo*-inositol 1,3,5-orthobenzoate (rac-1.179): Crystallization from ethyl acetate, chloroform, methanol, dichloromethane, nitromethane and acetone yielded solvent free squarish-hexagonal plate-like crystals[8] (form I) whereas thin, fibrous inclusion crystals were obtained from 2-propanol (form II) and toluene (form III). The appendix contains ^{1}H NMR spectra of the solvates. In some trials, form I and form II (form III) crystals were obtained concomitantly in 2-propanol and toluene.

2-*O*-acetyl *myo*-inositol 1,3,5-orthoformate (2.9): Crystallization of **2.9** by slow evaporation from ethyl acetate, acetone, dichloromethane and chloroform yielded hydrated crystals. Solvent free crystals were not obtained.

2.3 References

1. *Purification of Laboratory Chemicals*, Perrin, D. D. and Armarego, W. L. F. 2nd edition, Pergamon Press, Oxford, UK, 1988.
2. Beilstein, 2, IV, 1471.
3. *Vogel's Textbook of Practical Organic Chemistry*, 5th edition, Longman, UK, 1989.
4. P. Uhlmann and A. Vasella, *Helv. Chim. Acta.* **1992**, *75*, 1979-1994.

5. T. Das and M. S. Shashidhar, *Carbohydr. Res*., **1997**, *297*, 243-249.
6. U. Samanta, V. G. Puranik, P. Chakrabarti, P. Thoniyot and M. S. Shashidhar, *Acta Cryst. Sect. C*, **1998**, *54*, 1289-1291.
7. G. Bhosekar, C. Murali, R. G. Gonnade, M. S. Shashidhar, and M. M. Bhadbhade, *Cryst. Growth Des*., **2005**, *5*, 1977-1982.
8. C. Murali, M. S. Shashidhar, R. G. Gonnade and M. M. Bhadbhade, *Eur. J. Org. Chem.*, **2007**, 1153-1159.
9. R. G. Gonnade, M. M. Bhadbhade and M. S. Shashidhar, *CrystEngComm*, **2008**, *10*, 288-296.
10. R. G. Gonnade, M. M. Bhadbhade, M. S. Shashidhar and A. K. Sanki, *Chem. Commun.*, **2005**, 5870-5872.
11. K. M. Sureshan and M. S. Shashidhar, *Tetrahedron Lett.*, **2000**, *41*, 4185-4188.

2.4 Appendix (NMR and IR spectra)

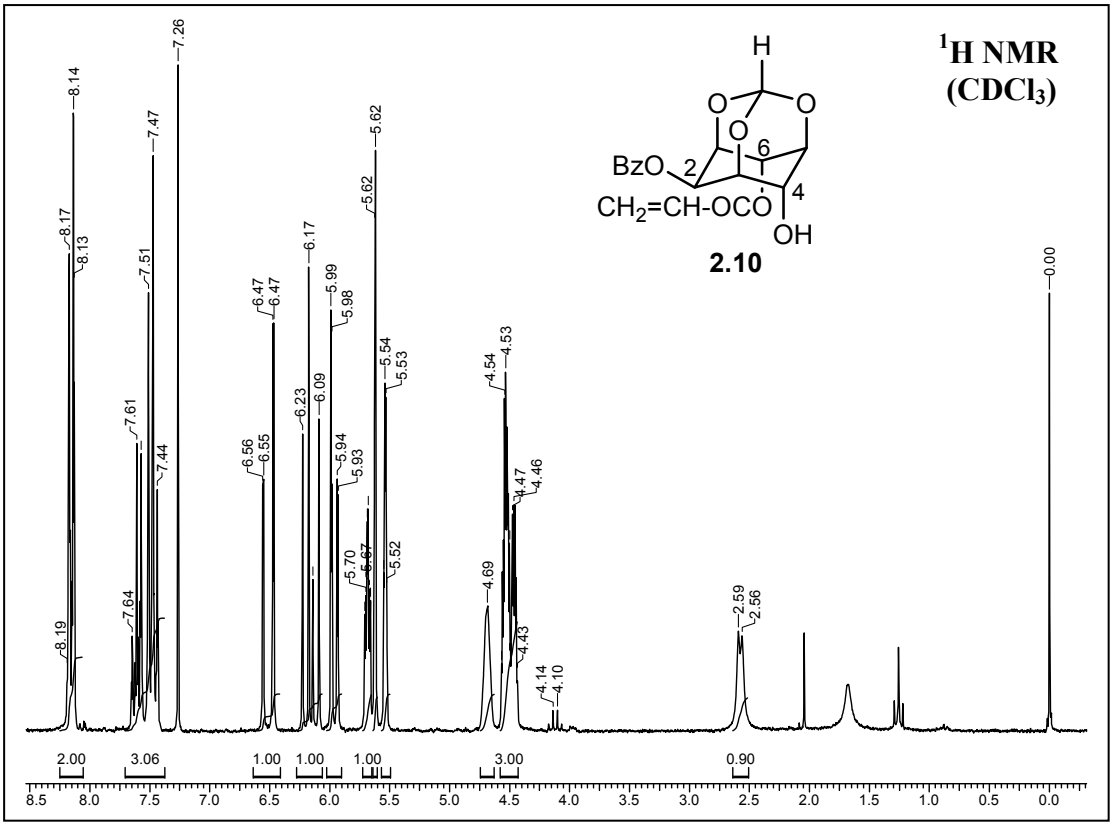

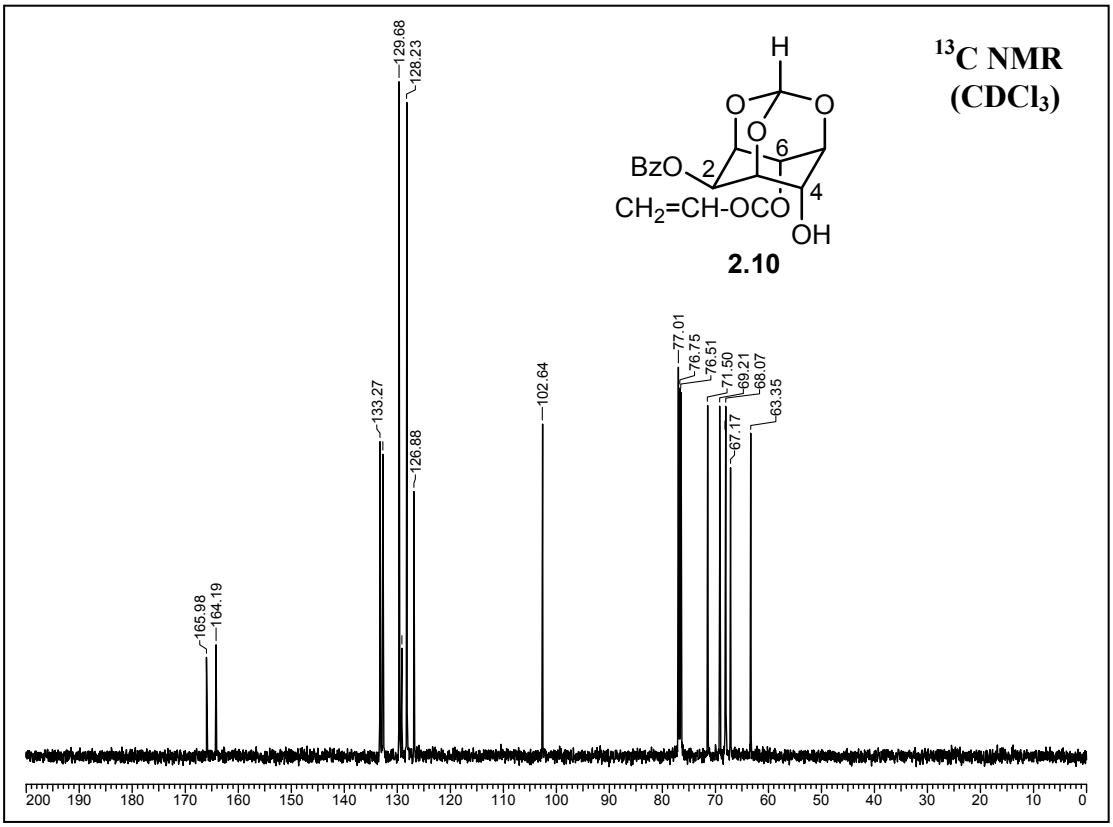

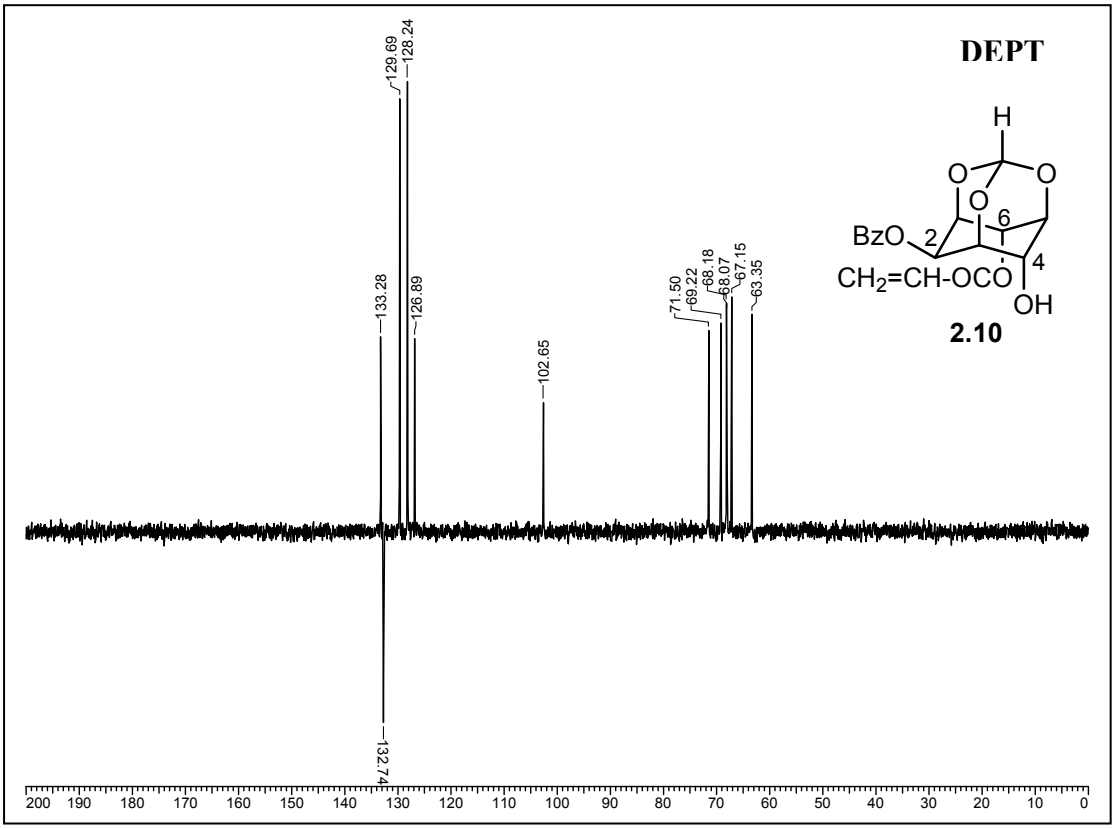
DEPT
129.69
128.24
133.28
126.89
102.65
71.50
69.22
68.18
68.07
67.15
63.35
132.74
H
O
O
O
6
BzO
2
4
CH2=CH-OCO
OH
2.10
200 190 180 170 160 150 140 130 120 110 100 90 80 70 60 50 40 30 20 10 0

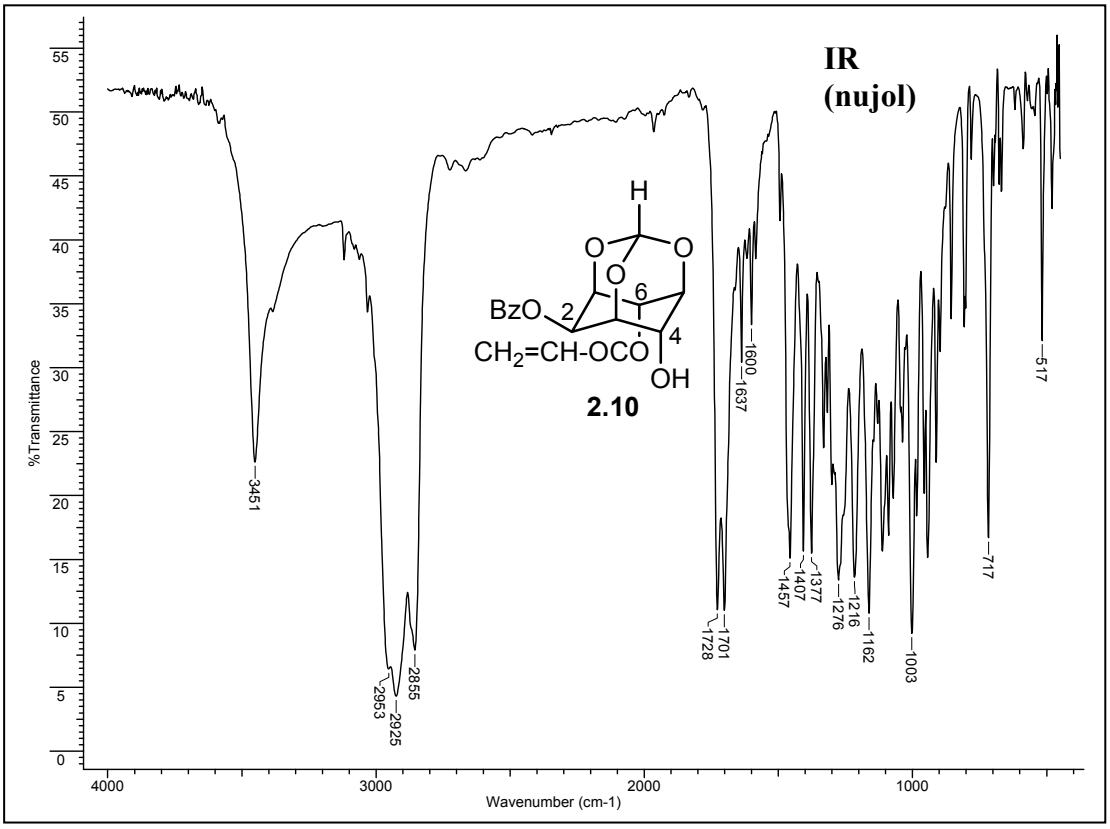
IR
(nujol)
%Transmittance
3451
2953
2925
2855
1728
1701
1637
1600
1457
1407
1377
1276
1216
1162
1003
717
517
H
O
O
O
6
BzO
2
4
CH2=CH-OCO
OH
2.10
4000
3000
2000
1000
Wavenumber (cm-1)

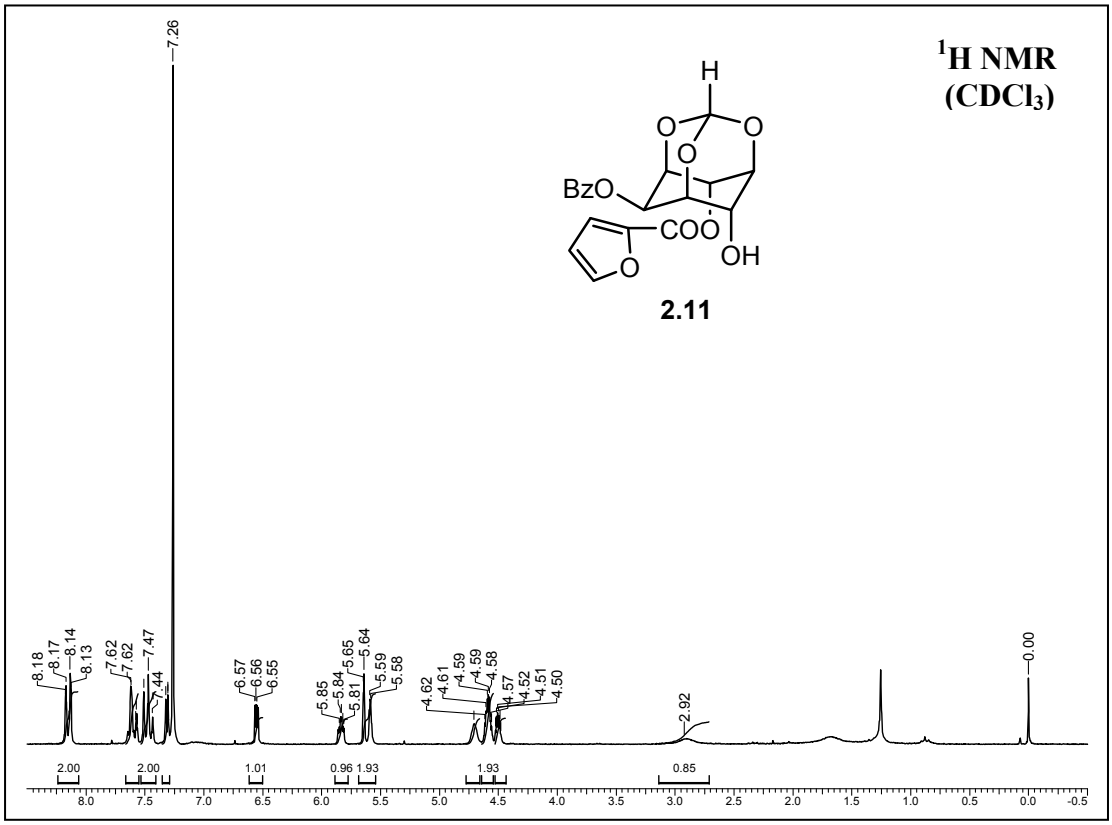
^{1}H NMR
(CDCl$_3$)
H
O
O
O
BzO
COO
OH
O
2.11
7.26
8.18
8.17
8.14
8.13
7.62
7.62
7.47
7.44
6.57
6.56
6.55
5.85
5.84
5.81
5.65
5.64
5.59
5.58
4.62
4.61
4.59
4.59
4.58
4.57
4.52
4.51
4.50
2.92
0.00
2.00
2.00
1.01
0.96
1.93
1.93
0.85

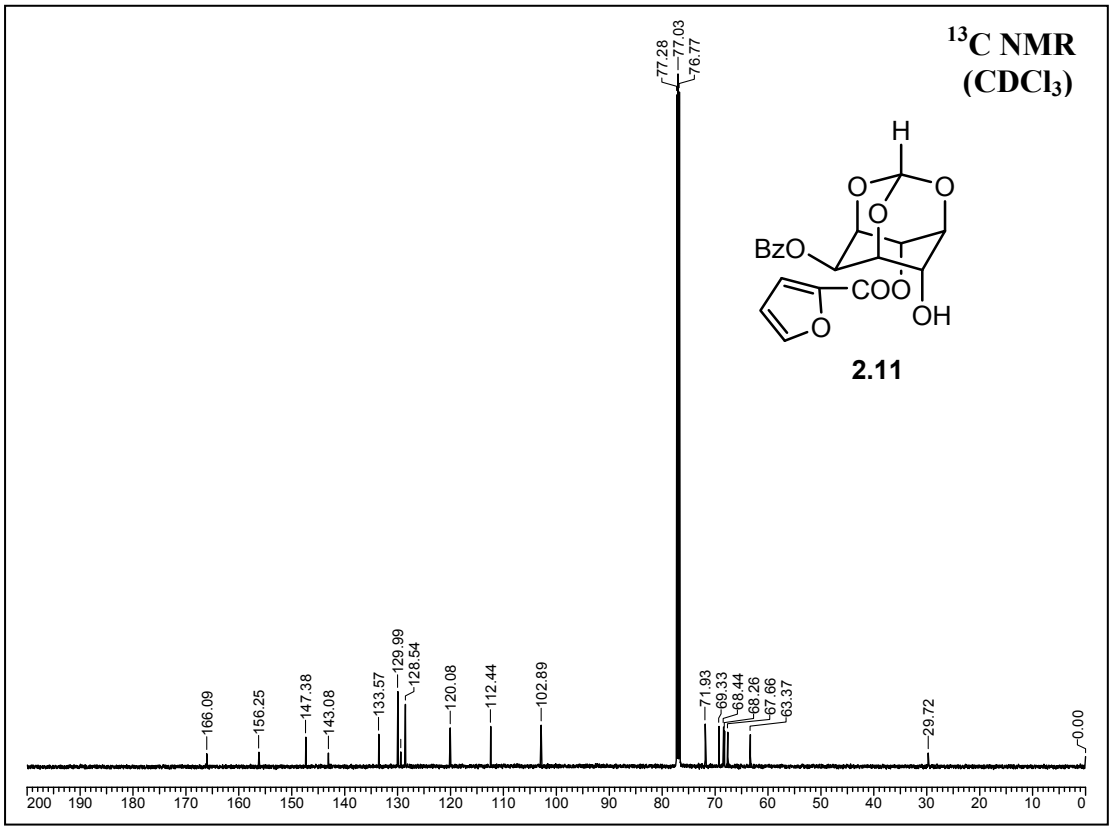
^{13}C NMR
(CDCl$_3$)
H
O
O
O
BzO
COO
OH
O
2.11
77.28
77.03
76.77
166.09
156.25
147.38
143.08
133.57
129.99
128.54
120.08
112.44
102.89
71.93
69.33
68.44
68.26
67.66
63.37
29.72
0.00

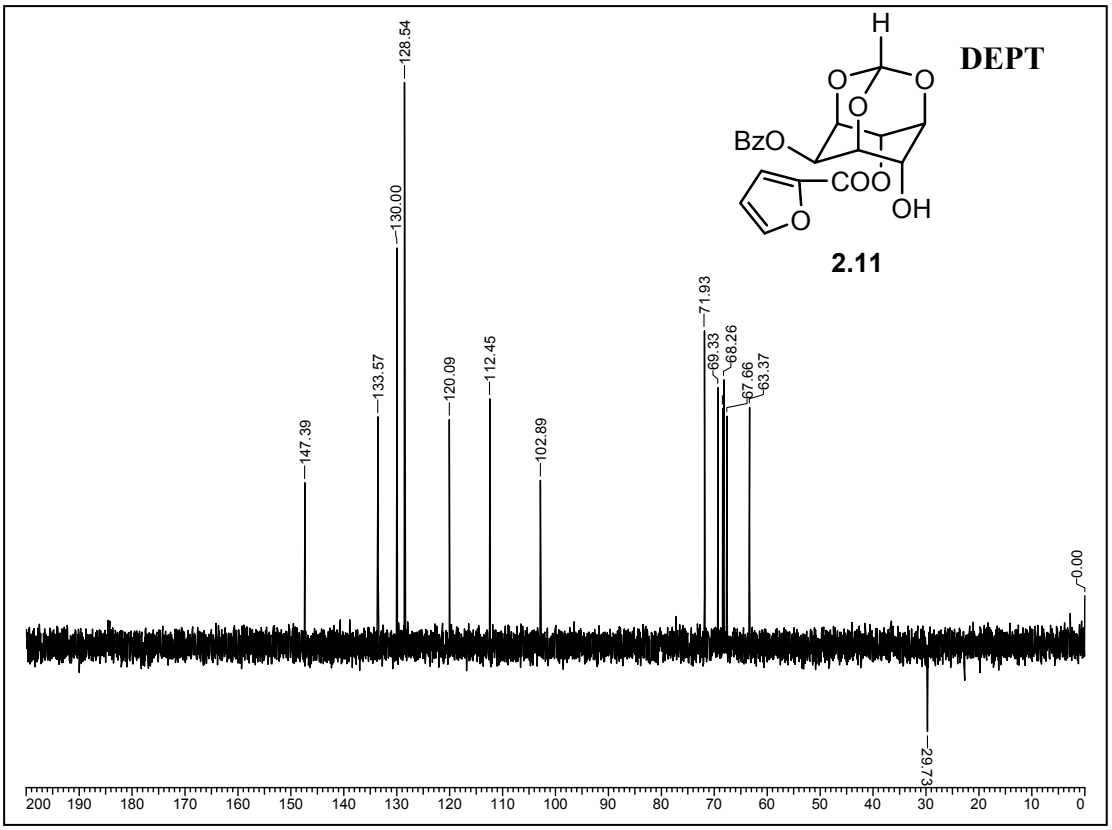
DEPT
2.11
128.54
130.00
147.39
133.57
120.09
112.45
102.89
71.93
69.33
68.26
67.66
63.37
0.00
29.73

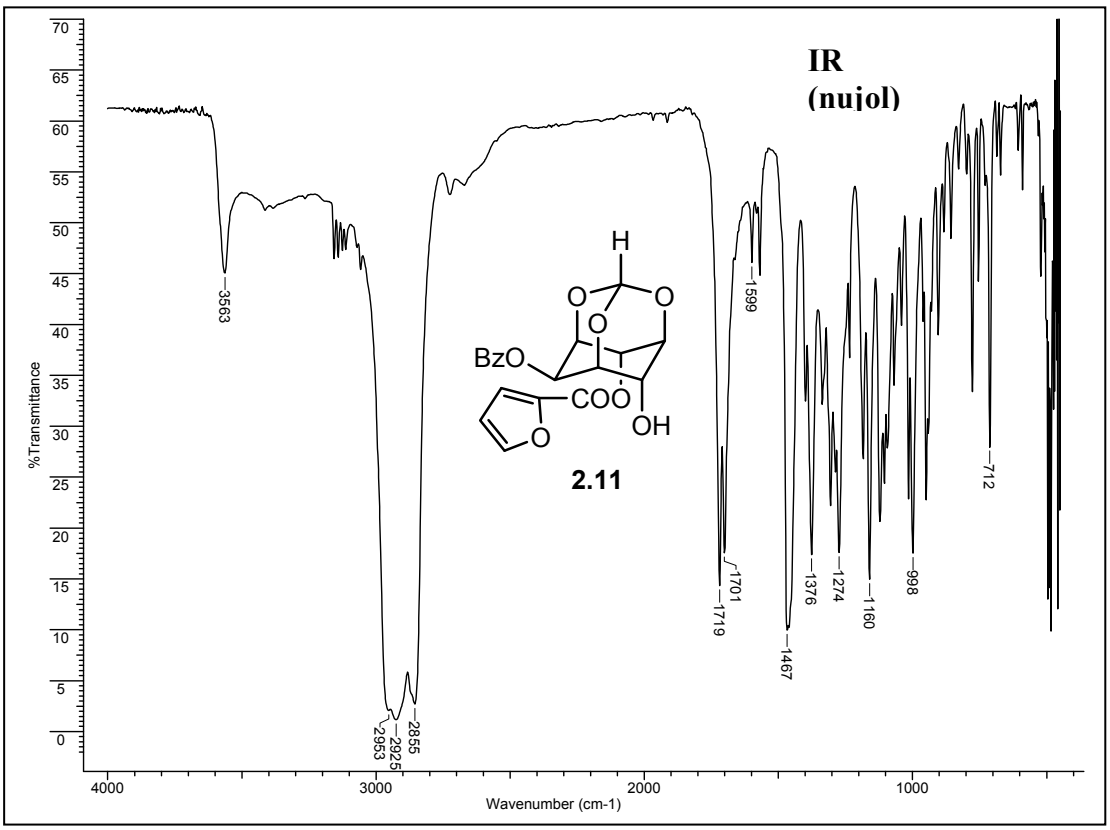
IR
(nujol)
2.11
%Transmittance
Wavenumber (cm-1)
3563
2953
2925
2855
1719
1701
1599
1467
1376
1274
1160
998
712

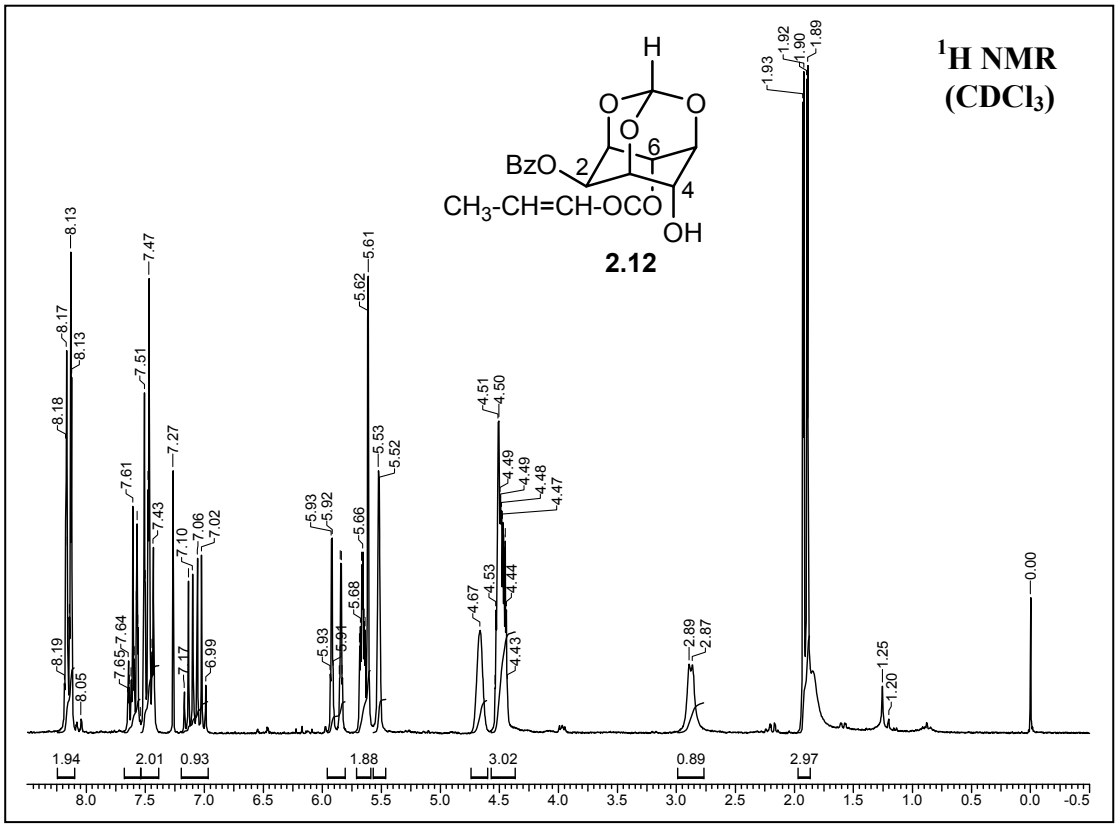
^{1}H NMR
(CDCl$_3$)
2.12

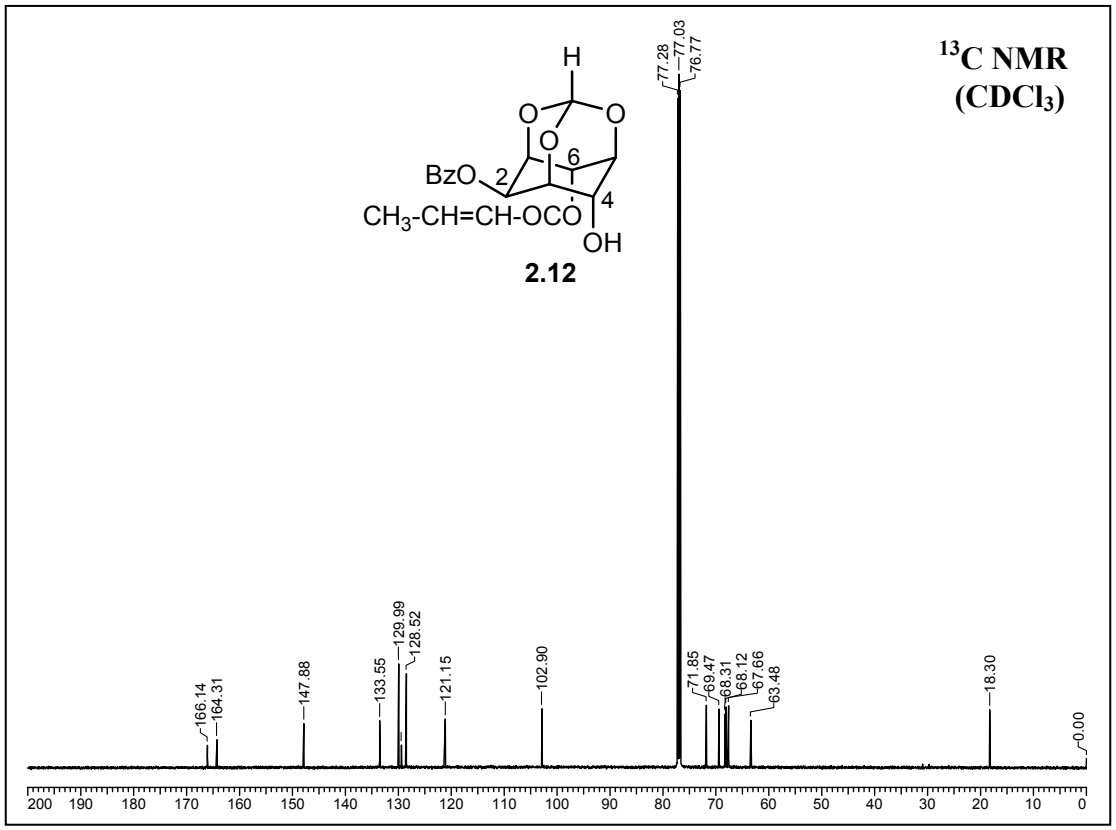
^{13}C NMR
(CDCl$_3$)
2.12

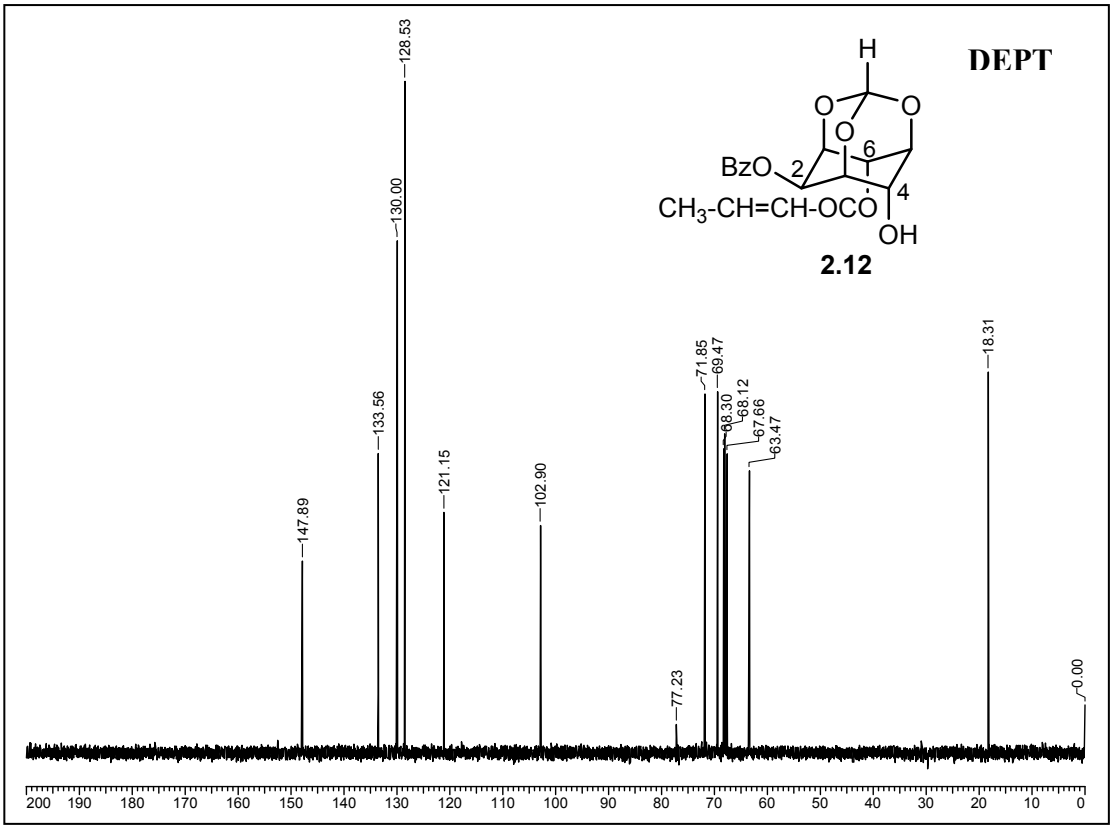
DEPT
128.53
130.00
133.56
147.89
121.15
102.90
71.85
69.47
68.30
68.12
67.66
63.47
77.23
18.31
0.00
H
O
O
O
6
BzO
2
4
CH3-CH=CH-OCO
OH
2.12
200 190 180 170 160 150 140 130 120 110 100 90 80 70 60 50 40 30 20 10 0

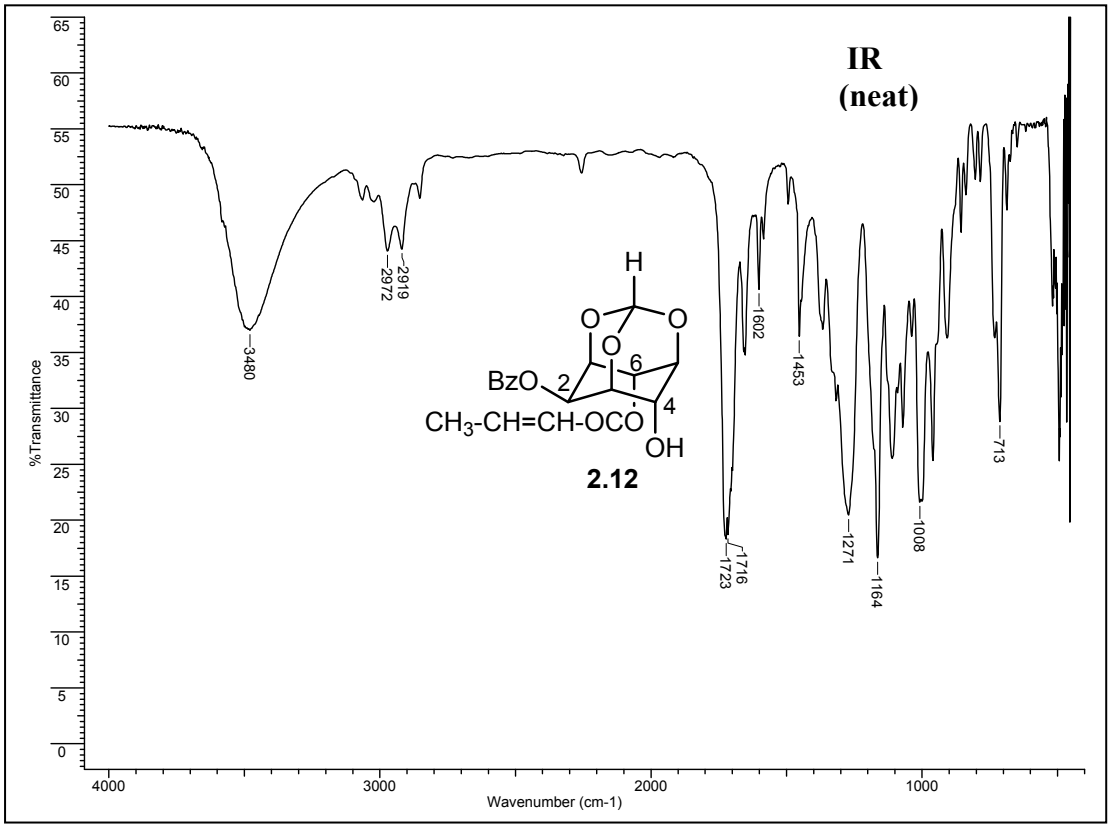
IR
(neat)
%Transmittance
65 60 55 50 45 40 35 30 25 20 15 10 5 0
3480
2972
2919
1602
1453
1723
1716
1271
1164
1008
713
H
O
O
O
6
BzO
2
4
CH3-CH=CH-OCO
OH
2.12
4000
3000
2000
1000
Wavenumber (cm-1)

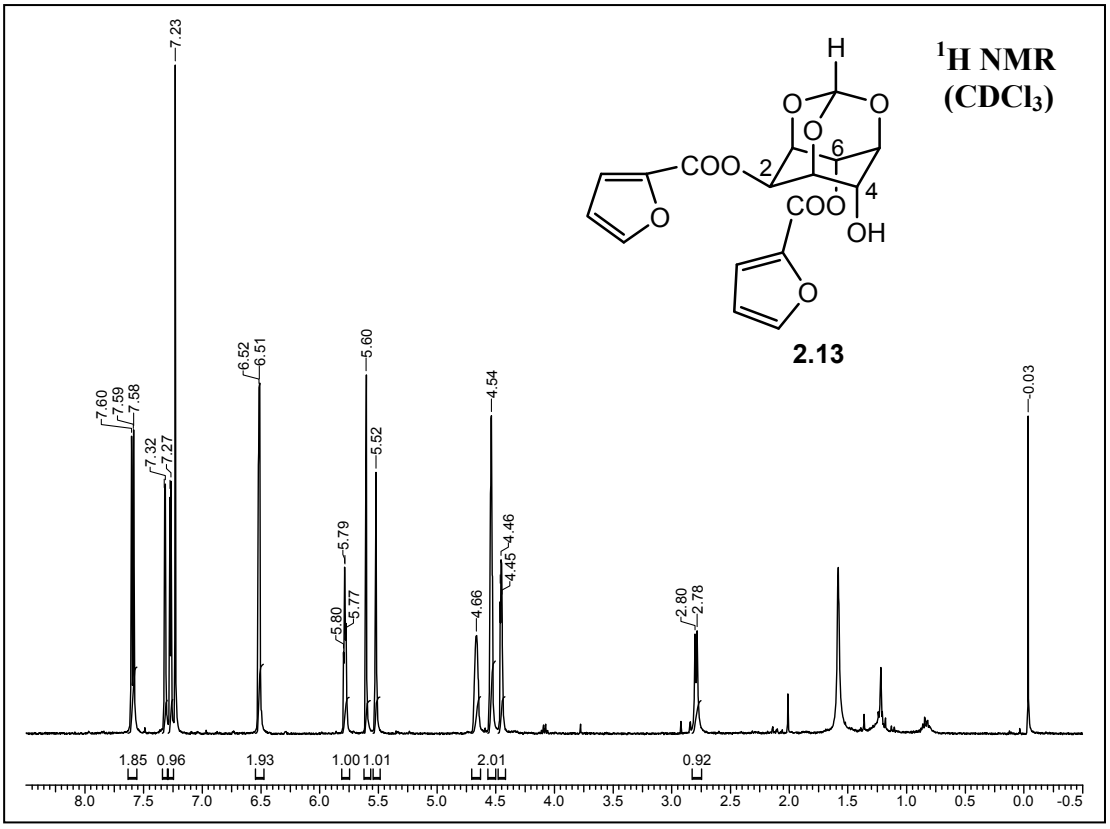
^{1}H NMR
(CDCl$_3$)
2.13
7.60
7.59
7.58
7.32
7.27
7.23
6.52
6.51
5.80
5.79
5.77
5.60
5.52
4.66
4.54
4.46
4.45
2.80
2.78
0.03
1.85
0.96
1.93
1.00
1.01
2.01
0.92

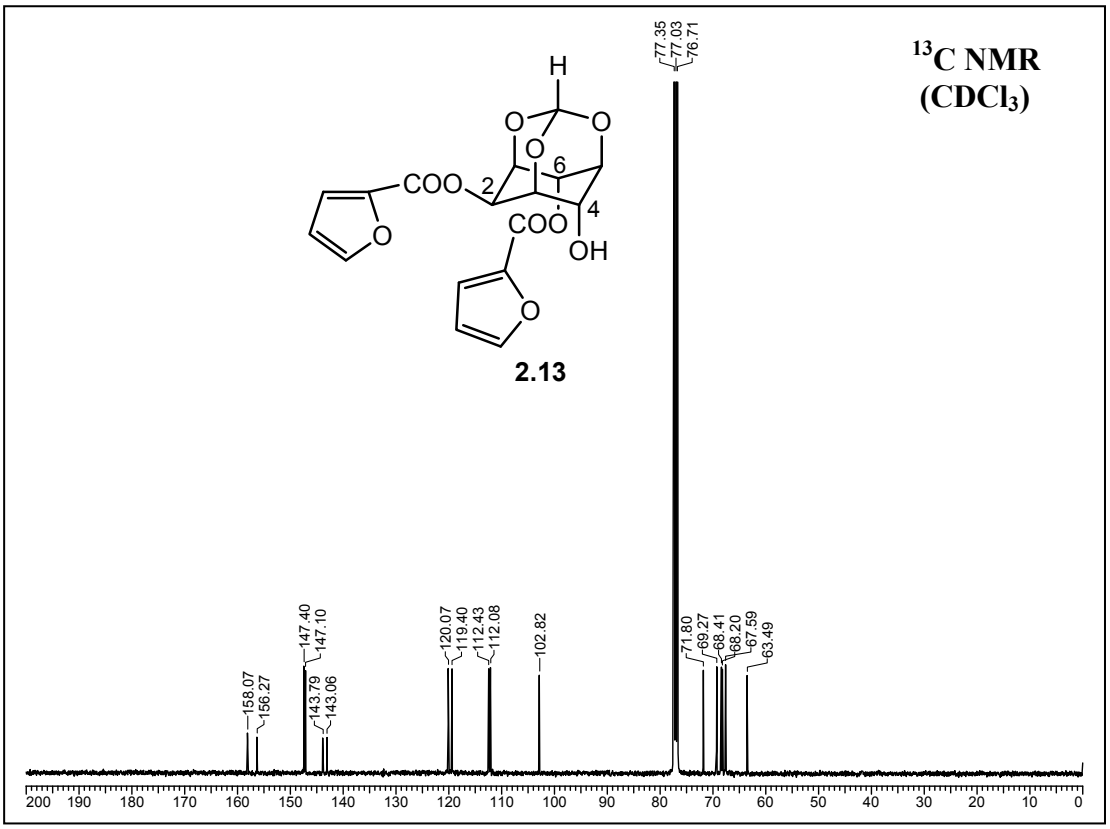
^{13}C NMR
(CDCl$_3$)
2.13
77.35
77.03
76.71
158.07
156.27
147.40
147.10
143.79
143.06
120.07
119.40
112.43
112.08
102.82
71.80
69.27
68.41
68.20
67.59
63.49

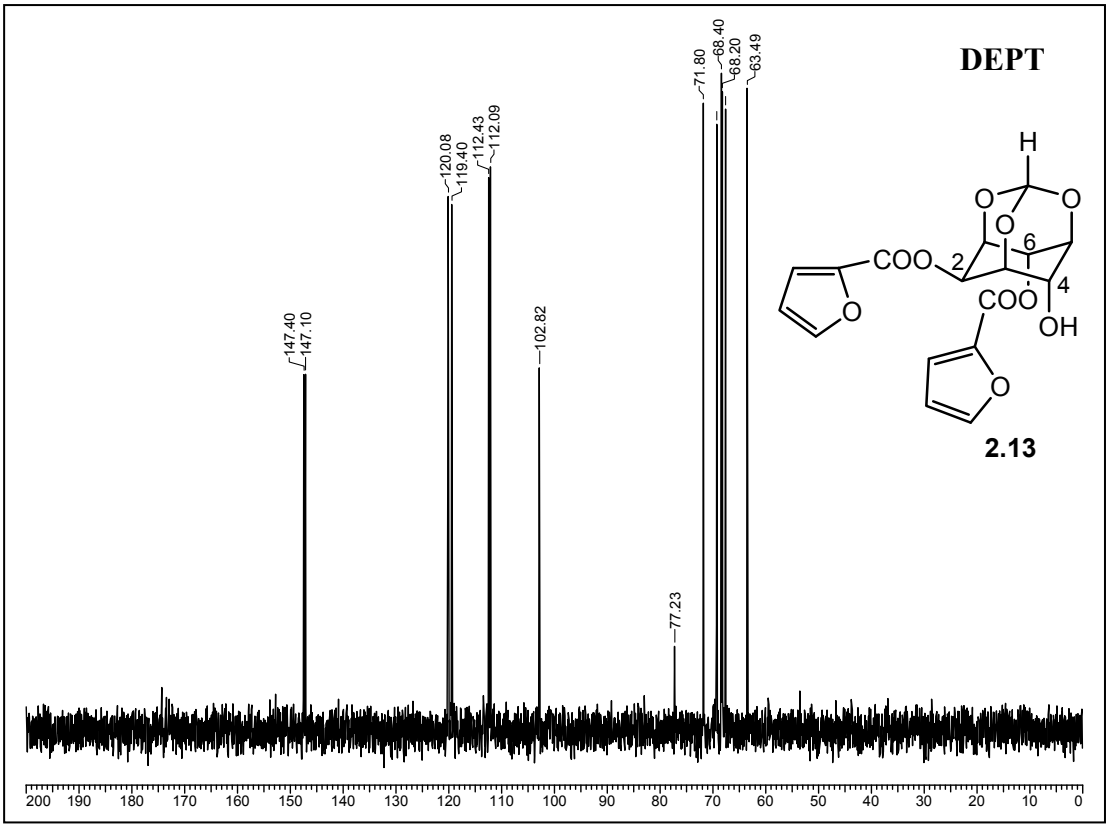
DEPT
147.40
147.10
120.08
119.40
112.43
112.09
102.82
77.23
71.80
68.40
68.20
63.49
2.13

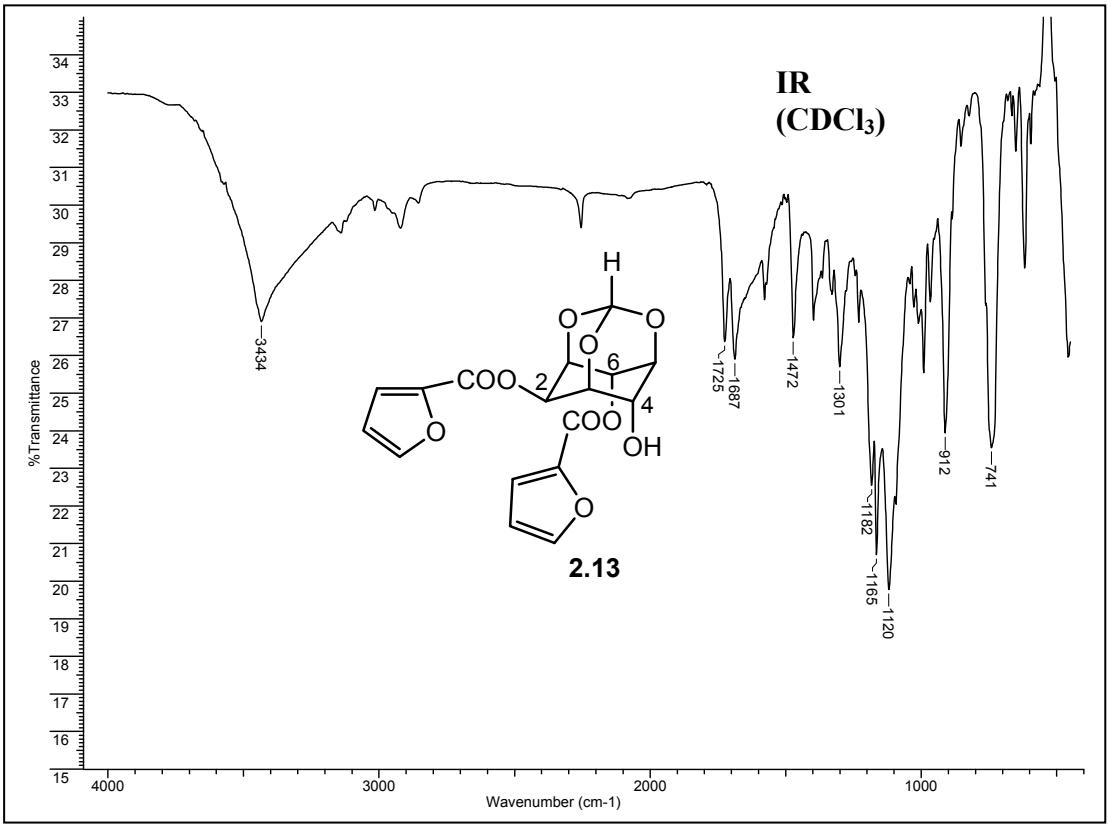
IR
(CDCl3)
%Transmittance
Wavenumber (cm-1)
3434
1725
1687
1472
1301
1182
1165
1120
912
741
2.13

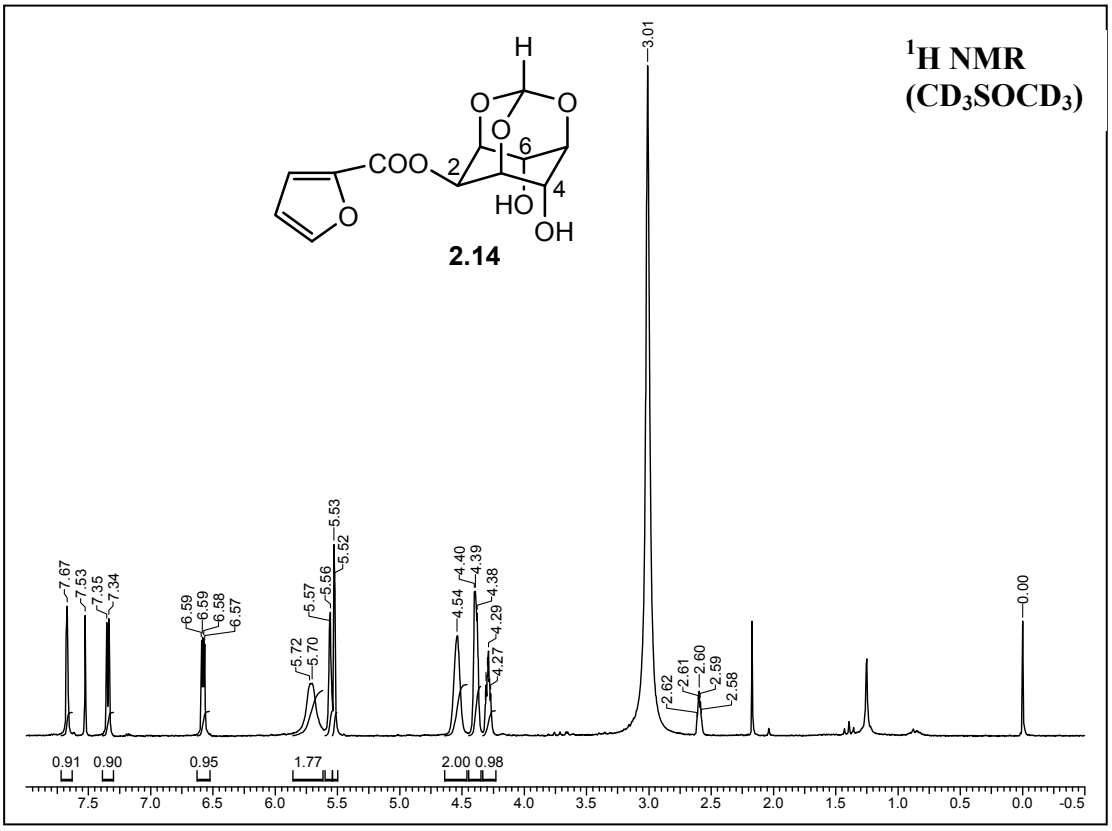
^{1}H NMR
(CD$_3$SOCD$_3$)
2.14
3.01
7.67
7.53
7.35
7.34
6.59
6.59
6.58
6.57
5.72
5.70
5.57
5.56
5.53
5.52
4.54
4.40
4.39
4.38
4.29
4.27
2.62
2.61
2.60
2.59
2.58
0.00
0.91
0.90
0.95
1.77
2.00
0.98

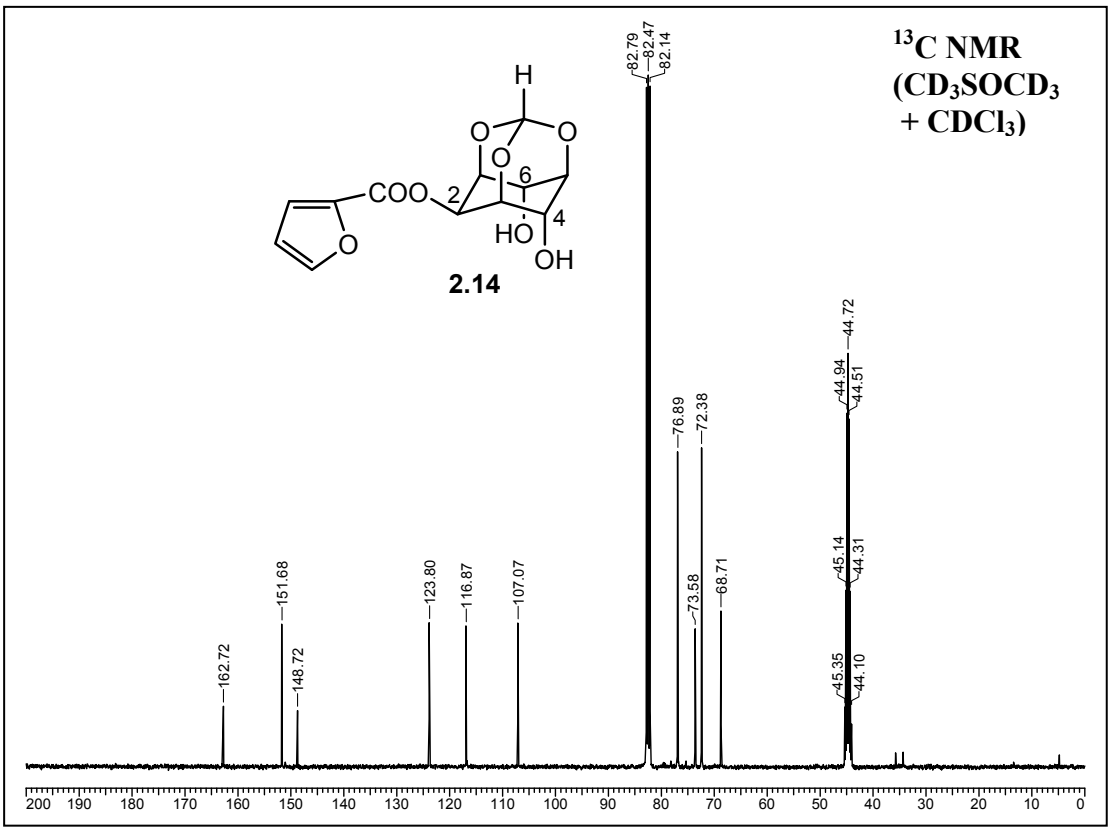
^{13}C NMR
(CD$_3$SOCD$_3$
+ CDCl$_3$)
2.14
82.79
82.47
82.14
76.89
72.38
73.58
68.71
44.72
44.94
44.51
45.14
44.31
45.35
44.10
162.72
151.68
148.72
123.80
116.87
107.07

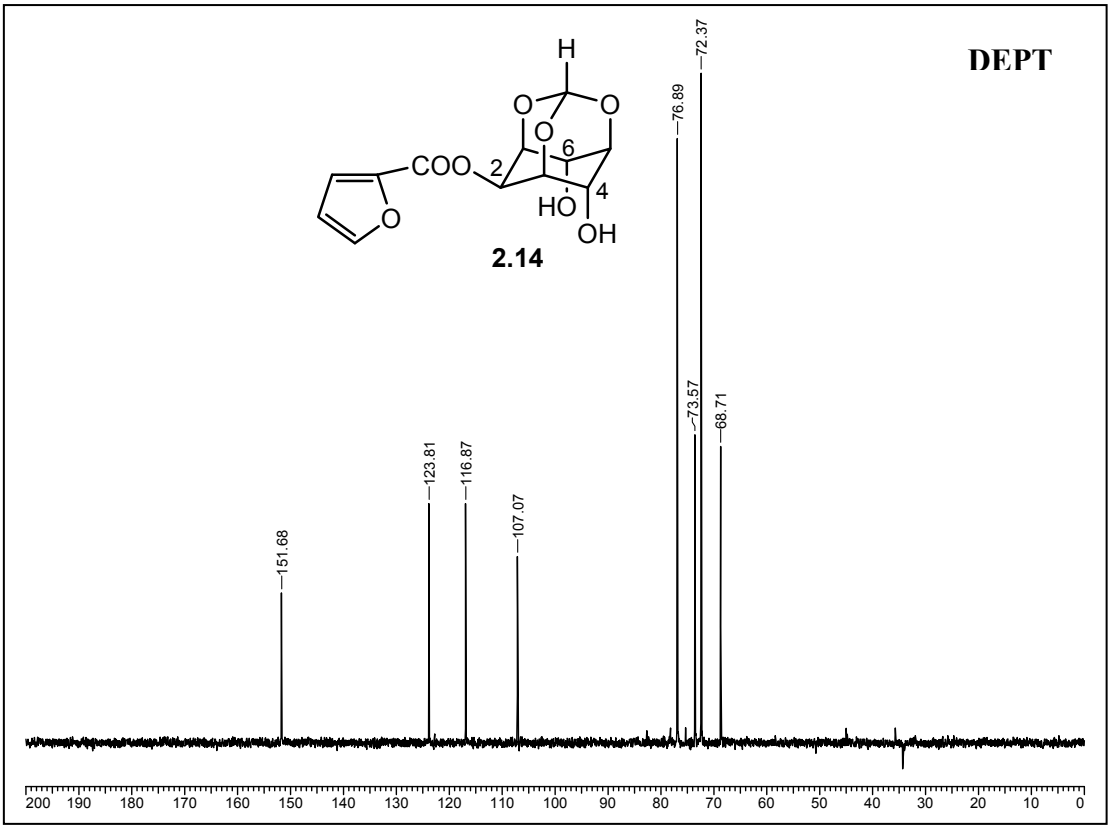
DEPT
H
O
O
O
6
COO
2
HO
4
OH
O
2.14
72.37
76.89
73.57
68.71
123.81
116.87
107.07
151.68
200 190 180 170 160 150 140 130 120 110 100 90 80 70 60 50 40 30 20 10 0

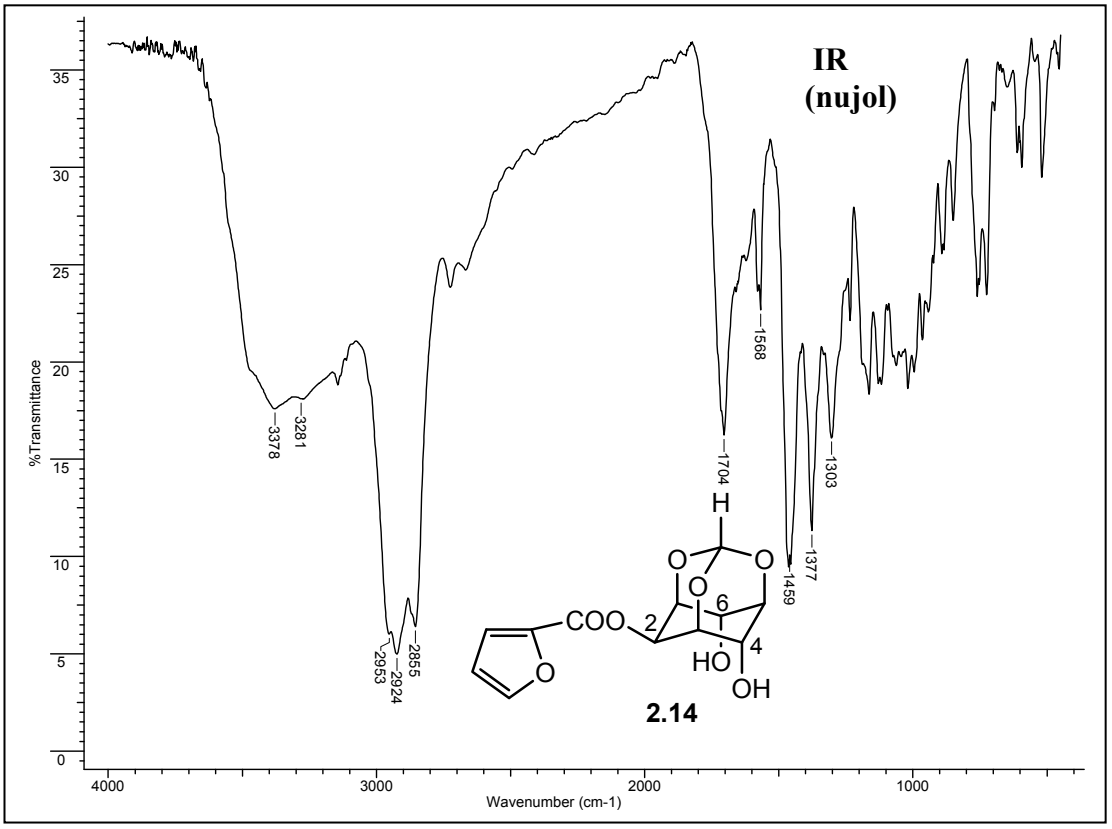
IR
(nujol)
%Transmittance
35
30
25
20
15
10
5
0
3378
3281
2953
2924
2855
1704
1588
1459
1377
1303
H
O
O
O
6
COO
2
HO
4
OH
O
2.14
4000
3000
2000
1000
Wavenumber (cm-1)

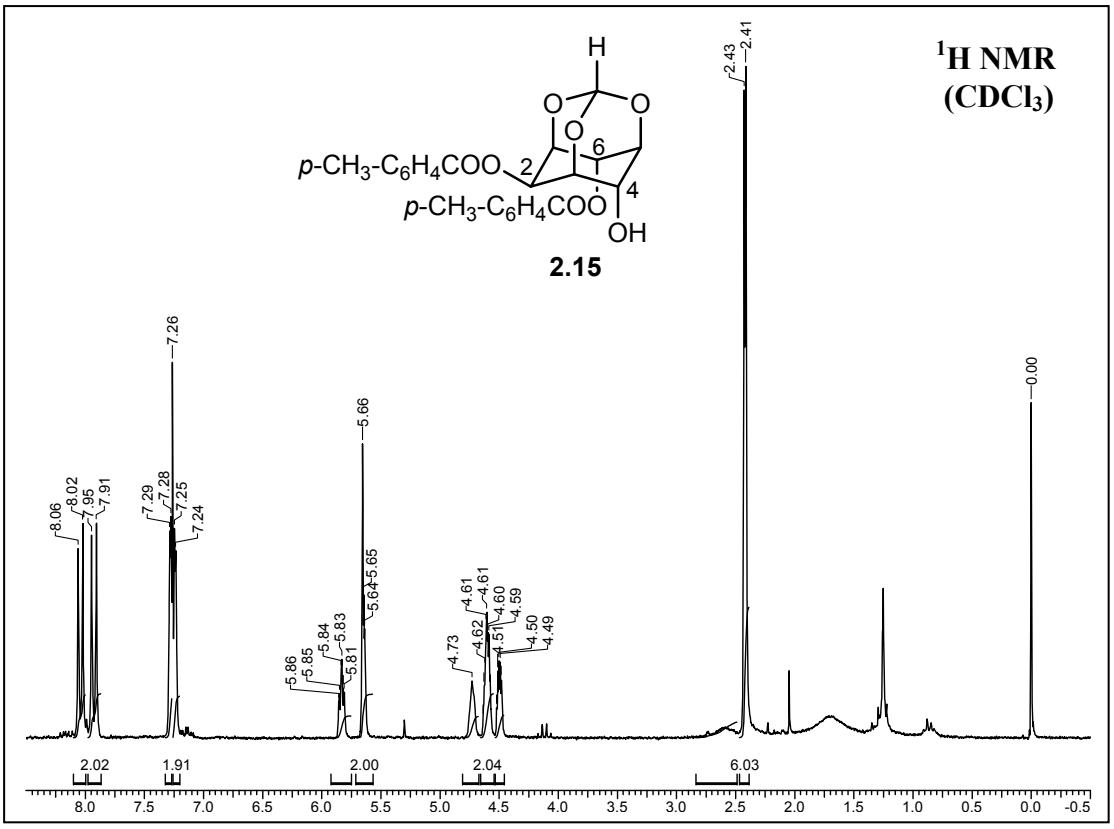
^{1}H NMR
(CDCl$_3$)
p-CH$_3$-C$_6$H$_4$COO
p-CH$_3$-C$_6$H$_4$COO
OH
2.15
8.06
8.02
7.95
7.91
7.29
7.28
7.25
7.24
7.26
5.86
5.85
5.84
5.83
5.81
5.66
5.64
5.65
4.73
4.62
4.61
4.61
4.60
4.59
4.51
4.50
4.49
2.43
2.41
0.00
2.02
1.91
2.00
2.04
6.03

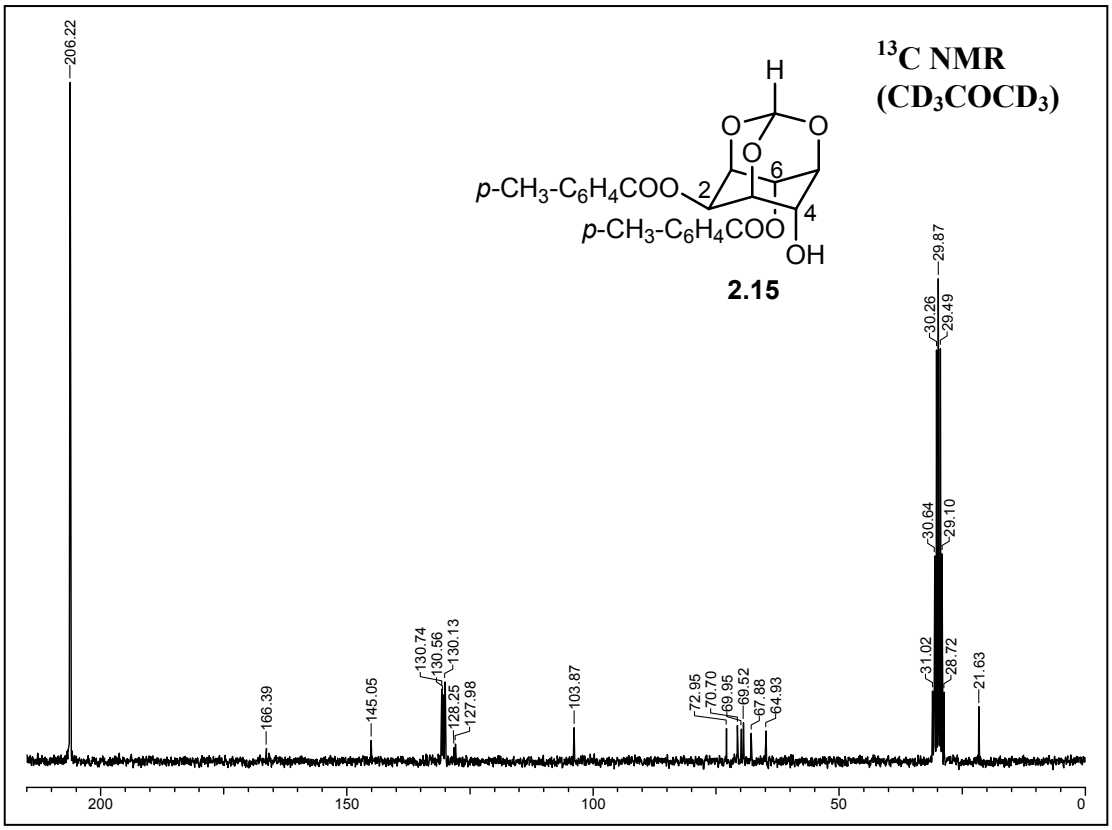
^{13}C NMR
(CD$_3$COCD$_3$)
p-CH$_3$-C$_6$H$_4$COO
p-CH$_3$-C$_6$H$_4$COO
OH
2.15
206.22
166.39
145.05
130.74
130.56
130.13
128.25
127.98
103.87
72.95
70.70
69.95
69.52
67.88
64.93
31.02
30.64
30.26
29.87
29.49
29.10
28.72
21.63

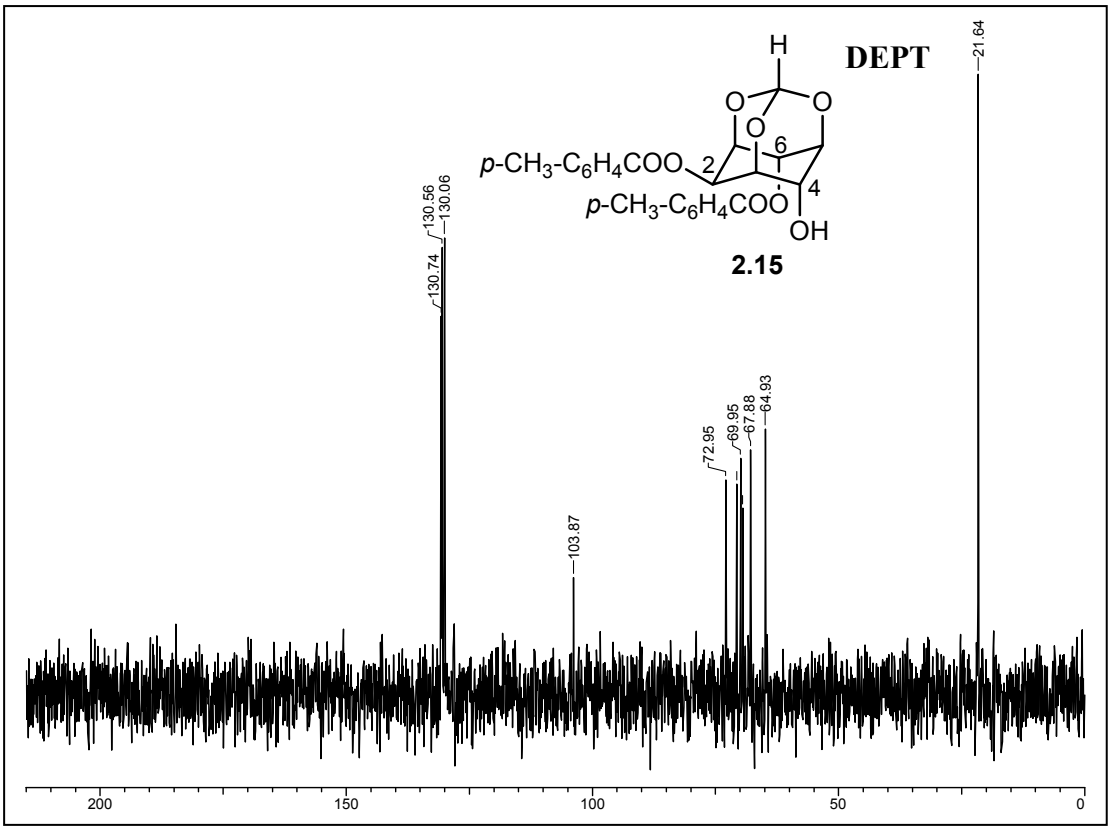
DEPT
H
O
O
O
6
p-CH3-C6H4COO
2
4
p-CH3-C6H4COO
OH
2.15
21.64
130.56
130.06
130.74
103.87
72.95
69.95
67.88
64.93
200
150
100
50
0

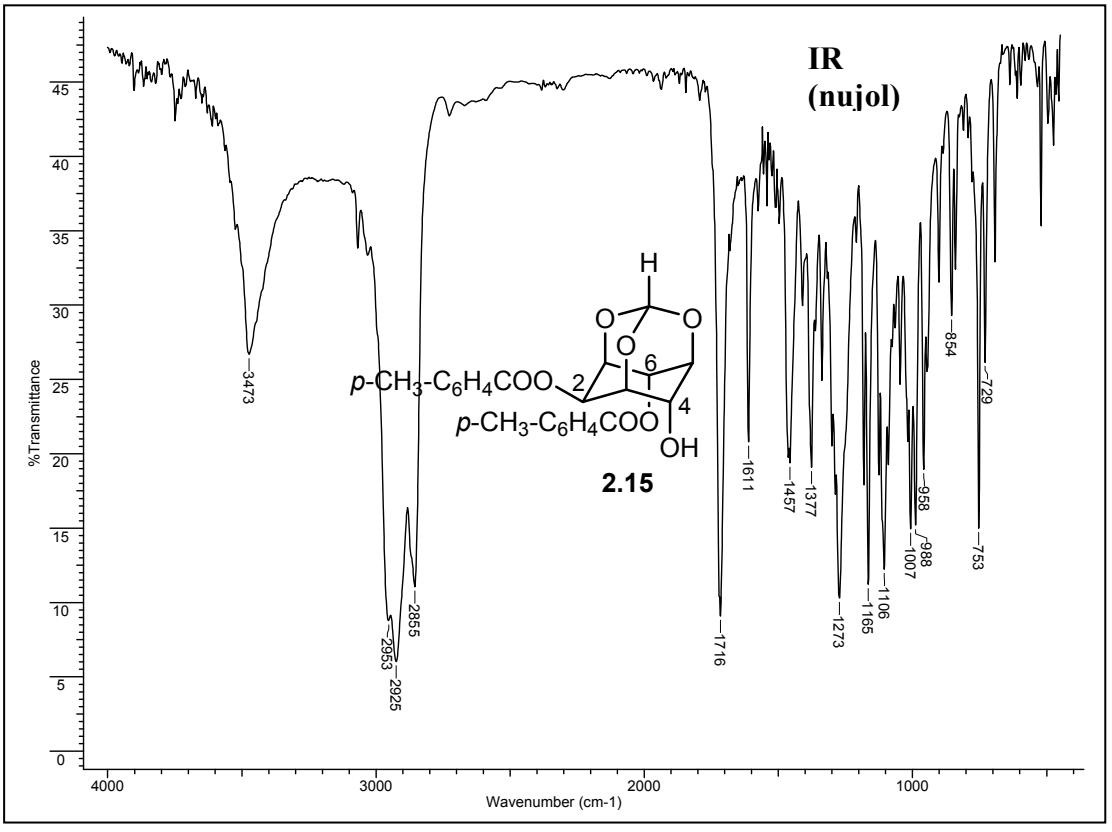
IR
(nujol)
%Transmittance
Wavenumber (cm-1)
4000
3000
2000
1000
3473
2953
2925
2855
1716
1611
1457
1377
1273
1165
1106
1007
988
958
854
753
729
H
O
O
O
6
p-CH3-C6H4COO
2
4
p-CH3-C6H4COO
OH
2.15

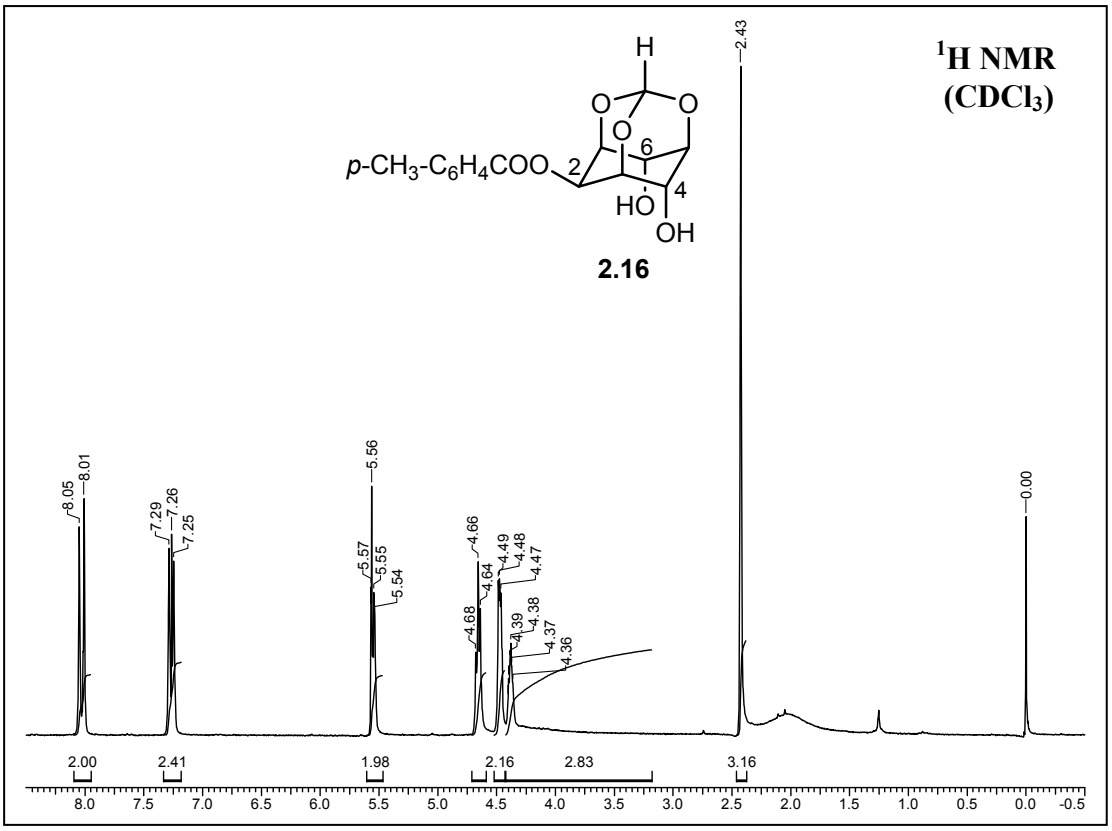
^{1}H NMR
(CDCl$_3$)
p-CH$_3$-C$_6$H$_4$COO
HO
OH
2.16
8.05
8.01
7.29
7.26
7.25
5.57
5.56
5.55
5.54
4.68
4.66
4.64
4.49
4.48
4.47
4.39
4.38
4.37
4.36
2.43
0.00
2.00
2.41
1.98
2.16
2.83
3.16

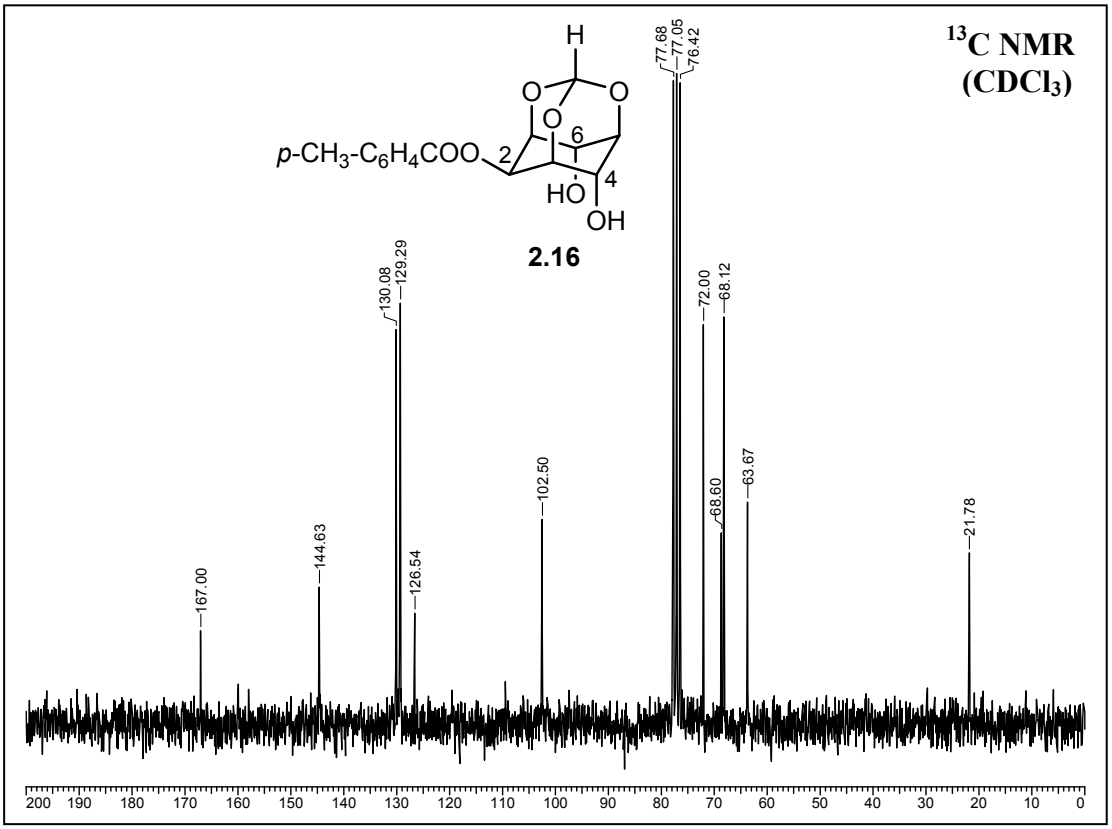
^{13}C NMR
(CDCl$_3$)
p-CH$_3$-C$_6$H$_4$COO
HO
OH
2.16
167.00
144.63
130.08
129.29
126.54
102.50
77.68
77.05
76.42
72.00
68.60
68.12
63.67
21.78

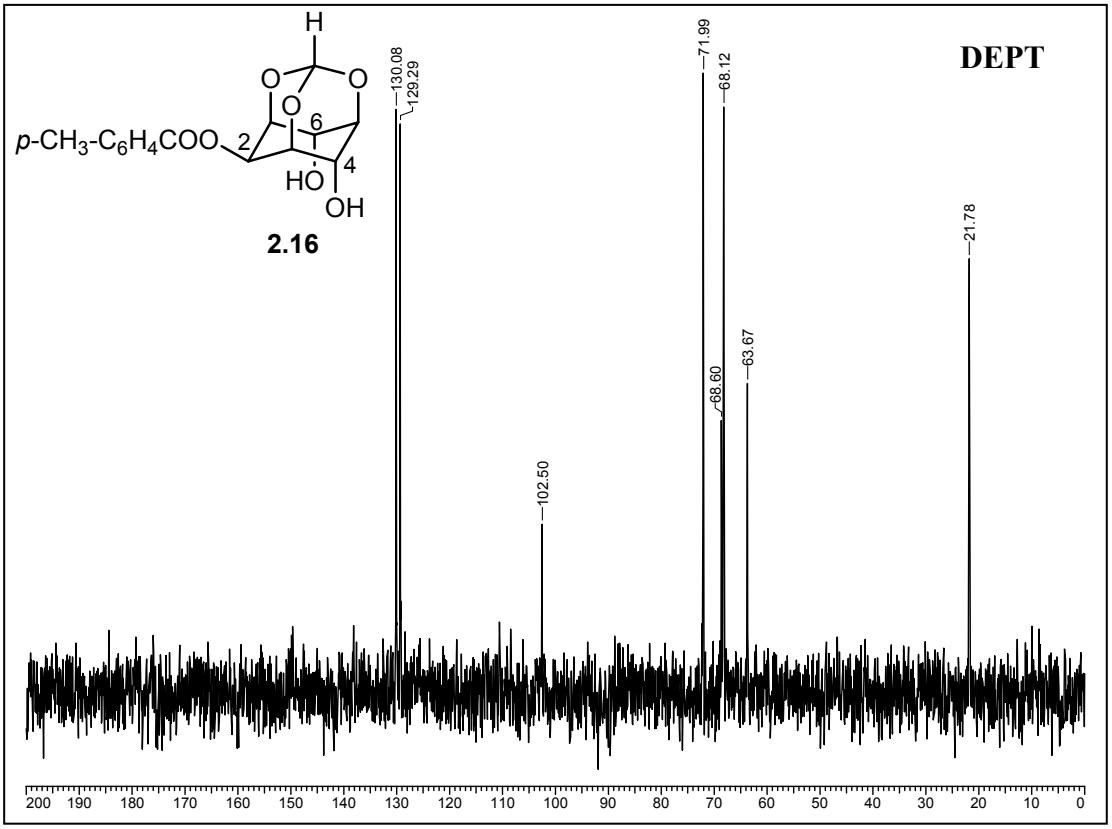
DEPT
H
O
O
O
6
2
4
HO
OH
p-CH3-C6H4COO
2.16
130.08
129.29
71.99
68.12
102.50
68.60
63.67
21.78
200 190 180 170 160 150 140 130 120 110 100 90 80 70 60 50 40 30 20 10 0

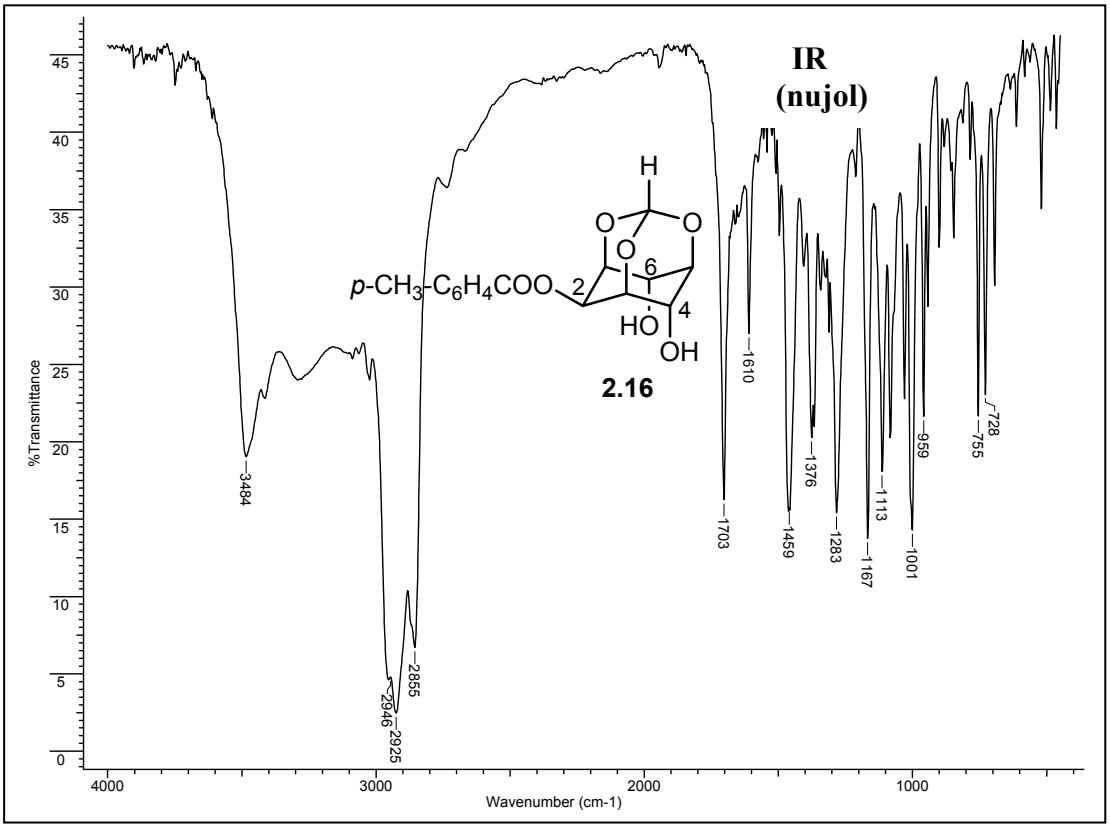
IR
(nujol)
%Transmittance
45 40 35 30 25 20 15 10 5 0
H
O
O
O
6
2
4
HO
OH
p-CH3-C6H4COO
2.16
3484
2946
2925
2855
1703
1610
1459
1376
1283
1167
1113
1001
959
755
728
4000
3000
2000
1000
Wavenumber (cm-1)

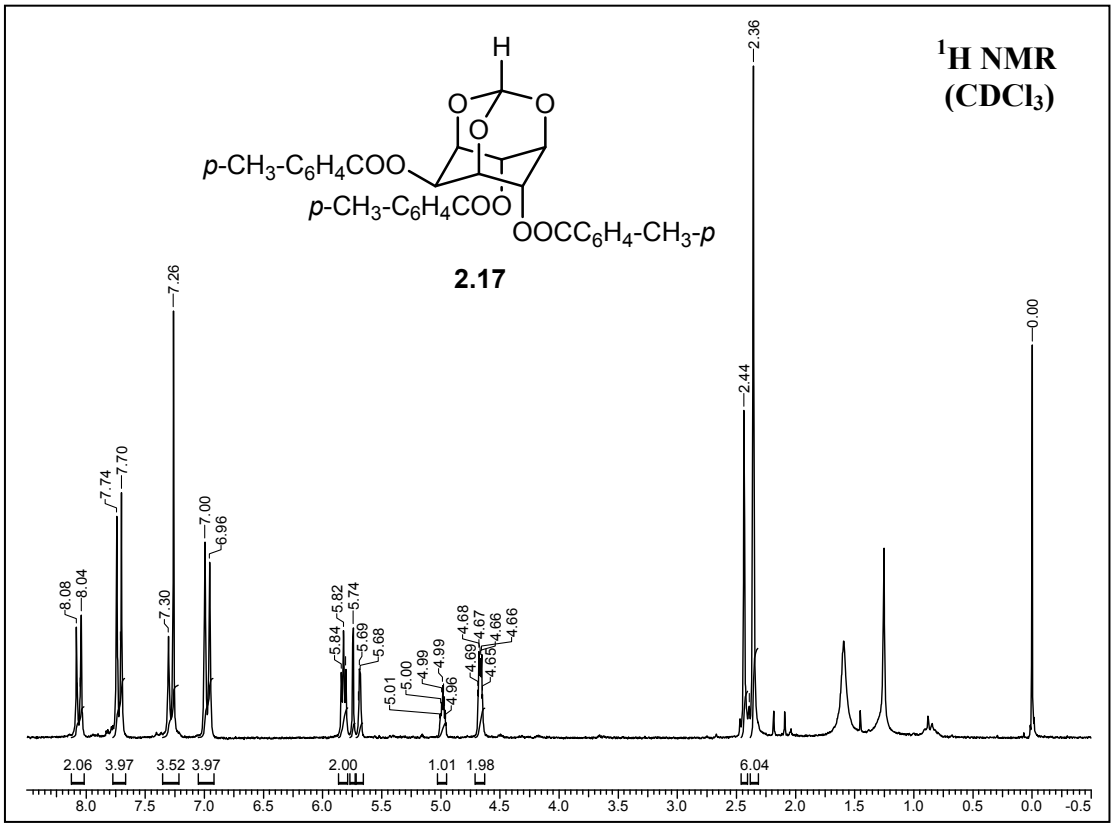
^{1}H NMR
(CDCl$_3$)
2.17
p-CH3-C6H4COO
p-CH3-C6H4COO
OOCC6H4-CH3-p
2.36
7.26
0.00
2.44
7.74
7.70
7.00
6.96
8.08
8.04
7.30
5.82
5.74
5.84
5.69
5.68
4.68
4.67
4.66
4.66
5.01
5.00
4.99
4.99
4.96
4.69
4.65
2.06
3.97
3.52
3.97
2.00
1.01
1.98
6.04

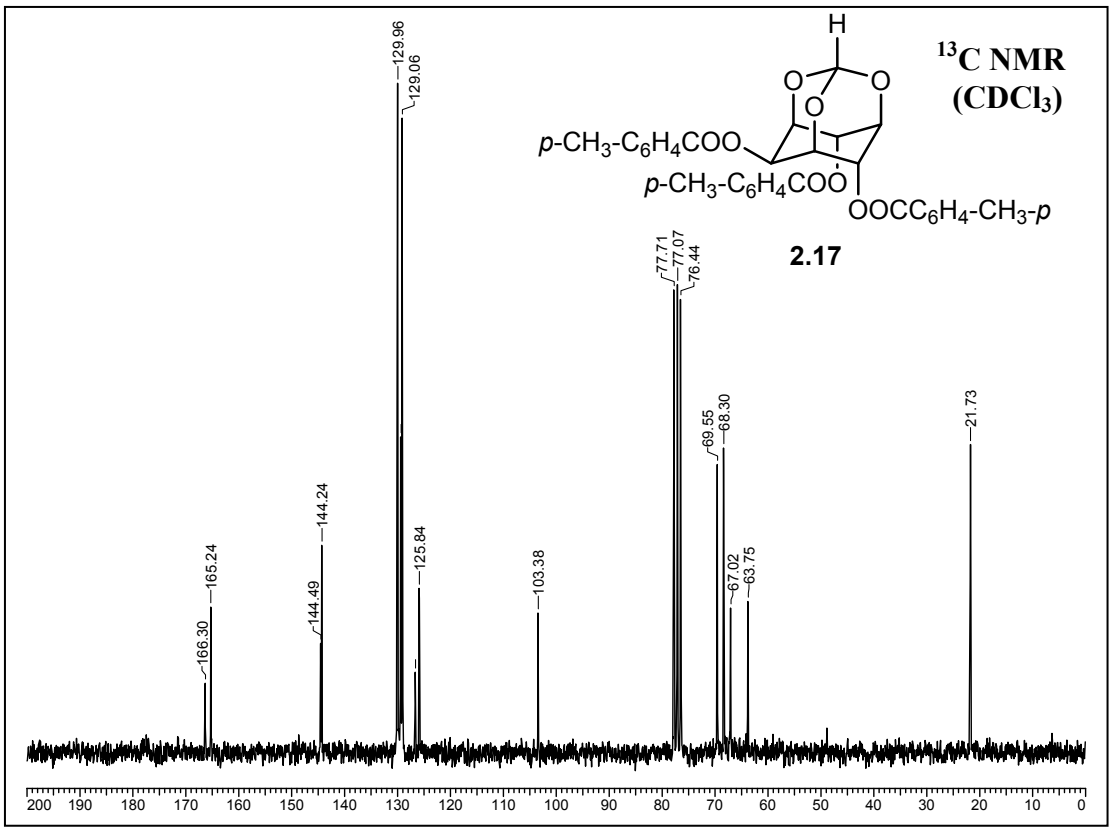
^{13}C NMR
(CDCl$_3$)
2.17
p-CH3-C6H4COO
p-CH3-C6H4COO
OOCC6H4-CH3-p
129.96
129.06
77.71
77.07
76.44
69.55
68.30
21.73
144.24
125.84
165.24
103.38
166.30
144.49
67.02
63.75

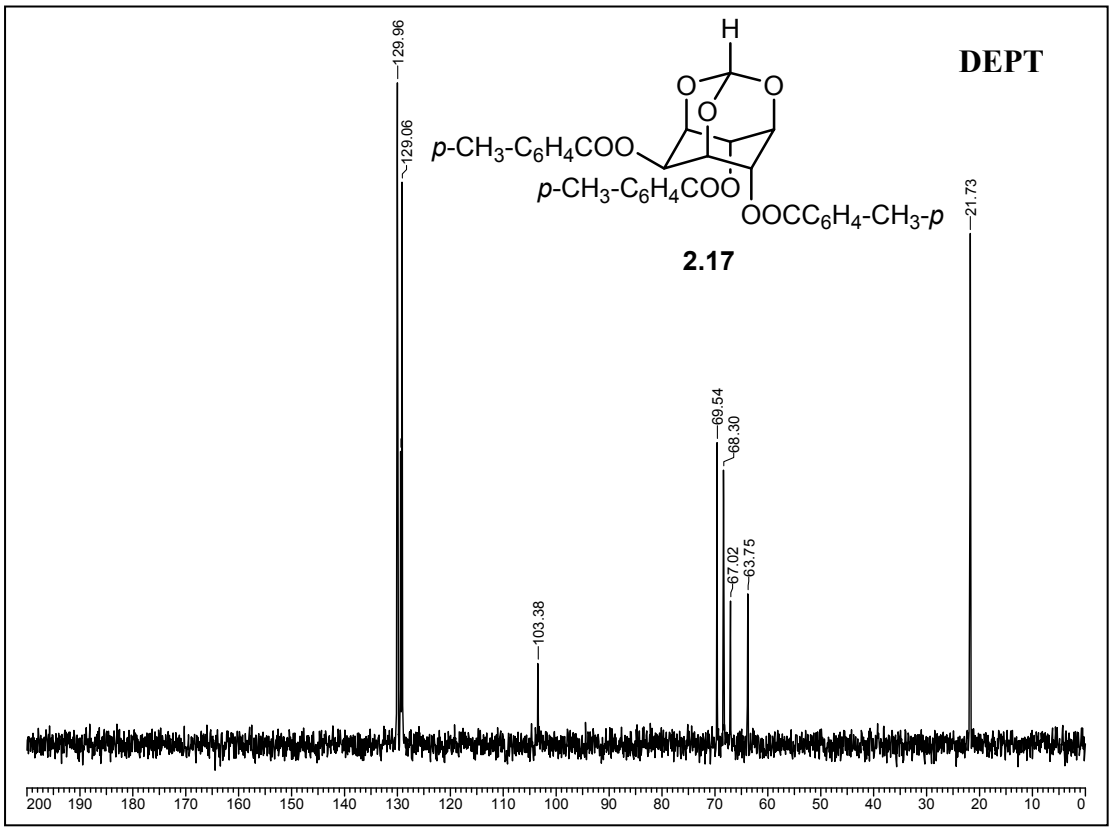
DEPT
129.96
129.06
103.38
69.54
68.30
67.02
63.75
21.73
H
O
O
O
p-CH3-C6H4COO
p-CH3-C6H4COO
OOCC6H4-CH3-p
2.17
200 190 180 170 160 150 140 130 120 110 100 90 80 70 60 50 40 30 20 10 0

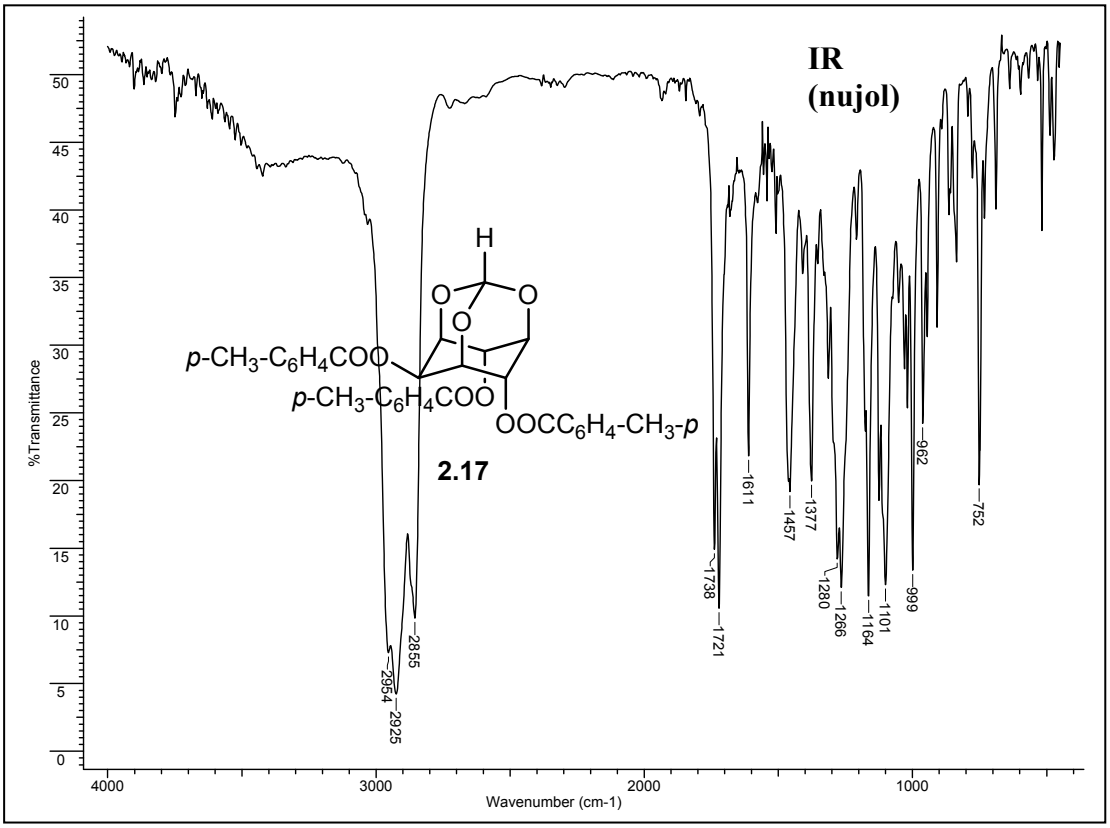
IR
(nujol)
%Transmittance
Wavenumber (cm-1)
4000
3000
2000
1000
0
5
10
15
20
25
30
35
40
45
50
2954
2925
2855
1738
1721
1611
1457
1377
1280
1266
1164
1101
999
962
752
H
O
O
O
p-CH3-C6H4COO
p-CH3-C6H4COO
OOCC6H4-CH3-p
2.17

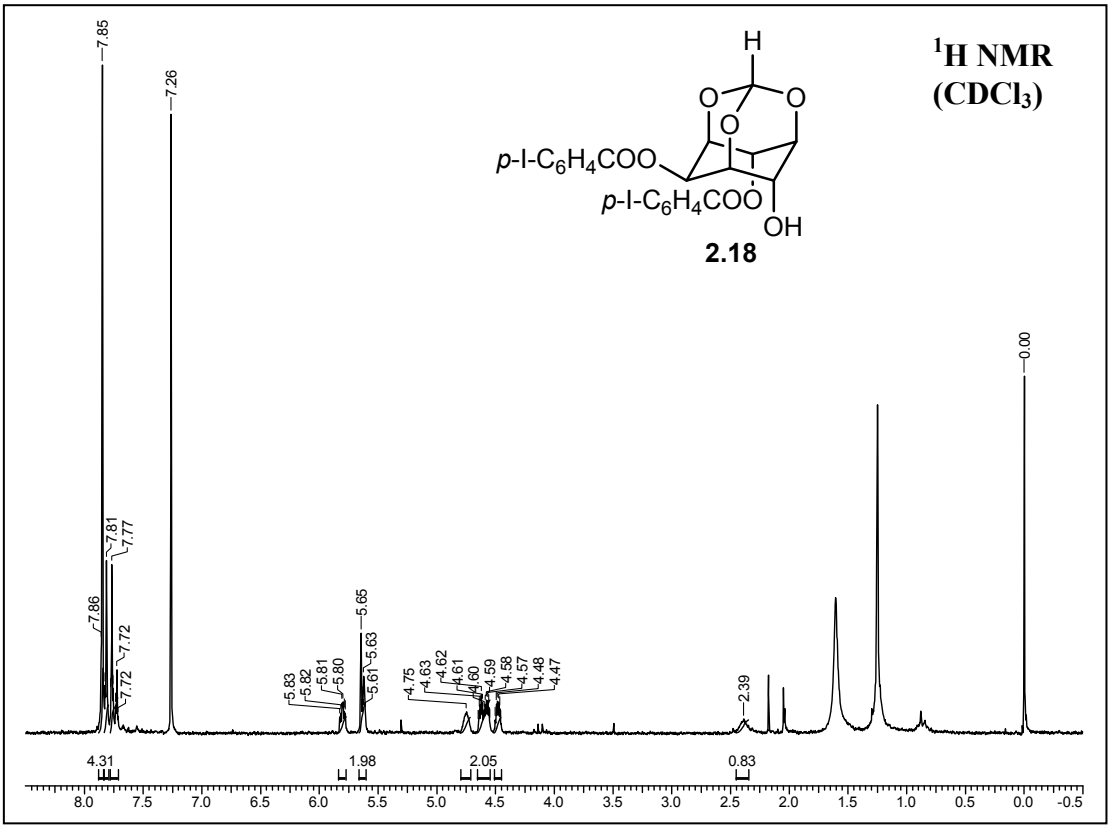
^{1}H NMR
(CDCl$_3$)
p-I-C$_6$H$_4$COO
p-I-C$_6$H$_4$COO
OH
2.18
7.85
7.26
7.81
7.77
7.86
7.72
7.72
5.65
5.83
5.82
5.81
5.80
5.63
5.61
4.75
4.63
4.62
4.61
4.60
4.59
4.58
4.57
4.48
4.47
2.39
0.00
4.31
1.98
2.05
0.83

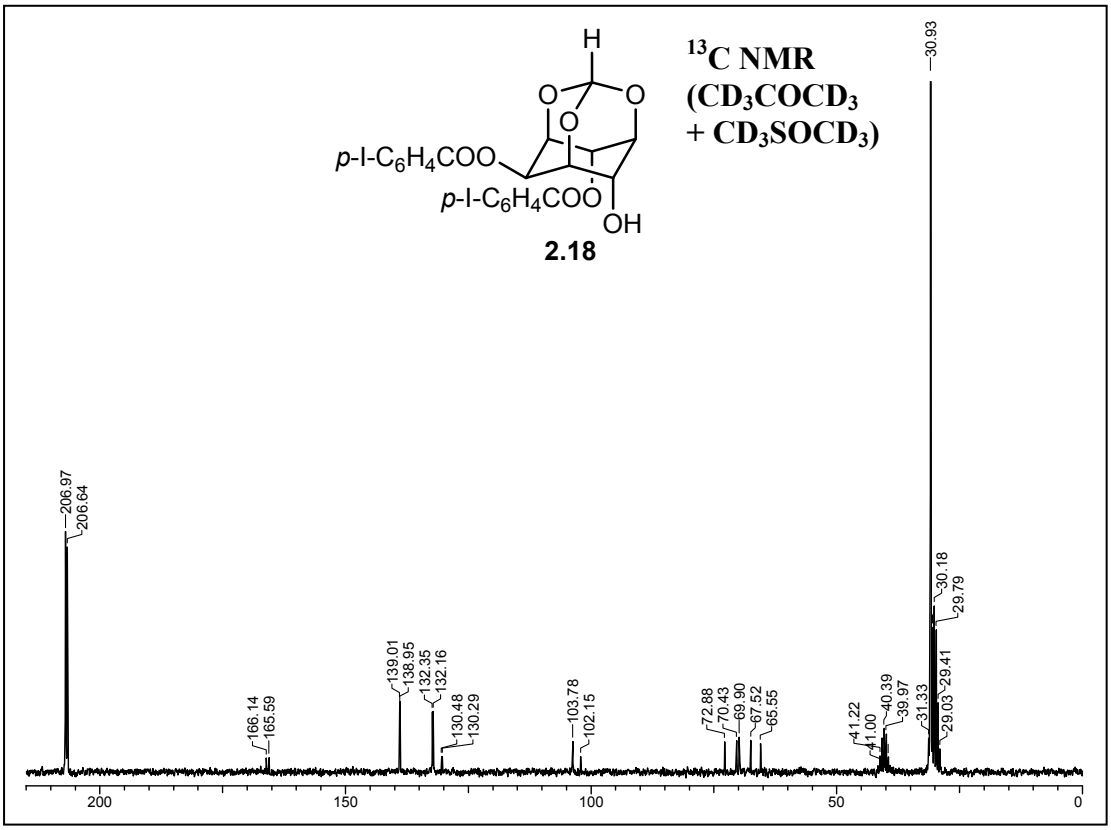
^{13}C NMR
(CD$_3$COCD$_3$
+ CD$_3$SOCD$_3$)
p-I-C$_6$H$_4$COO
p-I-C$_6$H$_4$COO
OH
2.18
206.97
206.64
166.14
165.59
139.01
138.95
132.35
132.16
130.48
130.29
103.78
102.15
72.88
70.43
69.90
67.52
65.55
41.22
41.00
40.39
39.97
31.33
30.93
30.18
29.79
29.41
29.03

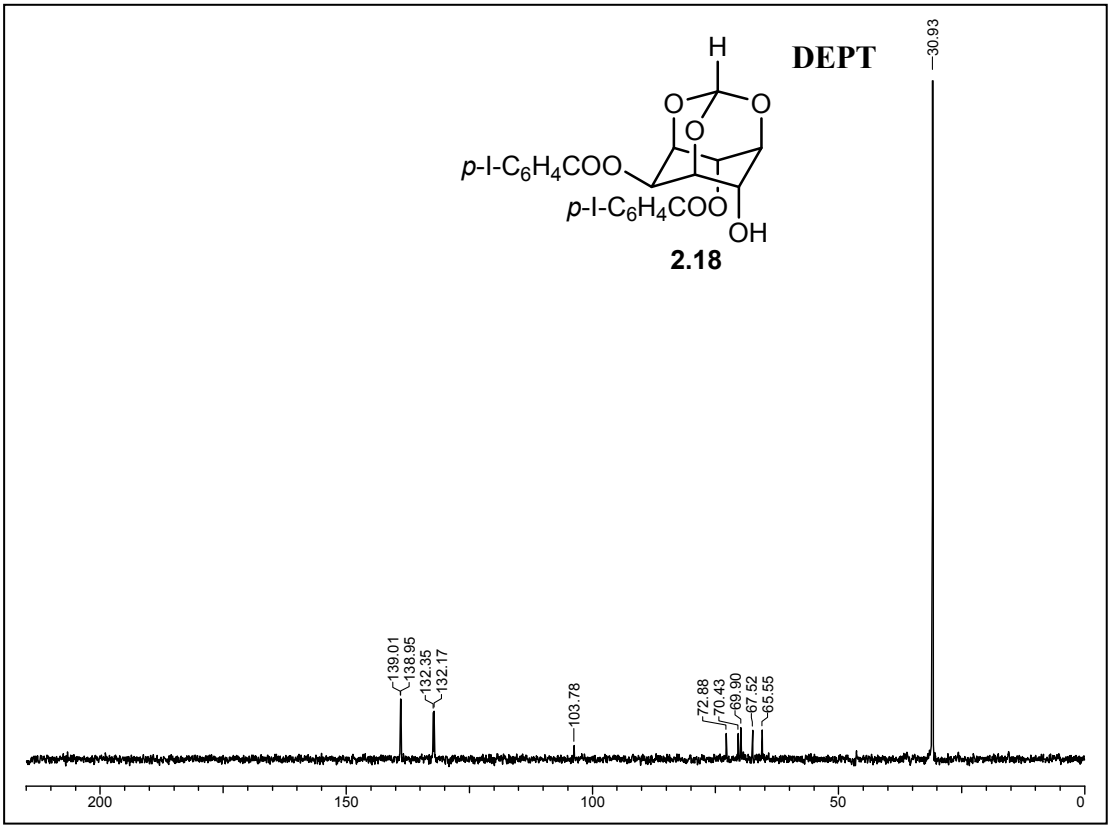
DEPT
H
O
O
O
p-I-C6H4COO
p-I-C6H4COO
OH
2.18
30.93
139.01
138.95
132.35
132.17
103.78
72.88
70.43
69.90
67.52
65.55
200
150
100
50
0

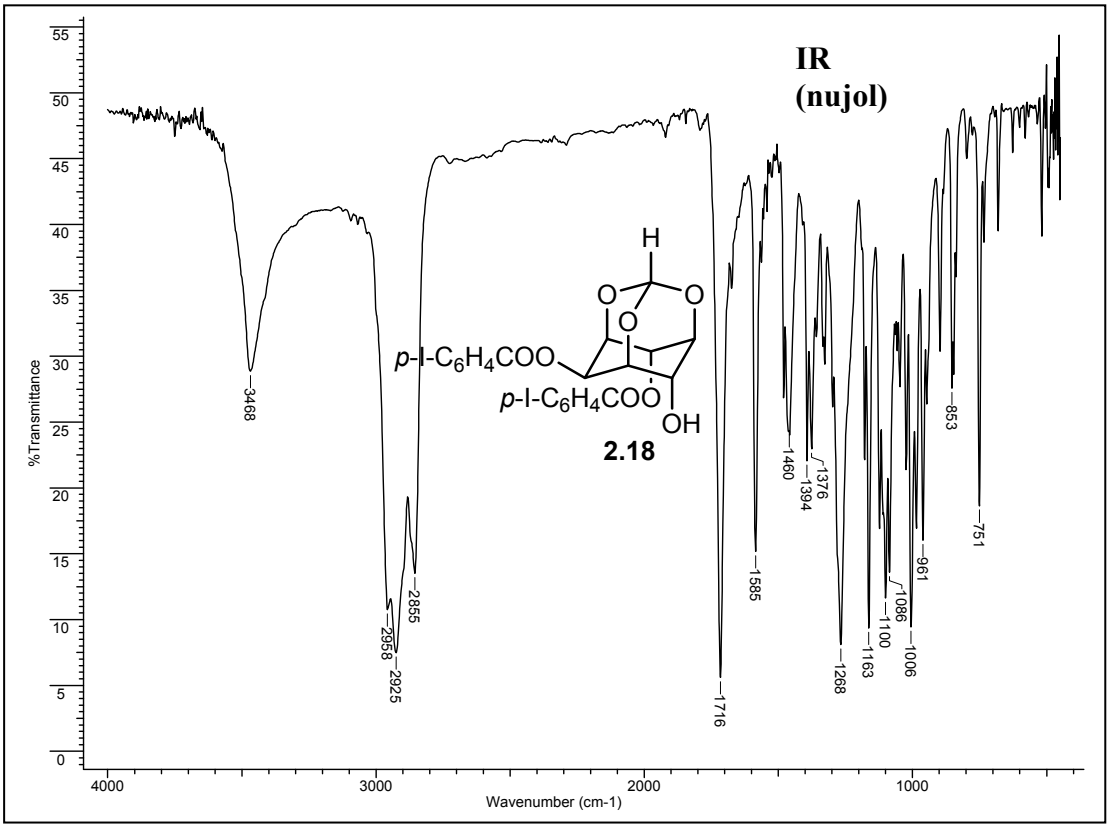
IR
(nujol)
%Transmittance
Wavenumber (cm-1)
4000
3000
2000
1000
3468
2958
2925
2855
1716
1585
1460
1394
1376
1268
1163
1100
1086
1006
961
853
751
H
O
O
O
p-I-C6H4COO
p-I-C6H4COO
OH
2.18

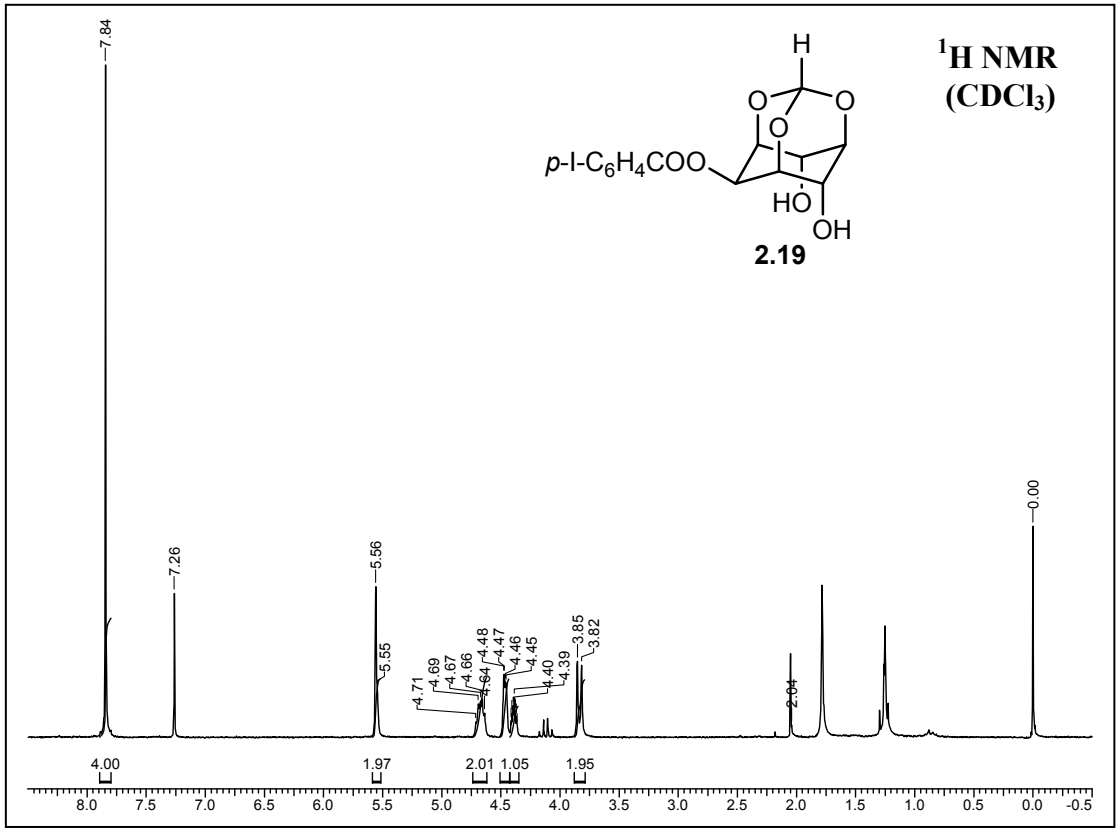
^{1}H NMR
(CDCl$_3$)
p-I-C$_6$H$_4$COO
HO
OH
2.19
7.84
7.26
5.56
5.55
4.71
4.69
4.67
4.66
4.64
4.48
4.47
4.46
4.45
4.40
4.39
3.85
3.82
2.04
0.00
4.00
1.97
2.01
1.05
1.95

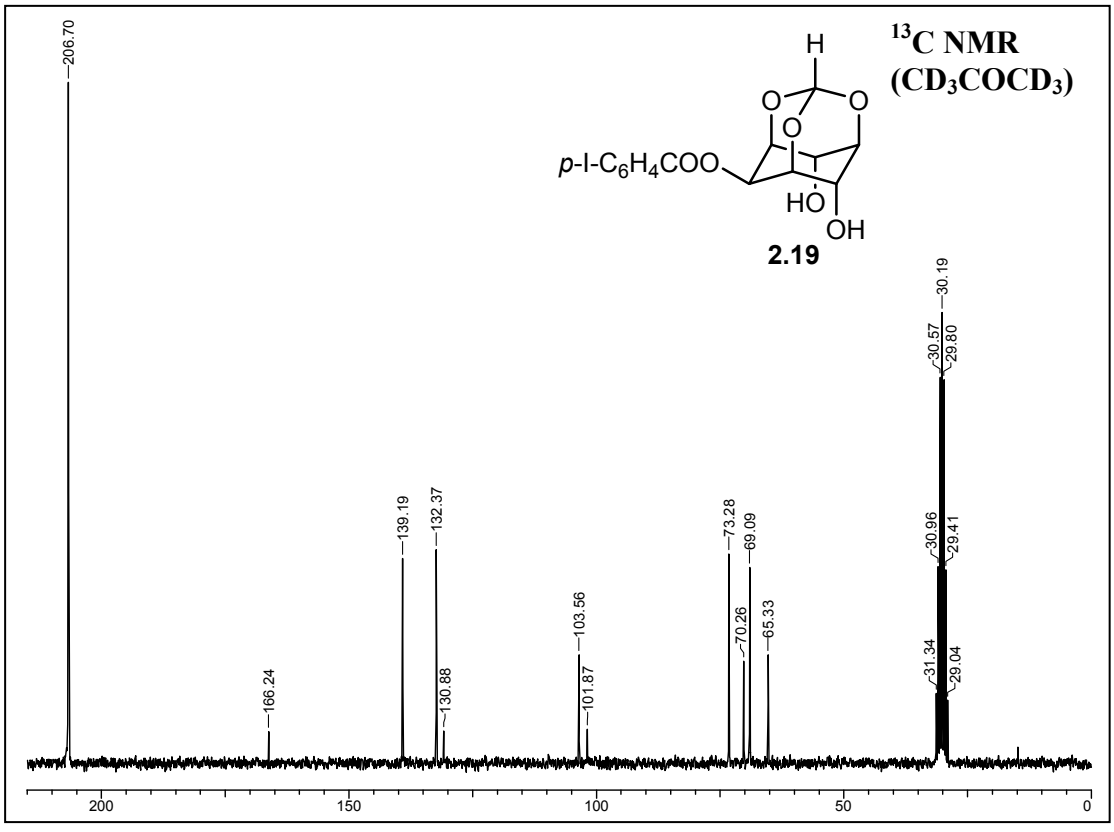
^{13}C NMR
(CD$_3$COCD$_3$)
p-I-C$_6$H$_4$COO
HO
OH
2.19
206.70
166.24
139.19
132.37
130.88
103.56
101.87
73.28
70.26
69.09
65.33
30.96
30.57
30.19
29.80
29.41
31.34
29.04

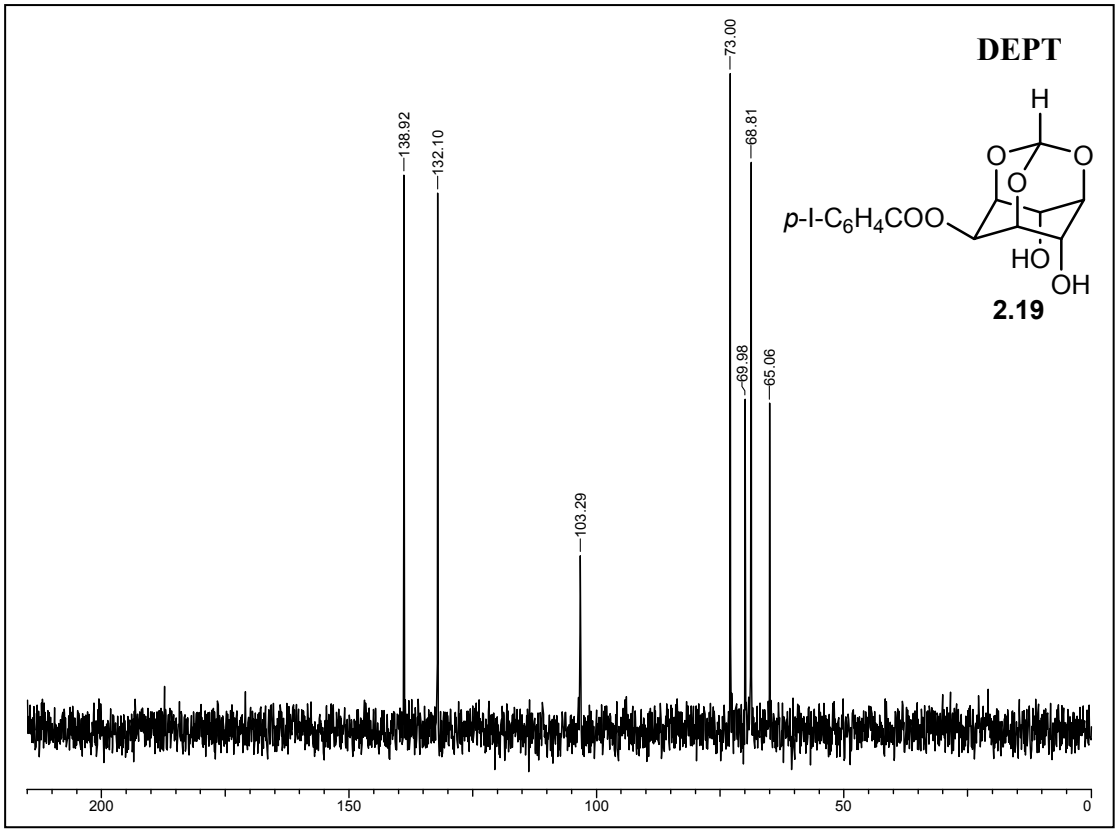
DEPT
73.00
138.92
132.10
68.81
69.98
65.06
103.29
p-I-C6H4COO
HO
OH
2.19
200
150
100
50
0

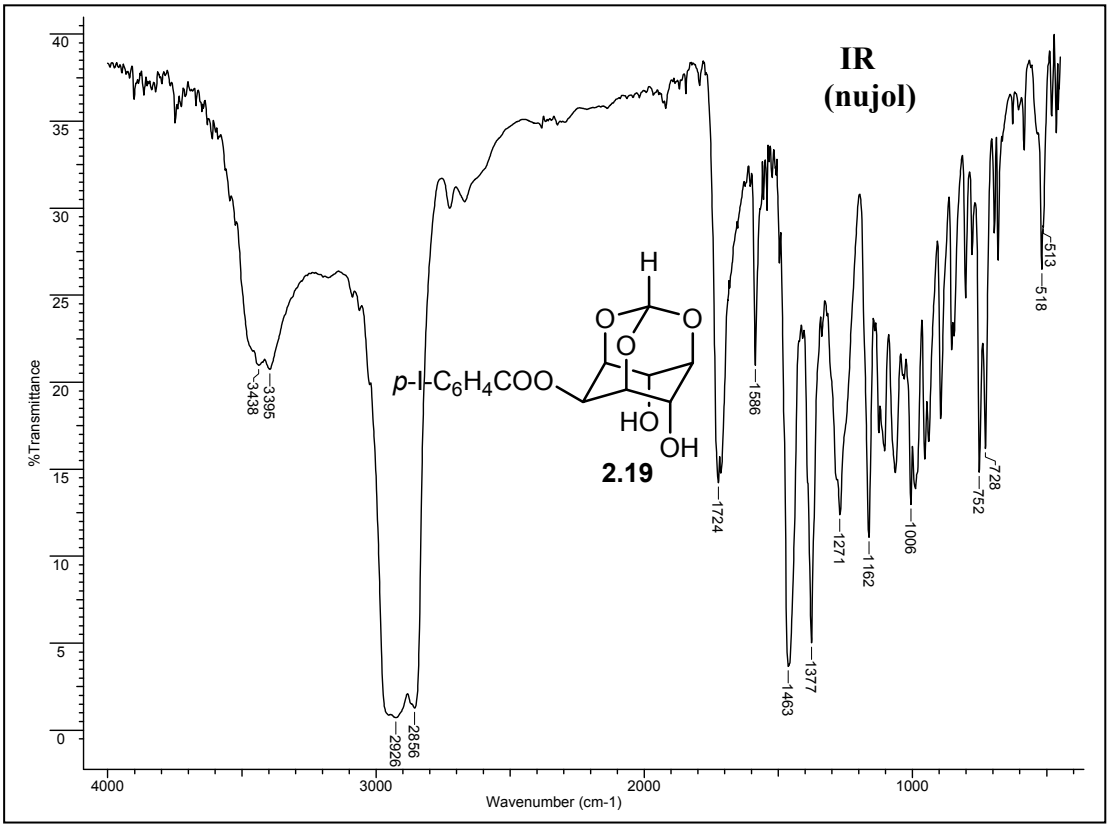
IR
(nujol)
%Transmittance
3438
3395
2926
2856
1724
1586
1463
1377
1271
1162
1006
752
728
518
513
p-I-C6H4COO
HO
OH
2.19
Wavenumber (cm-1)
4000
3000
2000
1000

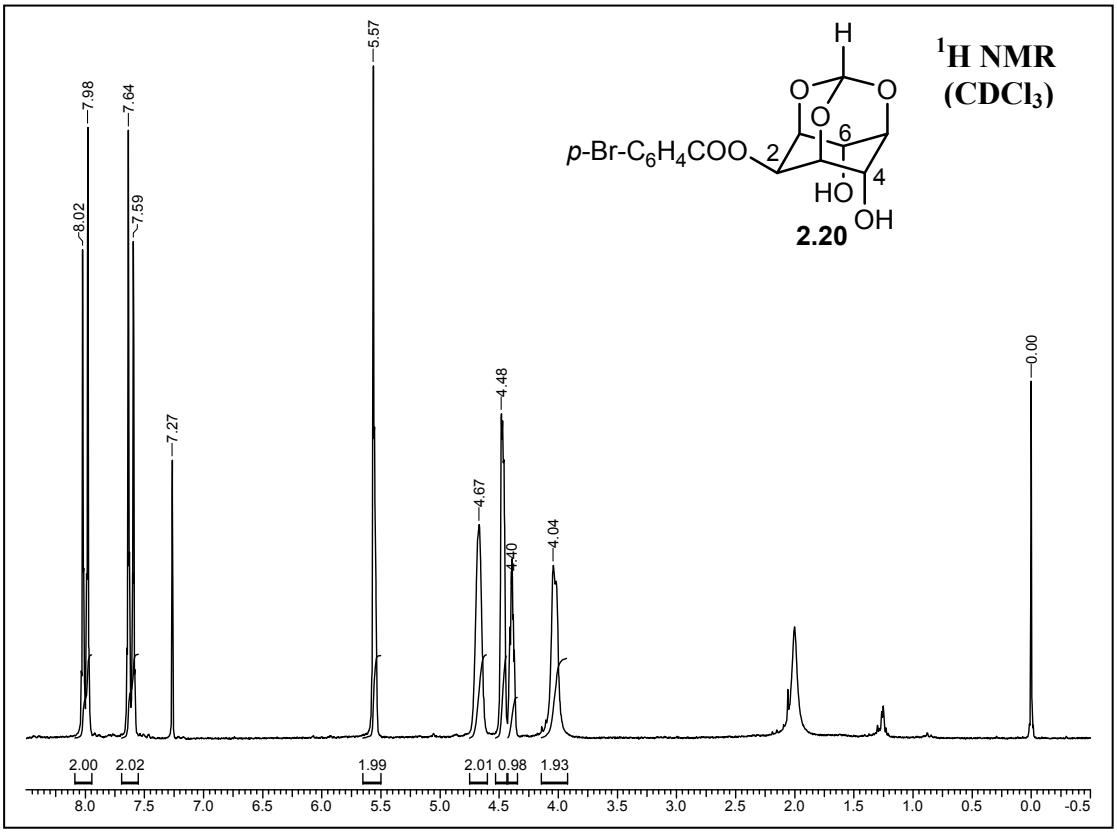
^{1}H NMR
(CDCl$_3$)
p-Br-C$_6$H$_4$COO
HO
OH
2.20
8.02
7.98
7.64
7.59
7.27
5.57
4.67
4.48
4.40
4.04
0.00
2.00
2.02
1.99
2.01
0.98
1.93

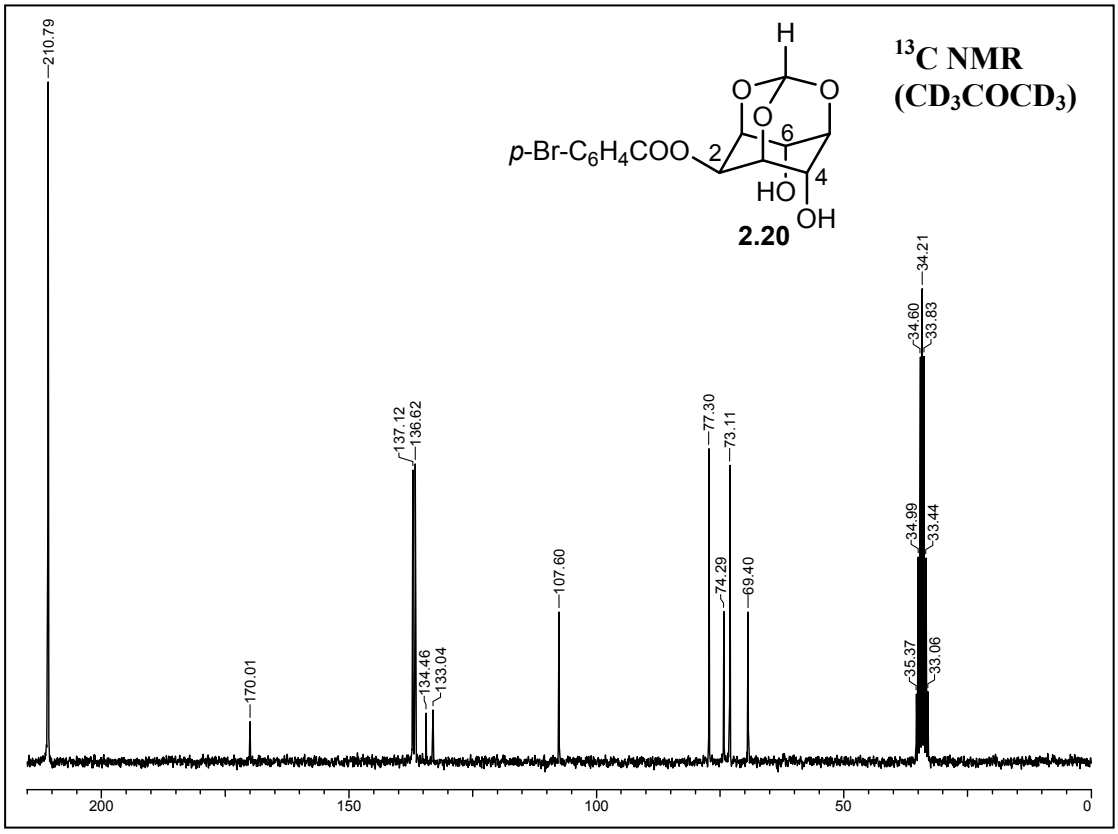
^{13}C NMR
(CD$_3$COCD$_3$)
p-Br-C$_6$H$_4$COO
HO
OH
2.20
210.79
170.01
137.12
136.62
134.46
133.04
107.60
77.30
74.29
73.11
69.40
34.60
34.21
33.83
34.99
33.44
35.37
33.06

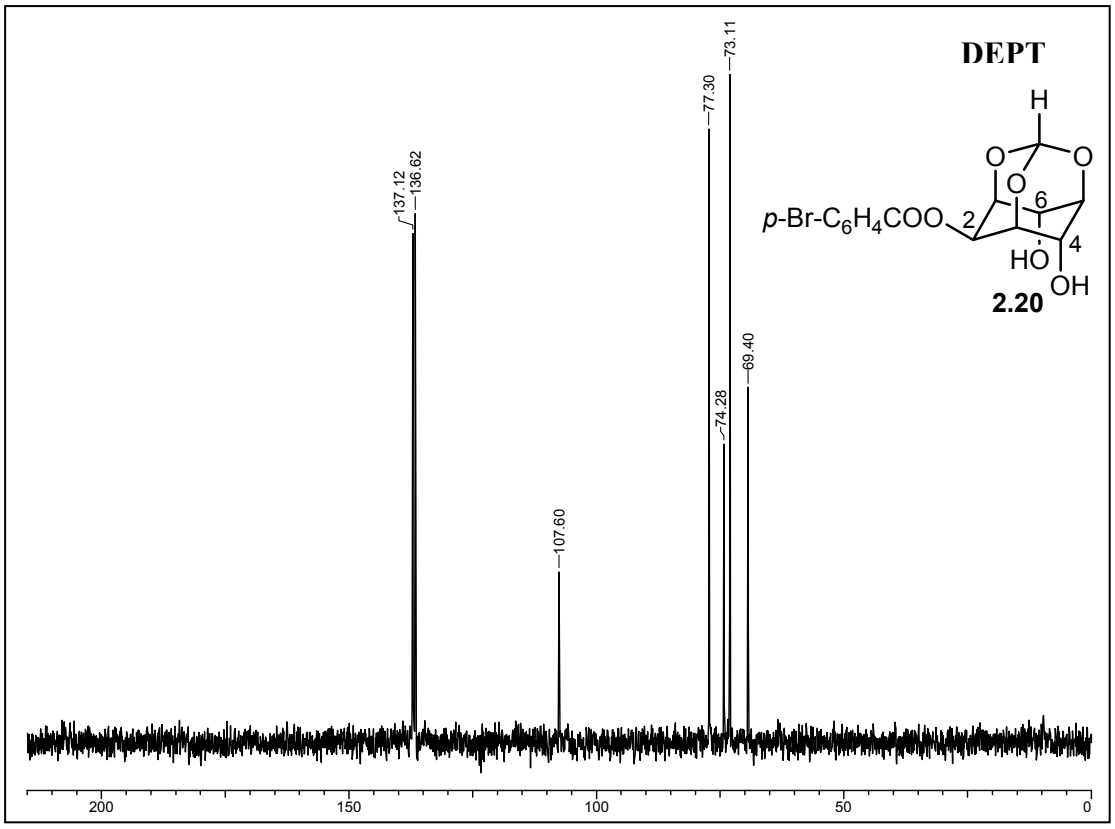
DEPT
137.12
136.62
107.60
77.30
74.28
73.11
69.40
p-Br-C6H4COO
2.20
200
150
100
50
0

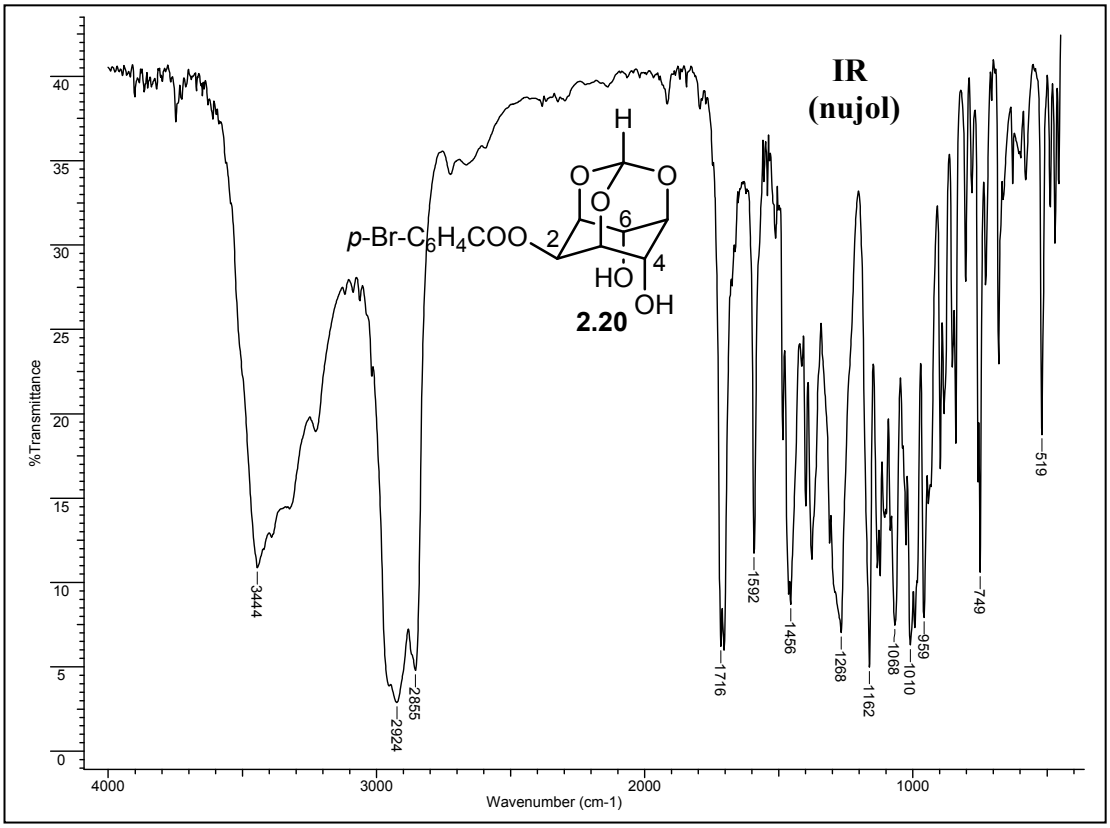
IR
(nujol)
%Transmittance
Wavenumber (cm-1)
3444
2924
2855
1716
1592
1456
1268
1162
1068
1010
959
749
519
p-Br-C6H4COO
2.20
4000
3000
2000
1000

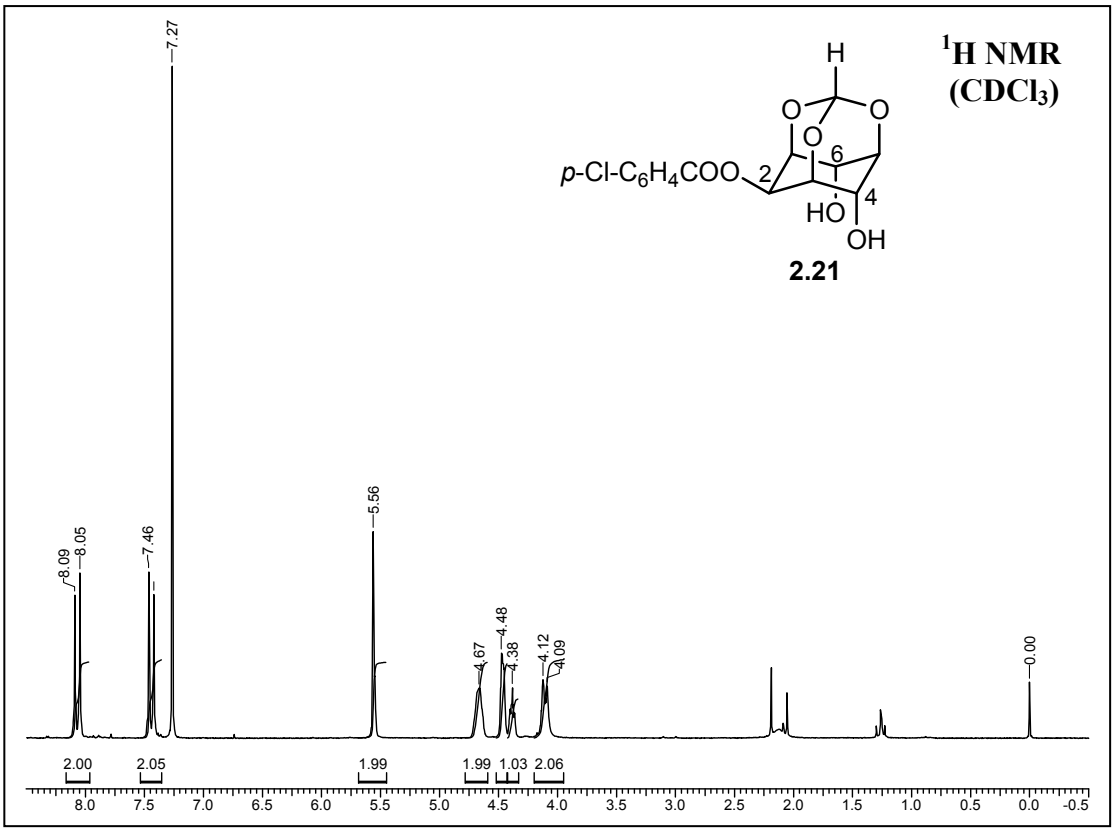
^{1}H NMR
(CDCl$_3$)
p-Cl-C$_6$H$_4$COO
HO
OH
2.21
7.27
8.09
8.05
7.46
5.56
4.67
4.48
4.38
4.12
4.09
0.00
2.00
2.05
1.99
1.99
1.03
2.06

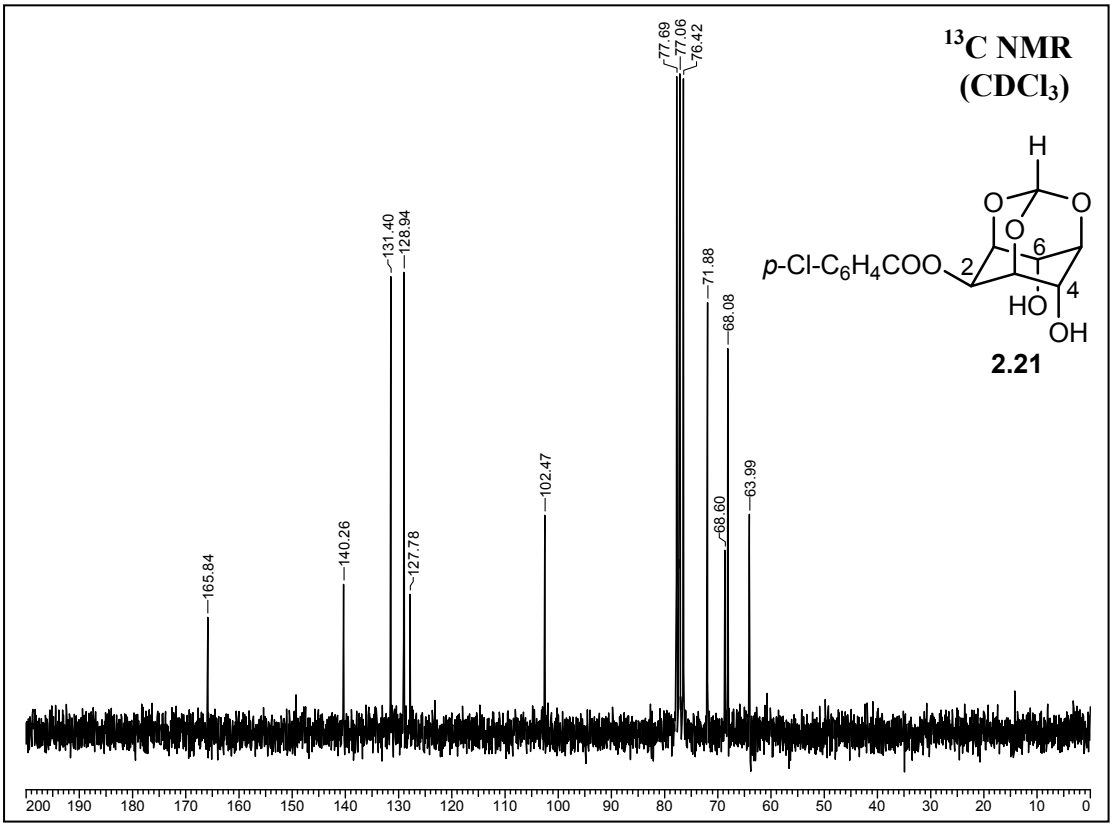
^{13}C NMR
(CDCl$_3$)
p-Cl-C$_6$H$_4$COO
HO
OH
2.21
77.69
77.06
76.42
131.40
128.94
71.88
68.08
102.47
68.60
63.99
165.84
140.26
127.78

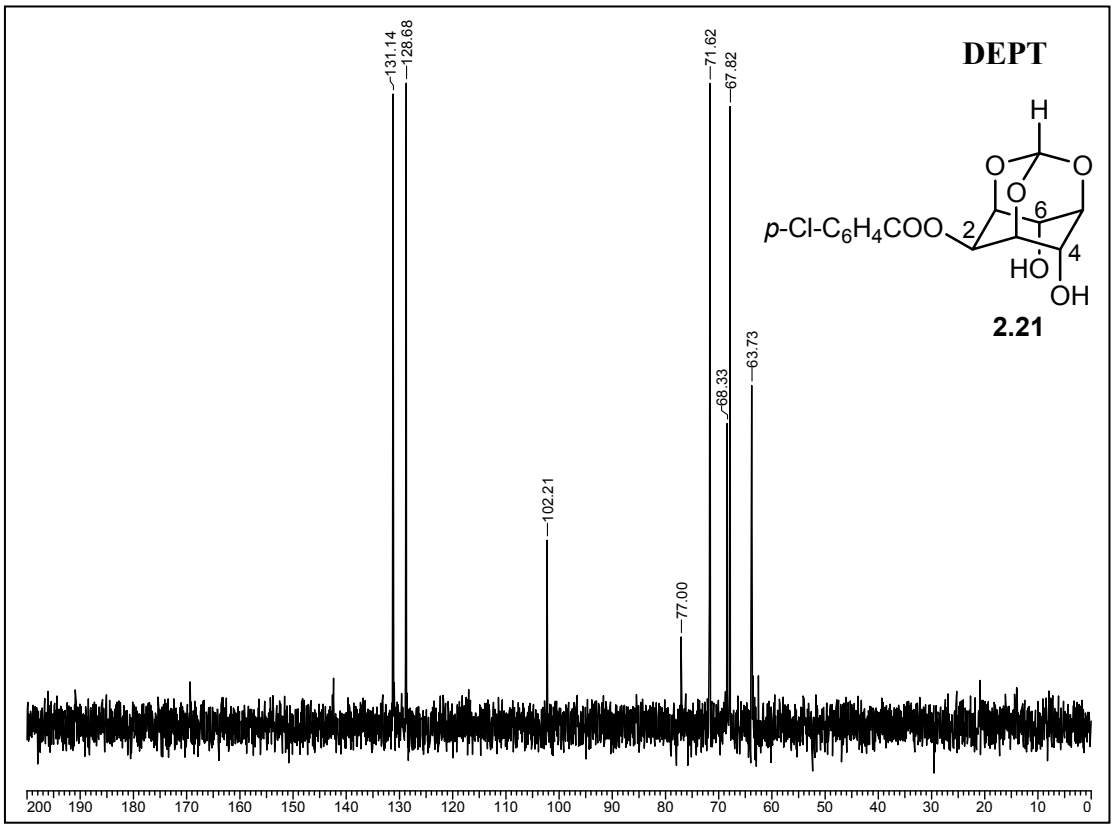
DEPT
131.14
128.68
71.62
67.82
68.33
63.73
102.21
77.00
p-Cl-C6H4COO
2.21

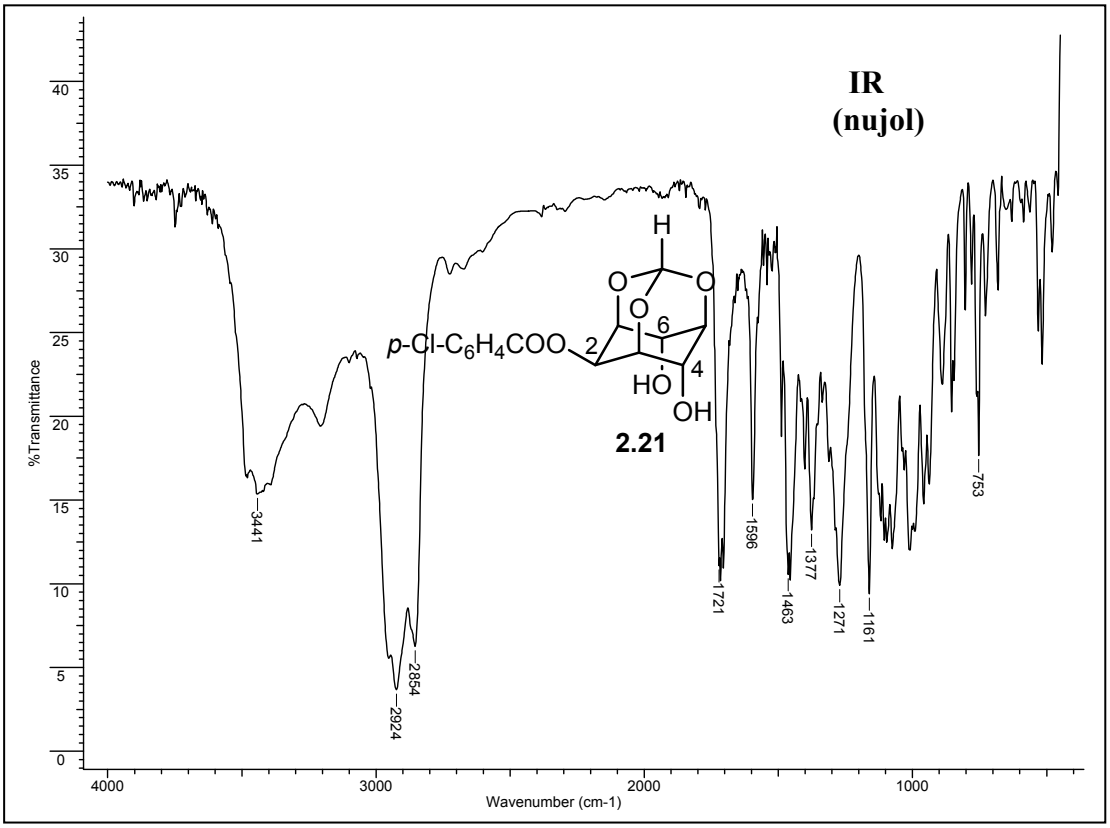
IR
(nujol)
%Transmittance
Wavenumber (cm-1)
3441
2924
2854
1721
1596
1463
1377
1271
1161
753
p-Cl-C6H4COO
2.21

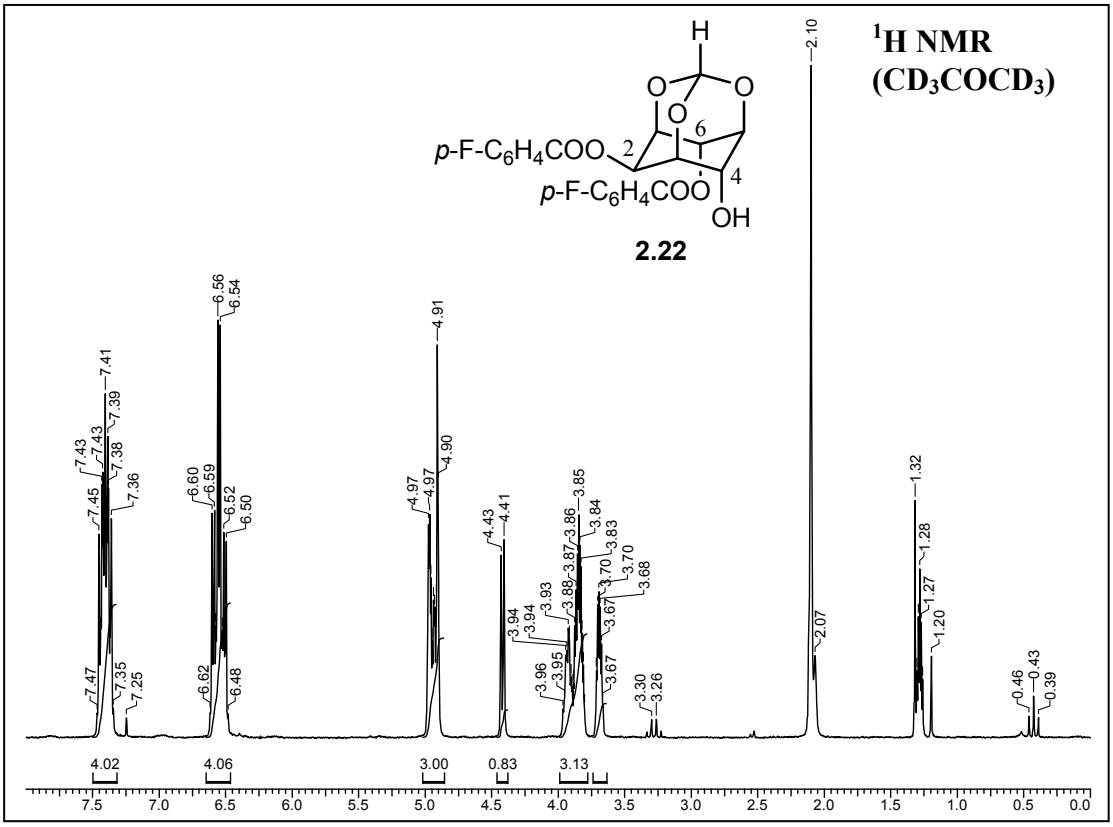
^{1}H NMR
(CD$_3$COCD$_3$)
p-F-C6H4COO
p-F-C6H4COO
OH
2.22
7.47
7.45
7.43
7.43
7.41
7.39
7.38
7.36
7.35
7.25
6.62
6.60
6.59
6.56
6.54
6.52
6.50
6.48
4.97
4.97
4.91
4.90
4.43
4.41
3.96
3.95
3.94
3.94
3.93
3.88
3.87
3.86
3.85
3.84
3.83
3.70
3.70
3.68
3.67
3.67
3.30
3.26
2.10
2.07
1.32
1.28
1.27
1.20
0.46
0.43
0.39
4.02
4.06
3.00
0.83
3.13

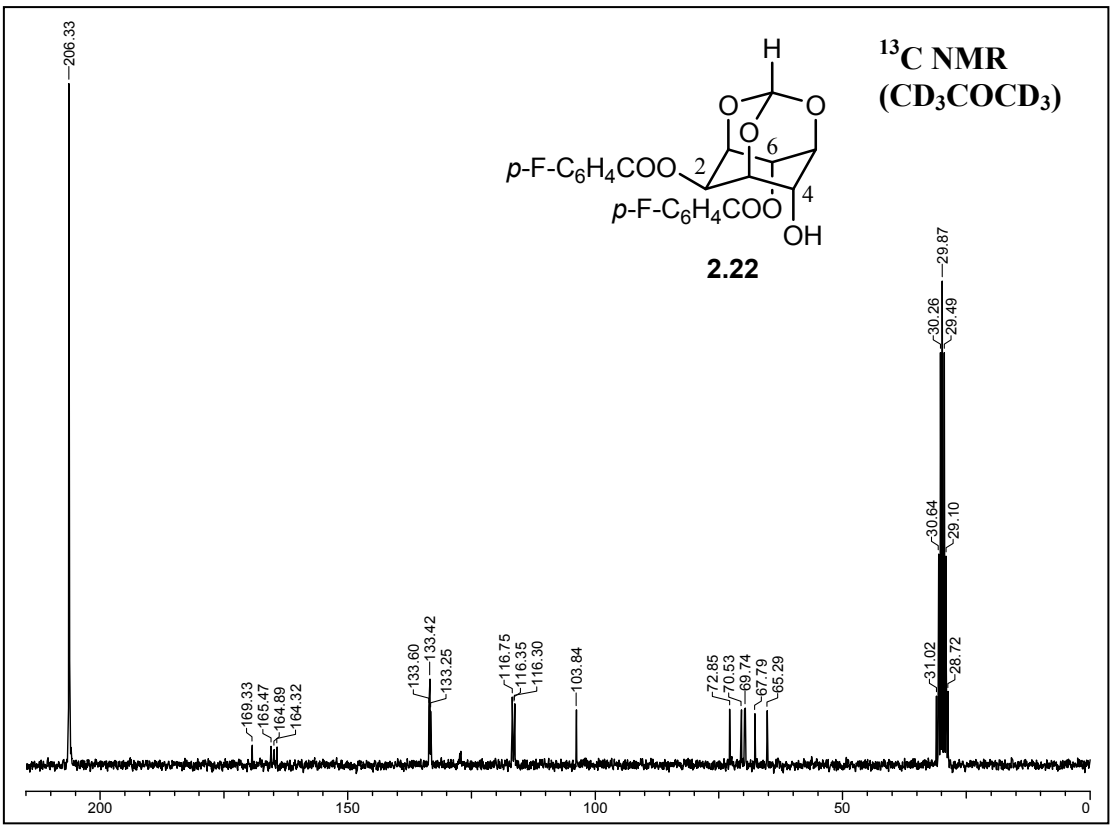
^{13}C NMR
(CD$_3$COCD$_3$)
p-F-C6H4COO
p-F-C6H4COO
OH
2.22
206.33
169.33
165.47
164.89
164.32
133.60
133.42
133.25
116.75
116.35
116.30
103.84
72.85
70.53
69.74
67.79
65.29
31.02
30.64
30.26
29.87
29.49
29.10
28.72

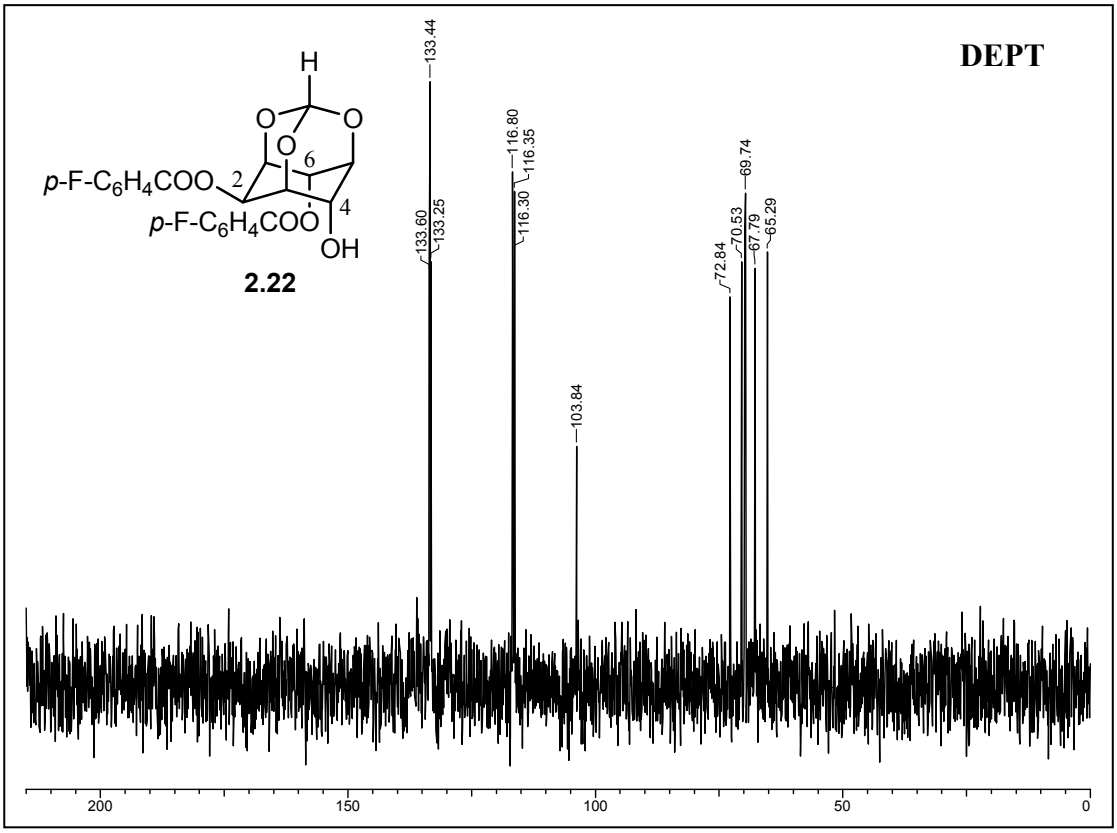
DEPT
H
O
O
O
6
p-F-C6H4COO 2
p-F-C6H4COO 4
OH
2.22
133.44
133.60
133.25
116.80
116.35
116.30
103.84
72.84
70.53
69.74
67.79
65.29
200
150
100
50
0

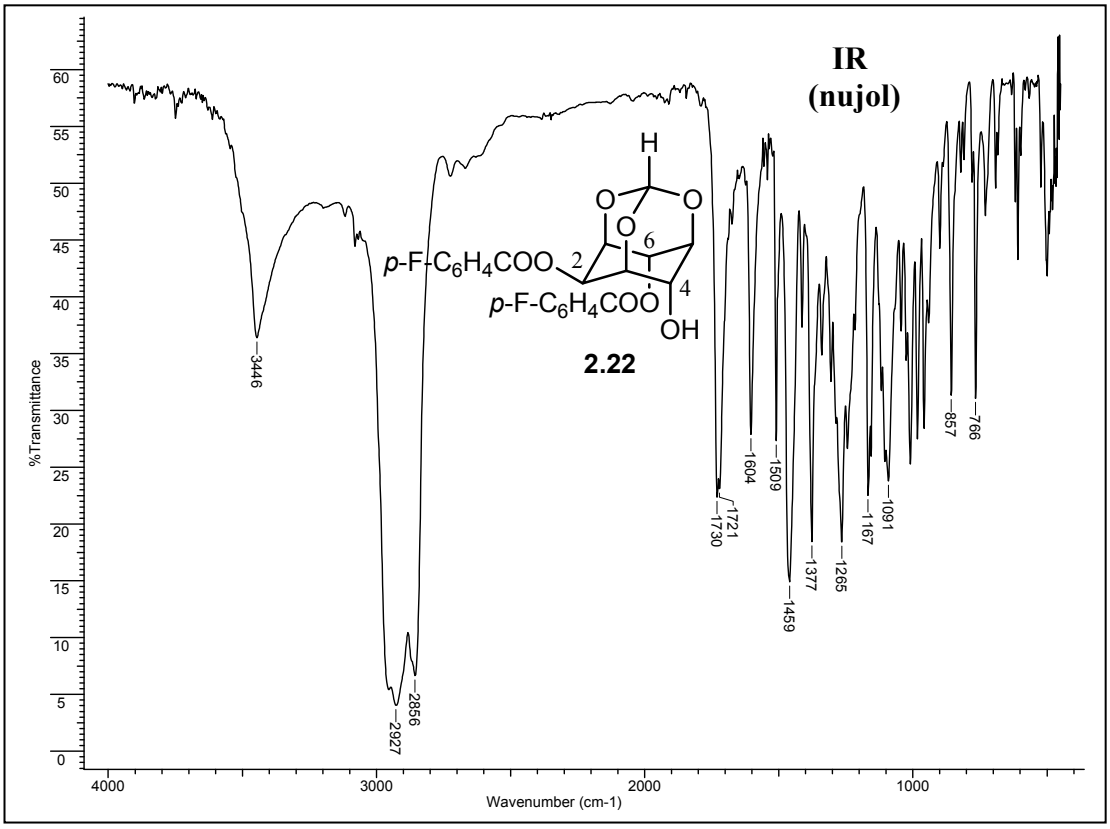
IR
(nujol)
H
O
O
O
6
p-F-C6H4COO 2
p-F-C6H4COO 4
OH
2.22
%Transmittance
3446
2927
2856
1730
1721
1604
1509
1459
1377
1265
1167
1091
857
766
4000
3000
2000
1000
Wavenumber (cm-1)

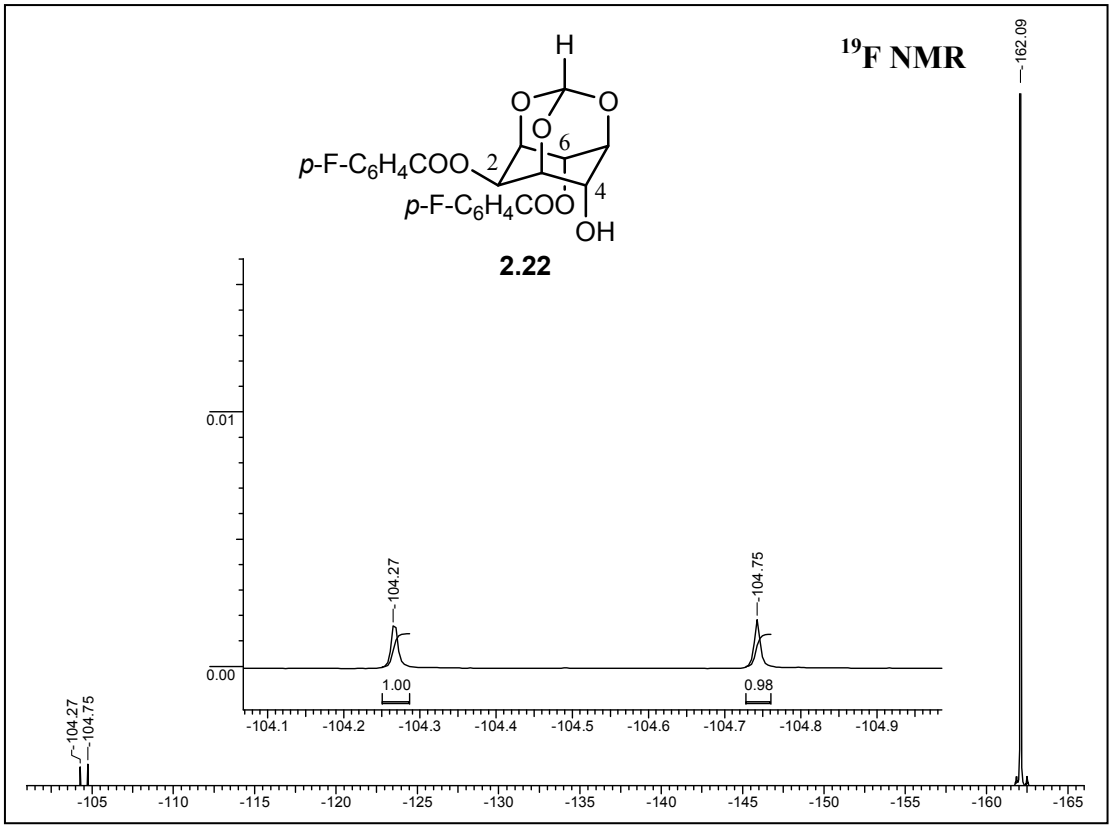
^{19}F NMR
H
O
O
O
O
6
p-F-C6H4COO
2
4
p-F-C6H4COO
OH
2.22
162.09
104.27
104.75
0.01
0.00
1.00
0.98
-104.1
-104.2
-104.3
-104.4
-104.5
-104.6
-104.7
-104.8
-104.9
-105
-110
-115
-120
-125
-130
-135
-140
-145
-150
-155
-160
-165

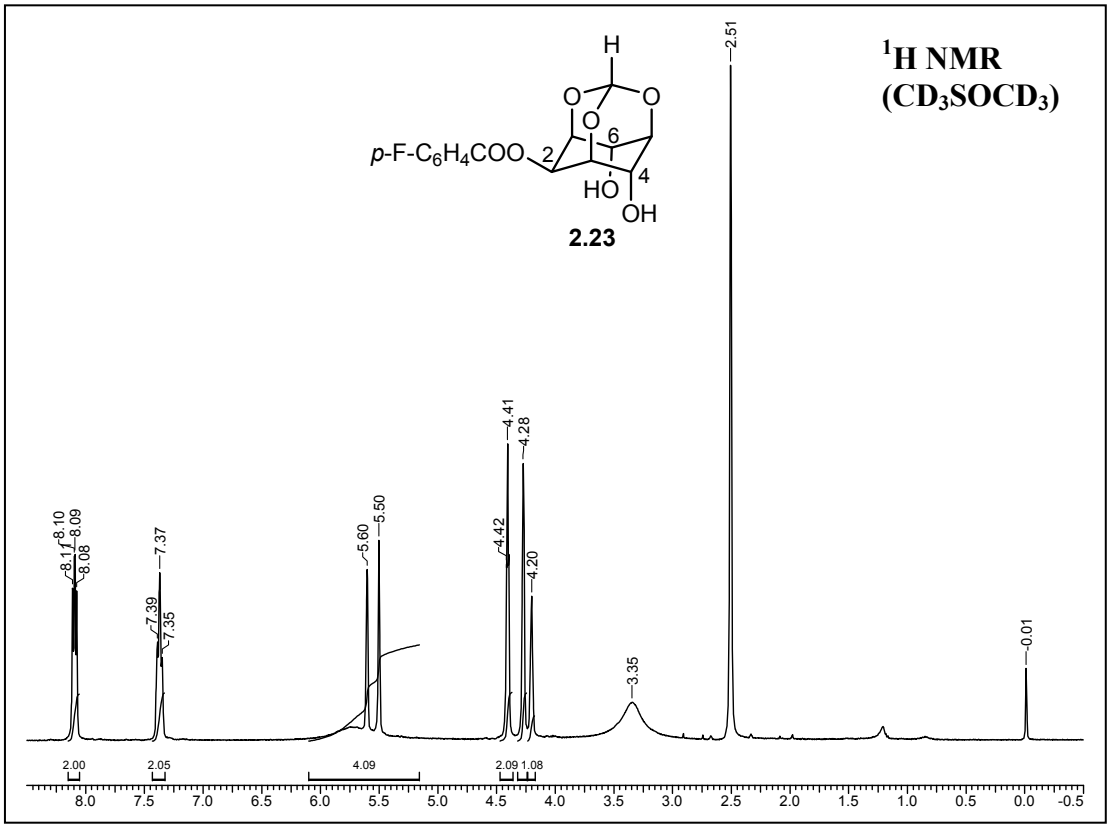
^{1}H NMR
(CD3SOCD3)
H
O
O
O
O
6
p-F-C6H4COO
2
HO
4
OH
2.23
2.51
4.41
4.28
4.42
4.20
5.60
5.50
8.11
8.10
8.09
8.08
7.39
7.37
7.35
3.35
0.01
2.00
2.05
4.09
2.09
1.08
8.0
7.5
7.0
6.5
6.0
5.5
5.0
4.5
4.0
3.5
3.0
2.5
2.0
1.5
1.0
0.5
0.0
-0.5

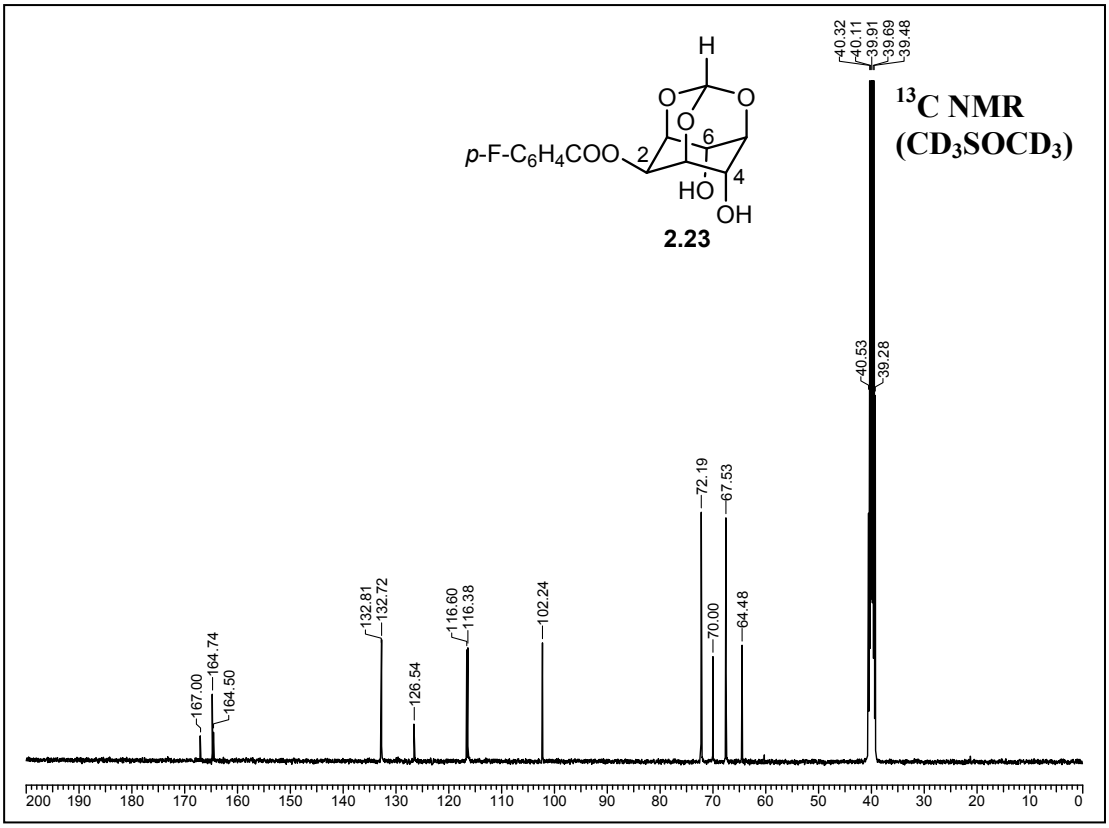
H
O
O
O
6
p-F-C6H4COO
2
4
HO
OH
2.23
13C NMR
(CD3SOCD3)
40.32
40.11
39.91
39.69
39.48
40.53
39.28
72.19
67.53
70.00
64.48
132.81
132.72
116.60
116.38
102.24
126.54
167.00
164.74
164.50
200 190 180 170 160 150 140 130 120 110 100 90 80 70 60 50 40 30 20 10 0

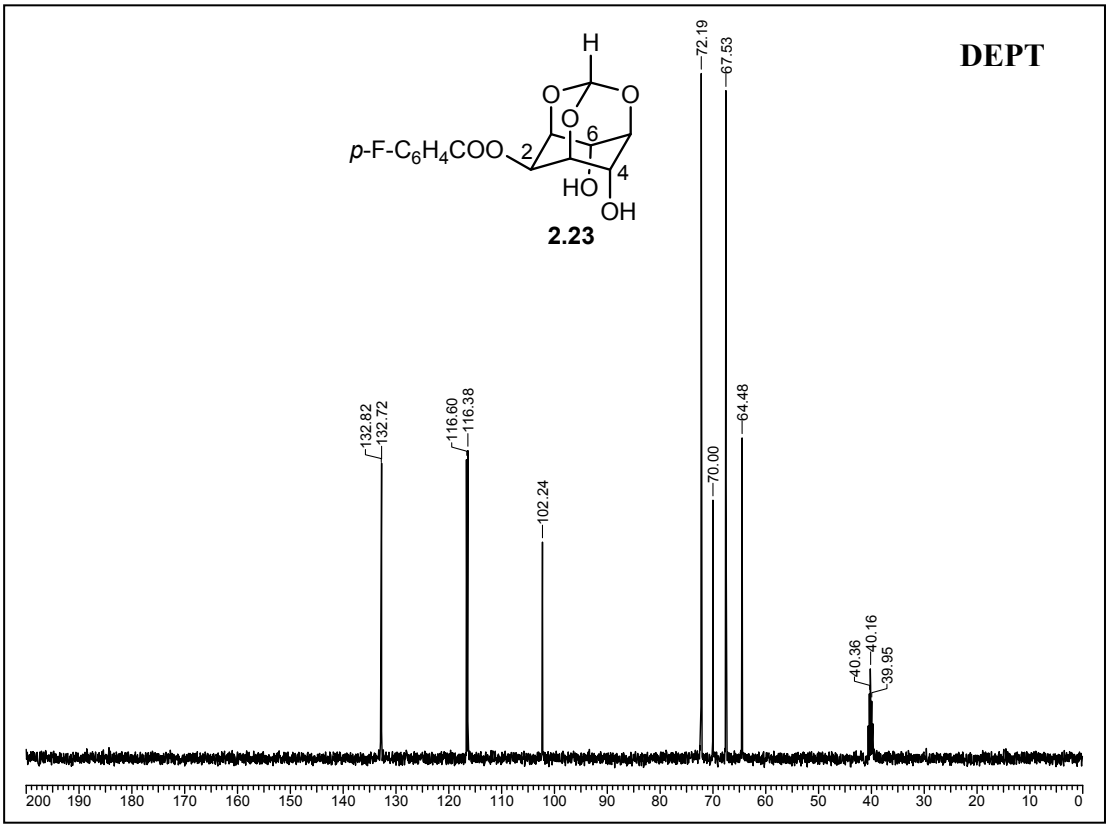
H
O
O
O
6
p-F-C6H4COO
2
4
HO
OH
2.23
DEPT
72.19
67.53
64.48
70.00
132.82
132.72
116.60
116.38
102.24
40.36
40.16
39.95
200 190 180 170 160 150 140 130 120 110 100 90 80 70 60 50 40 30 20 10 0

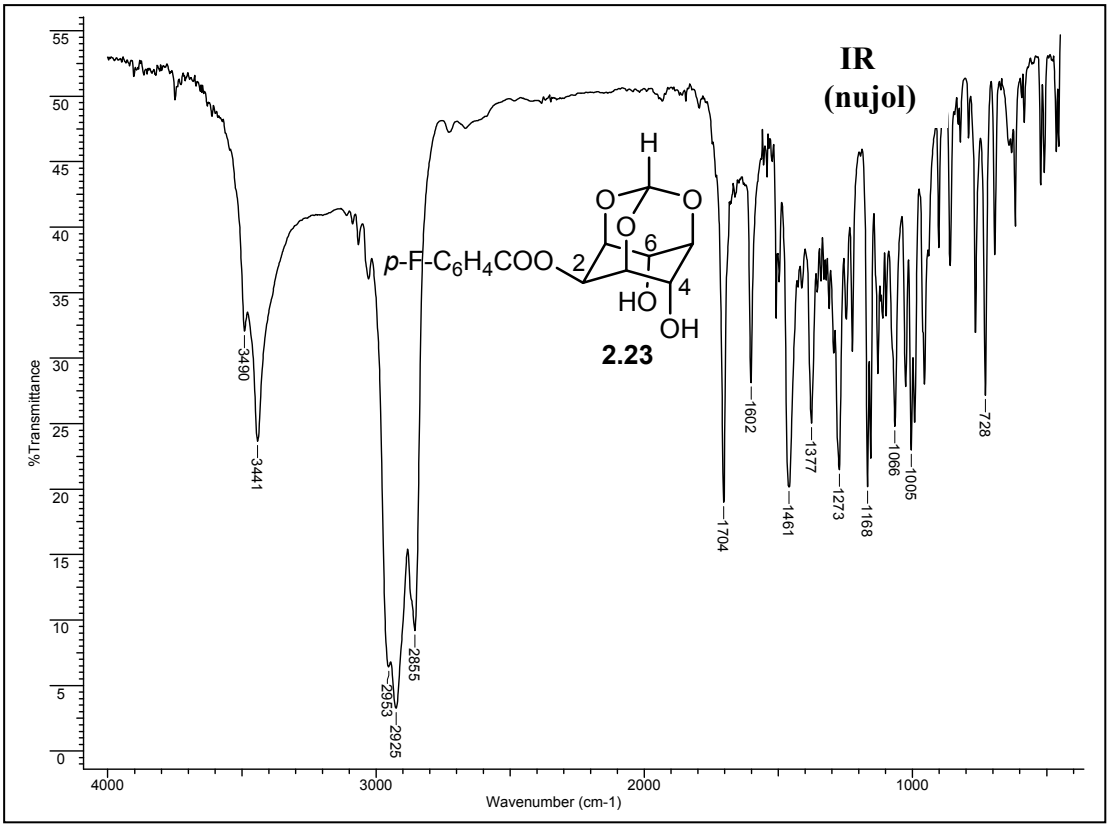
IR
(nujol)
p-F-C6H4COO
2.23
%Transmittance
Wavenumber (cm-1)
3490
3441
2953
2925
2855
1704
1602
1461
1377
1273
1168
1066
1005
728

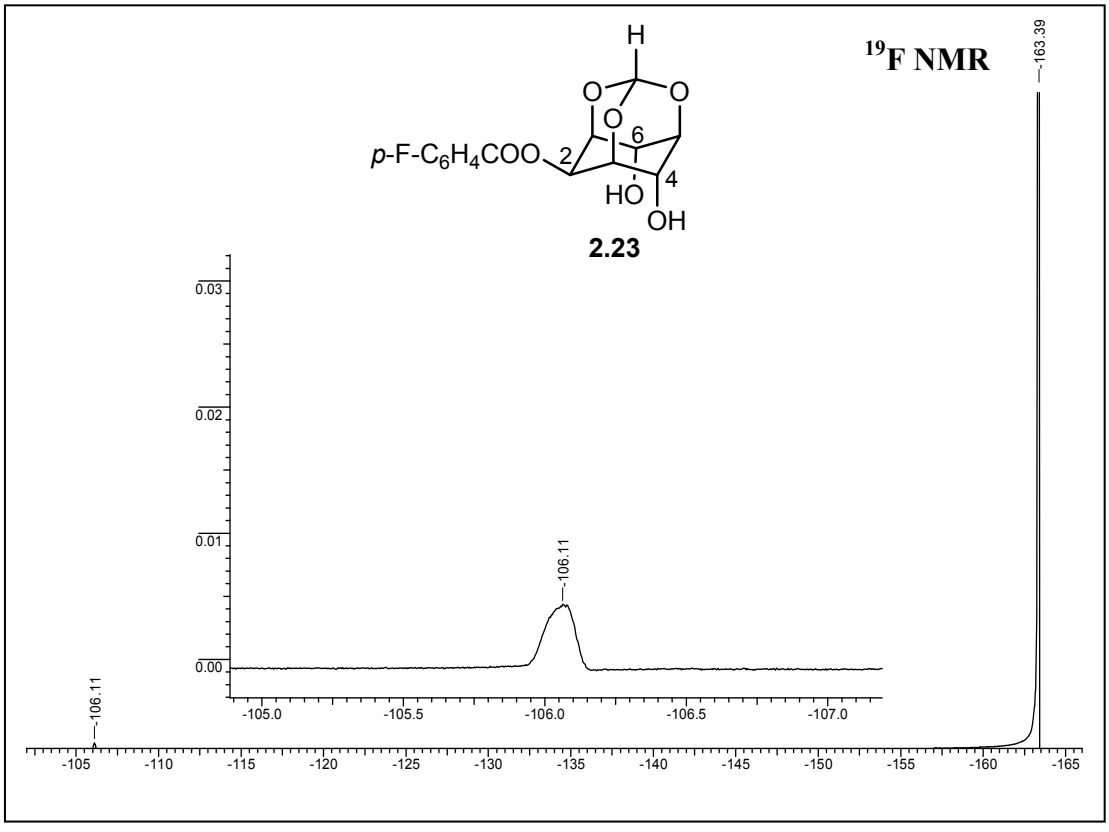
19F NMR
p-F-C6H4COO
2.23
163.39
106.11
106.11

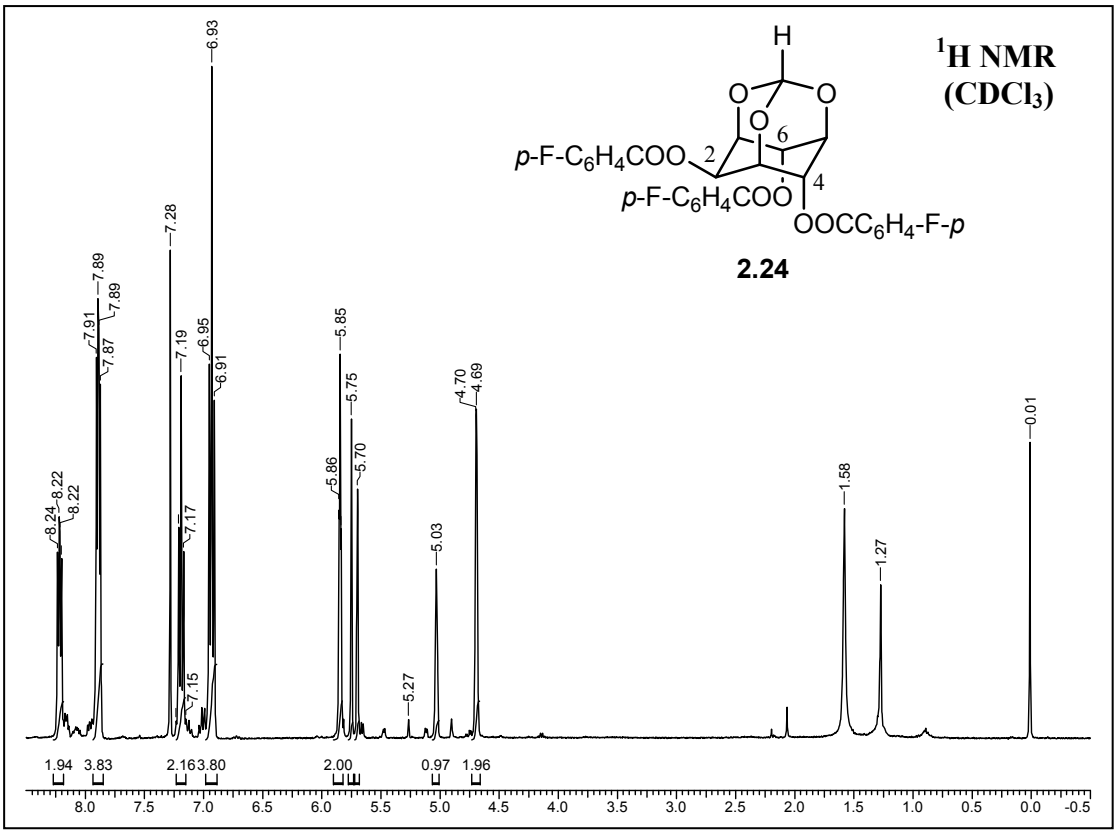
^{1}H NMR
(CDCl$_3$)
p-F-C6H4COO
p-F-C6H4COO
OOCC6H4-F-p
2.24
6.93
7.28
7.89
7.89
7.91
7.87
7.19
6.95
6.91
5.85
5.75
5.70
4.70
4.69
0.01
8.24
8.22
8.22
7.17
5.86
5.03
1.58
1.27
7.15
5.27
1.94 3.83 2.16 3.80 2.00 0.97 1.96

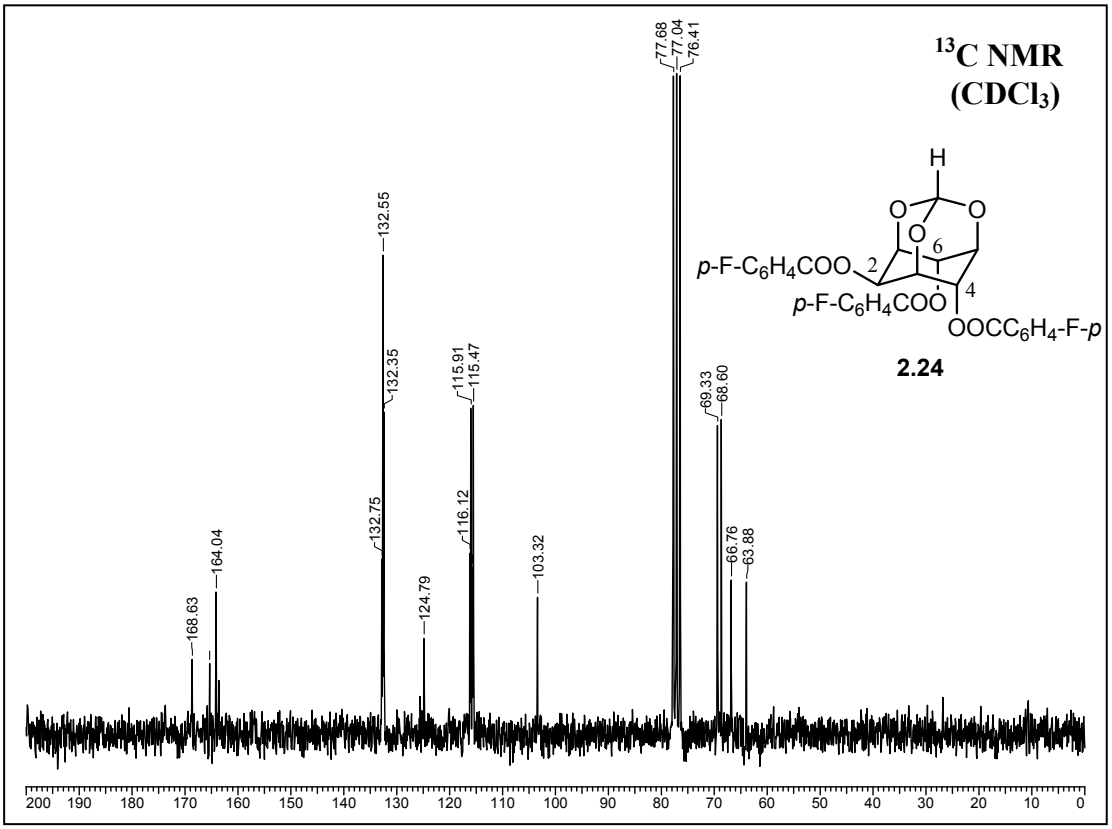
^{13}C NMR
(CDCl$_3$)
p-F-C6H4COO
p-F-C6H4COO
OOCC6H4-F-p
2.24
77.68
77.04
76.41
132.55
132.35
115.91
115.47
69.33
68.60
132.75
116.12
103.32
66.76
63.88
164.04
168.63
124.79

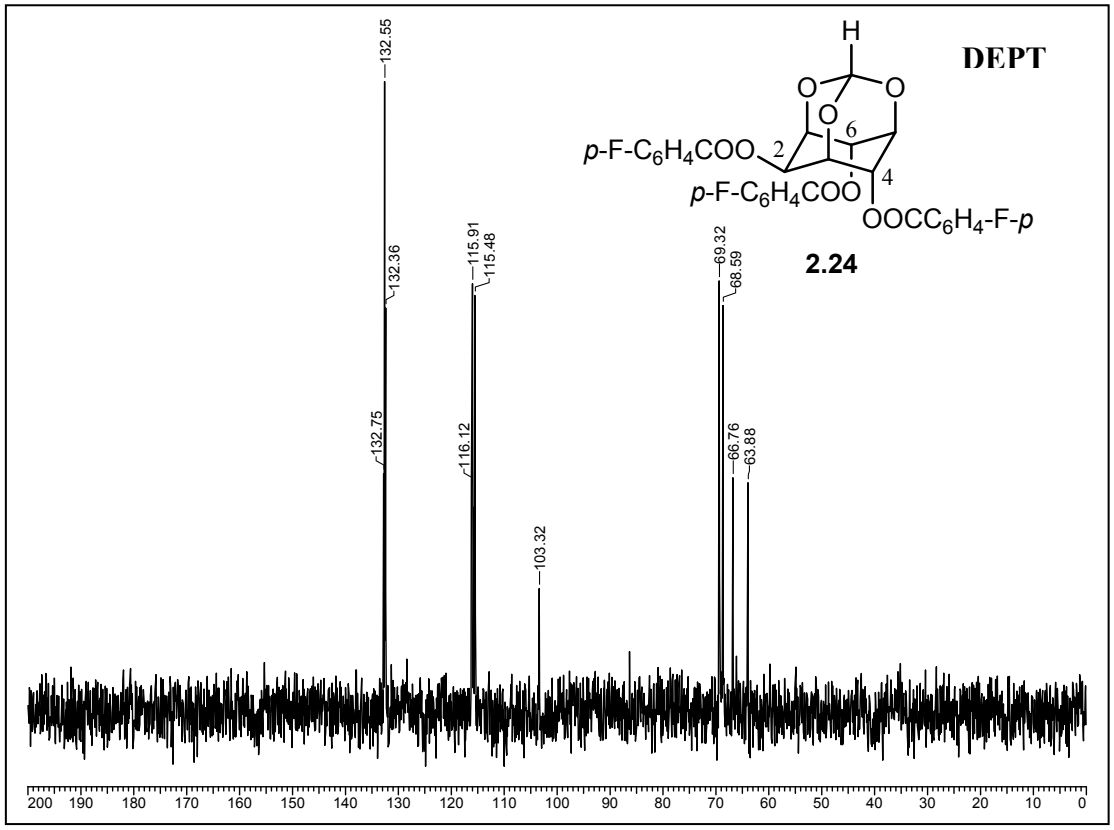
DEPT
132.55
132.36
132.75
115.91
115.48
116.12
103.32
69.32
68.59
66.76
63.88
p-F-C6H4COO
p-F-C6H4COO
OOCC6H4-F-p
2.24
200 190 180 170 160 150 140 130 120 110 100 90 80 70 60 50 40 30 20 10 0

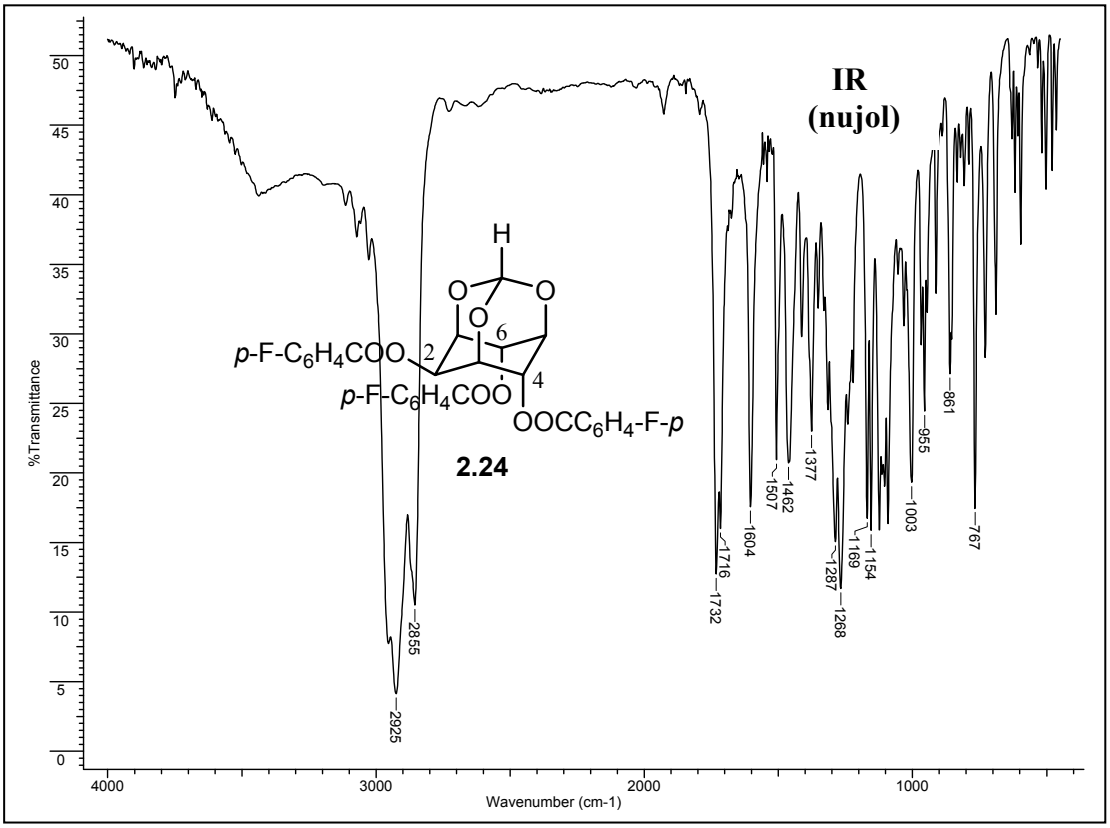
IR
(nujol)
%Transmittance
Wavenumber (cm-1)
4000
3000
2000
1000
2925
2855
1732
1716
1604
1507
1462
1377
1287
1268
1169
1154
1003
955
861
767
p-F-C6H4COO
p-F-C6H4COO
OOCC6H4-F-p
2.24

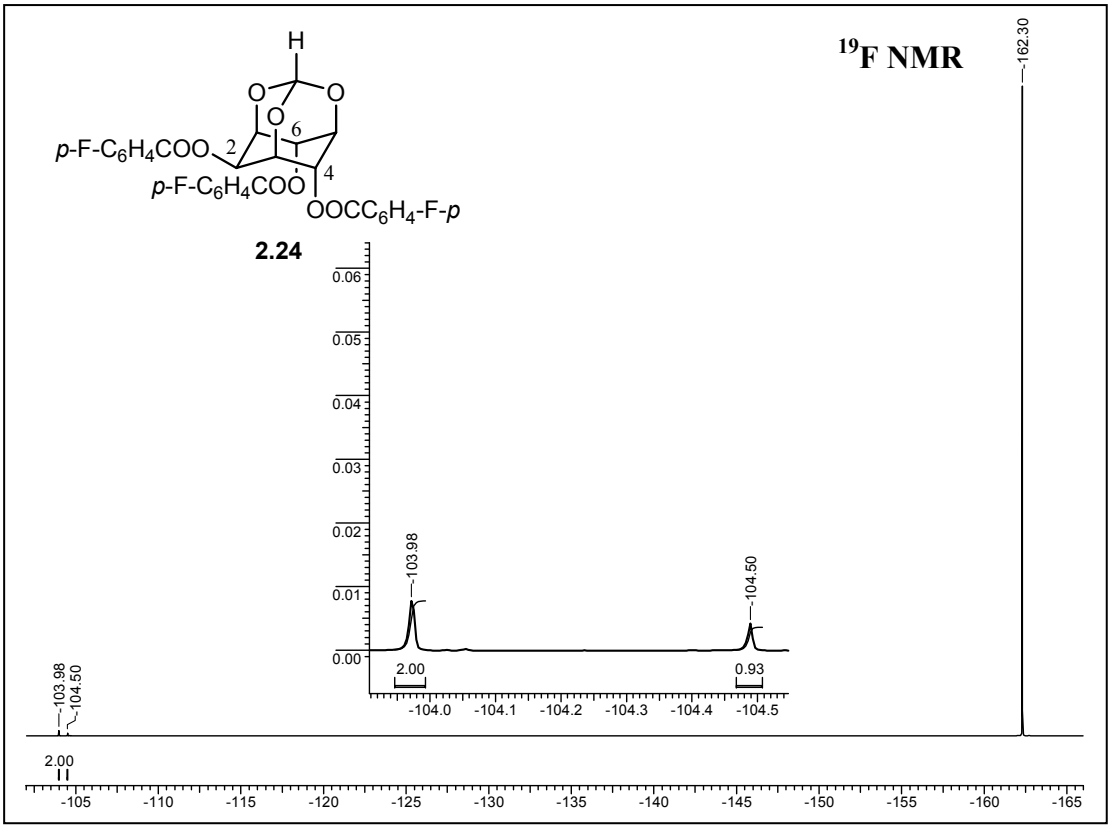
^{19}F NMR
H
O
O
O
O
6
p-F-C$_6$H$_4$COO
2
4
p-F-C$_6$H$_4$COO
OOCC$_6$H$_4$-F-*p*
2.24
162.30
103.98
104.50
2.00
0.93

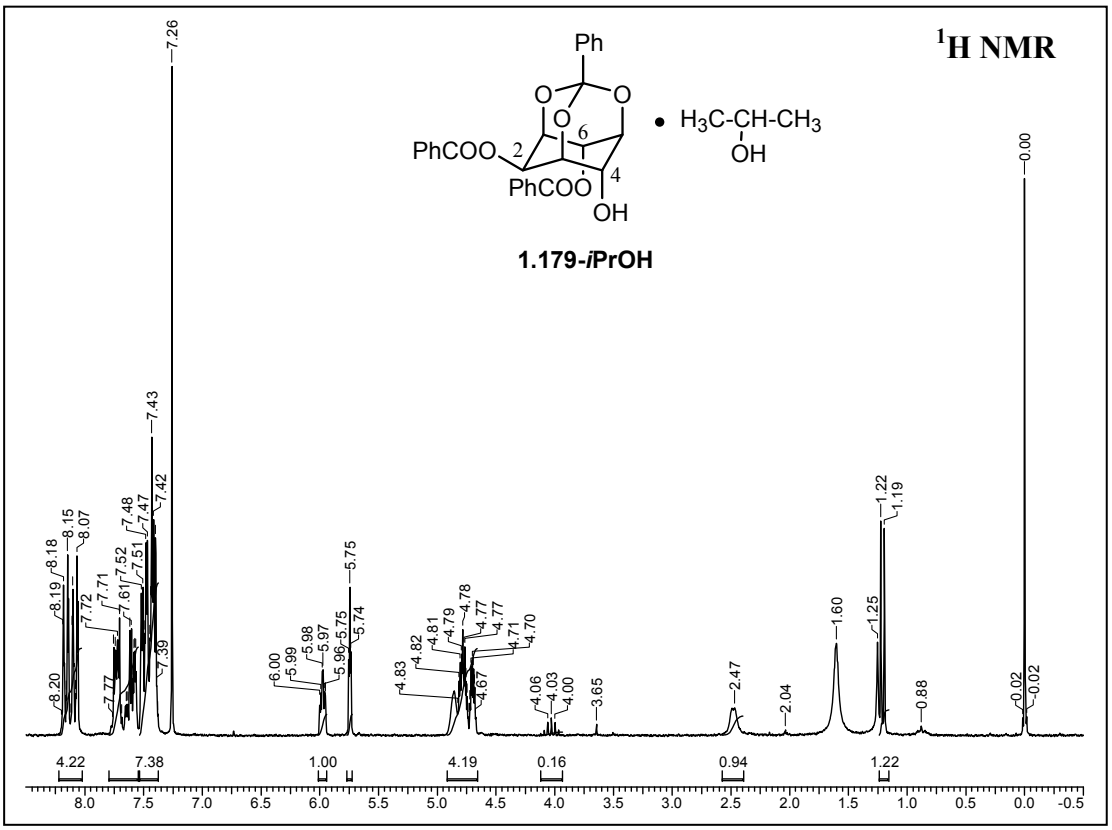
^{1}H NMR
Ph
O
O
O
O
6
PhCOO
2
4
PhCOO
OH
• H$_3$C-CH-CH$_3$
OH
1.179-*i*PrOH
7.26
0.00
7.43
7.42
7.48
7.47
7.52
7.51
7.61
7.71
7.72
8.07
8.15
8.18
8.19
8.20
7.77
7.39
5.75
5.74
5.98
5.97
5.96
5.75
6.00
5.99
4.83
4.82
4.81
4.79
4.78
4.77
4.77
4.71
4.70
4.67
4.06
4.03
4.00
3.65
2.47
2.04
1.60
1.25
1.22
1.19
0.88
0.02
0.02
4.22
7.38
1.00
4.19
0.16
0.94
1.22

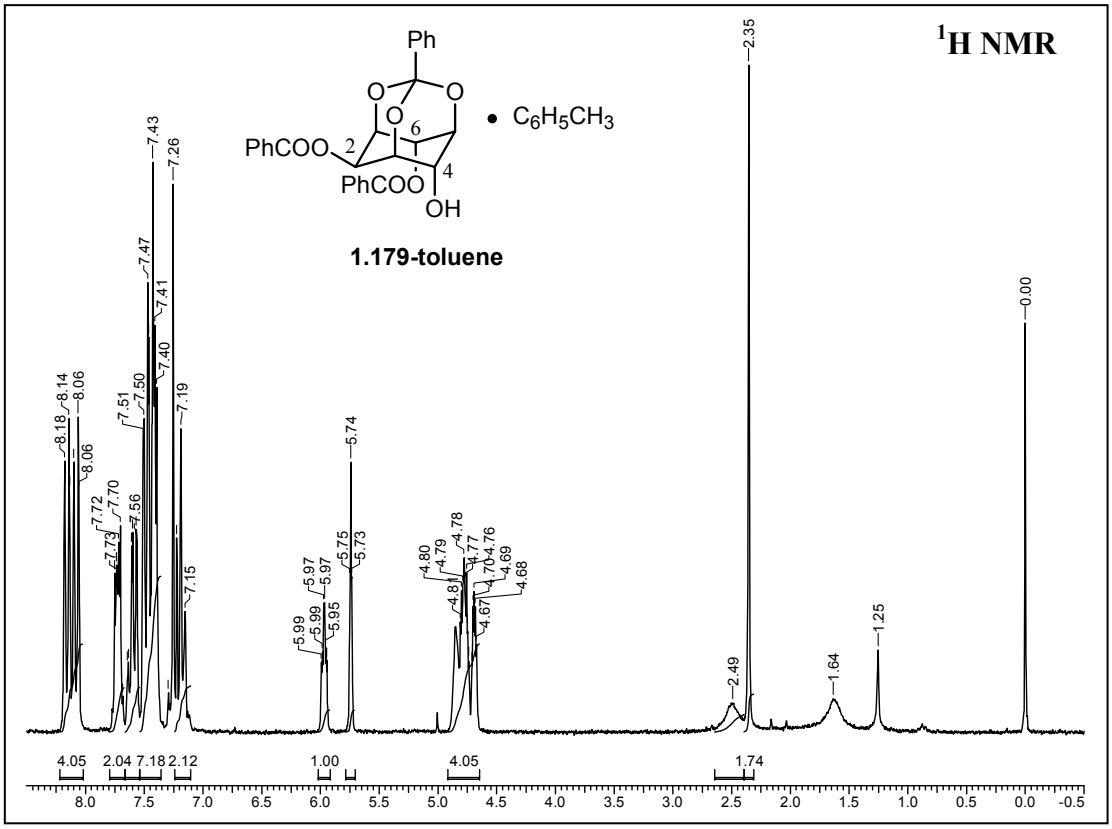
^{1}H NMR
Ph
O
O
O
6
PhCOO
2
4
PhCOO
OH
• $C_6H_5CH_3$
1.179-toluene
8.18
8.14
8.06
8.06
7.72
7.70
7.56
7.51
7.50
7.47
7.43
7.41
7.40
7.26
7.19
7.15
5.99
5.99
5.97
5.97
5.95
5.75
5.74
5.73
4.81
4.80
4.79
4.78
4.77
4.76
4.70
4.69
4.68
4.67
2.49
2.35
1.64
1.25
0.00
4.05
2.04
7.18
2.12
1.00
4.05
1.74

Chapter 3

Crystallization and reactivity of di-*O*-acylated *myo*-inositol derivatives

A great advantage of X-ray analysis as a method of chemical structure analysis is its power to show some totally unexpected and surprising structure with, at the same time, complete certainty.

- Dorothy Crowfoot Hodgkin

3.1 Introduction

Crystal engineering is the design and construction of molecular solids with desired physical and chemical properties, utilising molecular recognition through intermolecular interactions.[1] Non-covalent interactions such as hydrogen bonding, halogen bonding,[2] C-H···π,[3] halogen···halogen,[4] π···π,[5] and halogen···π[6] interactions between molecular building blocks have been exploited for the construction of useful molecular aggregates. However, the prediction of crystal structures and packing of analogues of even small molecules remains a challenging subject. One of the reasons for this is that the modification of even a small functionality in a reactive molecule can sometimes result in an undesirable change in the derivative crystal structure, because of the interplay of weak intermolecular interactions. While certain patterns of non-covalent interactions between molecules can be envisaged on the basis of functional groups and molecular geometry, the supramolecular structure is less predictable. The existence of polymorphs and pseudopolymorphs, arising from various solute-solute and solute-solvent interactions during the process of crystallization, also complicates efforts towards obtaining the desired molecular assembly.

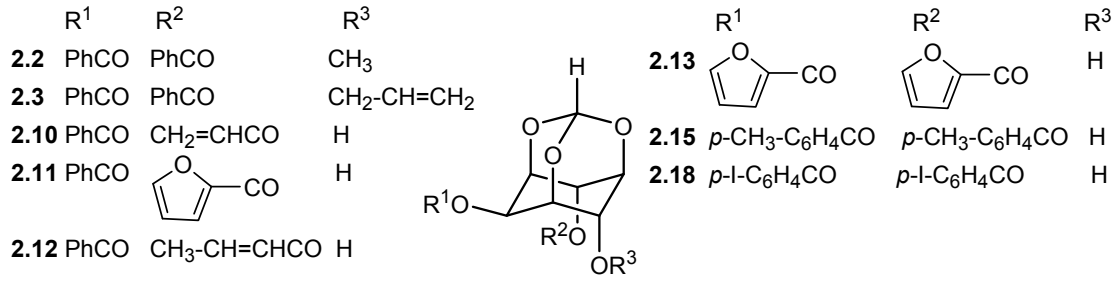

Scheme 3.1 Tri-substituted and di-*O*-acylated *myo*-inositol orthoformates.

In the introductory chapter of this thesis, the importance of helical hydrogen bonded molecular assemblies in crystals of benzoylated *myo*-inositol 1,3,5-orthoester derivatives in the context of benzoyl group transfer that occurs along adjacent molecules in these helices was described. The scope of this acyl transfer reaction was briefly examined by synthesising molecules containing esters other than benzoate groups at the equatorial and axial positions. It was consistently observed that the reactive crystals displayed (a) good electrophile-nucleophile geometry, (b) weak interactions which held the migrating group in the proper orientation for the reaction

and (c) discretely packed helices which acted as reaction tunnels for the acyl transfer resulting in high rate of conversion to products.[7] In order to examine the effect of other functional groups at different positions in the *myo*-inositol orthoformate framework on the molecular pre-organization and crystalline-state reactivity, the crystal structures of some trisubstituted *myo*-inositol orthoformates and di-*O*-acylated *myo*-inositol orthoformates were studied (Scheme 3.1).

3.2 General experimental details

X-ray crystallography: Intensity data was collected for all crystals on a Bruker SMART APEX CCD diffractometer with graphite-monochromatized (Mo K_α= 0.71073Å) radiation. Diffraction data were collected with a ω scan width of 0.3° at different settings of φ (0, 90, 180 and 270°) keeping the sample-to-detector distance fixed at 6.145 cm and the detector position (2θ) fixed at -28°. The X-ray intensities at low temperatures (in some experiments) were measured using an OXFORD LN2 cryosystem. The X-ray data acquisition was monitored by SMART program (Bruker, 2003).[8] All the data were corrected for Lorentz-polarization effects using SAINT programs (Bruker, 2003).[8] A semi-empirical absorption correction (multi-scan) based on symmetry equivalent reflections was applied using the SADABS program (Bruker, 2003).[8] Lattice parameters were determined from least-squares analysis of all reflections. The structures were solved by direct methods and refined by full matrix least squares, based on F^2, using SHELX-97 software package.[9] Thermal ellipsoid plots were generated using ORTEP-32,[10] packing diagrams were prepared using Mercury-2.3[11] and geometrical calculations were performed using PLATON.[12]

Differential Scanning Calorimetry (DSC): The thermal behaviour of crystals was investigated by measuring enthalpy change on a Mettler Differential Scanning Calorimeter. Crystals (2 - 4 mg) placed in a sealed aluminium pan (40 μL) were analyzed from ambient temperature to ~ 35 °C above the melting point of the compound using an empty pan as the reference. The heating rate was 5 °C min^{-1}(or 10 °C min^{-1} in some experiments) and nitrogen gas was used for purging.

Hot stage microscopy (HSM): Crystals heated on the stage (equipped with a temperature probe) were viewed through the eyepiece of a Leica polarizing microscope. Their images were captured using an on-board Leica camera.

General experimental procedure for solid-state reactions: Freshly grown crystals of the compound (1 equiv.) were ground together with activated solid Na_2CO_3 (8 equiv.) into a fine powder using a mortar and pestle. This powder was transferred to a hard glass test-tube and heated in an oil bath (in an inert atmosphere) maintained at a temperature below the melting point of the compound.

The acrylate rac-2.10: A mixture of form I crystals of **rac-2.10** (0.052 g, 0.15 mmol) and activated Na_2CO_3 (0.127 g, 1.2 mmol) ground together into a powder, was heated at 100 °C for 40 h. TLC analysis showed the presence of several products and absence of **rac-2.10**. The mixture was dissolved in dry pyridine and acetylated with excess acetic anhydride. Pyridine was evaporated under reduced pressure and the reaction mixture was diluted with ethyl acetate and washed with water, dilute HCl, $NaHCO_3$ solution, brine. The organic layer was dried with Na_2SO_4 and concentrated to obtain a gum. Analysis by proton NMR spectroscopy revealed the presence of di-acetylated **1.183**, i.e. 2-*O*-benzoyl 4,6-di-*O*-acetyl *myo*-inositol 1,3,5-orthoformate[13] amongst other unidentified products.

The di-*p*-toluate rac-2.15: A mixture of crystals of **rac-2.15** (0.149 g, 0.35 mmol) and activated Na_2CO_3 (0.297 g, 2.8 mmol) ground together into a powder, was initially heated at 110 °C for 17 h. TLC indicated the presence of only **rac-2.15**. The temperature was increased upto 130 °C and heating was continued for 47 h, at the end of which **rac-2.15** was recovered quantitatively.

The di-*p*-iodobenzoate rac-2.18: A mixture of crystals of **rac-2.18** (0.0195 g, 0.03 mmol) and activated Na_2CO_3 (0.0254 g, 0.24 mmol) ground together into a powder, was heated at 130 °C for 72 h. TLC analysis indicated a mixture of products, including **rac-2.18** and the diol **rac-2.19**, which were not separated.

The solid-state reactivities of **rac-2.10**-form II, **rac-2.11** and **rac-2.13** could not be studied due to the low yield of crystals of these compounds.

3.3 Synthesis, crystallization and X-ray crystallography

Racemic 2,6-di-*O*-benzoyl 4-*O*-methyl *myo*-inositol 1,3,5-orthoformate (**rac-2.2)** was synthesised earlier[13] in our laboratory for exploring the solvolysis of benzoyl groups in the presence of the methyl ether at C4.[14] Racemic 2,6-di-*O*-benzoyl 4-*O*-allyl *myo*-inositol 1,3,5-orthoformate (**rac-2.3**) was obtained by silver oxide assisted allylation of **rac-1.177**.[13] Intensity data for **rac-2.2,** when collected at low temperature

resulted in breakage of the crystal and poor quality diffraction patterns in some trials; hence the data were collected at ambient temperature. All non-hydrogen atoms were refined anisotropically and hydrogen atoms were included in the refinement as per the riding model. The racemic diesters **rac-2.10**, **rac-2.11**, **rac-2.13**, **rac-2.15** and **rac-2.18** were synthesised, characterised and crystallized as described in chapter 2. Diffraction data were collected as reported in **Sec. 3.2**. Hydroxyl (-OH) hydrogen atoms in all the structures were located in difference Fourier maps and refined isotropically. In the case of **rac-2.11** and **rac-2.18**, the O-H bond length was restrained using the DFIX instruction in SHELXL97. All other H-atoms were placed in geometrically idealized positions and non-hydrogen atoms were refined anisotropically. The experimental details are summarised in Table 3.3.1.

Table 3.3.1 Crystallographic data for tri- and di-substituted *myo*-inositol 1,3,5-orthoformates.

	rac-2.2	**rac-2.3**	**2.10 (Form I)**
Chemical formula	$C_{22}H_{20}O_8$	$C_{24}H_{22}O_8$	$C_{17}H_{16}O_8$
M_r	412.38	438.42	348.30
Temperature (K)	297(2)	100(2)	297(2)
Morphology	plate	plate	plate
Crystal size	0.29 × 0.20 × 0.10	0.38 × 0.30 × 0.25	0.56 × 0.43 × 0.19
Crystal system	Triclinic	Monoclinic	Triclinic
Space group	*P*-1	$P2_1/n$	*P*-1
a (Å)	10.4163(13)	10.3917(7)	8.8808(6)
b (Å)	14.6208(18)	14.2891(10)	9.5502(6)
c (Å)	14.7002(18)	13.8573(10)	9.7100(6)
α (°)	118.137(2)	90	102.266(1)
β (°)	90.812(2)	97.4360(10)	101.733(1)
γ (°)	90.347(2)	90	94.334(1)
V (Å^3)	1973.8(4)	2040.3(2)	781.83(9)
Z	4	4	2
D_{calc} (g cm^{-3})	1.388	1.427	1.480
μ (mm^{-1})	0.106	0.108	0.119
F(000)	864	920	364
T_{min}	0.970	0.960	0.936,
T_{max}	0.989	0.974	0.978
h, k, l (min, max)	(-12, 12), (-17, 17), (-17, 17)	(-10,12), (-16,16), (-15,16)	(-10, 10), (-11, 11), (-11, 11)
Reflns collected	19274	10071	9163
Unique reflns	6947	3589	2755
Observed reflns	4595	3328	2374
R_{int}	0.0291	0.0163	0.014
No. of parameters	543	289	230
GoF	1.041	1.046	1.03
$R_1[I > 2\sigma(I)]$	0.0539	0.0344	0.0535
$wR_2[I > 2\sigma(I)]$	0.1170	0.0895	0.1449
R_1_all data	0.0882	0.0367	0.0596
wR_2_all data	0.1327	0.0912	0.1514
$\Delta\rho_{max}$,$\Delta\rho_{min}$(eÅ^{-3})	0.18, -0.13	0.25, -0.18	0.44, -0.14

Table 3.3.1 Contd...

	2.10 (Form II)	**2.11**	**2.13**
Chemical formula	$C_{17}H_{16}O_8$	$C_{19}H_{16}O_9$	$C_{17}H_{14}O_{10}$
M_r	348.30	388.32	378.28
Temperature (K)	133(2)	297(2)	297(2)
Morphology	needle	plate	plate
Crystal size	0.19 × 0.12 × 0.05	0.38 × 0.31 × 0.05	0.44×0.15×0.01
Crystal system	Monoclinic	Orthorhombic	Triclinic
Space group	$P2_1$	$Pca2_1$	P-1
a (Å)	13.813(4)	33.481(11)	8.0783(10)
b (Å)	19.279(5)	7.786(2)	9.8959(12)
c (Å)	5.9801(15)	6.671(2)	10.9889(14)
α (°)	90	90	76.081(2)
β (°)	96.665(4)	90	69.424(2)
γ (°)	90	90	80.923(2)
V (Å^3)	1581.8(7)	1739.0(9)	795.69(17)
Z	4	4	2
D_{calc} (g cm^{-3})	1.463	1.483	1.579
μ (mm^{-1})	0.118	0.120	0.133
F(000)	728	808	392
T_{min}	0.978,	0.956,	0.944
T_{max}	0.994	0.994	0.999
h, k, l (min, max)	(-16, 16), (-22, 22), (-7, 7)	(-39, 39), (-5, 9), (-7, 7)	(-9, 9), (-11, 11), (-13, 13)
Reflns collected	15127	8351	7724
Unique reflns	2870	2983	2791
Observed reflns	2669	2215	1976
R_{int}	0.075	0.0507	0.0198
No. of parameters	453	257	248
GoF	1.136	1.094	1.027
$R_1[I > 2\sigma(I)]$	0.0482	0.0463	0.0468
$wR_2[I > 2\sigma(I)]$	0.1119	0.0972	0.1238
R_1_all data	0.0528	0.0750	0.0677
wR_2_all data	0.1143	0.1277	0.1377
$\Delta\rho_{max}$,$\Delta\rho_{min}$(eÅ^{-3})	0.29, -0.21	0.21, -0.23	0.23, -0.16

Table 3.3.1 Contd...

	2.15	**2.18**
Chemical formula	$C_{23}H_{22}O_8$	$C_{21}H_{16}I_2O_8$
M_r	426.41	650.14
Temperature (K)	297(2)	297(2)
Morphology	thin plate	Thin plate
Crystal size	0.15 × 0.05 × 0.03	0.15 × 0.07 × 0.04
Crystal system	Triclinic	Monoclinic
Space group	*P*-1	$P2_1/c$
a (Å)	6.8474(15)	6.8984(12)
b (Å)	11.558(3)	36.230(7)
c (Å)	13.858(3)	8.3985(15)
α (°)	108.274(4)	90
β (°)	98.891(4)	96.013(3)
γ (°)	90.870(4)	90
V (Å^3)	1026.6(4)	2087.5(6)
Z	2	4
D_{calc} (g cm^{-3})	1.379	2.069
μ (mm^{-1})	0.105	3.060
F(000)	448	1248
T_{min}	0.984	0.664
T_{max}	0.996	0.877
h, k, l (min, max)	(-8, 8), (-13, 13), (-16, 16)	(-7, 8), (-33, 43), (-9, 9)
Reflns collected	9911	10546
Unique reflns	3606	3668
Observed reflns	2342	3286
R_{int}	0.0447	0.0287
No. of parameters	286	284
GoF	1.149	1.083
$R_1[I > 2\sigma(I)]$	0.0775	0.0294
$wR_2[I > 2\sigma(I)]$	0.1410	0.0619
R_1_all data	0.1209	0.0353
wR_2_all data	0.1570	0.0642
$\Delta\rho_{max}$,$\Delta\rho_{min}$(eÅ^{-3})	0.17, -0.20	0.87, -0.42

3.4 Results and discussion

3.4.1 Structural features

(A) The tri-substituted *myo*-inositol 1,3,5-orthoformates

Although **rac-2.2** and **rac-2.3** do not contain any reactive functional groups (for acyl transfer), examination of their crystal structures revealed interesting similarities with the crystal structure of the reactive 2,6-di-*O*-benzoyl *myo*-inositol 1,3,5-orthoformate (**rac-1.177**). The crystal structure of **rac-2.2** is reported previously[14] (CSD code: MEYBIB). Though the molecular arrangement in **rac-2.2** indicated approximate $P2_1/c$ symmetry, the space group was retained as P-1 based on data processing and refinement statistics. Hence a redetermination of the crystal structure was undertaken and is reported here with a slight improvement in the R-factor with respect to the previously reported data. The crystals of **rac-2.2** are triclinic, belonging to the space group P-1, with two molecules (*A* and *B*) in the asymmetric unit (Fig. 3.4.1a) while crystals of **rac-2.3** are monoclinic, space group $P2_1/n$ (Fig. 3.4.1b). The two molecules in the asymmetric unit of **rac-2.2** are not significantly different except for minor conformational difference in the axial aryl rings.

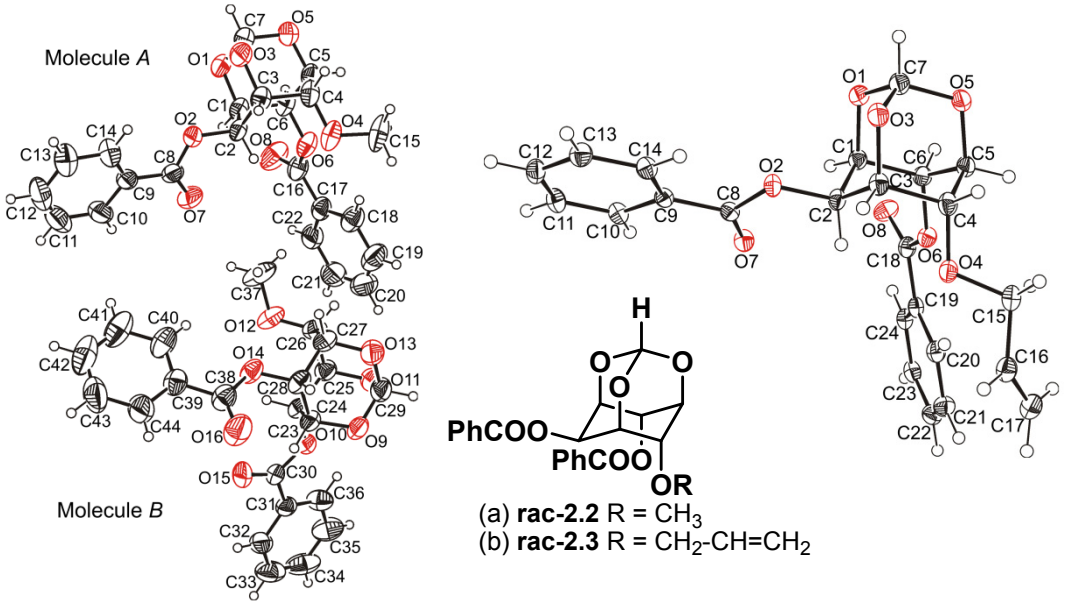

Figure 3.4.1 The molecular structure of (a) **rac-2.2** and (b) **rac-2.3**, showing the atom-labelling scheme. Thermal ellipsoids are drawn at the 40% probability level and hydrogen atoms are shown as small spheres of arbitrary radii.

In the crystals of the methyl ether **rac-2.2**, C-H···O interactions between the *O*-methyl group and the equatorial ester carbonyl oxygen (C15-H15B···O15 and C37-H37B···O7, Fig. 3.4.2a) are instrumental in the formation of a helix-like assembly along the *a*-axis similar to the spiral assembly adopted by the molecules of **rac-1.177** in their crystals through O-H···O hydrogen bonding.[15]

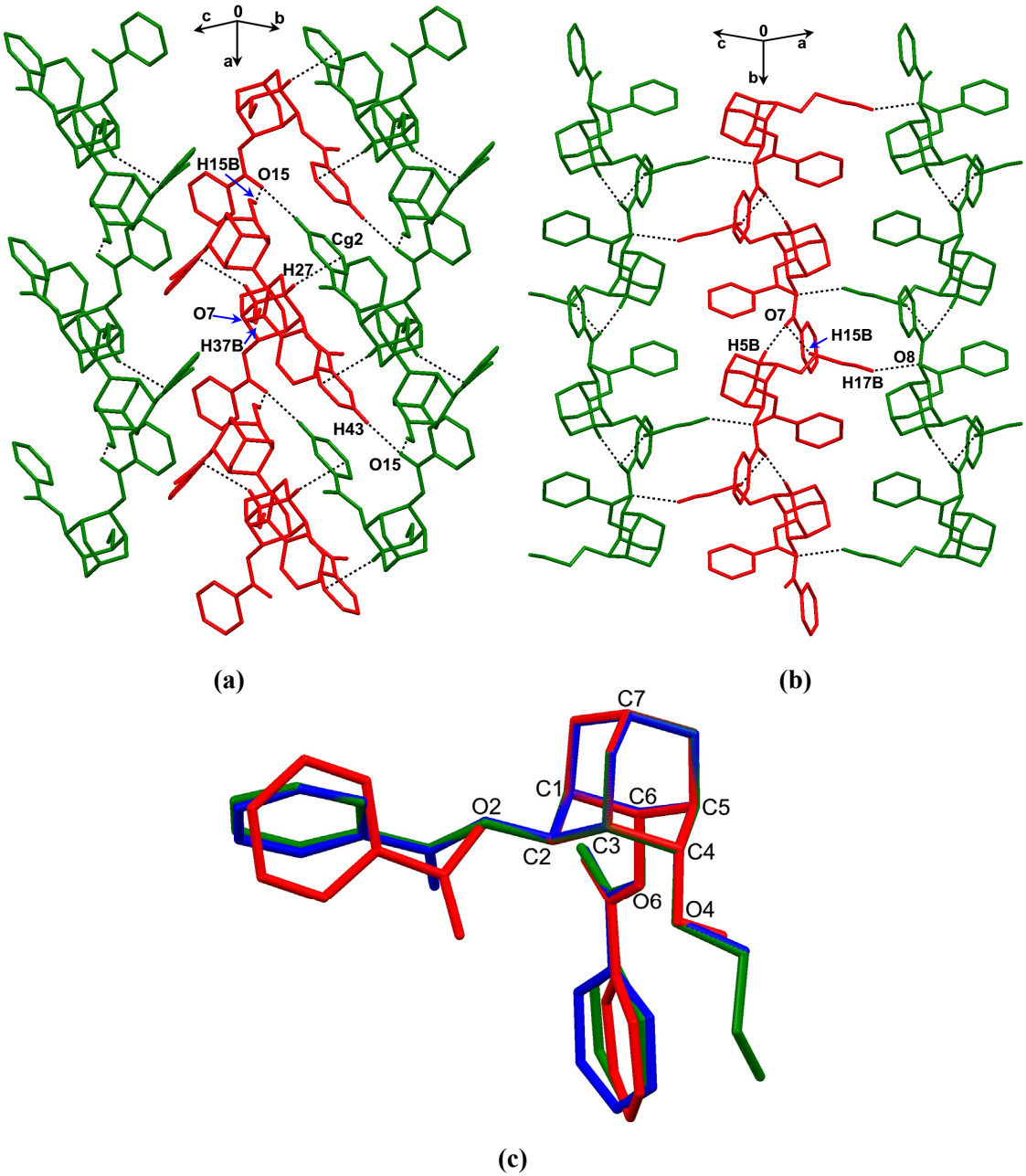

Figure 3.4.2 Helix-like assembly *via* hydrogen bonding interactions in crystals of (a) **rac-2.2** and (b) **rac-2.3**. Red and green indicate the two enantiomers. H-atoms not involved in hydrogen bonding are omitted for the sake of clarity. (c) shows the molecular overlap of **rac-1.177** (red)**, rac-2.2** (blue) and **2.3** (green).

The molecules of the allyl ether **rac-2.3** assemble in helical fashion along the crystallographic two-fold *b*-axis *via* bifurcated moderately strong C-H···O interactions between the hydrogen atoms H15B (of the allyl group) and H5 (of the inositol ring) and the equatorial ester carbonyl oxygen atom O7 (C5-H5···O7 and C15-H15B···O7, Fig. 3.4.2b, Table 3.4.1).

Table 3.4.1 Intermolecular interactions in crystals of **rac-2.2** and **rac-2.3**.

	D-H···A	D-H (Å)	H···A (Å)	D···A (Å)	D-H···A (°)
2.2	C15-H15B···O15^{i}	0.96	2.51	3.388(3)	153
	C37-H37B···O7	0.96	2.50	3.259(4)	136
	C43-H43···O15^{ii}	0.93	2.56	3.402(4)	150
	C5-H5···Cg1*^{iii}	0.98	2.55	3.471(3)	156
	C27-H27···Cg2*^{iv}	0.98	2.58	3.506(3)	157
2.3	C5-H5···O7^{v}	1.00	2.37	3.359(2)	172
	C15-H15B···O7^{v}	0.99	2.52	3.330(2)	139
	C13-H13B···O5^{vi}	0.95	2.58	3.384(2)	142
	C17-H17B···O8^{vii}	0.95	2.61	3.486(2)	154

Symmetry codes: (i) *x* - 1, *y*, *z*; (ii) –*x* + 2, -*y* + 1, -*z*; (iii) -*x*, -*y* + 1, -*z* + 1; (iv) –*x* + 1, -*y* + 1, -*z*; (v) –*x* + 1/2, *y* – 1/2, -*z* + 1/2; (vi) *x* – 1/2, -*y* + 3/2, *z* - 1/2; (vii) *x* + 1/2, -*y* + 3/2, *z* – 1/2.

*Cg1 = Centroid of ring C17-C22; *Cg2 = centroid of ring C39-C44.

C-H···π interactions in **rac-2.2** between the inositol ring proton and the axial ester aryl ring (C5-H5···Cg1 and C27-H27···Cg2, Fig. 3.4.2a) link the adjacent helices along the *c*-axis along with moderately strong C43-H43···O15 interactions (Table 3.4.1). In the case of **rac-2.3** the adjacent helices along the *bc*-diagonal are linked by weak C-H···O interactions between the hydrogen of the allyl group and the axial carbonyl oxygen O8 (C17-H17B···O8 contacts, Fig. 3.4.2b) and along the *ac*-diagonal by C13-H13···O5 interactions. As observed in **rac-1.177** each helix is built up of a single enantiomer and the adjacent helix contains molecules of the other enantiomer. Examination of the unit cell parameters of **rac-2.2** and **rac-2.3** reveals a close correspondence in the *a* and *b* axis lengths while the *c*-axis is longer by ~ 1 Å in the methyl ether (Table 3.3.1). The molecular overlap of the methyl and allyl ethers

with the reactive dibenzoate **rac-1.177** (Fig. 3.4.2c) reveals that while the equatorial benzoyl groups of the methyl and allyl ethers overlap almost completely with each other, there is a torsional difference of ~ 58° in their overlap with the equatorial benzoate of **rac-1.177**. The methyl and allyl groups almost perfectly overlap with the hydroxyl group of **rac-1.177**, while there is a minor torsional difference in the overlap of the axial esters, explaining the similar patterns of molecular organization in their crystals.

(B) The di-substituted *myo*-inositol 1,3,5-orthoformates

Crystal structure solution revealed that form I crystals of **rac-2.10** belonged to triclinic *P*-1 (Table 3.3.1, Fig. 3.4.3a) while the form II crystals belonged to the chiral space group $P2_1$ with two molecules in the asymmetric unit of different chirality (Table 3.3.1, Fig. 3.4.3b). The furoate ester **rac-2.11** crystallised in the polar orthorhombic space group $Pca2_1$ (Fig.3.4.3c) and the di-furoate **rac-2.13** in triclinic *P*-1 (Fig. 3.4.3d) while the crotonate ester **rac-2.12** solidified into amorphous matter, but did not yield crystals.

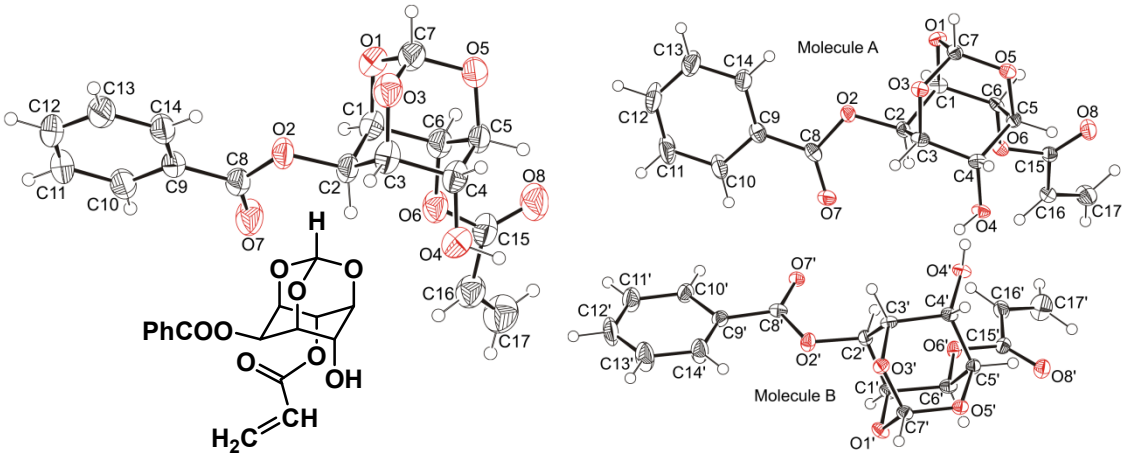

(a) **(b)**

Fig. 3.4.3 ORTEPs of molecules in crystals of (a) **rac-2.10** (form I), (b) **rac-2.10** (form II). Contd…

Recognising that the presence of benzoate groups could be possibly essential for the creation of the helical molecular assembly (from the structures of the tri-substituted *myo*-inositol orthoformates), the structures of orthoformates with *p*-methylbenzoate **rac-2.15** (Fig. 3.4.1e) and *p*-iodobenzoate **rac-2.18** (Fig. 3.4.1f) were investigated.

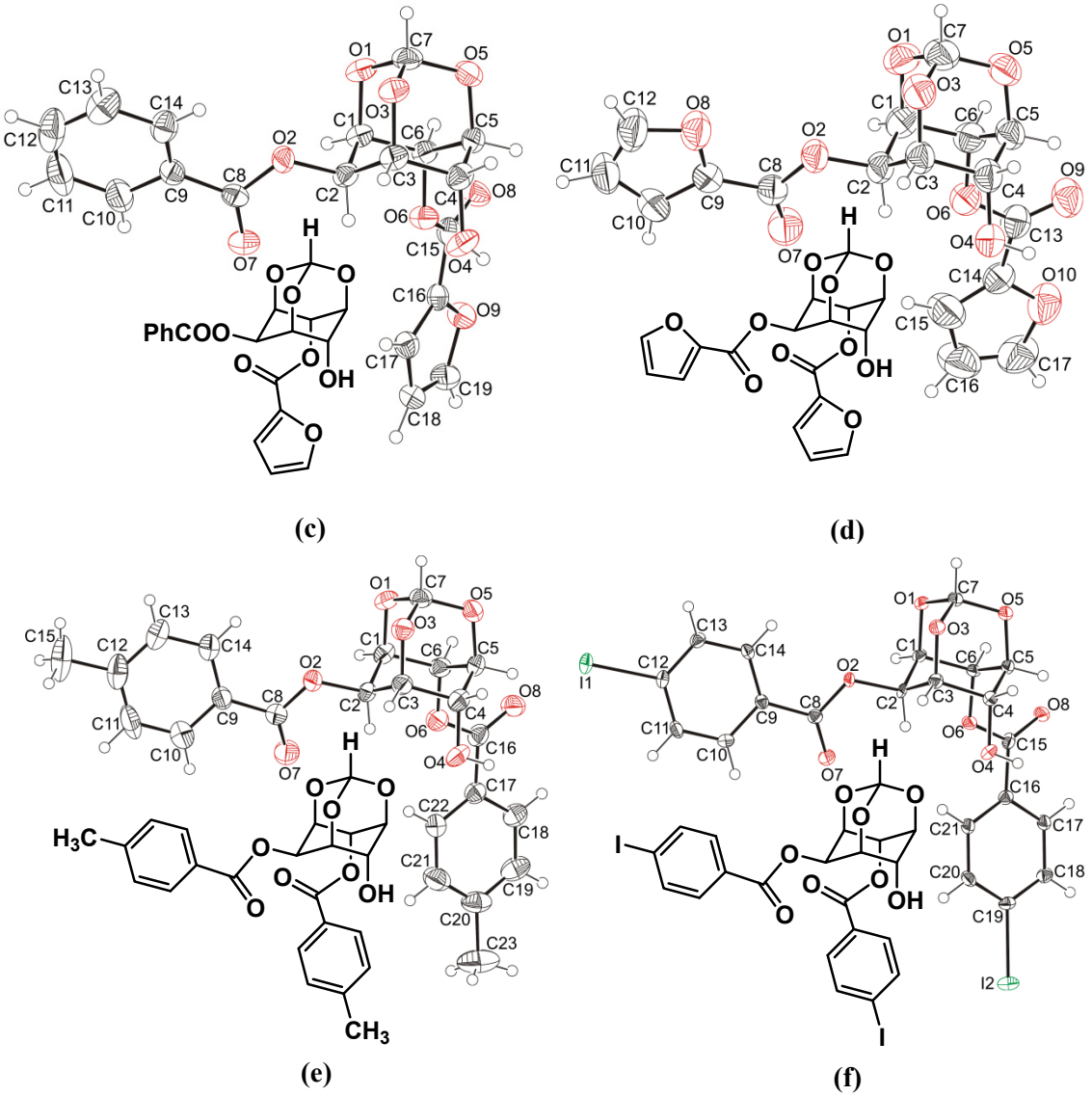

Fig. 3.4.3 Contd…(c) **rac-2.11**, (d) **rac-2.13**, (e) **rac-2.15** and (f) **rac-2.18**. Thermal ellipsoids are drawn at 40% probability and hydrogen atoms are depicted as small spheres of arbitrary radii.

The diesters **rac-2.15** and **rac-2.18** crystallized in the triclinic *P*-1 and monoclinic $P2_1/c$ space groups respectively.

(a) Structure of the acrylate rac-2.10

The acrylate, **rac-2.10** yielded conformational dimorphs (forms I and II) upon crystallization from different solvents as described in chapter 2. The molecular overlap of form I crystals and molecule 1 of form II crystals revealed major conformational change in the hydroxyl groups as well as benzoyl groups (Fig. 3.4.4a). The orientations of the -OH groups were almost reversed (113°) whereas benzoyl

groups showed a difference of ~ 52° in their torsion angles. The difference in torsion angles of the acryloyl group (C1-C6-O6-C15) was 13°. These conformational changes in the three functional groups have a profound influence on the molecular association in the dimorphs.

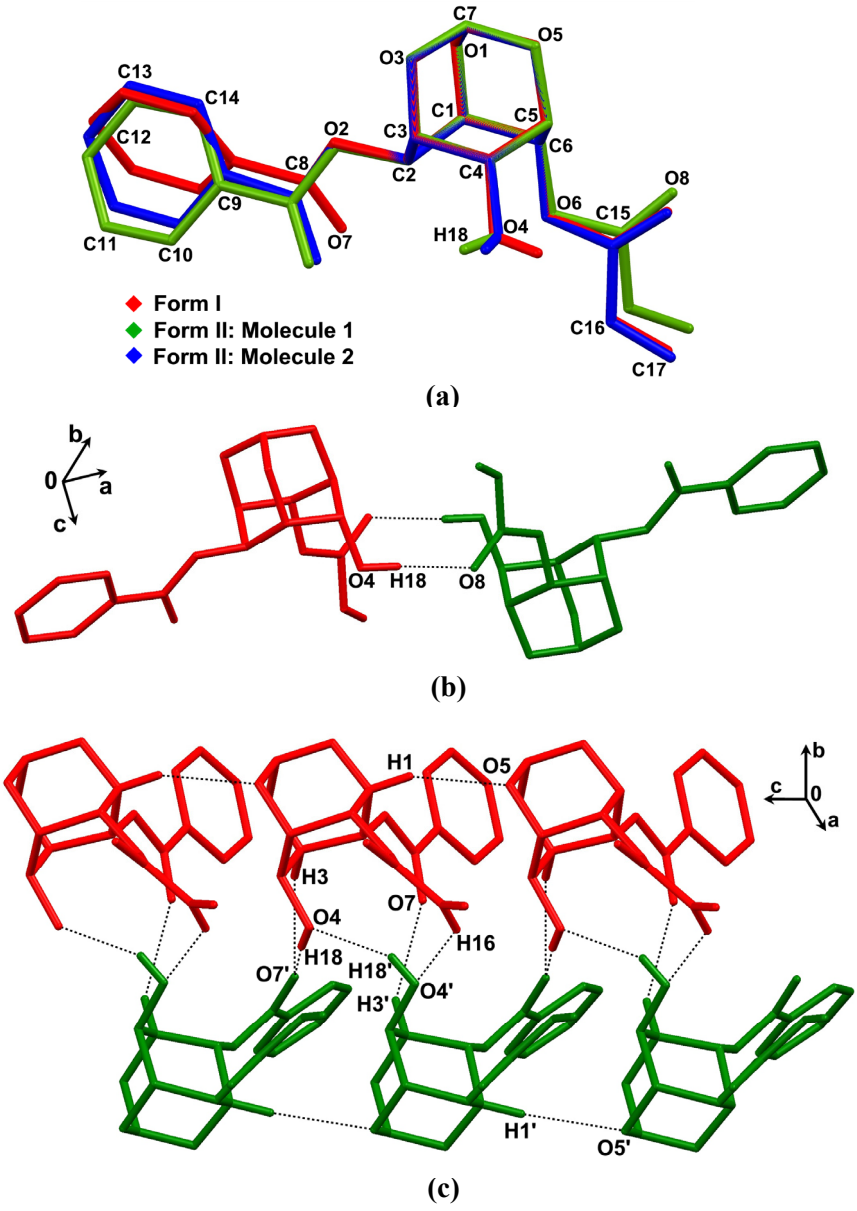

Figure 3.4.4 (a) Molecular overlap of form I and form II crystals of **rac-2.10** shows the conformational differences in the dimorphs. Hydrogen bonding interactions in crystals of: (b) form I - O-H···O linked dimers and (c) form II - catemeric association along the *c*-axis. Red and green indicate the two enantiomers; hydrogen atoms not involved in hydrogen bonding are omitted for the sake of clarity.

The hydroxyl group makes different O-H···O intermolecular hydrogen bonds in crystals of forms I and II. In form I, the adjacent molecules make centrosymmetric dimers *via* O-H···O hydrogen bonds involving OH group (O4-H18) and carbonyl oxygen O8 of the acryloyl group (Fig. 3.4.4b). In the form II crystals the –OH groups of the two symmetry independent molecules are involved in a hydrogen bonding interaction (O4'-H18'···O4, Fig. 3.4.4c). The acceptor oxygen O4 also acts as a donor in forming a conventional hydroxyl···carbonyl interaction (O4-H18···O7'), thus forming a catemeric arrangement along the *c*-axis. Additionally, five supporting C-H···O interactions (C1-H1···O5, C1'-H1'···O5', C3-H3···O7', C3'-H3'···O7, C16-H16···O4', Fig. 3.4.4c) hold the molecules along the chain direction. The hydrogen bonded units thus formed make different three-dimensional patterns of molecular organization in the polymorphs. In form I crystals O-H···O linked centrosymmetric dimers form a planar structure (Fig. 3.4.5a).

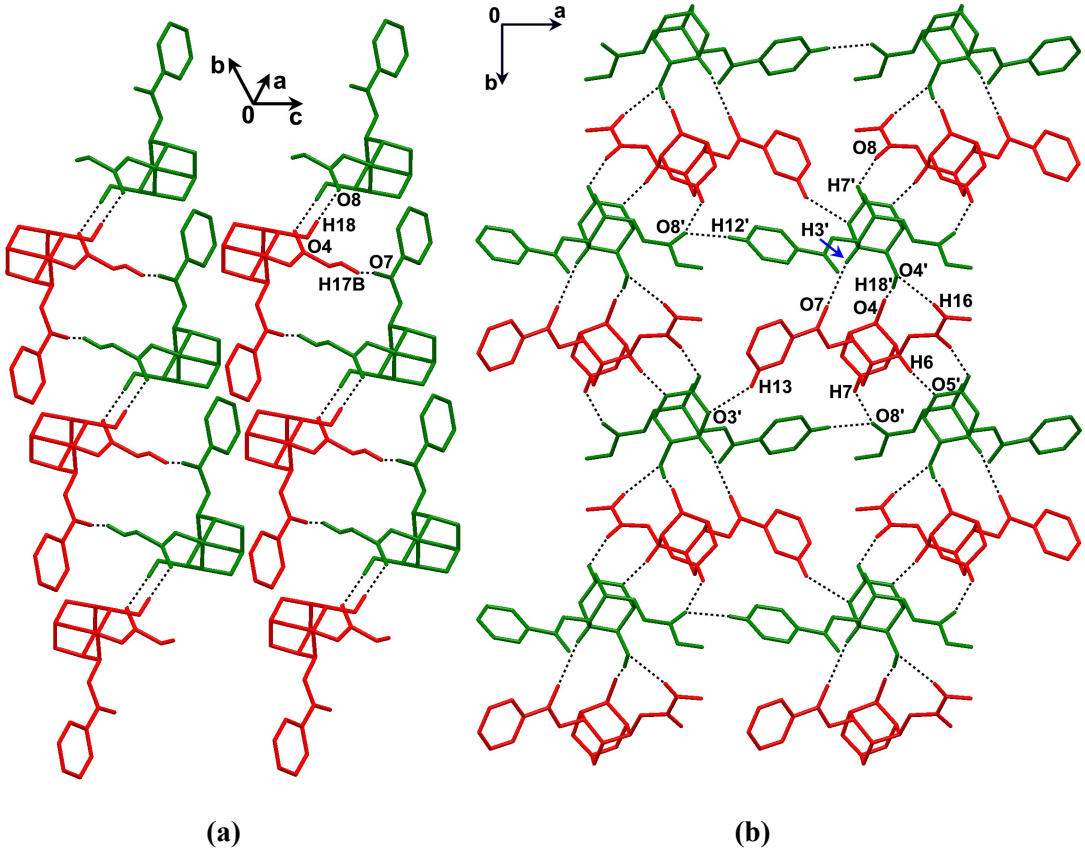

Figure 3.4.5 Molecular packing in (a) form I - dimers and (b) form II - catemers. Red and green indicate the two enantiomers; hydrogen atoms not involved in hydrogen bonding are omitted for the sake of clarity.

In form II, each molecule in the asymmetric unit forms a dimer by aggregating sideways, bringing orthoformate groups closer by non-centrosymmetric C-H···O interactions (C7-H7···O8', C6-H6···O5', C7'-H7'···O8) of comparable strength. These dimeric units are stitched together *via* O4'-H18'···O4, C3-H3···O7' and C16-H16···O4' hydrogen bonding interactions, thus forming a chain extended along the *b*-axis. The neighboring chains are weakly associated along the *a*-axis *via* C12'-H12'···O8' and C13-H13···O3' contacts thus forming a layered arrangement (Fig. 3.4.5b; Table 3.4.2).

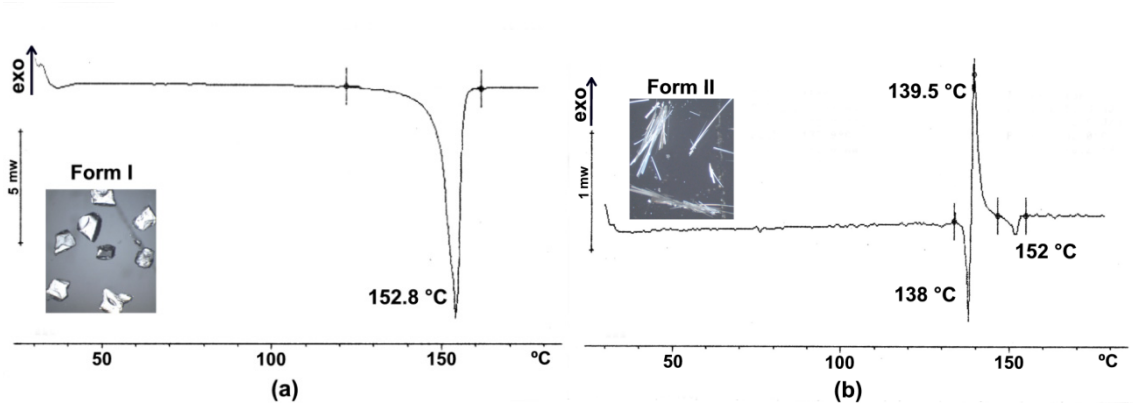

Figure 3.4.6 DSC curve of (a) form I crystals of **rac-2.10**, showing one endotherm and (b) form II crystals of **rac-2.10** with an endotherm, followed by an exotherm with a second endotherm indicating melting. Inset shows the crystal morphology of the two dimorphs.

A DSC study of crystals of form I showed only a single endotherm at 153 °C (Fig. 3.4.6a), while crystals of form II showed two endothermic peaks (Fig. 3.4.6b). The first of these, at 138 °C, was established by hot-stage microscopy (Fig. 3.4.7) to be the structural phase transition to form I *via* a molten phase. The second endotherm at 152 °C corresponds to the melting of the crystals of form I. While single-crystal to single-crystal thermal phase transitions have been reported earlier in *myo*-inositol derivatives,[16] in this instance the conversion of form II to form I occurs *via* melt crystallization, often observed amongst polymorphs of pharmaceutical crystals.[17] Thus, form II crystals upon heating transform irreversibly to form I crystals.

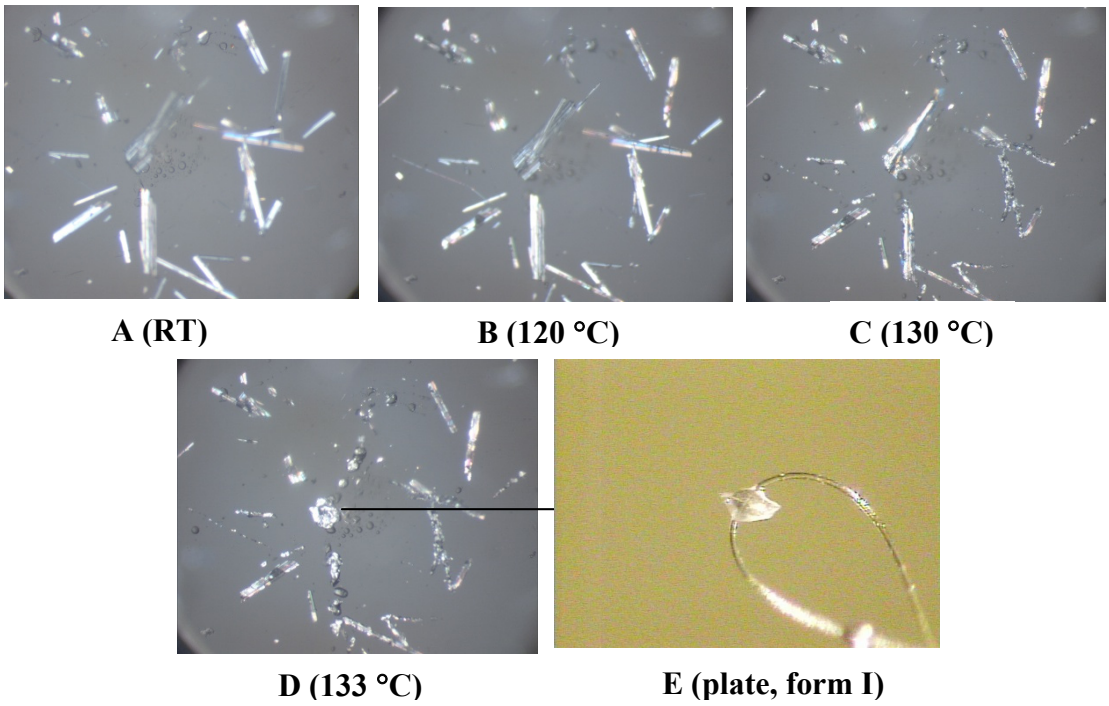

Figure 3.4.7 HSM images of form II crystals of **rac-2.10**: (A) at ambient temperature; (B) onset of melting; (C) melt recrystallization; (D) plate like fragments and (E) form I (plate).

(b) The structures of furoates rac-2.11 and rac-2.13

The molecular packing in **rac-2.11** seems to have been influenced by the excellent π···π stacking interaction between furan moieties (Fig. 3.4.8a, Cg···Cg distance between two furan rings is 3.594(3) Å and the dihedral angle between them is 0.62˚). O···C=O interactions between molecules along the *c*-axis (O4···C8=O7) form homochiral molecular chains (Fig. 3.4.8a, green or red). Adjacent homochiral molecular chains are interlinked by O-H···O and weak C-H···O interactions (C5-H5···O8, O4-H4A···O9) between the hydroxyl group and furanyl group of heterochiral glide related molecules (Fig. 3.4.8a). These molecular chains are connected across the *b*-axis (Fig. 3.4.8b, Table 3.4.2) by moderately strong C-H···O interactions (C17-H17···O5, C7-H7···O7 and C18-H18···O8, Table 3.4.1).

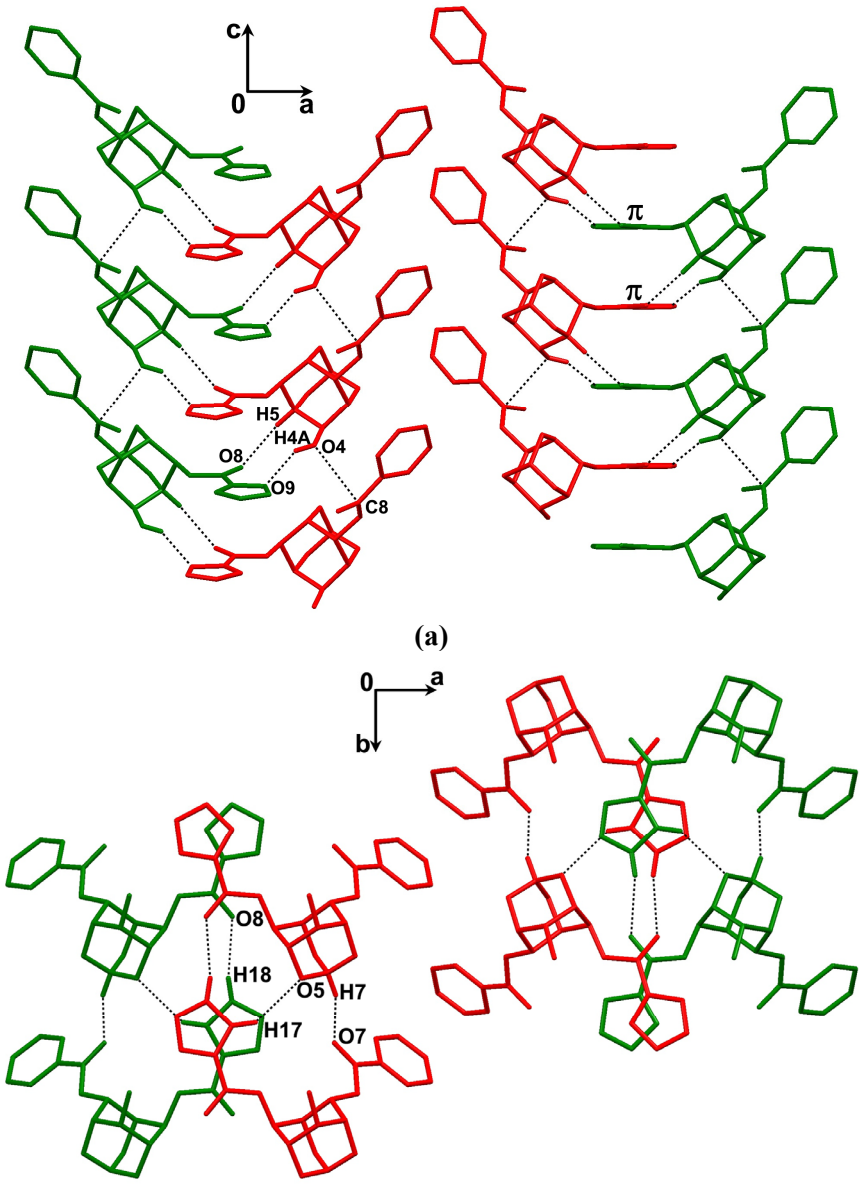

Figure 3.4.8 (a) Hydrogen bonding interactions form chains of glide related molecules in crystals of **rac-2.11** and (b) View down *c*-axis shows linkage of adjacent chains. Red and green indicate the two enantiomers.

On the other hand, in **rac-2.13**, the hydroxyl group of one enantiomer is involved in O-H···O hydrogen bonding (O4-H4A···O9) with the carbonyl group of the axial ester of the other enantiomer, similar to that observed in the form I crystals of **rac-2.10**, resulting in the formation of centrosymmetric dimers. The molecular association within this dimeric unit is strengthened by a bifurcated hydrogen bonding interaction of the furanyl oxygen O10 with inositol protons H4 and H5. The dimers are interconnected *via* weak C-H···O interactions along the *a* and *c*-axes (C16- H16···O7 contacts) forming a planar arrangement (Fig. 3.4.9).

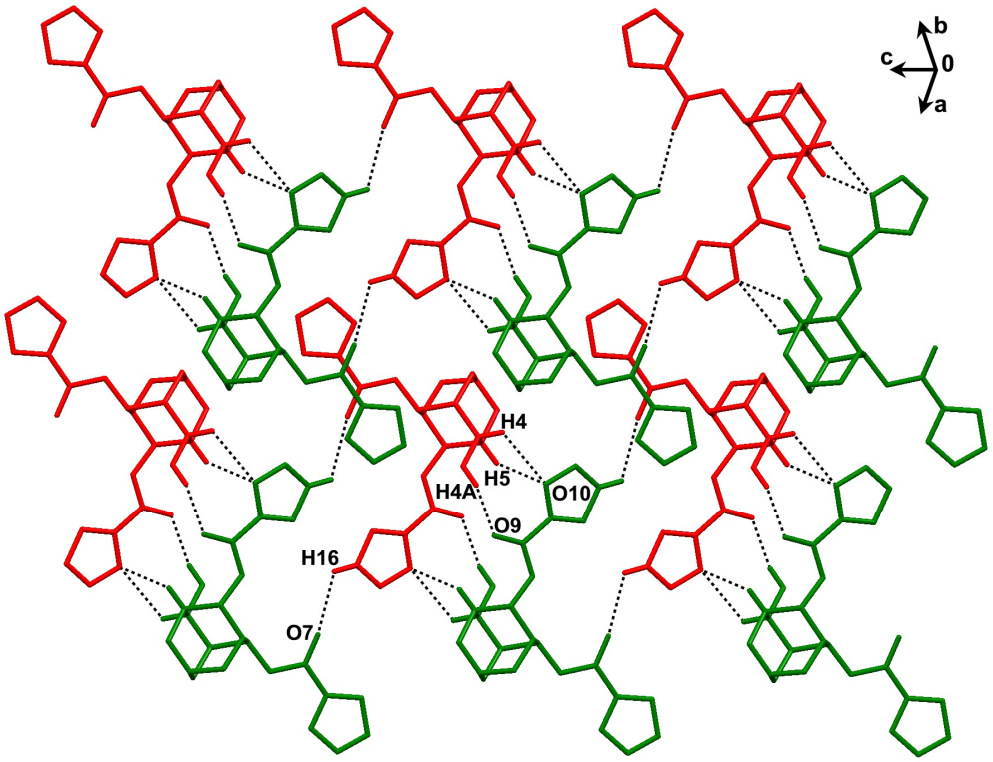

Figure 3.4.9 Centrosymmetric molecular dimers forming a layered arrangement in crystals of **rac-2.13**. Red and green indicate the two enantiomers.

(c) Structures of di-*p*-methylbenzoate (rac-2.15) and di-*p*-iodobenzoate (rac-2.18)

Replacement of the hydrogen at the *para* position in the benzoyl groups of **rac-1.177** with methyl and iodo substituents resulted in major changes in the molecular organization in the resultant crystal structures. The hydroxyl group in **rac-2.15** and **rac-2.18** is engaged in hydrogen bonding with the orthoester oxygen (O4-H4A···O1) and aromatic proton of the equatorial ester (C14-H14···O4) forming a homochiral molecular chain along the *a*-axis, in contrast to the hydrogen bonding observed between the hydroxyl group and equatorial ester carbonyl oxygen in **rac-1.177**. Weak C-H···π interactions (C1-H1···Cg) are observed between adjacent molecules in the chain. Neighbouring homochiral molecular chains (red and green, Fig. 3.4.10a) are linked by C5-H5···O8 contacts and a pair of centrosymmetric C-H···O interactions (C7-H7···O8, C6-H6···O5), forming bilayers.

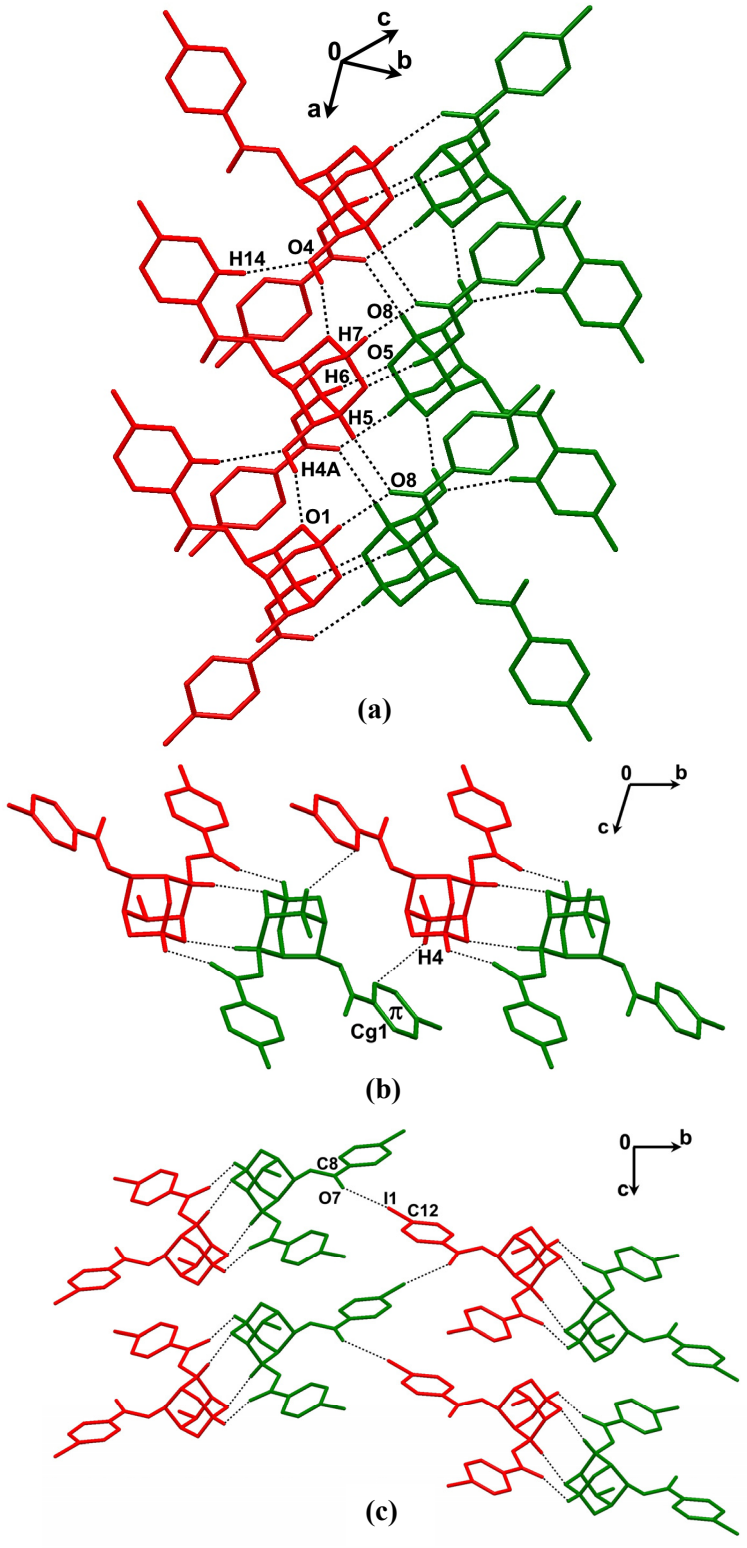

Figure 3.4.10 Bilayers formed through O-H···O and C-H···O interactions in (a) **rac-2.15** and linked *via*: (b) weak C-H···π interactions in **rac-2.15** and (c) halogen bonding C12-I1···O7 contacts in **rac-2.18**. Red and green indicate the two enantiomers, which form molecular strings. Hydrogen atoms not involved in hydrogen bonding are omitted for the sake of clarity.

This assembly of bilayers is reminiscent of that observed in the solvent free dimorphs of the bromo and chloro analogues **rac-2.5** and **rac-2.7** respectively.[18] Hence, there exists a one-dimensional iso-structurality in these crystal structures. The difference in their molecular organization arises in the linkage of the bilayers in shaping a three-dimensional arrangement. Centrosymmetric C-H···π interactions link adjacent bilayers along the *bc*-diagonal in the crystals of **rac-2.15** (Fig. 3.4.10b). In the case of **rac-2.18**, the bilayers are linked by halogen bonding (C12-I1···O7=C8) interactions (Fig. 3.4.10c) between the iodine atom of the equatorial *p*-iodobenzoate group and the carbonyl oxygen of an adjacent equatorial *p*-iodobenzoate group. Interestingly, in the case of the solvent free dimorphs of the bromo and chloro derivatives, these bilayers are linked by C-H···X (form I crystals) and C-X···O (form II crystals) halogen bonding interactions (X = Cl, Br).[18]

Table 3.4.2. Intermolecular interactions in crystals of di-*O*-acylated *myo*-inositol orthoformates.

Crystal	D-H···A	D-H /Å	H···A /Å	D···A /Å	D-H···A /°
2.10(form I)	O4-H18···O8^{i}	0.95(5)	1.98(5)	2.930(3)	174(4)
	C17-H17B···O7^{ii}	0.93	2.48	3.046(3)	119
2.10(form II)	O4'-H18'···O4	0.84(6)	2.09(6)	2.858(5)	151(5)
	O4-H18···O7'^{iii}	0.82(5)	1.98(5)	2.785(4)	165(4)
	C1-H1···O5^{iv}	1.00	2.43	3.364(5)	155
	C1'-H1'···O5'^{iv}	1.00	2.59	3.533(5)	157
	C3-H3···O7'^{iii}	1.00	2.39	3.161(5)	133
	C3'-H3'···O7	1.00	2.58	3.482(5)	150
	C16-H16···O4'	0.95	2.55	3.308(5)	136
	C7-H7···O8'^{v}	1.00	2.50	3.328(5)	140
	C6-H6···O5'^{v}	1.00	2.39	3.208(5)	138
	C7'-H7'···O8^{vi}	1.00	2.43	3.202(5)	133
	C12'-H12'···O8'^{vii}	0.95	2.60	3.540(6)	171
	C13-H13···O3'^{viii}	0.95	2.59	3.416(6)	145
2.11	C17-H17···O5^{ix}	0.93	2.55	3.347(5)	143
	C18-H18···O8^{ix}	0.93	2.56	3.410(5)	153
	O4-H4A···O9^{x}	0.803(19)	2.35(4)	3.016(4)	141(5)
	C5-H5···O8^{x}	0.98	2.57	3.365(5)	139
	C7-H7···O7^{xi}	0.98	2.32	3.230(5)	155
2.13	C16-H16···O7^{xii}	0.93	2.55	3.161(3)	124
	O4-H4A···O9^{xiii}	0.87(3)	2.03(3)	2.879(2)	165(3)
	C5-H5···O10^{xiii}	0.98	2.58	3.204(3)	122
	C4-H4···O10^{xiii}	0.98	2.55	3.063(3)	113
2.15	C7-H7···O8^{xiv}	0.98	2.49	3.236(4)	133
	C6-H6···O5^{xiv}	0.98	2.42	3.393(4)	172
	C5-H5···O8^{xv}	0.98	2.52	3.372(4)	146
	C14-H14···O4^{xvi}	0.93	2.54	3.408(5)	155
	O4-H4A···O1^{xvii}	0.82(4)	2.10(5)	2.886(3)	159(4)
	C1-H1···Cg1*^{xvi}	0.98	2.57	3.522(4)	164
2.18	C7-H7···O8^{xviii}	0.98	2.53	3.212(5)	127
	C6-H6···O5^{xviii}	0.98	2.49	3.458(5)	172
	C5-H5···O8^{xii}	0.98	2.44	3.293(5)	145
	O4-H4A···O1^{xvi}	0.80(2)	2.10(2)	2.880(4)	166(5)
	C1-H1···Cg1†^{xvii}	0.98	2.58	3.539(4)	167

Symmetry codes: (i) $-x + 2, -y + 2, -z+2$; (ii) $-x + 2, -y + 1, -z + 2$; (iii) $x, y, z + 1$; (iv) $x, y, z - 1$; (v) $-x + 2, y + 1/2, -z + 2$; (vi) $-x + 2, y - 1/2, -z + 2$; (vii) $x - 1, y, z - 1$; (viii) $-x + 1, y + 1/2, -z + 1$; (ix) $x, y - 1, z$; (x) $-x + 1/2, y, z - 1/2$; (xi) $x, y + 1, z$; (xii) $-x + 1, -y + 1, -z + 1$; (xiii) $-x + 1, -y + 1, -z$; (xiv) $-x, -y + 2, -z + 1$; (xv) $-x + 1, -y + 2, -z + 1$; (xvi) $x - 1, y, z$; (xvii) $x + 1, y, z$; (xviii) $-x + 2, -y + 1, -z + 1$.

*Cg1 = centroid of the axial ester phenyl ring (C17-C22), †Cg2 = centroid of the axial ester phenyl ring (C16-C21).

3.4.2 Analysis of electrophile-nucleophile (El-Nu) geometry: correlation with reactivity

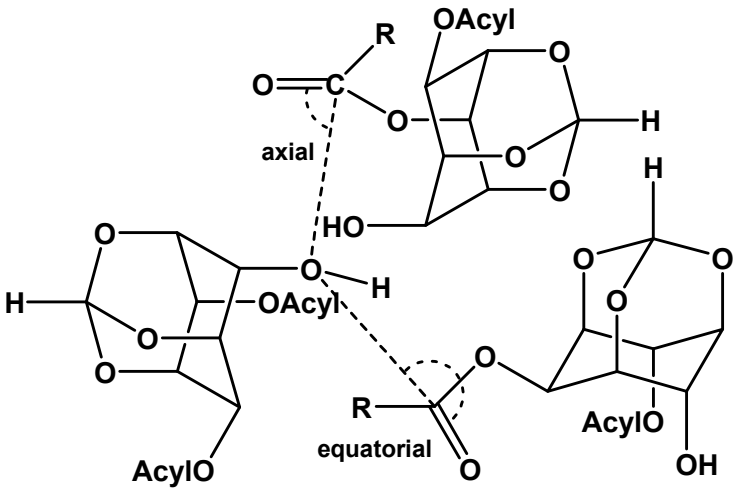

Figure 3.4.11 Schematic representation of El-Nu geometry in crystals of reactive di-benzoylated *myo*-inositol orthoesters.

Earlier work in our laboratory showed that the facility of transesterification reactions in crystalline dibenzoylated *myo*-inositol orthoesters is due to the favourable geometry of the C4(6)-hydroxyl group (Nu) and the C6(4)-acyl carbonyl group (El), brought about by the helical pre-organization of the molecules.[7] Examination of the crystal structures of the diesters **rac-2.10**, **rac-2.11**, **rac-2.13**, **rac-2.15** and **rac-2.18** reveals that none of them exhibit such a helical assembly of molecules in the solid-state. Further, the ester substitutions at the C6(4) position exert control on the hydrogen bonding patterns of the hydroxyl group which results in different non-helical molecular assemblies. The El-Nu geometrical parameters for these crystals are summarised in Table 3.4.3. Intermolecular El-Nu geometry for the hydroxyl group and the axial and equatorial ester carbonyl of nearest neighbouring molecules (Fig.

3.4.11) is analysed. In case of the reactive diesters the C4(6)-axial benzoyl group migrates, giving the corresponding tribenzoate and the diol (Chapter 1, Scheme 1.14).[7] However, in crystals of the diesters reported in the present chapter, the geometry required for the reaction is not observed. Absence of good El...Nu geometry between the constituent molecules in crystals of the acrylate **rac-2.10** (form I) and the di-furoate **rac-2.13** is due to the formation of closed dimers (Fig. 3.4.4b, Fig. 3.4.5a, Fig. 3.4.9). The hydroxyl group and the equatorial benzoate of the furoate **rac-2.11** seem to be oriented in the right geometry for acyl transfer, however the solid-state reactivity could not be tested because of the poor yield of crystals of the pure compound. While the form I crystals of the acrylate **rac-2.10** and crystals of the di-*p*-iodobenzoate **rac-2.18** reacted in the solid-state yielding a mixture of products, the di-*p*-methylbenzoate **rac-2.15** was unreactive under similar conditions. The lack of specificity observed for the acyl transfer reaction in form I crystals of **rac-2.10**, **rac-2.15** and **rac-2.18** could be because of preference for molecular organization through hydrogen bonding which does not bring the El-Nu in proximity for the reaction.

Table 3.4.3 Electrophile nucleophile geometry in the crystals of di-esters.

Crystal	Distance Å/Angle °	d (O...C=O) Å	∠ (O...C=O) °
rac-1.177	^{a}O4...C15=O8	3.226, 3.249	88.1, 89.9
rac-1.179	^{a}O4...C15=O8	3.144(2)	85.6
rac-1.178B	^{a}O4...C15=O8	3.135(4)	87.6
rac-2.10 (form II)	^{a}O4'...C15=O8^{i} ^{e}O4'...C8=O7^{i}	3.689(5) 4.881(6)	147 35
rac-2.11	^{a}O4...C15=O8^{ii} ^{e}O4...C8=O7^{iii}	3.989(5) 3.989(5)	48 89
rac-2.15	^{a}O4...C16=O8^{iv} ^{e}O4...C8=O7^{v}	5.269(5) 4.332(4)	15 143
rac-2.18	^{a}O4...C15=O8^{vi} ^{e}O4...C8=O7^{vii}	5.159(5) 4.436(5)	18 145

Symmetry codes: (i) *x*, *y*, *z*; (ii) -*x* + 1/2, *y*, *z* - 1/2; (iii) *x*, *y*, *z* - 1; (iv) -*x* + 1, *y* + 2, -*z* + 1; (v) *x* + 1, *y*, *z*; (vi) -*x* + 1, -*y* + 1, -*z* + 1; (vii) *x* - 1, *y*, *z*.

a = axial ester carbonyl; *e* = equatorial ester carbonyl

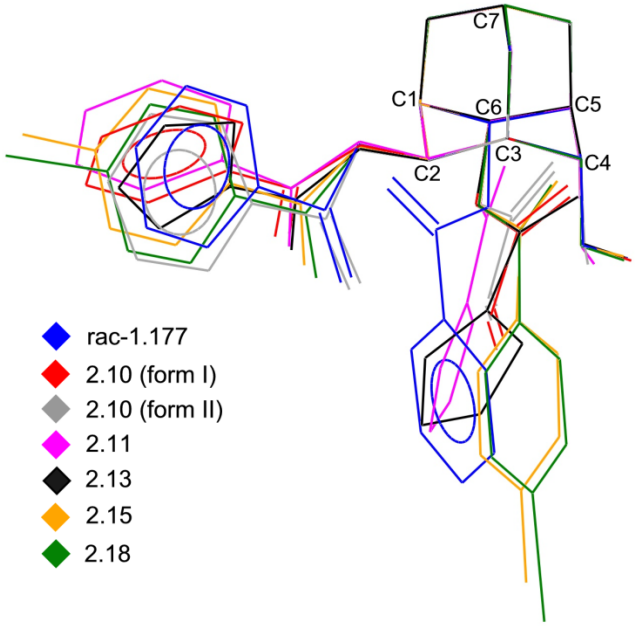

Figure 3.4.12 Overlap of molecules in the crystals of **rac-1.177**, **2.10**, **2.11**, **2.13**, **2.15** and **2.18**, showing the conformational differences in the functional groups; some hydrogen atoms are omitted for the sake of clarity.

The overlap of the molecules in the crystals of the reactive dibenzoate **rac-1.177** and the diesters studied in this chapter (Fig. 3.4.12), shows that the equatorial ester group has moved away from the hydroxyl group while the axial ester group has moved towards the hydroxyl group in the various diesters as compared to the conformation of the benzoyl groups in **rac-1.177**. These conformational changes along with the different patterns of O-H···O hydrogen bonding (perhaps an outcome of replacing the benzoates with other ester groups) could have resulted in the pre-organization of these molecules, not conducive for the acyl transfer reaction in crystals.

3.5 Conclusions

The relationship between the structure and solid-state reactivity of di-*O*-acylated *myo*-inositol orthoformate derivatives, was studied by varying the acyl group at the C6(4) position of the diol **1.183**. Examination of the crystal structures revealed that acryloyl and the furoyl groups do not induce a helical self-assembly of molecules in the solid-state, as the benzoyl group did. Though **rac-2.10** crystallised in two different modifications, none of them possessed the geometry required for acyl transfer reactions. Replacing the benzoyl groups by 4-iodobenzoyl and 4-methylbenzoyl

groups resulted in molecular organization in the form of bilayers similar to that observed in the polymorphs of the analogous bromo and chloro derivatives. The hydrogen bonding patterns observed in these compounds seem to arise from the weak interactions due to the ester substitutions at the C6 position and different substituents at the *para* position in the benzene rings. Evidently, even small perturbations in the chemical structure of a compound can affect the molecular pre-organization in the modified derivatives. Molecules with closely related chemical structures may assemble in radically different fashion in the crystalline-state, which determines their solid-state properties. While reactions in the solid state and single crystals are attractive as 'green reactions', designing molecules which contain reactive groups and growing their crystals wherein the reactive centers are in a favourable orientation for the reaction is still a challenging goal.

3.6 References

1. (*a*) G. R. Desiraju, *Crystal Engineering. The Design of Organic Solids*, Elsevier, Amsterdam, 1989; (*b*) G. R. Desiraju, *Angew. Chem. Int. Ed. Engl.*, **2007**, *46*, 8342-8356.
2. (*a*) P. Metrangolo, G. Resnati, T. Pilati and S. Biella, *Struct. Bond*, **2008**, *126*, 105-136; (*b*) M. Fourmigue, *Curr. Opin. Solid State Mater. Sci.*, **2009**, *13*, 36-45.
3. M. Nishio, Y. Umezawa, K. Honda, S. Tsuboyama and H. Suezawa, *CrystEngComm*, **2009**, *11*, 1757-1788.
4. G. Cavallo, P. Metrangolo, T. Pilati, G. Resnati, M. Sansotera and G. Terraneo, *Chem. Soc. Rev.*, **2010**, *39*, 3772-3783.
5. (*a*) D. L. Reger, J. D. Elgin, R. F. Semeniuc, P. J. Pellechia and M. D. Smith, *Chem. Commun.*, **2005**, 4068-4070; (*b*) Y. Chang, Y. Chen, C. Chen, Y. Wen, J. T. Lin, H. Chen, M. Kuo and I. Chao, *J. Org. Chem.*, **2008**, *73*, 4608-4614.
6. (*a*) R. Bishop, M. L. Scudder, D. C. Craig, A. Noman, M. M. Rahman and S. F. Alshahateet, *Mol. Cryst. Liq. Cryst.*, **2005**, *440*, 173-186; (*b*) M. C. Aragoni, M. Arca, F. Demartin, F. A. Devillanova, T. Gelbrich, A. Garau, M. B. Hursthouse and F. Isaia and V. Lippolis, *Cryst. Growth Des.*, **2007**, *7*, 1284-1290.
7. C. Murali, M. S. Shashidhar, R. G. Gonnade and M. M. Bhadbhade, *Chem. Eur. J.*, **2009**, *15*, 261-269.

8. Bruker 2003. SADABS (Version 2.05), SMART (Version 5.631) and SAINT (Version 6.45). Bruker AXS Inc., Madison, Wisconsin, USA.
9. G. M. Sheldrick, *Acta Crystallogr., Sect. A: Found. Crystallogr.*, **2008**, *64*, 112-122.
10. L. J. Farrugia, *J. Appl. Crystallogr.*, **1997**, *30*, 565.
11. C. F. Macrae, P. R. Edgington, P. McCabe, E. Pidcock, G. P. Shields, R. Taylor, M. Towler and J. van de Streek, *J. Appl. Crystallogr.*, **2006**, *39*, 453-457.
12. A. L. Spek, *J. Appl. Crystallogr.*, **2003**, *36*, 7-13.
13. T. Das and M. S. Shashidhar, *Carbohydr. Res*., **1997**, *297*, 243-249.
14. T. Praveen, T. Das, K. M. Sureshan, M. S. Shashidhar, U. Samanta, D. Pal and P. Chakrabarti, *J. Chem. Soc. Perkin Trans. 2*, **2002**, 358-365.
15. M. P. Sarmah, R. G. Gonnade, M. S. Shashidhar and M. M. Bhadbhade, *Chem. Eur. J.* **2005**, *11*, 2103-2110.
16. (*a*) T. Steiner, W. Hinrichs, W. Saenger, and R. Gigg, *Acta Cryst. Sect. B*, **1993**, *49*, 708-718; (*b*) R. G. Gonnade, M. S. Shashidhar, M. M. Bhadbhade, and A. K. Sanki, *Chem. Commun.*, **2005**, 5870-5872; (*c*) R. G. Gonnade, M. S. Shashidhar, and M. M. Bhadbhade, *CrystEngComm*, **2008,** 10, 288-296.
17. (*a*) S. D. Cosgrove, G. Steele, T. K. Austin, A. P. Plumb, B. Stensland, E. Ferrari and K. J. Roberts, *J. Pharm. Sci.*, **2005**, *94*, 2403-2415; (*b*) S. Wishkerman and J. Bernstein, *CrystEngComm*, **2006**, *8*, 245-249; (*c*) D. Vega, A. Petragalli, D. Fernandez and J. A. Ellena, *J. Pharm. Sci.*, **2006**, *95*, 1075-1083; (*d*) S. Roy, P. M. Bhatt, A. Nangia and G. J. Kruger, *Cryst. Growth Des.*, **2007**, *7*, 476-480; (*e*) D. Grooff, M. M. De Villiers, and W. Liebenberg, *Thermochim. Acta*, **2007,** *454*, 33-42.
18. R. G. Gonnade, M. M. Bhadbhade and M. S. Shashidhar, *CrystEngComm*, **2008**, *10*, 288-296.

Chapter 4

Creating helical assemblies of *myo*-inositol derivatives for acyl transfer reactivity in their crystals

Theory guides. Experiment decides.

-I. M. Kolthoff

Section A: Polymorphism and reactivity

4A.1 Introduction

Polymorphism and pseudopolymorphism of molecular crystals (and the associated phase changes in them) is a widely researched phenomenon in recent times because of the valuable information their structures provide to advance our understanding of the process of crystallization.[1] Polymorphic modifications of a compound, by definition, imply differing arrangements of molecules in their crystals, and hence show significant variation in chemical behaviour and reactivity in the solid-state. One of the earliest and well studied examples is the differential photodimerization response of the three polymorphs of *trans*-cinnamic acid investigated by Cohen and co-workers.[2] Other examples include the reactivity of indomethacin with ammonia,[3] the reactivities of polymorphs of barbituric acid with amines,[4] the dissimilar photochemical reactivity of dimorphs of α-adamantyl-*p*-chloroacetophenone[5] and the thermal response of polymorphs of tetrakis(4-vinylpyridine) diisothiocyanatocobalt(II).[6] Since the crystalline-state properties of a compound are determined by the molecular arrangement and weak non-covalent intermolecular interactions between the constituent molecules in crystals, it is reasonable to expect that the facility of solid-state reactions of organic compounds could be controlled by understanding their polymorphic behavior and by growing crystals having the structure that facilitates a chemical reaction. Introduction of smaller guest (solvent) molecules in molecular crystals gives rise to solvated crystals (pseudopolymorphic forms), which often have different structures compared to the structures of host crystals (devoid of guest molecules), provides a way of perturbing the intermolecular interactions and hence the reactivity of molecules in the solid state. Ability to increase or decrease the reactivity of molecules in crystals is of great relevance to the development of functional assemblies of organic molecules.[7] Amongst these, helical molecular assemblies have a very special functional role in biological systems,[8] and applications in organic and inorganic systems.[9] Helical assemblies have been realized *via* synthetic routes by employing metals,[10] polymers,[11] hydrogen bonds,[12] π···π stacking[13] and ion pairing within ligand strands.[14] A few synthetic examples of anion induced helical assemblies[15] are also known.

The solvent of crystallization is known to have an impact on crystal morphology[16] though its function in the growth of polymorphic crystals and inclusion complexes is not so well understood. The solvent of crystallization was found to influence the formation of capsular assemblies[17] and tubular complexes[18] of pyrrogallolarenes and cone formation in tripyridoxycalix[4]arenes,[19] stabilise the crystal packing in 3,4-dihydroxybenzophenone,[20] promote the formation of hydrogen-bonded hollow crystals in (1*R*,5*R*)-7,7-diallyl-5-hydroxylmethyl-6-oxabicyclo[3.3.1]-octane-1-carboxylic acid (±)9.H_2O[21] and support the cage-like structures of tetrol-boronic ester complexes.[22] Helical assemblies derived by mediation of solvent molecules are much less common. A few reports in the literature mention the role of solvent molecules in inducing helical assemblies in *p-tert*-butylcalix[4]dihydroquinone,[23] poly(phenylene ethynylene),[24] poly(*N*-octylcarbazole ethylene)[25] and cyclodextrins.[26]

From our laboratory we reported that the extremely facile and neat intermolecular acyl transfer reactivity (comparable to that carried out with high specificity only by enzymes[27]) in crystals of racemic 2,6-di-*O*-benzoyl *myo*-inositol 1,3,5-orthoformate (**rac-1.177**) and racemic 2,6-di-*O*-benzoyl *myo*-inositol 1,3,5-orthobenzoate (**rac-1.179**)[28] is due to the favourable helical molecular pre-organization which brings the electrophile and nucleophile in the right orientation for reaction. Deviation from this 'reactive pre-organization' showed a marked decrease in the acyl transfer activity. Our initial attempts described in chapter 3 to achieve this helical reactive organization in *myo*-inositol orthoformates with acrylate, crotonate, furoate, *p*-iodobenzoate and *p*-methylbenzoate esters at the C2, C6 positions were not successful. On the other hand, 2,6-di-*O*-(4-bromobenzoyl) *myo*-inositol 1,3,5-orthoformate (**rac-2.5**) and 2,6-di-*O*-(4-chlorobenzoyl) *myo*-inositol 1,3,5-orthoformate (**rac-2.7**) produced dimorphs each from methanol (**2.5FI**, **2.7FI**) and ethyl acetate (**2.5FII**, **2.7FII**) and revealed one-dimensional isostructurality in their organization, bridging the O-H···O linked molecular chain *via* C-H···O contacts across the inversion center[29] unlike **rac-1.177** and **rac-1.179**. However, crystallizations of **rac-2.5** and **rac-2.7** from a range of solvents (other than methanol and ethyl acetate) yielded solvatomorphs with helical assembly of the host molecules around the crystallographic 2_1-screw axis, akin to reactive molecular packing of **rac-1.177**.[28*b*] 2,6-Di-*O*-(4-fluorobenzoyl) *myo*-inositol 1,3,5-orthoformate (**rac-2.22**) also produced solvatomorphs from most organic

solvents except methanol which yielded solvent free crystals (**2.22FI**). However, crystallization of **rac-1.179** from 2-propanol produced solvated crystals, which exhibited a non-helical assembly of molecules. The solvent induced helical assembly of molecules in the crystals of racemic 2,6-di-*O*-halobenzoyl *myo*-inositol 1,3,5-orthoformates (halo = fluoro, chloro, bromo), their thermal behaviour and correlation with solid-state reactivities will be discussed here in section 4A.3-4A.4 and the structures and solid-state reactivities of solvates of **rac-1.179** will be discussed in section 4A.5-4A.6.

4A.2 General experimental details

X-ray crystallography: Intensity data were collected for all crystals on a Bruker SMART APEX CCD diffractometer with graphite-monochromatized (Mo K_α= 0.71073 Å) radiation. Diffraction intensities were measured with a ω scan width of 0.3° at different settings of φ (0, 90, 180 and 270°) keeping the sample-to-detector distance fixed at 6.145 cm and the detector position (2θ) fixed at -28°. The X-ray intensities at low temperatures (in some experiments) were measured using an OXFORD LN2 cryosystem. The X-ray data acquisition was monitored by SMART program (Bruker, 2003).[30] All the data were corrected for Lorentz-polarization effects using SAINT programs (Bruker, 2003).[30] A semi-empirical absorption correction (multi-scan) based on symmetry equivalent reflections was applied using the SADABS program (Bruker, 2003).[30] Lattice parameters were refined from least-squares analysis of all reflections. The structures were solved by direct methods and refined by full matrix least squares, based on F^2, using SHELX-97 software package.[31] Thermal ellipsoid plots were generated using ORTEP-32,[32] packing diagrams were prepared using Mercury-2.3[33] and geometrical calculations were performed using PLATON.[34]

Differential Scanning Calorimetry (DSC): The thermal behaviour of freshly grown crystals was investigated by measuring enthalpy change on a Mettler Differential Scanning Calorimeter. Freshly grown crystals (2 - 4 mg) were placed in a sealed aluminium pan (40 µl) and were analyzed from ambient temperature to ~ 35 °C above the melting point of the compound (recorded earlier, see Chap. 2.) using an empty pan as the reference. The heating rate was 5 °C min^{-1}(or 10 °C min^{-1} in some experiments)

and nitrogen gas was used for purging.

Hot stage microscopy (HSM): Crystals were heated on the stage (equipped with a temperature probe) and viewed through the eyepiece of a Leica polarizing microscope. Crystal images were captured using an on-board Leica camera.

4A.3 The 2,6-di-*O*-(4-halobenzoyl) *myo*-inositol 1,3,5-orthoformates

4A.3.1 Synthesis, crystallization and X-ray crystallography

The diesters **rac-2.5**, **rac-2.7** and **rac-2.22** were synthesised and characterised as described in Chapter 2. Crystallization of **rac-2.5**, **rac-2.7** and **rac-2.22** from most organic solvents (except methanol and ethyl acetate) yielded inclusion crystals, summarised in (Scheme 4A.3.1). Most of the inclusion crystals were robust square or hexagonal plates and were stable in the open atmosphere for 3-7 days with the exception of benzene inclusion crystals of **rac-2.7**, which were highly unstable. Crystals of **2.7**K were stabilized by applying paraffin oil coat and immediately taken into the liquid nitrogen stream maintained at 133(2) K for data collection. The hydroxyl H-atoms in the crystal structures of **2.5A** - **2.5H**, **2.7A** - **2.7J, 2.22A** - **2.22M**, the hydrogen atoms of the inositol and phenyl ring in **2.7G**, **2.7I** and all hydrogen atoms in **2.22K** were located in difference Fourier maps and refined isotropically. All the other hydrogen atoms (including hydroxyl H-atom in **2.7K**) in all the solvates were placed in geometrically idealized positions and refined isotropically. The crystallographic data are summarized in Table 4A.3.1.

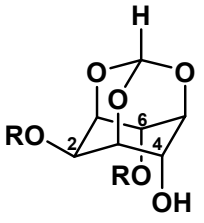

2.5 R = *p*-Br-C_6H_4-CO
2.7 R = *p*-Cl-C_6H_4-CO
2.22 R = *p*-F-C_6H_4-CO

2.5A = 2.5•$CHCl_3$
2.5B = 2.5•CH_3COCH_3
2.5C = 2.5•CH_2Cl_2
2.5D = 2.5•CH_3NO_2
2.5E = 2.5•C_4H_8O
2.5F = 2.5•$C_4H_8O_2$
2.5G = 2.5•CH_3SOCH_3
2.5H = 2.5•$ClCH_2CH_2Cl$

2.7A = 2.7•$CHCl_3$
2.7B = 2.7•CH_3COCH_3
2.7C = 2.7•CH_2Cl_2
2.7D = 2.7•CH_3NO_2
2.7E = 2.7•C_4H_8O
2.7F = 2.7•$C_4H_8O_2$
2.7G = 2.7•CH_3SOCH_3
2.7H = 2.7•$ClCH_2CH_2Cl$
2.7I = 2.7•CH_3CN
2.7J = 2.7•*p*-$C_6H_4(CH_3)_2$
2.7K = 2.7•C_6H_6

2.22A = 2.22•$CHCl_3$
2.22B = 2.22•CH_3COCH_3
2.22C = 2.22•CH_2Cl_2
2.22D = 2.22•CH_3NO_2
2.22E = 2.22•C_4H_8O
2.22G = 2.22•CH_3SOCH_3
2.22H = 2.22•$ClCH_2CH_2Cl$
2.22I = 2.22•CH_3CN
2.22J = 2.22•*p*-$C_6H_4(CH_3)_2$
2.22K = 2.22•C_6H_6
2.22L = 2.22•$C_6H_5CH_3$
2.22M = 2.22•*o*-$C_6H_4(CH_3)_2$

Scheme 4A.3.1 Solvates of **rac-2.5**, **rac-2.7** and **rac-2.22**

Table 4A.3.1 Crystallographic data for solvates of **rac-2.5**, **rac-2.7** and **rac-2.22**.

	2.5•$CHCl_3$	**2.5•CH_3COCH_3**	**2.5•CH_2Cl_2**	**2.5•CH_3NO_2**
Chemical formula	$C_{21}H_{16}Br_2O_8$·($CHCl_3$)	$C_{21}H_{16}Br_2O_8$·(C_3H_6O)	$C_{21}H_{16}Br_2O_8$·(CH_2Cl_2)	$C_{21}H_{16}$ Br_2O_8·(CH_3NO_2)
M_r	675.53	614.24	641.08	617.20
Temperature (K)	133(2)	133(2)	133(2)	133(2)
Morphology	Plate	Square plate	plate	plate
Crystal size	0.34×0.18×0.08	0.30×0.21×0.06	0.54×0.20×0.17	0.19×0.17×0.06
Crystal system	Monoclinic	Monoclinic	Monoclinic	Monoclinic
Space group	$P2_1/n$	$P2_1/n$	$P2_1/n$	$P2_1/n$
a (Å)	12.8141(17)	12.8133(15)	12.8524(11)	12.1747(15)
b (Å)	10.2601(14)	10.2045(12)	10.2018(8)	10.1533(12)
c (Å)	18.756(3)	18.814(2)	18.525(15)	19.261(2)
β (°)	102.832(2)	103.599(4)	102.870(10)	103.231(2)
V (Å^3)	2404.3(6)	2391.1(5)	2367.9(3)	2317.7(5)
Z	4	4	4	4
D_{calc} (g cm^{-3})	1.866	1.706	1.798	1.769
μ (mm^{-1})	3.753	3.443	3.696	3.557
F(000)	1336	1232	1272	1232
T_{min}	0.365	0.425	0.240	0.550
T_{max}	0.758	0.812	0.577	0.807
h, k, l (min, max)	(-15,10), (-12,12), (-21,22)	(-15,15), (-11,12), (-15,22)	(-15,12), (-8,12), (-17,22)	(-13,14), (-12,12), (-19,22)
Reflns collected	11791	11778	11686	11343
Unique reflns	4223	4208	4166	4067
Observed reflns	3873	3597	3739	3666
R_{int}	0.0231	0.0286	0.0240	0.0436
No. of parameters	328	322	359	338
GoF	1.029	1.037	1.050	1.021
$R_1[I > 2\sigma(I)]$	0.0268	0.0340	0.0340	0.0327
$WR_2[I > 2\sigma(I)]$	0.0651	0.0836	0.0865	0.0812
R_1_all data	0.0301	0.0422	0.0385	0.0372
Wr_2_all data	0.0665	0.0879	0.0890	0.0839
$\Delta\rho_{max}$, $\Delta\rho_{min}$(e Å^{-3})	0.55, -0.54	0.82, -0.59	0.78, -0.62	0.74, -0.33
CCDC dep No.	752175	752176	752177	752178

Table 4A.3.1 Contd…

	2.5•C_4H_8O	**2.5•$C_4H_8O_2$**	**2.5•CH_3SOCH_3**	**2.5•$ClCH_2CH_2Cl$**
Chemical formula	$C_{21}H_{16}Br_2O_8$·(C_4H_8O)	$C_{21}H_{16}Br_2O_8$·($C_4H_8O_2$)	$C_{21}H_{16}Br_2O_8$·(C_2H_6SO)	$C_{21}H_{16}Br_2O_8$·($C_2H_4Cl_2$)
M_r	628.26	644.26	634.29	655.11
Temperature (K)	133(2)	133(2)	133(2)	133(2)
Morphology	plate	plate	plate	plate
Crystal size	0.55×0.37×0.18	0.19×0.13×0.06	0.26×0.11×0.03	0.37×0.16×0.04
Crystal system	Monoclinic	Monoclinic	Monoclinic	Monoclinic
Space group	$P2_1/c$	$P2_1/n$	$P2_1/n$	$P2_1/c$
a (Å)	13.181(4)	13.1856(16)	13.0322(15)	12.1687(8)
b (Å)	10.046(3)	10.2483(13)	10.2499(11)	10.0099(7)
c (Å)	18.813(5)	18.966(2)	18.415(2)	20.3518(14)
β (°)	102.436(4)	104.704(2)	103.579(2)	92.677(10)
V (Å^3)	2432.7(11)	2478.9(5)	2391.0(5)	2476.3(3)
Z	4	4	4	4
D_{calc} (g cm^{-3})	1.715	1.726	1.762	1.757
μ (mm^{-1})	3.386	3.328	3.530	3.536
F(000)	1264	1296	1272	1304
T_{min}	0.245	0.570	0.455	0.357
T_{max}	0.544	0.818	0.892	0.886
h, k, l (min, max)	(-15,15), (-11,11), (-22,22)	(-15,15), (-6,12), (-22,21)	(-15,15), (-12,10), (-21,19)	(-14,11), (-11,10), (-18,24)
Reflns collected	15536	12106	11699	12144
Unique reflns	4268	4352	4201	4335
Observed reflns	3714	3577	3768	3763
R_{int}	0.0776	0.0332	0.0288	0.0269
No. of parameters	374	356	322	347
GoF	1.082	1.023	1.164	1.065
$R_1[I > 2\sigma(I)]$	0.0690	0.0363	0.0457	0.0406
$WR_2[I > 2\sigma(I)]$	0.1833	0.0855	0.0936	0.1063
R_1_all data	0.0751	0.0482	0.0528	0.0476
Wr_2_all data	0.1914	0.0912	0.0976	0.1107
$\Delta\rho_{max}$, $\Delta\rho_{min}$(e Å^{-3})	0.99, -1.05	0.67, -0.74	1.03, -0.51	0.79, -0.94
CCDC dep No.	752179	752180	752181	752182

Table 4A.3.1 Contd…

	2.7•$CHCl_3$	**2.7•CH_3COCH_3**	**2.7•CH_2Cl_2 (F)**[a]	**2.7•CH_3NO_2**
Chemical formula	$C_{21}H_{16}Cl_2O_8$·($CHCl_3$)	$C_{21}H_{16}Cl_2O_8$·(C_3H_6O)	$C_{21}H_{16}Cl_2O_8$·(CH_2Cl_2)	$C_{21}H_{16}Cl_2O_8$·(CH_3NO_2)
M_r	586.61	525.32	552.16	528.28
Temperature (K)	133(2)	133(2)	133(2)	133(2)
Morphology	plate	plate	Thick plate	Thick plate
Crystal size	0.12×0.07×0.03	0.28×0.18×0.10	0.49×0.27×0.10	0.40×0.36×0.19
Crystal system	Monoclinic	Monoclinic	Monoclinic	Monoclinic
Space group	$P2_1/n$	$P2_1/n$	$P2_1/n$	$P2_1/n$
a (Å)	12.9486(9)	12.751(2)	12.8921(11)	12.6835(7)
b (Å)	10.2705(7)	10.221(18)	10.1356(9)	10.0712(5)
c (Å)	18.0539(12)	18.520(3)	18.0788(16)	18.298(10)
β (°)	101.398(10)	103.209(3)	101.584(10)	103.100(10)
V (Å^3)	2353.5(3)	2349.8(7)	2314.2(4)	2276.5(2)
Z	4	4	4	4
D_{calc} (g cm^{-3})	1.656	1.485	1.585	1.541
μ (mm^{-1})	0.665	0.330	0.559	0.345
F(000)	1192	1088	1128	1088
T_{min}	0.924	0.913	0.773	0.874
T_{max}	0.984	0.969	0.946	0.937
h, k, l (min, max)	(-15,15), (-12,12), (-21,21)	(-15,15), (-11,12), (-18,22)	(-15,15), (-12,12), (-21,21)	(-15,11), (-11,11), (-21,20)
Reflns collected	16706	11486	16329	11138
Unique reflns	4146	4136	4073	3999
Observed reflns	3906	3812	3780	3767
R_{int}	0.0221	0.0202	0.0175	0.0122
No. of parameters	320	322	338	358
GoF	1.087	1.079	1.030	1.048
$R_1[I > 2\sigma(I)]$	0.0386	0.0402	0.0433	0.0303
$WR_2[I > 2\sigma(I)]$	0.0884	0.0976	0.1057	0.0798
R_1_all data	0.0413	0.0440	0.0460	0.0318
Wr_2_all data	0.0901	0.1003	0.1076	0.0811
$\Delta\rho_{max}$, $\Delta\rho_{min}$(e Å^{-3})	0.75, -0.58	0.43, -0.29	1.08, -0.58	0.37, -0.24
CCDC dep No.	752183	752184	752185	752186

[a]F – Full occupancy of solvent.

Table 4A.3.1 Contd…

	2.7•C_4H_8O	**2.7•$C_4H_8O_2$**	**2.7•CH_3SOCH_3**	**2.7•$ClCH_2CH_2Cl$**
Chemical formula	$C_{21}H_{16}Cl_2O_8$·(C_4H_8O)	$C_{21}H_{16}Cl_2O_8$·($C_4H_8O_2$)	$C_{21}H_{16}Cl_2O_8$·(C_2H_6SO)	$C_{21}H_{16}Cl_2O_8$·($C_2H_4Cl_2$)
M_r	539.34	555.34	545.37	566.19
Temperature (K)	133(2)	133(2)	133(2)	133(2)
Morphology	Square plate	plate	plate	plate
Crystal size	0.22×0.16×0.07	0.22×0.18×0.06	0.27×0.22×0.11	0.17×0.14×0.09
Crystal system	Monoclinic	Monoclinic	Monoclinic	Monoclinic
Space group	$P2_1/n$	$P2_1/n$	$P2_1/n$	$P2_1/c$
a (Å)	12.908(3)	13.047(3)	12.9731(13)	12.093(2)
b (Å)	10.135(2)	10.141(3)	10.2342(11)	9.9108(17)
c (Å)	18.299(4)	18.678(5)	18.0469(19)	20.260(3)
β (°)	101.682(4)	103.518(4)	102.585(2)	92.433(3)
V (Å^3)	2344.3(9)	2402.8(10)	2338.5(4)	2426.1(7)
Z	4	4	4	4
D_{calc} (g cm^{-3})	1.528	1.535	1.549	1.550
μ (mm^{-1})	0.333	0.330	0.421	0.536
F(000)	1120	1152	1128	1160
T_{min}	0.930	0.931	0.896	0.916
T_{max}	0.977	0.981	0.956	0.955
h, k, l (min, max)	(-15,9), (-12,11), (-21,21)	(-15,15), (-11,12), (-15,22)	(-15,12), (-12,11), (-21,21)	(-12,14), (-9,11), (-24,22)
Reflns collected	11470	11795	11333	11676
Unique reflns	4120	4212	4119	4214
Observed reflns	3351	3490	3752	3277
R_{int}	0.0391	0.0308	0.0224	0.0377
No. of parameters	356	392	382	338
GoF	1.103	1.055	1.148	1.034
$R_1[I > 2\sigma(I)]$	0.0605	0.0540	0.0509	0.0716
$WR_2[I > 2\sigma(I)]$	0.1240	0.1203	0.1139	0.1553
R_1_all data	0.0770	0.0674	0.0565	0.0930
Wr_2_all data	0.1313	0.1276	0.1169	0.1685
$\Delta\rho_{max}$, $\Delta\rho_{min}$(e Å^{-3})	0.36, -0.27	0.60, -0.67	0.66, -0.31	0.97, -0.77
CCDC dep No.	752187	752188	752189	752190

Table 4A.3.1 Contd…

	2.7•CH_3CN	**2.7•*p*-$C_6H_4(CH_3)_2$**	**2.7•C_6H_6**	**2.7•CH_2Cl_2 (T)**[a]
Chemical formula	$C_{21}H_{16}Cl_2O_8$·(CH_3CN)	$C_{21}H_{16}Cl_2O_8$·0.5($C_6H_4(CH_3)_2$)	$C_{21}H_{16}Cl_2O_8$·(C_6H_6)	$C_{21}H_{16}Cl_2O_8$·0.06(CH_2Cl_2)
M_r	508.29	520.32	545.35	472.33
Temperature (K)	133(2)	133(2)	133(2)	133(2)
Morphology	Square plate	plate	plate	Thin plate
Crystal size	0.72×0.68×0.19	0.26×0.16×0.04	0.51×0.23×0.12	0.33×0.33×0.13
Crystal system	Monoclinic	Monoclinic	Monoclinic	Monoclinic
Space group	$P2_1/c$	$P2_1/c$	$C2/c$	$P2_1/n$
a (Å)	12.074(10)	11.6917(18)	32.22(3)	12.962(2)
b (Å)	9.861(8)	9.6018(15)	9.584(8)	10.1406(17)
c (Å)	20.003(16)	21.103(3)	21.386(19)	18.391(3)
β (°)	94.894(13)	94.329(3)	129.72(3)	102.627(3)
V (Å^3)	2373(3)	2362.3(6)	5080(8)	2358.8(7)
Z	4	4	8	4
D_{calc} (g cm^{-3})	1.423	1.463	1.393	1.330
μ (mm^{-1})	0.322	0.325	0.304	0.331
F(000)	1048	1076	2190	970.2
T_{min}	0.800	0.920	0.859	0.902
T_{max}	0.942	0.987	0.964	0.960
h, k, l (min, max)	(-14,14), (-11,11), (-23,23)	(-13,10), (-11,11), (-25,25)	(-36,38), (-11,11), (-25,25)	(-15,15), (-12,8), (-21,21)
Reflns collected	21364	11522	14943	11414
Unique reflns	4178	4133	4438	4128
Observed reflns	3590	3510	2776	2902
R_{int}	0.0628	0.0234	0.1232	0.0285
No. of parameters	372	321	350	337
GoF	1.077	1.046	1.115	1.034
$R_1[I > 2\sigma(I)]$	0.0518	0.0357	0.1154	0.0551
$WR_2[I > 2\sigma(I)]$	0.1277	0.0818	0.2338	0.1410
R_1_all data	0.0597	0.0434	0.1790	0.0789
Wr_2_all data	0.1340	0.0862	0.2626	0.1586
$\Delta\rho_{max}$, $\Delta\rho_{min}$(e Å^{-3})	0.42, -0.51	0.29 –0.23	0.89, -0.42	0.41, -0.43
CCDC dep No.	752191	752192	752193	752863

[a]T – Trace occupancy of solvent

Table 4A.3.1 Contd….

	2.22 •$CHCl_3$	**2.22 •CH_3COCH_3**	**2.22 •CH_2Cl_2**	**2.22 •CH_3NO_2**
Chemical formula	$C_{21}H_{16}F_2O_8$·($CHCl_3$)	$C_{21}H_{16}F_2O_8$·(C_3H_6O)	$C_{21}H_{16}F_2O_8$·(CH_2Cl_2)	$C_{21}H_{16}F_2O_8$·(CH_3NO_2)
M_r	553.71	492.42	519.26	495.38
Temperature (K)	133(2)	133(2)	133(2)	133(2)
Morphology	plate	plate	plate	Plate
Crystal size	0.30×0.14×0.05	0.37×0.17×0.12	0.55×0.18×0.14	0.32×0.26×0.07
Crystal system	monoclinic	monoclinic	Monoclinic	monoclinic
Space group	$P2_1/n$	$P2_1/c$	$P2_1/n$	$P2_1/c$
a (Å)	12.869(3)	11.476(2)	12.8215(15)	11.5876(16)
b (Å)	10.168(2)	9.5127(17)	10.1040(12)	9.6180(13)
c (Å)	17.234(3)	20.424(4)	17.172(2)	19.653(3)
	90	90	90	90
β (°)	99.870(4)	90.219(3)	100.146(2)	95.241(2)
	90	90	90	90
V (Å^3)	2221.6(9)	2229.6(7)	2189.8(4)	2181.2(5)
Z	4	4	4	4
D_{calc} (g cm^{-3})	1.655	1.467	1.575	1.509
μ (mm^{-1})	0.479	0.123	0.362	0.131
F(000)	1128	1024	1064	1024
T_{min}	0.871	0.956	0.827	0.959
T_{max}	0.976	0.986	0.952	0.991
h, k, l (min, max)	(-14, 15)	(-12, 13)	(-15, 13)	(-13, 13)
	(-12, 12)	(-11, 11)	(-12, 10)	(-11, 9)
	(-20, 20)	(-22, 24)	(-20, 20)	(-23, 19)
Reflns collected	30894	21208	10790	10575
Unique reflns	3917	3917	3862	3840
Observed reflns	3484	3708	3633	3419
R_{int}	0.0650	0.0494	0.0159	0.0165
No. of parameters	320	322	311	321
GoF	1.157	1.091	1.036	1.067
$R_1[I > 2\sigma(I)]$	0.0507	0.0621	0.0411	0.0631
$WR_2[I > 2\sigma(I)]$	0.1185	0.1732	0.0975	0.1787
R_1_all data	0.0588	0.0643	0.0433	0.0683
Wr_2_all data	0.1241	0.1758	0.0992	0.1840
$\Delta\rho_{max,}$ $\Delta\rho_{min}$(e Å^{-3})	0.49, -0.35	0.48, -0.39	0.85, -0.57	1.06, -0.51

Table 4A.3.1 Contd….

	2.22 •C_4H_8O	**2.22 •CH_3SOCH_3**	**2.22 •$ClCH_2CH_2Cl$**	**2.22 •CH_3CN**
Chemical formula	$C_{21}H_{16}F_2O_8$·(C_4H_8O)	$C_{21}H_{16}F_2O_8$·(C_2H_6SO)	$C_{21}H_{16}F_2O_8$·($C_2H_4Cl_2$)	$C_{21}H_{16}F_2O_8$·(CH_3CN)
M_r	506.44	512.47	533.29	475.39
Temperature (K)	133(2)	133(2)	133(2)	133(2)
Morphology	Plate	Plate	Plate	Plate
Crystal size	0.24×0.19×0.10	0.38×0.16×0.14	0.21×0.16×0.10	0.40×0.39×0.21
Crystal system	Monoclinic	monoclinic	monoclinic	Monoclinic
Space group	$P2_1/n$	$P2_1/c$	$P2_1/n$	$P2_1/c$
a (Å)	12.6350(14)	11.5353(10)	13.3061(12)	11.790(3)
b (Å)	10.2016(11)	9.5572(8)	10.0518(9)	9.537(3)
c (Å)	17.8698(19)	20.5755(17)	17.0729(15)	19.753(6)
	90	90	90	90
β (°)	101.388(2)	91.3960(10	98.5050(10)	96.425(5)
	90	90	90	90
V (Å^3)	2258.0(4)	2267.7(3)	2258.4(3)	2207.2(11)
Z	4	4	4	4
D_{calc} (g cm^{-3})	1.490	1.501	1.568	1.431
μ (mm^{-1})	0.124	0.213	0.354	0.119
F(000)	1056	1064	1096	984
T_{min}	0.971	0.924	0.928	0.954
T_{max}	0.988	0.971	0.967	0.976
h, k, l (min, max)	(-15, 14)	(-10, 13)	(-15, 15)	(-13, 8)
	(-10, 12)	(-11, 11)	(-11, 11)	(-3, 11)
	(-21, 21)	(-24, 24)	(-20, 20)	(-23, 23)
Reflns collected	11011	10996	15898	5676
Unique reflns	3970	3983	3962	3552
Observed reflns	3494	3486	3678	3185
R_{int}	0.0546	0.0168	0.0261	0.0215
No. of parameters	338	351	347	312
GoF	1.080	1.050	1.153	1.063
$R_1[I > 2\sigma(I)]$	0.0532	0.0602	0.0546	0.0416
$WR_2[I > 2\sigma(I)]$	0.1247	0.1519	0.1329	0.1009
R_1_all data	0.0602	0.0678	0.0585	0.0462
Wr_2_all data	0.1293	0.1578	0.1353	0.1043
$\Delta\rho_{max}$, $\Delta\rho_{min}$(e Å^{-3})	0.40, -0.21	0.65, -0.53	0.37, -0.40	0.26, -0.22

Table 4A.3.1 Contd….

	2.22 •***p*-C$_6$H$_4$(CH$_3$)$_2$**	**2.22** •**C$_6$H$_6$**	**2.22** •**C$_6$H$_5$CH$_3$**	**2.22** •***o*-C$_6$H$_4$(CH$_3$)$_2$**
Chemical formula	$C_{21}H_{16}F_2O_8$·0.5 *p*-$C_6H_4(CH_3)_2$	$C_{21}H_{16}F_2O_8$· 2(C_6H_6)	$C_{21}H_{16}F_2O_8$· ($C_6H_5CH_3$)	$C_{29}H_{26}F_2O_8$· *o*-($C_6H_4(CH_3)_2$)
M_r	487.42	512.45	526.47	540.50
Temperature (K)	133(2)	133(2)	133(2)	133(2)
Morphology	Plate	Block	Block	Rect plate
Crystal size	0.43×0.22×0.14	0.25×0.24×0.12	0.26×0.08×0.07	0.25×0.19×0.14
Crystal system	monoclinic	triclinic	triclinic	Triclinic
Space group	$P2_1/c$	P-1	P-1	P-1
a (Å)	11.2679(13)	6.7449(4)	6.8762(8)	6.7954(10)
b (Å)	9.3620(11)	11.5178(8)	11.6387(13)	11.6754(17)
c (Å)	20.990(2)	15.5671(10)	15.4094(18)	16.069(2)
	90	77.7590(10)	81.028(2)	95.891(2)
β (°)	93.908(2)	88.9710(10)	89.700(2)	90.066(2)
	90	88.3540(10)	87.389(2)	91.056(2)
V (Å^3)	2209.1(4)	1181.28(13)	1216.9(2)	1267.9(3)
Z	4	2	2	2
D_{calc} (g cm^{-3})	1.466	1.441	1.437	1.416
μ (mm^{-1})	0.120	0.116	0.115	0.112
F(000)	1012	532	548	564
T_{min}	0.951	0.972	0.971	0.972
T_{max}	0.984	0.987	0.992	0.985
h, k, l (min, max)	(-13, 12)	(-8, 8)	(-8, 8)	(-8, 8)
	(-11, 10)	(-13, 13)	(-13, 13)	(-13, 13)
	(-24, 24)	(-18, 18)	(-18, 18)	(-19, 19)
Reflns collected	10818	11463	10385	12240
Unique reflns	3870	4139	4257	4431
Observed reflns	3524	3935	3648	4144
R_{int}	0.0184	0.0162	0.0324	0.0215
No. of parameters	321	422	348	358
GoF	1.033	1.103	1.213	1.064
$R_1[I > 2\sigma(I)]$	0.0347	0.0351	0.0691	0.0624
$WR_2[I > 2\sigma(I)]$	0.0865	0.0859	0.1552	0.1758
R_1_all data	0.0380	0.0370	0.0798	0.0653
Wr_2_all data	0.0891	0.0873	0.1602	0.1788
$\Delta\rho_{max}$, $\Delta\rho_{min}$(e Å^{-3})	0.30, -0.21	0.24, -0.18	0.48, -0.24	1.20, -0.38

Table 4A.3.1 Contd….

	2.22FI	**2.23**	**2.24**
Chemical formula	$C_{21}H_{16}F_2O_8$	$C_{14}H_{13}FO_7$	$C_{28}H_{19}F_3O_9$
M_r	434.34	312.24	556.43
Temperature (K)	297(2)	297(2)	297(2)
Morphology	block	Plate	plate
Crystal size	0.45×0.10×0.03	0.49×0.35×0.11	0.30×0.20×0.07
Crystal system	Monoclinic	orthorhombic	monoclinic
Space group	$P2_1/n$	*Pbcn*	$P2_1/n$
a (Å)	11.5791(18)	19.047(4)	14.060(3)
b (Å)	6.7493(10)	10.1896(19)	10.592(3)
c (Å)	24.277(4)	13.462(3)	17.702(4)
	90	90	90
β (°)	92.685(3)	90	110.548(4)
	90	90	90
V (Å^3)	1895.2(5)	2612.8(9)	2468.4(10)
Z	4	8	4
D_{calc} (g cm^{-3})	1.522	1.588	1.497
μ (mm^{-1})	0.130	0.137	0.127
F(000)	896	1296	1144
T_{min}	0.945	0.935	0.963
T_{max}	0.996	0.985	0.991
h, k, l (min, max)	(-13, 13)	(-22, 17)	(-16, 11)
	(-8, 8)	(-12, 11)	(-12, 12)
	(-28, 28)	(-16, 15)	(-21, 21)
Reflns collected	17496	12331	12125
Unique reflns	3315	2297	4342
Observed reflns	2200	1938	3400
R_{int}	0.0449	0.0282	0.0223
No. of parameters	284	207	361
GoF	1.004	1.051	1.039
$R_1[I > 2\sigma(I)]$	0.0399	0.0355	0.0427
$WR_2[I > 2\sigma(I)]$	0.0804	0.0872	0.0946
R_1_all data	0.0726	0.0429	0.0566
Wr_2_all data	0.0923	0.0929	0.1015
$\Delta\rho_{max}$, $\Delta\rho_{min}$(e Å^{-3})	0.17, -0.14	0.16, -0.25	0.23, -0.20

4A.3.2 Thermal response of solvates

The DSC curves of the inclusion complexes showed an endotherm much before the final melting curve of the crystals, attributed to the escape of solvent molecules from the inclusion crystal lattice, followed by a second melting endotherm (Fig. 4A.3.1). In some cases a small endothermic peak was observed before melting in the case of **rac-2.5** (**2.5•CH_3SOCH_3**) and **rac-2.7** solvates (**2.7•$C_4H_8O_2$**, **2.7•CH_3SOCH_3**, **2.7•CH_3CN**, **2.7•*p*-$C_6H_4(CH_3)_2$**).

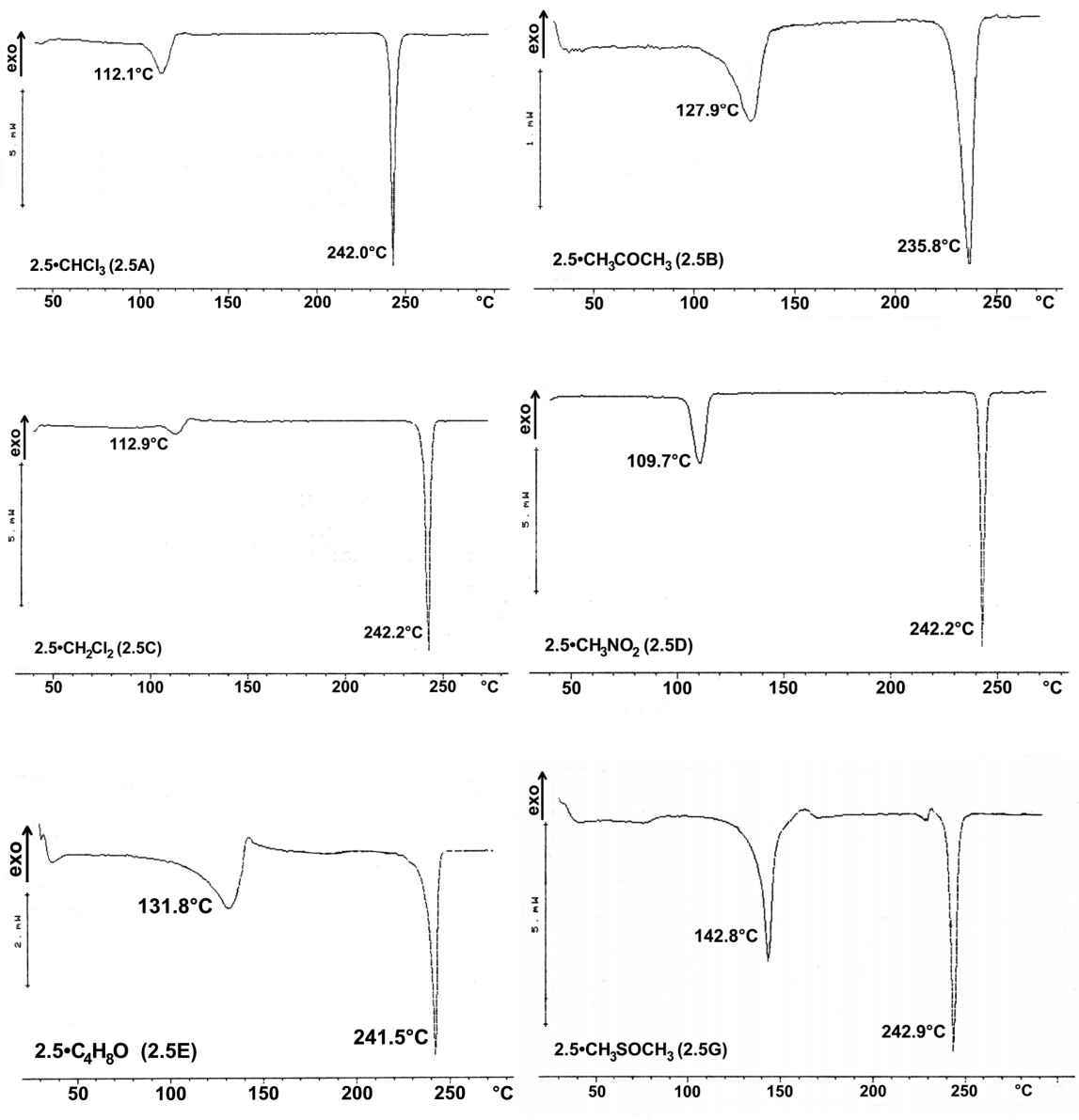

Figure 4A.3.1 DSC curves for solvates of **2.5**, **2.7** and **2.22**.

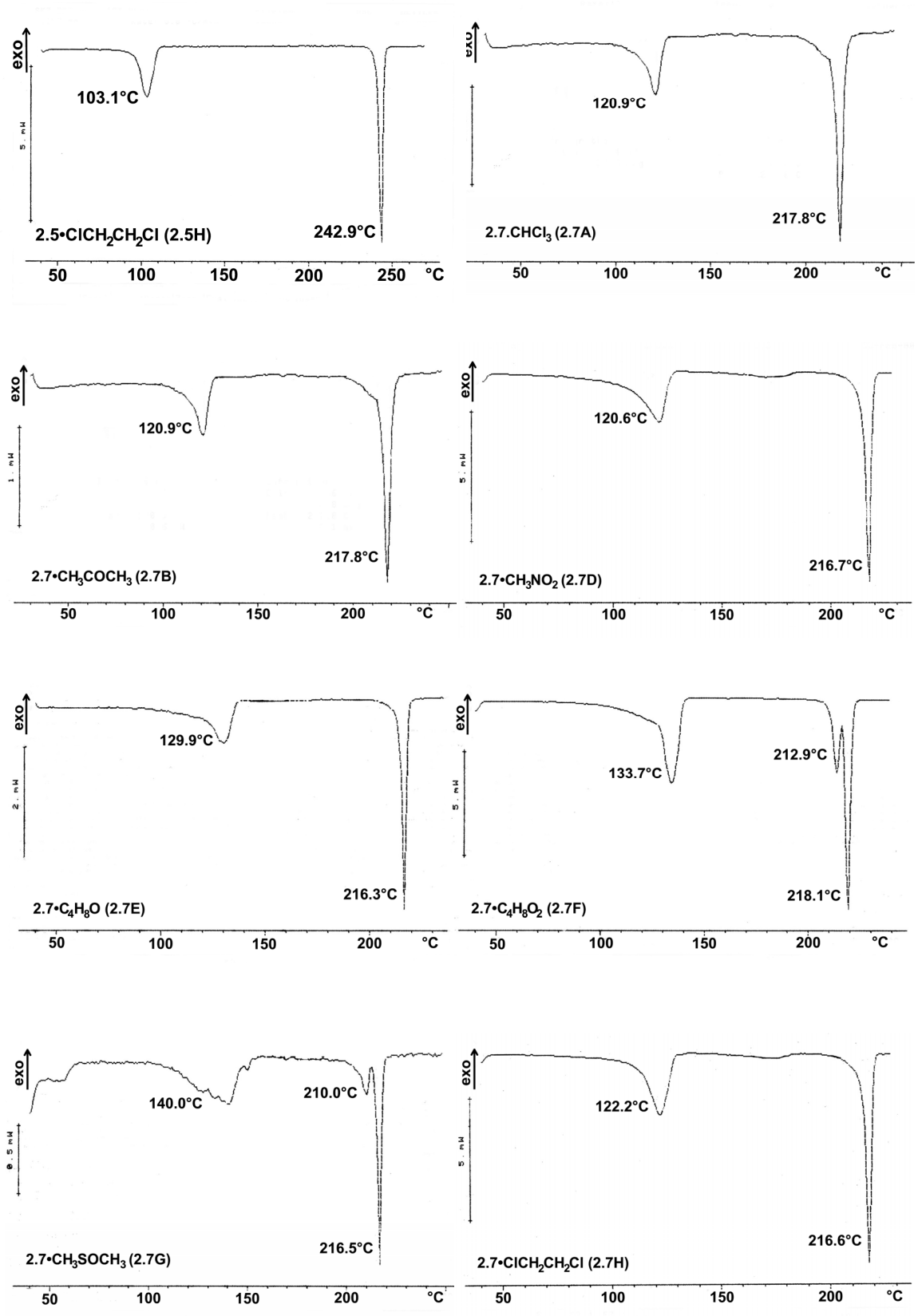

Figure 4A.3.1 Contd...

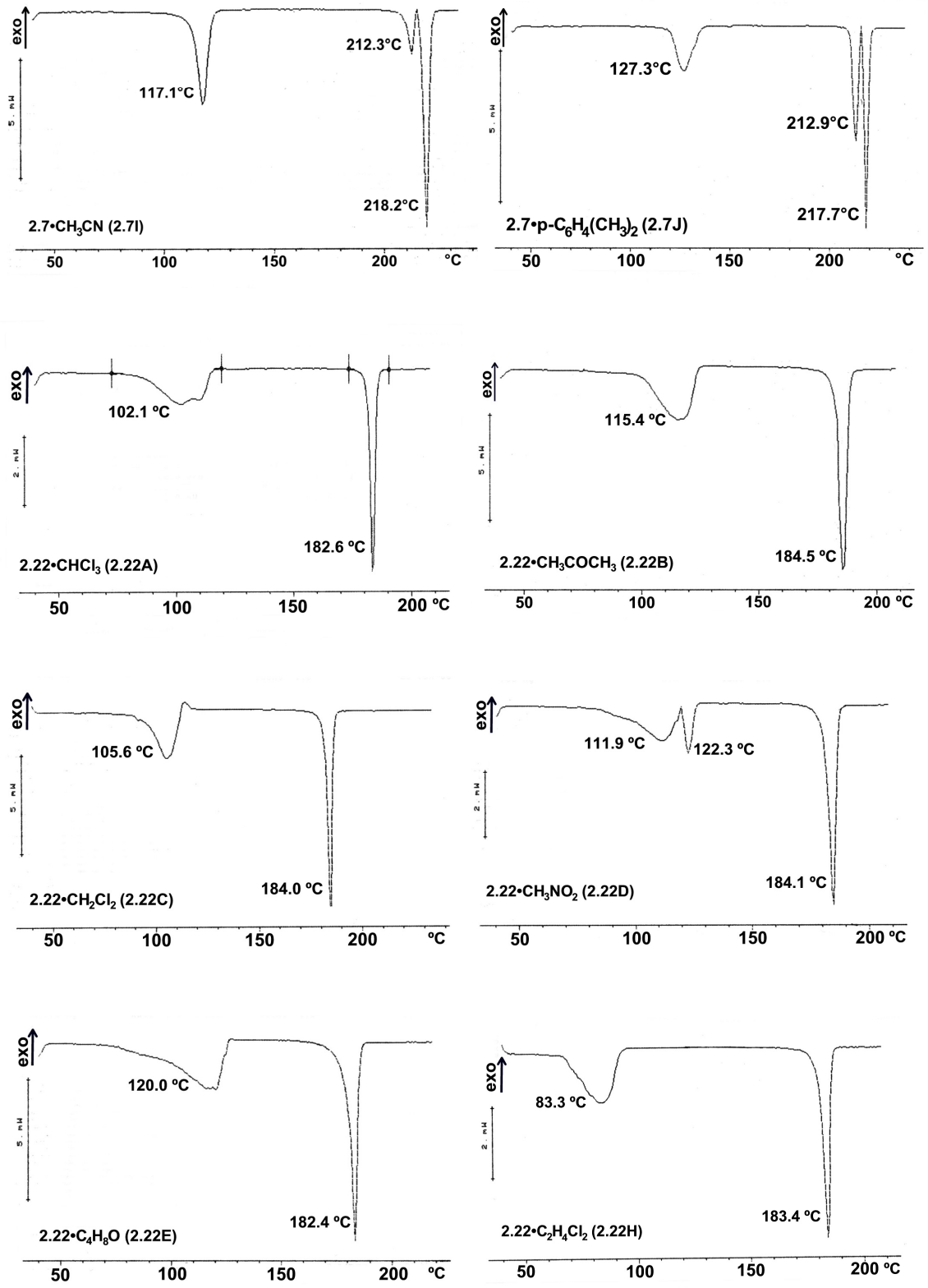

Figure 4A.3.1 Contd...

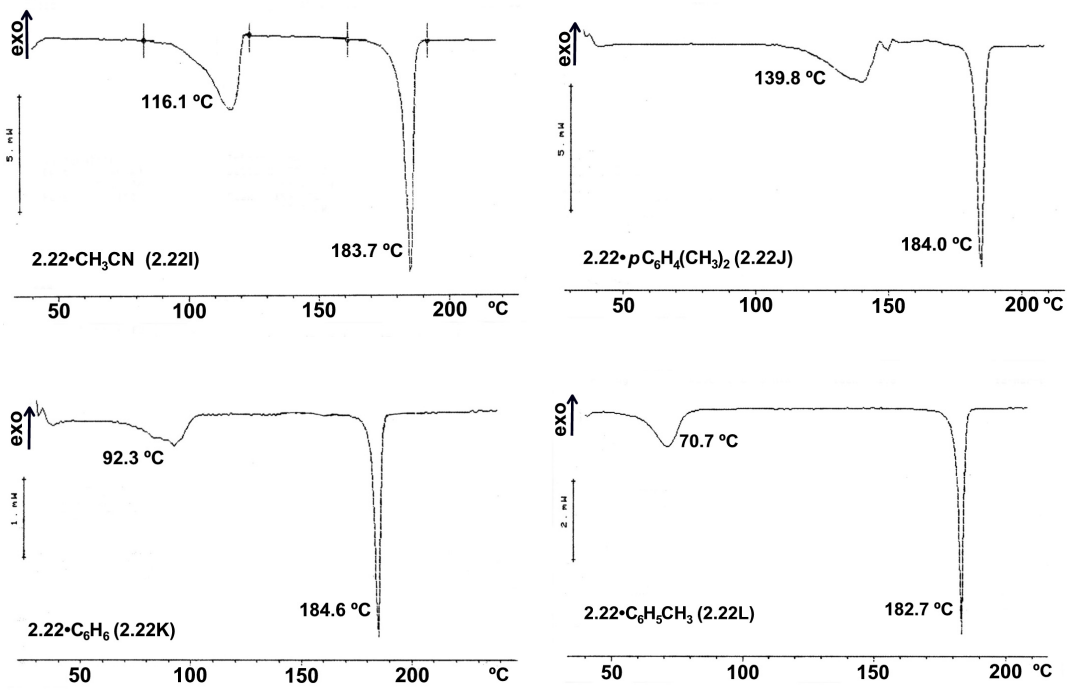

Figure 4A.3.1 Contd...

The thermal response of the solvent free dimorphs of **2.5** (**FI** and **FII**) and the single crystal-to-crystal transformation of **2.5FI** to **2.5FII** has been described earlier.[29] Heating the solvated crystals of **2.5•ClCH$_2$CH$_2$Cl** and **2.7•CH$_3$NO$_2$** upto the temperature of solvent escape (as indicated in the DSC curves) resulted in loss of the included solvent and apparent loss of crystallinity (Fig. 4A.3.2). The opaque mass when touched with a pin, revealed the formation of small rectangular crystals. The unit cell parameters of these crystals revealed that they were Form I solvent free crystals (**2.5FI / 2.7FI**). When these crystals were further heated upto a few degrees below the melting point of the compound (below the melting endotherm indicated by the DSC curve), unit cell determination of crystals from this sample revealed the presence of Form II solvent-less crystals (**2.5FII / 2.7FII**). Heating other bromo and chloro solvates also yielded similar results, indicating the phase transition of the solvated crystal to a solvent free form which further undergoes a single-crystal-to-single crystal phase transition to the halogen bonded solvent free crystals. Heating the solvates of **rac-2.22** also resulted in loss of solvent and apparent loss of crystallinity, but suitable crystals could not be obtained for structural analysis.

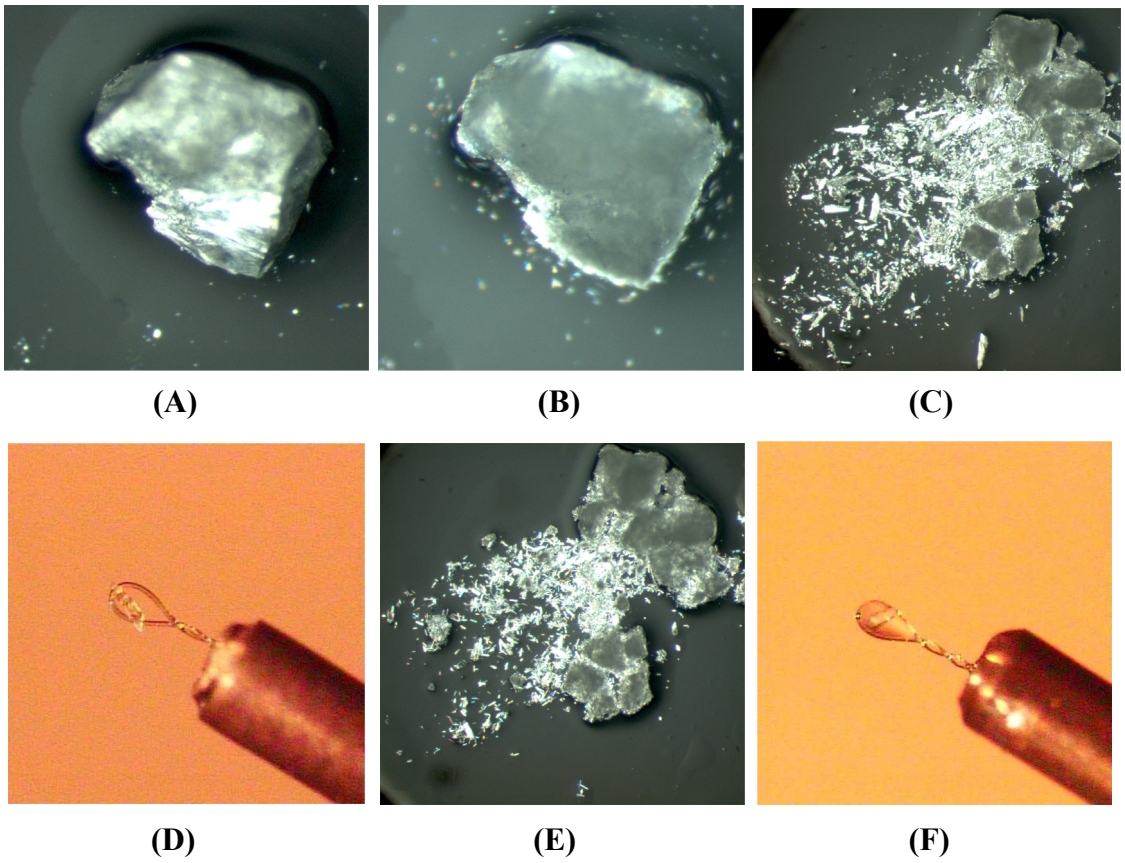

Figure 4A.3.2 Hot stage microscopy images for **2.7•CH_3NO_2**: (A) 100 °C: onset of solvent escape; (B) 140 °C: loss of solvent and crystallinity; (C) smaller crystalline fragments obtained from larger opaque crystal; (D) unit cell determination: solvent free form I crystal (**2.7FI**); (E) fragments in (C) reheated to 220 °C; (F) plate-like solvent free form II crystals (**2.7FI**).

4A.3.3 Solid-state reactivity of solvates

General experimental procedure for solid-state reactions: Solid Na_2CO_3 was activated by placing a finely powdered sample in a furnace maintained at 270 °C for 12 h. Freshly grown crystals of the compound (~ 1 equiv.) were ground together with (anhydrous) activated solid Na_2CO_3 (~ 8 equiv.) into a fine powder using a mortar and pestle. This powder was transferred to a hard glass test-tube and heated under an inert atmosphere in an oil bath maintained at or below the temperature of solvent escape (according to DSC) from the solvate.

2.5•$CHCl_3$: Crystals of **2.5•$CHCl_3$** (0.028 g, 0.05 mmol) were ground together with activated Na_2CO_3 (0.050 g, 0.45 mmol) and heated at 80 °C for 72 h. TLC analysis showed the presence of the unreacted diester **2.5**, the triester **2.6** and the diol **2.20**.

2.5•CH_3COCH_3: Crystals of **2.5•CH_3COCH_3** (0.028 g, 0.05 mmol) were ground together with activated Na_2CO_3 (0.043 g, 0.4 mmol) and heated at 80 °C for 42 h, after which no further change was observed by TLC analysis which showed the presence of the triester **2.6** and the diol **2.20** along with the unreacted diester **2.5**.

2.5•CH_2Cl_2: Crystals of **2.5•CH_2Cl_2** (0.028 g, 0.05 mmol) were ground together with activated Na_2CO_3 (0.043 g, 0.4 mmol) and heated at 90 °C for 72 h. TLC analysis showed only the presence of the unreacted diester **2.5**.

2.5•CH_3NO_2: Crystals of **2.5•CH_3NO_2** (0.028 g, 0.05 mmol) were ground together with activated Na_2CO_3 (0.043 g, 0.4 mmol) and heated at 90 °C for 71 h. TLC analysis showed only the presence of the unreacted diester **2.5**.

2.5•$ClCH_2CH_2Cl$: Crystals of **2.5•$ClCH_2CH_2Cl$** (0.035 g, 0.06 mmol) were ground together with activated Na_2CO_3 (0.050 g, 0.48 mmol) and heated at 82 °C for 72 h, after which no further change was observed by TLC analysis which showed the presence of the triester **2.6** and the diol **2.20** along with the unreacted diester **2.5**.

2.7•$CHCl_3$: Crystals of **2.7•$CHCl_3$** (0.024 g, 0.05 mmol) were ground together with activated Na_2CO_3 (0.045 g, 0.4 mmol) and heated at 90 °C for 72 h. TLC analysis showed the presence of the unreacted diester **2.7**, the triester **2.8** and the diol **2.21** along with two unidentified products.

2.7•CH_3COCH_3: Crystals of **2.7•CH_3COCH_3** (0.027 g, 0.05 mmol) were ground together with activated Na_2CO_3 (0.045 g, 0.4 mmol) and heated at 80 °C for 72 h. TLC analysis showed the presence of the unreacted diester **2.7**, the triester **2.8** and the diol **2.21** along with two unidentified products.

2.7•CH_3NO_2: Crystals of **2.7•CH_3NO_2** (0.026 g, 0.05 mmol) were ground together with activated Na_2CO_3 (0.042 g, 0.4 mmol) and heated at 90 °C for 48 h, after which no further change was observed by TLC analysis, which showed presence of the unreacted diester **2.7**, the triester **2.8** and the diol **2.21** along with two unidentified products.

2.7•$ClCH_2CH_2Cl$: Crystals of **2.7•$ClCH_2CH_2Cl$** (0.024 g, 0.05 mmol) were ground together with activated Na_2CO_3 (0.043 g, 0.4 mmol) and heated at 85 °C for 48 h,

after which no further change was observed. TLC analysis showed the presence of the triester **2.8** and the diol **2.21** along with the unreacted diester **2.7**. Increase in reaction temperature (100 °C) resulted in the formation of two unidentified products.

2.7•CH_3CN: Crystals of **2.7•CH_3CN** (0.024 g, 0.05 mmol) were ground together with activated Na_2CO_3 (0.045 g, 0.4 mmol) and heated at 90 °C for 82 h. TLC analysis showed the presence of the unreacted diester **2.7**, the triester **2.8** and the diol **2.21** along with two unidentified products.

2.22•CH_3COCH_3: Crystals of **2.22•CH_3COCH_3** (0.022 g, 0.05 mmol) were ground together with activated Na_2CO_3 (0.043 g, 0.4 mmol) and heated at 80 °C for 47 h. TLC analysis showed the presence of the diester **2.22**, the diol **2.23** and the triester **2.24**.

2.22•CH_2Cl_2: Crystals of **2.22•CH_2Cl_2** (0.023 g, 0.053 mmol) were ground together with activated Na_2CO_3 (0.045 g, 0.424 mmol) and heated at 80 °C for 71 h. TLC analysis showed the presence of the unreacted diester **2.22**.

2.22•CH_3NO_2: Crystals of **2.22•CH_3NO_2** (0.080 g, 0.2 mmol) were ground together with activated Na_2CO_3 (0.170 g, 1.6 mmol) and heated at 105 °C for 72 h. TLC analysis showed the presence of the unreacted diester as well as the diol **2.23** and the triester **2.24**. The organic material was extracted with $CHCl_3$ (5 × 5 mL), concentrated and dried under vacuum. ^{19}F NMR spectrum indicated the presence of the diol **2.23** and the triester **2.24** along with large amount of the unreacted diester **2.22** (see end of this section for NMR spectra).

2.22•C_4H_8O: Crystals of **2.22•C_4H_8O** (0.043 g, 0.1 mmol) were ground together with activated Na_2CO_3 (0.085 g, 0.8 mmol) and heated at 60 °C for 41 h. TLC analysis showed the presence of the unreacted diester **2.22**.

2.22•$ClCH_2CH_2Cl$: Crystals of **2.22•$ClCH_2CH_2Cl$** (0.026 g, 0.06 mmol) were ground together with activated Na_2CO_3 (0.051 g, 0.48 mmol) and heated at 70 °C for 40 h. TLC analysis showed the presence of the unreacted diester **2.22**.

2.22•CH_3CN: Crystals of **2.22•CH_3CN** (0.106 g, 0.25 mmol) were ground together with activated Na_2CO_3 (0.212 g, 2 mmol) and heated at 80 °C for 46 h. TLC analysis showed the presence of the diester **2.22**, the diol **2.23** and the triester **2.24**. When the temperature was increased to 100 °C, other unidentified products were observed by TLC analysis.

2.22•*p*-$C_6H_4(CH_3)_2$: Crystals of **2.22•*p*-$C_6H_4(CH_3)_2$** (0.024 g, 0.05 mmol) were ground together with activated Na_2CO_3 (0.045 g, 0.4 mmol) and heated at 100 °C for 72 h. TLC analysis showed the presence of the diester **2.22**, the diol **2.23** and the triester **2.24** along with two other unidentified products.

2.22FI: Crystals of **2.22FI** (0.027 g, 0.05 mmol) were ground together with activated Na_2CO_3 (0.045 g, 0.4 mmol) and heated at 115 °C for 48 h. TLC analysis showed the presence of the diester **2.22**, the diol **2.23** and the triester **2.24** along with other unidentified products. The mixture was extracted with ethyl acetate (5 x 5 mL), concentrated, dried under vacuum. ^{19}F NMR spectrum indicated the presence of the triester **2.24**, the unreacted diester **2.22** amongst two other unidentified products (see end of this section for NMR spectra).

^{19}F NMR spectrum (in $CDCl_3$ + CD_3SOCD_3 + C_6F_6) of product mixture of the solid-state reaction of **2.22•CH_3NO_2.**

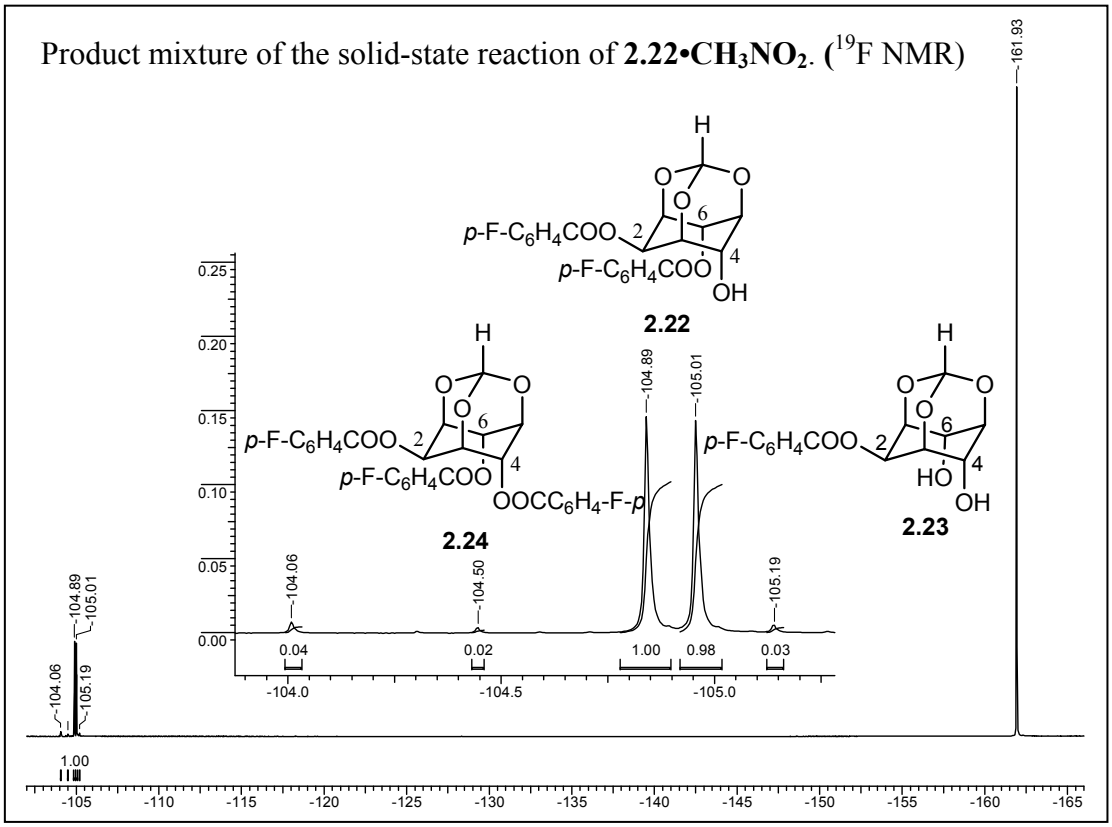

^{19}F NMR spectrum (in $CDCl_3$ + CD_3SOCD_3 + C_6F_6) of product mixture of the solid-state reaction of **2.22FI.**

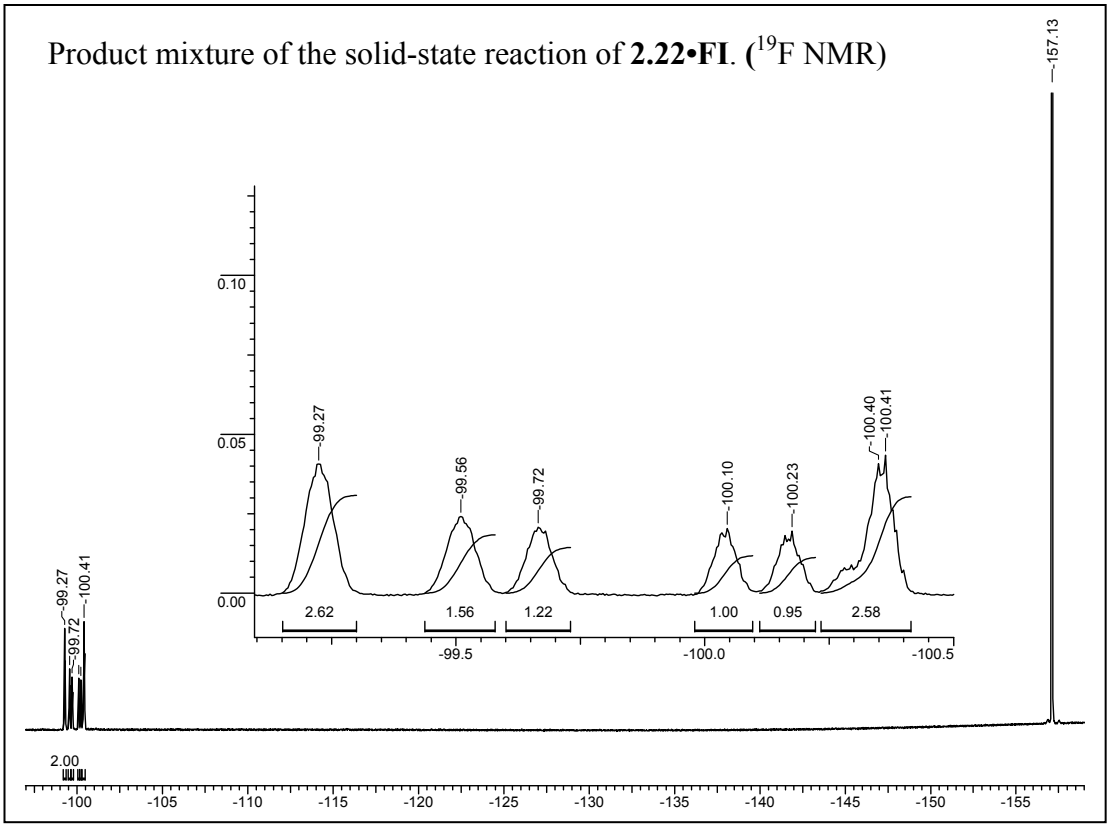

4A.4 Results and Discussion

4A.4.1 Structural features

The inclusion crystals of **rac-2.5** and **rac-2.7** (for a representative ORTEP see Fig. 4A.4.1a) could be categorized into three groups, based on the differences in the organization of molecules in their crystals: group I (**2.5A-2.5G** and **2.7A-2.7G**) belonging to the monoclinic space group $P2_1/n$, group II (**2.5H**, **2.7H**, **2.7I**, **2.7J**) belonging to the monoclinic space group $P2_1/c$ and group III (**2.7K**) belonging to the monoclinic space group $C2/c$. The two space groups $P2_1/n$ and $P2_1/c$ are crystallographically equivalent and are simply related by cell transformations, which is purely coincidental in the present case. The molecules in the space groups have different environments and modes of association in their crystal structures. As often observed in many systems, the crystals of chloro and bromo derivatives are isomorphous.[35] The solvates of **rac-2.22** can be divided into two groups: group IV (**2.22A-2.22J**) belonging to the monoclinic space groups $P2_1/n$ and $P2_1/c$ and group V (**2.22K-2.22M**) belonging to the triclinic space group P-1. Solvent free crystals of **2.22** (**2.22FI**, monoclinic, $P2_1/n$), were obtained from methanol (Fig. 4A.4.1b).

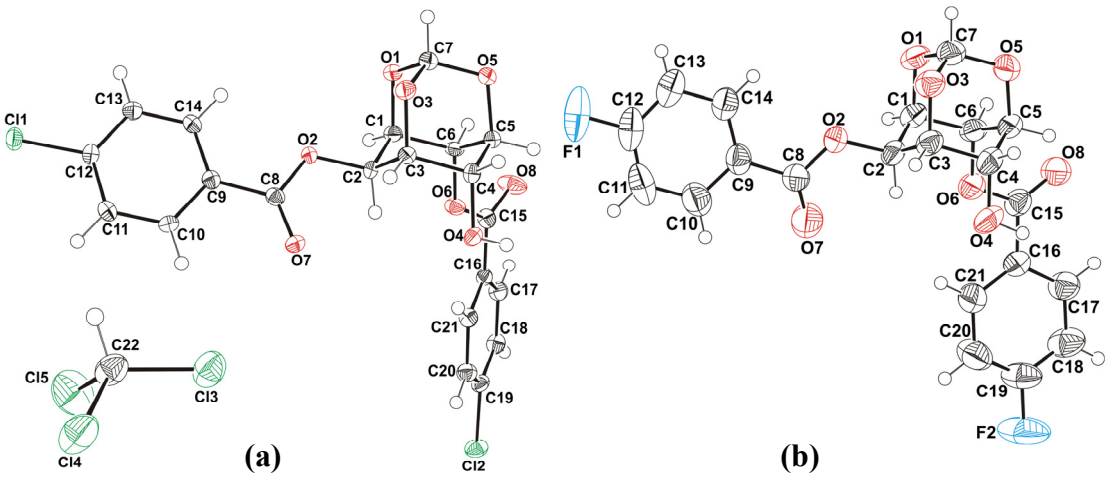

Figure 4A.4.1 Representative ORTEP of the molecule in crystals of (a) **2.7•CHCl$_3$** and (b) **2.22FI**. Thermal ellipsoids are drawn at 50% probability and hydrogen atoms are shown as small spheres of arbitrary radii.

The *a* and *b* axes are very similar in groups I, II and IV but the *c*-axis in group II and in $P2_1/c$ solvates of group IV is longer by ~2 Å. The unique axis length is similar (~ 10 Å) in all the monoclinic solvates. The group V triclinic solvates (**2.22K- 2.22M**) are also isomorphous, but unit cell parameters differ greatly from those of the monoclinic solvates. In all the solvates of **rac-2.5**, **rac-2.7** and **rac-2.22** the crystal lattice contained one molecule of host per one molecule of the guest (guests showed full occupancy) except in **2.7•C_6H_6**, **2.7•*p*-$C_6H_4(CH_3)_2$**, **2.22•*p*-$C_6H_4(CH_3)_2$** and **2.22•C_6H_6**. In **2.7•C_6H_6** two molecules of benzene (half benzene molecule with full occupancy and full benzene molecule with half occupancy) were present per molecule of the host, thus the host : guest ratio was 1 : 1. In **2.7•*p*-$C_6H_4(CH_3)_2$** and **2.22•*p*-$C_6H_4(CH_3)_2$** half molecule of *p*-xylene with full occupancy was present per molecule of the host. In **2.22•C_6H_6** two molecules of benzene were present per molecule of the host, thus host : guest ratio was 1 : 2. Interestingly, when the X-ray measurements for an approximately one month-old crystal of **2.7•CH_2Cl_2 (T)** were recorded, crystal structure solution (Table 4A.3.1) revealed that over time the occupancy of dichloromethane in the crystals of **2.7•CH_2Cl_2** had reduced to 0.06.

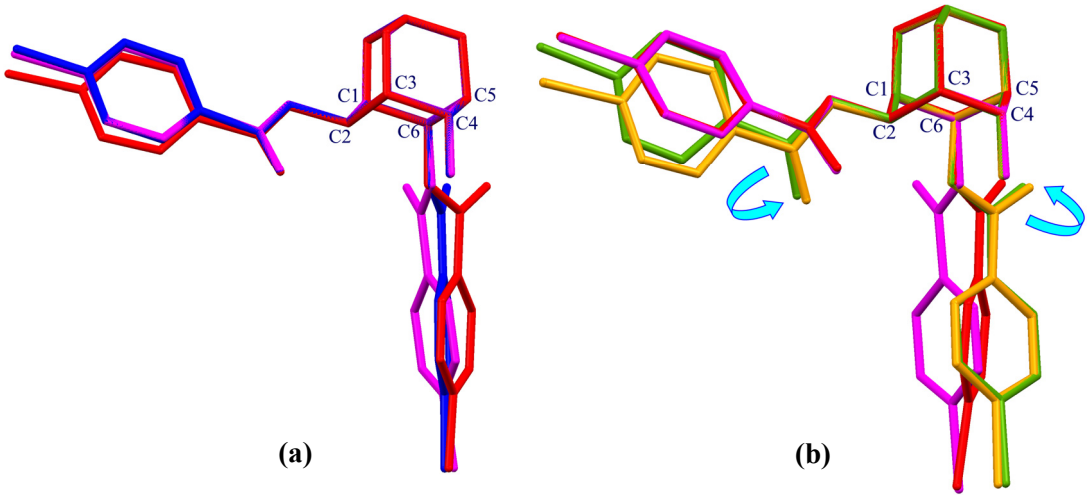

Figure 4A.4.2 Molecular overlap of (a) host molecules in inclusion crystals of **2.7•$CHCl_3$** (red), **2.7•CH_2Cl_2** (blue), **2.7•$C_4H_8O_2$** (magenta) and (b) overlap of solvent free polymorphs of **2.7** (orange and green) and host molecules in **2.7•$CHCl_3$** (red) and **2.7•$C_4H_8O_2$** (magenta) showing relative orientation of benzoyl groups.

Host molecules in inclusion crystals of **rac-2.5**, **rac-2.7** and **rac-2.22** were superimposed to examine their conformational differences (Fig. 4A.4.2). The C2-*O*-

(*p*-halobenzoyl) group overlapped reasonably well in solvates of **rac-2.5** whereas in solvates of **rac-2.7** it revealed slight differences (2–11°) in the orientation. Marked conformational differences in the relative orientation of C6-*O*-*p*-halobenzoyl groups were observed due to free rotation about O–C bond in solvates of **rac-2.5** and **rac-2.7**. There are three major conformations observed for the C6-*O*-(*p*-halobenzoyl) group in the inclusion crystals of **rac-2.5** and **rac-2.7** irrespective of their space group (Fig. 4A.4.2a). The orientation of the C6-*O*-(*p*-halobenzoyl) group in **2.7•CH_2Cl_2** (blue) differs by about 25° each from that in **2.7•$CHCl_3$** (red) and **2.7•$C_4H_8O_2$** (magenta). The conformation of C6-*O*-(*p*-halobenzoyl) group in DMSO and acetone solvates of **rac-2.5** and **rac-2.7** matches with **2.7•$CHCl_3$** whereas in THF inclusion crystals of **rac-2.5** and **rac-2.7** it matches with **2.7•CH_2Cl_2**. In acetonitrile, benzene, 1,2-dichloroethane, *p*-xylene solvates of **rac-2.7** and 1,2-dichloroethane solvate of **rac-2.5** the conformation of C6-*O*-(*p*-halobenzoyl) group matches with **2.7•$C_4H_8O_2$**. Interestingly, the orientation of C6-*O*-(*p*-halobenzoyl) group in **2.5•CH_3NO_2** matches with that of **2.7•$CHCl_3$** whereas that of **2.7•CH_3NO_2** overlaps well with **2.7•$C_4H_8O_2$**. Superimposing solventless polymorphs of **rac-2.7** and host molecules of chloroform and dioxane inclusion crystals showed major difference in relative orientation of the C2 and C6-*O*-benzoyl groups (Fig. 4A.4.2b). The C6-*O*-(*p*-halobenzoyl) group of host molecules in inclusion crystals of **rac-2.5** and **rac-2.7** moved away from the axial –OH group in anticlockwise direction while the C2-*O*-(*p*-halobenzoyl) group moved closer to the –OH group. The C6-*O*-(*p*-halobenzoyl) group in polymorphs of **rac-2.7** showed difference of about 26-28° with C6-*O*-(*p*-halobenzoyl) group of chloroform solvate of **rac-2.7**. The difference in the relative orientation of the C2-*O*-benzoyl group in solvent-free polymorphs and solvates of **rac-2.7** is about 56-68°.

The overlap of host molecules in solvates and solventless crystals of **rac-2.22** revealed four major conformations adopted by the C6-*O*-(*p*-fluorobenzoyl) group (Fig. 4A.4.3a) while the equatorial and axial esters of triclinic solvates **2.22•$C_6H_5CH_3$**, **2.22•C_6H_6** and **2.22•*o*-$C_6H_4(CH_3)_2$** overlapped well with the solvent free crystals **2.22FI** (Fig. 4A.4.3b). In the case of the monoclinic solvates, two major conformations for the C6-*O*-(*p*-fluorobenzoyl) group were observed represented by **2.22•$CHCl_3$** (blue) and **2.22•*p*-$C_6H_4(CH_3)_2$** (red). The conformation of the axial ester in **2.22•C_4H_8O** and **2.22•CH_2Cl_2** matches with **2.22•$CHCl_3$** while that in

2.22•CH_3CN, 2.22•CH_3COCH_3, **2.22•CH_3SOCH_3** and **2.22•CH_3NO_2** matches with **2.22•*p*-$C_6H_4(CH_3)_2$**. The conformation of the axial ester in **2.22•$ClCH_2CH_2Cl$** (orange) lies in between **2.22•$CHCl_3$** and **2.22•*p*-$C_6H_4(CH_3)_2$**. The conformation difference of C6-*O*-(*p*-halobenzoyl) groups in **2.22•$CHCl_3$** (blue) and **2.22•$ClCH_2CH_2Cl$** (orange) is ~ 8° while that between **2.22•$ClCH_2CH_2Cl$** (orange) and **2.22•*p*-$C_6H_4(CH_3)_2$** (red) is ~ 25°. The C2-*O*-(*p*-halobenzoyl) groups in **2.22FI** (purple) and **2.22•$CHCl_3$** (blue) are ~ 47° apart.

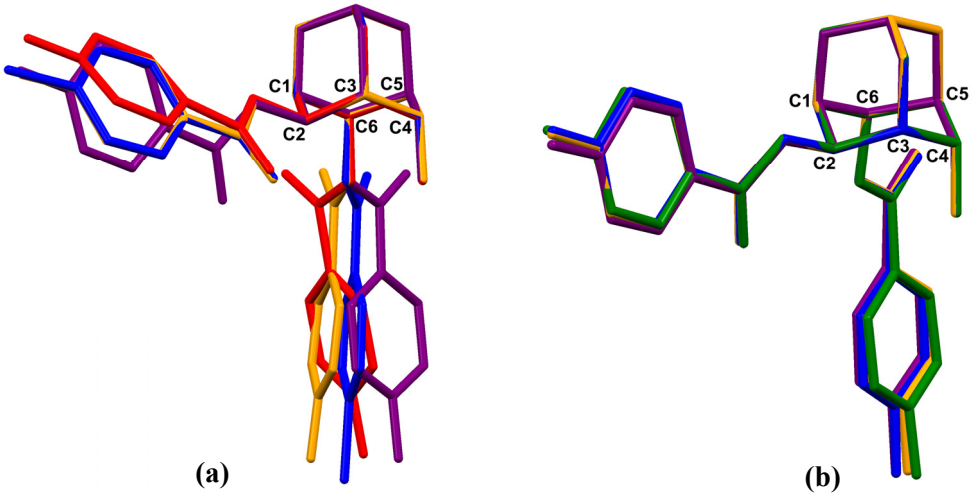

Figure 4A.4.3. Molecular overlap of (a) host molecules in solvates and solventless crystals of group IV (purple-**2.22FI**; blue-**2.22•$CHCl_3$**; orange-**2.22•$ClCH_2CH_2Cl$** and red-**2.22•*p*-$C_6H_4(CH_3)_2$**) and (b) overlap of triclinic solvates of group V and solventless crystals of **2.22** (purple-**2.22FI**; orange-**2.22•C_6H_6**; green-**2.22•$C_6H_5CH_3$** and blue-***o*-$C_6H_4(CH_3)_2$**) shows relative orientation of benzoyl groups.

Assembly of the host molecules in solvates

Host molecules in the monoclinic inclusion crystals belonging to groups I-IV assemble around the crystallographic two-fold screw axis (*b*-axis) to form a helical assembly (Fig. 4A.4.4a) exhibiting one-dimensional isostructurality[36] justified by the near equality of the *b*-axis. Each helix is composed of only a single enantiomer of the racemic host while the neighboring helix is comprised of the other enantiomer. The successive molecules along the helix are linked by conventional O-H···O hydrogen bonding; the -OH group at the C-4 position donates its H atom to the carbonyl oxygen

O7 of the equatorial C2-*O*-*p*-halobenzoyl group. This is similar to the assembly of molecules observed in crystals of **rac-1.177**.[28b]

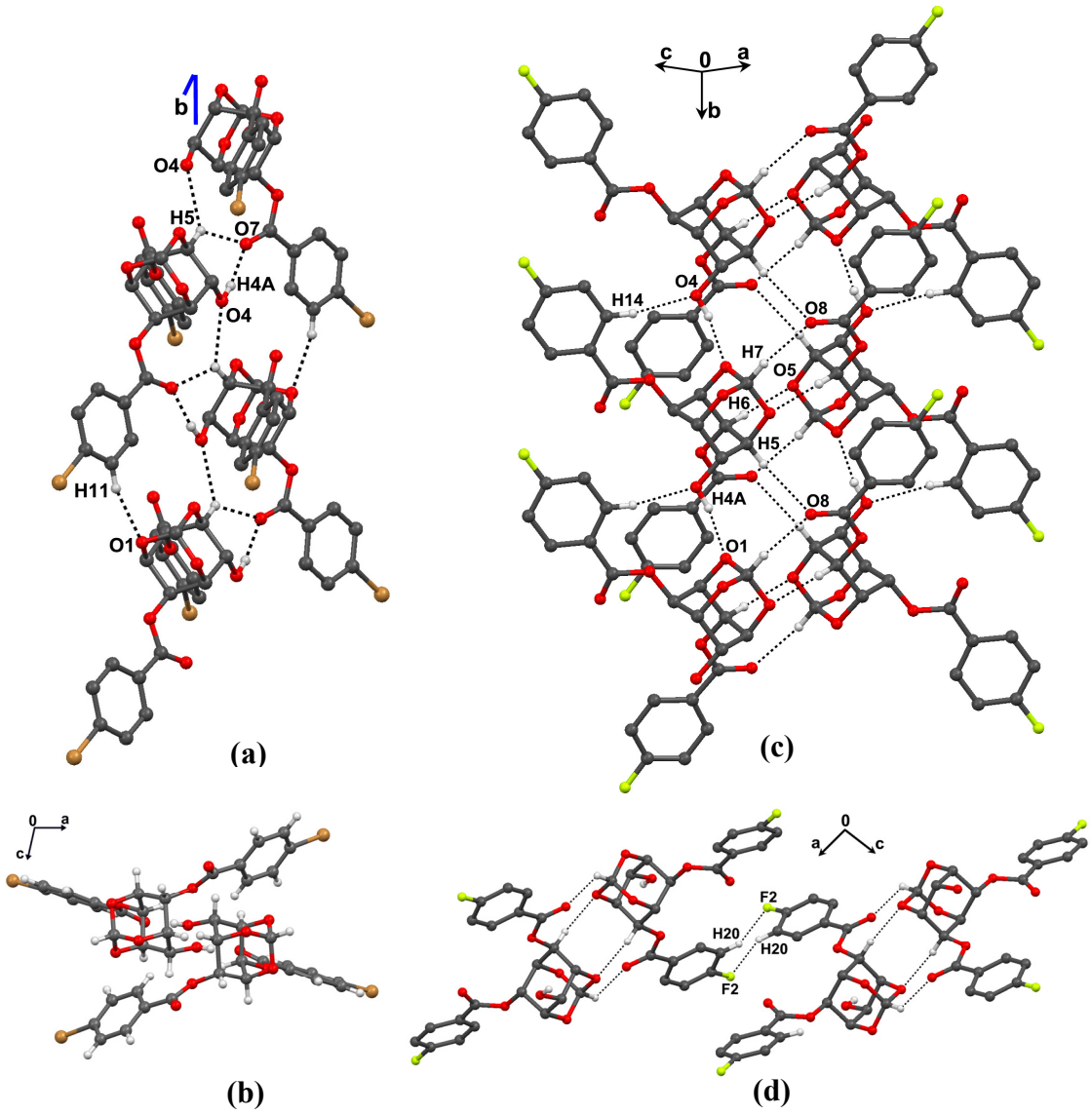

Figure 4A.4.4. (a) Helical assembly across crystallographic 2_1 axis *via* O-H···O and C-H···O interactions in **2.5•CH_3COCH_3**. Hydrogen atoms not involved in bonding are omitted for the sake of clarity. (b) Dancing pair like association of host molecules viewed down the *b*-axis in **2.5•CH_3COCH_3**. (c) Bilayer assembly in **2.22FI** (solvent free crystal of **rac-2.22**) and (d) Linkage of bilayers *via* weak C-H···F interactions.

The H4A···O7 distances are in the range 1.95-2.11 Å but the angle of approach varies (164-178°, Table 4A.4.1). In the monoclinic inclusion crystals, in addition to O-

H···O, some weak C-H···O contacts also hold the molecules along the helix. The C5-H5 of the inositol ring makes C-H···O contacts with the hydroxyl oxygen O4 (C5-H5···O4) of the neighboring 2_1-screw related molecules along the helix. Further along the helical assembly, the unit-translated molecules are linked *via* more linear C11-H11···O1 contacts as compared to C5-H5···O4 interactions (Table 4A.4.1). The helical assembly across crystallographic two-fold axis mainly linked *via* O-H···O bonding is a consistent feature in the organization of the host molecules in all monoclinic solvates. The C-H···π interactions which were observed along the helix (holding the migrating group in place for the reactions) in **rac-1.177** are weak (> 3 Å) and marginal in the solvates. A perpendicular view of the helix down *b*-axis shows 'dancing pair' like organization of the molecules (Fig. 4A.4.4b). Interestingly, molecules in the solvent less crystals of **rac-2.22** (**2.22FI**) do not assemble in helical fashion. Strong O-H···O hydrogen bonding (Table 4A.4.1) between the hydroxyl group and orthoester oxygen along with weak C1-H1···π interactions leads to the formation of homochiral molecular chains which are linked by C-H···O interactions (C7-H7···O8, C6-H6···O5 and C5-H5···O8) between the orthoformate and inositol ring protons and orthoester and axial ester carbonyl oxygen to form bilayers (Fig.4A.4.4c, Table 4A.4.1). These bilayers are interlinked by weak C20-H20···F2 interactions (Fig.4A.4.4d).[37] The host molecules in the triclinic solvates of **rac-2.22** also assemble in the form of molecular bilayers, with a perfect overlap of the axial and equatorial ester groups in their structures and the solvent less crystals (Fig. 4A.4.3b). This pattern of bilayer formation is similar to that observed in the solvent less crystals of **rac-2.5** and **rac 2.7**[29] (and **rac-2.15** and **rac-2.18**, discussed in chapter 3).

Table 4A.4.1 Interactions building helices in crystals of groups I-IV and bilayers in group V.

Solvate	D-H···A	D-H (Å)	H-A (Å)	D-A (Å)	D-H···A (°)
Group I					
2.5•$CHCl_3$	O4-H4A···O7^{i}	0.804(18)	2.00(2)	2.782(2)	165(4)
	C5-H5···O4^{i}	1.00	2.56	3.296(3)	131
	C11-H11···O1^{ii}	0.95	2.70	3.524(4)	146
2.5•CH_3COCH_3	O4-H4A···O7^{iii}	0.81(3)	1.98(4)	2.780(3)	171(3)
	C5-H5···O4^{iii}	1.00	2.52	3.231(3)	128
	C11-H11···O1^{ii}	0.95	2.66	3.489(3)	146
2.5•CH_2Cl_2	O4-H4A···O7^{iv}	0.805(18)	1.992(19)	2.794(3)	174(4)
	C5-H5···O4^{iv}	1.00	2.60	3.337(3)	131
	C11-H11···O1^{ii}	0.95	2.59	3.435(3)	149
2.5•CH_3NO_2	O4-H4A···O7^{iv}	0.812(19)	1.97(2)	2.767(3)	167(4)
	C5-H5···O4^{i}	1.00	2.45	3.160(3)	127
2.5•C_4H_8O	O4-H4A···O7^{iii}	0.82(7)	2.00(8)	2.800(4)	168(7)
	C5-H5···O4^{iii}	1.00	2.54	3.261(5)	129
	C11-H11···O1^{ii}	0.95	2.57	3.387(5)	144
2.5•$C_4H_8O_2$	O4-H4A···O7^{iv}	0.86(4)	1.99(5)	2.830(3)	166(4)
	C5-H5···O4^{i}	1.00	2.69	3.381(4)	126
	C11-H11···O1^{ii}	0.95	2.64	3.491(4)	149
2.5•CH_3SOCH_3	O4-H4A···O7^{v}	0.83(7)	1.96(7)	2.776(4)	169(6)
	C5-H5···O4^{v}	1.00	2.55	3.277(5)	129
	C11-H11···O1^{ii}	0.95	2.58	3.437(5)	151
2.7•$CHCl_3$	O4-H4A···O7^{iv}	0.804(18)	2.004(18)	2.803(2)	172(3)
	C5-H5···O4^{i}	1.00	2.58	3.336(3)	132
	C11-H11···O1^{ii}	0.95	2.51	3.385(3)	153
2.7•CH_3COCH_3	O4-H4A···O7^{iii}	0.84(3)	1.97(3)	2.786(2)	165(3)
	C5-H5···O4^{iii}	1.00	2.53	3.240(2)	128
	C11-H11···O1^{ii}	0.95	2.61	3.450(2)	148
2.7•CH_2Cl_2	O4-H4A···O7^{i}	0.81(3)	1.99(4)	2.798(2)	173(3)
	C5-H5···O4^{i}	1.00	2.58	3.316(3)	131
	C11-H11···O1^{ii}	0.95	2.53	3.371(3)	148
2.7•CH_3NO_2	O4-H4A···O7^{v}	0.791(15)	2.012(15)	2.800(2)	174(2)
	C5-H5···O4^{v}	1.00	2.58	3.287(2)	128
	C11-H11···O1^{ii}	0.95	2.56	3.381(2)	145
2.7•C_4H_8O	O4-H4A···O7^{iii}	0.834(19)	1.97(2)	2.795(3)	171(4)
	C5-H5···O4^{iii}	1.00	2.61	3.338(4)	130
	C11-H11···O1^{ii}	0.95	2.55	3.397(4)	148
2.7•$C_4H_8O_2$	O4-H4A···O7^{iii}	0.82(4)	2.02(2)	2.828(3)	171(5)
	C5-H5···O4^{iii}	1.00	2.61	3.294(4)	126
	C11-H11···O1^{ii}	0.95	2.66	3.474(4)	145

Table 4A.4.1 Contd...

2.7•CH_3SOCH_3	O4-H4A···O7^{iii}	0.831(18)	1.96(2)	2.770(3)	166(4)
	C5-H5···O4^{iii}	0.91(3)	2.55(3)	3.263(3)	135(2)
	C11-H11···O1^{ii}	0.89(3)	2.60(3)	3.411(3)	151(2)
Group II					
2.5•$ClCH_2CH_2Cl$	O4-H4A···O7^{vi}	0.81(4)	2.03(2)	2.822(4)	166(4)
	C5-H5···O4^{vi}	1.00	2.64	3.348(5)	128
	C11-H11···O1^{ii}	0.95	2.50	3.315(5)	144
2.7•$ClCH_2CH_2Cl$	O4-H4A···O7^{vii}	0.82(5)	2.01(5)	2.825(4)	175(6)
	C5-H5···O4^{vii}	1.00	2.56	3.265(5)	127
	C11-H11···O1^{ii}	0.95	2.50	3.294(5)	141
2.7•CH_3CN	O4-H4A···O7^{vii}	0.80(3)	2.01(3)	2.813(2)	176(3)
	C5-H5···O4^{vii}	0.93(2)	2.61(2)	3.332(3)	134(2)
	C11-H11···O1^{ii}	0.96(3)	2.52(3)	3.307(3)	139(2)
2.7•*p*-$C_6H_4(CH_3)_2$	O4-H4A···O7^{viii}	0.83(2)	1.99(3)	2.811(2)	172(2)
	C11-H11···O1^{ii}	0.95	2.51	3.237(2)	134
Group III					
2.7•C_6H_6	O4-H4A···O7^{iii}	0.84	1.98	2.813(6)	174
	C11-H11···O1^{ii}	0.95	2.49	3.227(8)	135
Group IV					
2.22•$CHCl_3$	O4-H4A···O7^{iv}	0.77(4)	2.04(4)	2.802(3)	171(4)
	C5-H5···O4^{iv}	1.00	2.53	3.244(3)	128
	C11-H11···O1^{ii}	0.95	2.47	3.328(3)	150
2.22•CH_3COCH_3	O4-H4A···O7^{ix}	0.83(3)	1.97(3)	2.803(2)	178(3)
	C5-H5···O4^{ix}	1.00	2.62	3.269(3)	123
	C11-H11···O1^{x}	0.95	2.53	3.223(3)	130
2.22•CH_2Cl_2	O4-H4A···O7^{iv}	0.79(3)	2.01(3)	2.793(2)	169(3)
	C5-H5···O4^{iv}	1.00	2.49	3.196(2)	128
	C11-H11···O1^{ii}	0.95	2.54	3.367(2)	145
2.22•CH_3NO_2	O4-H4A···O7^{xi}	0.86(4)	1.95(4)	2.803(3)	171(4)
	C5-H5···O4^{xi}	1.00	2.62	3.289(3)	125
	C11-H11···O1^{ii}	0.95	2.60	3.305(3)	131
2.22•C_4H_8O	O4-H4A···O7^{iii}	0.90(3)	1.89(3)	2.789(2)	172(3)
	C5-H5···O4^{iii}	1.00	2.62	3.355(3)	131
	C11-H11···O1^{ii}	0.95	2.56	3.414(3)	149
2.22•CH_3SOCH_3	O4-H4A···O7^{xii}	0.84(4)	1.95(4)	2.793(3)	175(4)
	C5-H5···O4^{xii}	1.00	2.62	3.250(3)	121
	C11-H11···O1^{x}	0.95	2.55	3.246(4)	130
2.22•$ClCH_2CH_2Cl$	O4-H4A···O7^{v}	0.72(3)	2.11(3)	2.816(3)	170(3)
	C5-H5···O4^{v}	1.00	2.52	3.231(3)	128
	C11-H11···O1^{ii}	0.95	2.51	3.331(3)	145

Table 4A.4.1 Contd...

2.22•CH_3CN	O4-H4A···O7^{xi}	0.81(2)	2.03(3)	2.839(2)	175(2)
	C5-H5···O4^{xi}	1.00	2.62	3.270(2)	123
	C11-H11···O1^{ii}	0.95	2.65	3.315(2)	128
2.22•	O4-H4A···O7^{xiii}	0.85(2)	1.98(2)	2.819(2)	170(2)
***p*-$C_6H_4(CH_3)_2$**	C5-H5···O4^{xiii}	1.00	2.72	3.356(2)	122
	C11-H11···O1^{x}	0.95	2.56	3.223(2)	127
Group V					
2.22•F1	O4-H4A···O1^{ii}	0.87(3)	1.98(3)	2.836(2)	167(2)
	C1-H1···π^{x}		2.61	3.549(2)	161
	C5-H5···O8^{xiv}	0.98	2.52	3.380(3)	146
	C6-H6···O5^{xv}	0.98	2.43	3.400(2)	173
	C7-H7···O8^{xv}	0.98	2.45	3.191(3)	132
	C14-H14···O4^{x}	0.93	2.44	3.333(3)	162
2.22•C_6H_6	O4-H4A···O7^{xvi}	0.88(2)	1.92(2)	2.788(2)	170.1(18)
	C1-H1···π^{xvii}		2.539(15)	3.442(2)	161.6(12)
	C5-H5···O8^{xviii}	0.979(14)	2.450(14)	3.293(2)	144.2(11)
	C6-H6···O5^{xiv}	0.975(15)	2.433(15)	3.399(2)	170.3(11)
	C7-H7···O8^{xiv}	0.959(13)	2.497(13)	3.249(2)	135.2(10)
	C14-H14···O4^{xvii}	0.952(16)	2.354(16)	3.287(2)	166.2(12)
2.22•$C_6H_5CH_3$	O4-H4A···O7^{xvii}	0.84(3)	2.00(3)	2.830(3)	167(3)
	C1-H1···π^{xvi}		2.52	3.474(3)	160
	C5-H5···O8^{xix}	1.00	2.47	3.314(3)	142
	C6-H6···O5^{xx}	1.00	2.43	3.424(3)	173
	C7-H7···O8^{xx}	1.00	2.54	3.264(3)	129
	C14-H14···O4^{xvi}	0.95	2.45	3.376(4)	165
2.22•	O4-H4A···O7^{xvii}	0.79(4)	2.05(4)	2.818(2)	165(4)
***o*-$C_6H_4(CH_3)_2$**	C1-H1···π^{xvi}		2.56	3.525(3)	162
	C5-H5···O8^{xxi}	1.00	2.45	3.301(3)	143
	C6-H6···O5^{xiv}	1.00	2.37	3.365(3)	171
	C7-H7···O8^{xiv}	1.00	2.50	3.248(3)	132
	C14-H14···O4^{xvi}	0.95	2.38	3.295(3)	162

Symmetry codes: (i) $-x + 3/2, y - 1/2, -z + 3/2$; (ii) $x, y + 1, z$; (iii) $-x + 1/2, y - 1/2, -z + ½$; (iv) $-x + 3/2, y - 1/2, -z + ½$; (v) $-x + 1/2, y - 1/2, -z + 3/2$; (vi) $-x + 1, y - 1/2, -z + 3/2$; (vii) $-x + 2, y - 1/2, -z + ½$; (viii) $-x + 1, y + 1/2, -z + 3/2$; (ix) $-x + 2, y + 1/2, -z + 3/2$; (x) $x, y - 1, z$; (xi) $-x + 1, y - 1/2, -z + 1/2$; (xii) $-x + 1, y + 1/2, -z + 1/2$; (xiii) $-x, y + 1/2, -z + ½$; (xiv) $-x + 1, -y + 2, -z$; (xv) $-x + 1, -y + 1, -z$; (xvi) $x - 1, y, z$; (xvii) $x + 1, y, z$; (xviii) $-x, -y + 2, -z$; (xix) $-x + 1, -y, -z$; (xx) $-x, -y, -z$; (xxi) $-x + 2, -y + 2, -z$.

Interlinking of the helices and bilayers

The helices in all the solvates of **rac-2.5** and **rac-2.7** are packed compactly diagonal to the *ac*-plane in group I and group III and along *c*-axis in group II, leaving no accessible space for solvent inclusion along these directions. A view of O-H···O linked helices in other directions revealed that they are packed discretely providing a well-guided tunnel throughout the crystal lattice as observed in crystals of **rac-1.177**.[28b] Helices in group I solvates are linked *via* halogen bonding[38] contacts (C19-Br2···O3 and C19-Cl2···O3 contacts in inclusion crystals of **2.5** and **2.7** respectively) diagonal to the *ac*-plane creating a cavity of size ~ 6 × 6 Å to accommodate the guest molecules in between the two orthoformate bridgeheads (Fig. 4A.4.5a). In group II solvates, the separation between the adjacent helices increased by ~2.5 Å with the orthoformate groups moving away from each other resulting into the overall increase of cavity size to 8 × 10 Å. This change leads to the breaking of halogen bonding contacts between the neighbouring helices with the generation of new links between C13-H13 of the equatorial benzoyl group and halogen atom (Br2/Cl2) of the axial benzoyl group *via* C13-H13···Br2 (Cl2) interactions (Fig. 4A.4.5b). In group III benzene solvate (Fig. 4A.4.5c), the slight change in the orientation of both the benzoyl groups of the host molecule as compared to the group II solvates, brings the halogens of the axial and equatorial benzoyl groups of neighbouring helices closer to form short halogen···halogen (Cl2···Cl1) contacts thus bridging the adjacent helical assemblies without changing the cavity size much. In group I inclusion crystals of **2.5** and **2.7**, the halogen atom (Cl2 or Br2) of the axial C6-*O*-(*p*-halobenzoyl) group approaches the orthoformate bridge ether oxygen O3 almost linearly to form C19-Br2(Cl2)···O3 halogen bond (Table 4A.4.2).In all the inclusion crystals of **2.5** the Br2···O3 contact is much less than sum of van der Waals radii (3.37 Å) except in the dioxane solvate where Br2···O3 contact is somewhat longer (3.44 Å), however the angle of approach is better in the latter than in the former. In solvates of **2.7**, the halogen bonding interaction is somewhat weaker as compared to that in **2.5**. In acetone, dichloromethane and DMSO solvates of **2.7** the halogen bonding interaction is shorter than the sum of van der Waals radii of Cl and O atoms (3.27 Å) whereas in the other solvates of **2.7** the contacts are longer and the angle of approach varies from 140-157°.

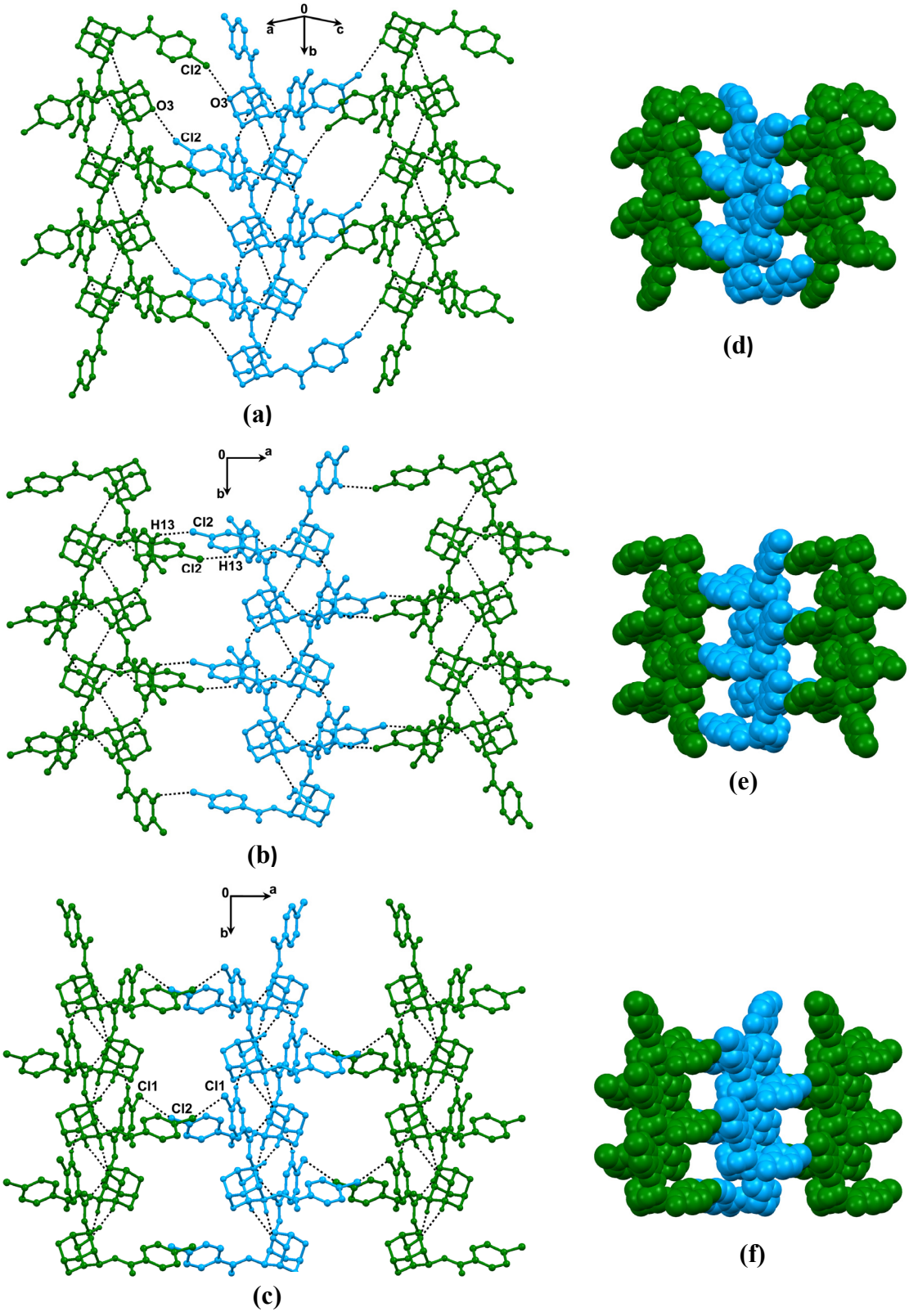

Figure 4A.4.5. Association of the helices in (a) **2.7•CH_2Cl_2**, (b) **2.7•CH_3CN** and (c) **2.7•C_6H_6** and CPK view (d), (e), (f) in respective modifications. Guest solvents are omitted for the sake of clarity.

In group II solvates of **2.5** and **2.7** (**2.5•$ClCH_2CH_2Cl$**, **2.7•CH_3CN**, **2.7•$ClCH_2CH_2Cl$** and **2.7•*p*-$C_6H_4(CH_3)_2$**), the C-H···Br(Cl) contacts which link the neighboring helices are long and deviate from linearity. In **2.7•C_6H_6** (group III), the Cl···Cl contacts that link the neighboring helices are of type II[39] (∠Cl2 = 170° and ∠Cl1 = 104°) and the Cl2···Cl1 distance (3.378 Å) is much less than the sum of van der Waals radii (3.50 Å, Table 4A.4.2).

A view of the molecular organization down the helical axis (*b*-axis) reveals a pairwise association of molecules (red or blue), akin to dancing pairs (Fig. 4A.4.4b). The packing of these dancing pairs viewed down the *b*-axis reveals linking of adjacent helices (Fig. 4A.4.6). In groups I (except 2.5•$C_4H_8O_2$ and 2.7•$C_4H_8O_2$) and II the dancing pairs are weakly associated *via* centrosymmetric off-centered π···π contact between the phenyl rings of the C2-*O*-*p*-halobenzoyl group along the *c*-axis forming identical dimers (blue–red, Fig. 4A.4.6a and b) but with slight change in orientation. In turn, these dimeric units (blue–red) are weakly associated with adjacent dimeric units (blue–red) in the same direction *via* centrosymmetric C13-H13···O8 contacts in group I and C14-H14···O8 contacts in group II inclusion complexes.

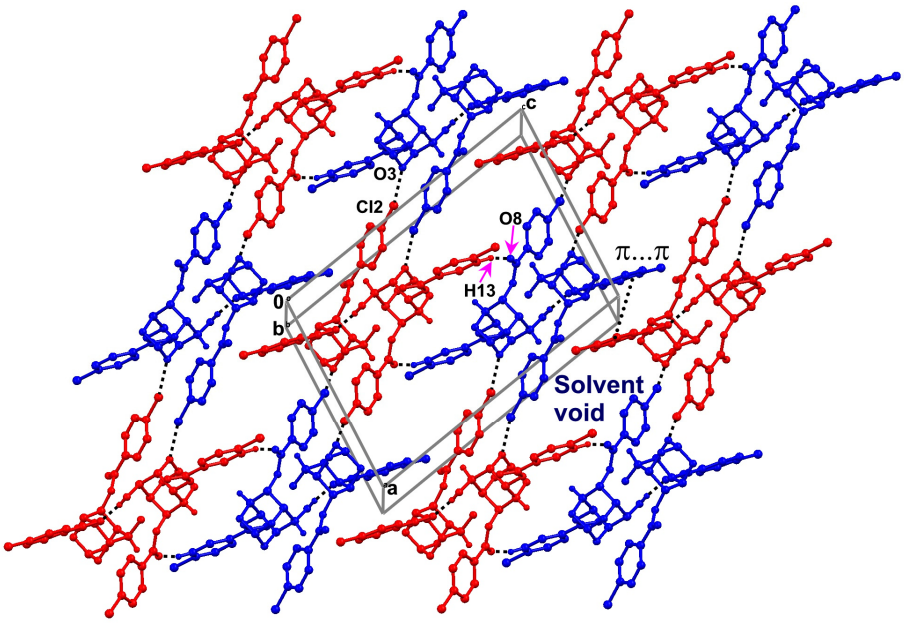

(a)

Figure 4A.4.6. Association of dancing pairs: (a) group I, (b) group II and (c) group III solvates.

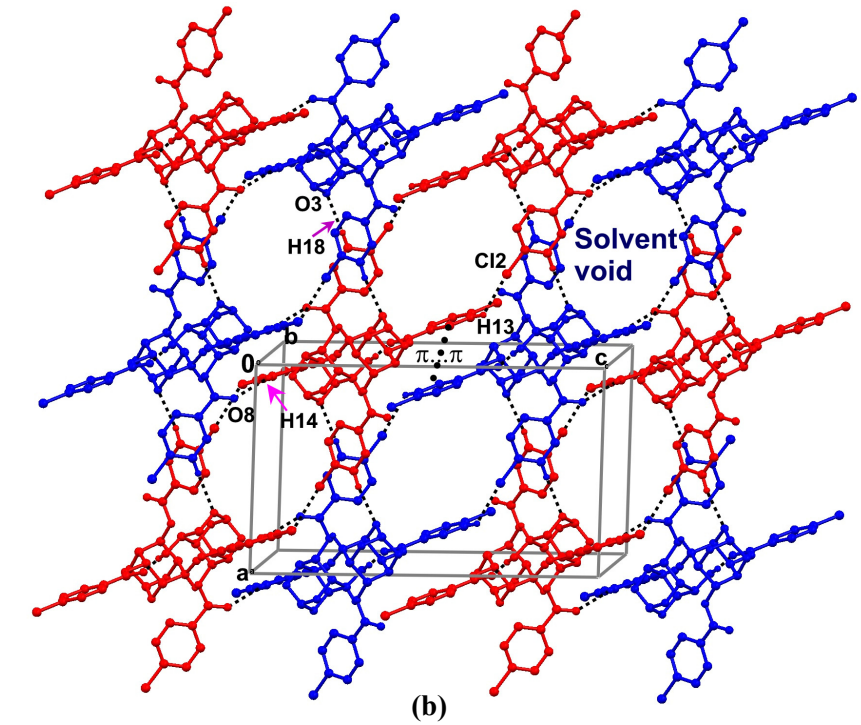

(b)

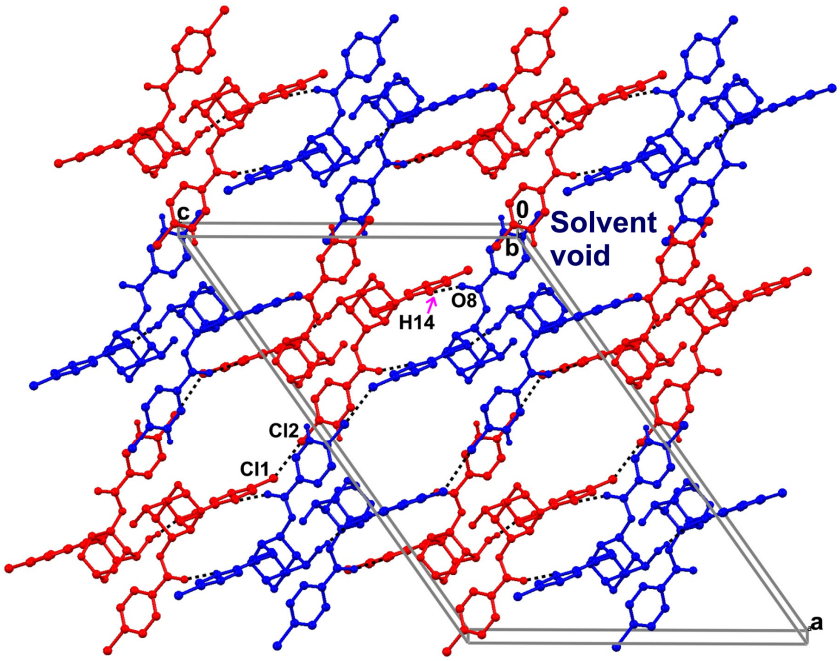

(c)

Figure 4A.4.6 Contd...

In dioxane solvates of group I crystals (**2.5•$C_4H_8O_2$** and **2.7•$C_4H_8O_2$**) due to significant difference (~25°) in the orientation of the axial C6-*O*-*p*-halobenzoyl group, the carbonyl oxygen O8 moved away resulting in breaking of C13-H13···O8 contact whereas centrosymmetric π···π interaction remained intact. Furthermore as discussed earlier, the conformation of the C6-*O*-*p*-halobenzoyl group in **2.7•CH_3NO_2** is

different from that of **2.5•CH_3NO_2** but similar to **2.7•$C_4H_8O_2$**, thus C13-H13···O8 contact in **2.5•CH_3NO_2** is replaced by C14-H14···O8 in **2.7•CH_3NO_2**. The crossover from C13-H13···O8 in group I to C14–H14···O8 in group II inclusion crystals is due to the same conformational change as well as due to the orientation of the C2-*O*-*p*-halobenzoyl group. The bridging of these dancing pairs along the direction of *a*-axis is also similar in group I and group II but they are associated *via* different types of interactions. In group I solvates, the dancing pairs are linked *via* C19-Br2(Cl2)···O3 contact (halogen bond) whereas in group II solvates the major change in the conformation of the C6-*O*-*p*-halobenzoyl group compared to group I solvates results in the breaking of halogen bond with the formation of new weak centrosymmetric C18-H18···O3 contacts between the dancing pairs (Fig. 4A.4.6b). The diagonally related dancing pairs (blue–blue or red–red) in group I solvates are ~6 Å apart and there are no contacts between them but in group II inclusion crystals, they draw closer by 1.5 Å to make C13-H13···Cl2 interactions. In group III inclusion crystals, the dancing pairs are linked *via* C14–H14···O8 contacts along *c*-axis and the relative movements of the dancing pairs diagonal to the *ac*-plane bring the obliquely related dancing pairs close to each other (blue-blue or red-red) *via* Cl1···Cl2 contact (Fig. 4A.4.6c). The expansion of the *c*-axis in both group I and group III inclusion crystals could be due to these relative movements of the dancing pairs.

Helices in the $P2_1/n$ and $P2_1/c$ group IV solvates are linked differently along the *c*-axis and the diagonal to *ac*-plane. The linkage of helices in group IV $P2_1/c$ solvates is similar to that observed in the group II solvates (Figure 4A.4.5b). In the case of the $P2_1/c$ solvates the helices diagonal to the *ac* plane are linked by weak C13-H13···F2 interactions (Fig. 4A.4.7a, analogous to the C-H···Br/Cl interactions in group II solvates), creating a 6 × 6 Å cavity occupied by the guest. In the case of the dichloroethane solvate **2.22•$ClCH_2CH_2Cl$** ($P2_1/n$) due to a slight change in the conformation of the C6-O-*p*-fluorobenzoyl group, the helix linkage along the *ac* diagonal is achieved by weak C3-H3···F2 and π···π interactions (Fig. 4A.4.7b). In case of the other $P2_1/n$ solvates (**2.22•CH_2Cl_2**, **2.22•$CHCl_3$** and **2.22•CCl_4** and **2.22•C_4H_8O**) helices along the *ac*-diagonal are linked by weak C18-H18···π and π···π interactions (Fig. 4A.4.7c, Table 4A.4.2).

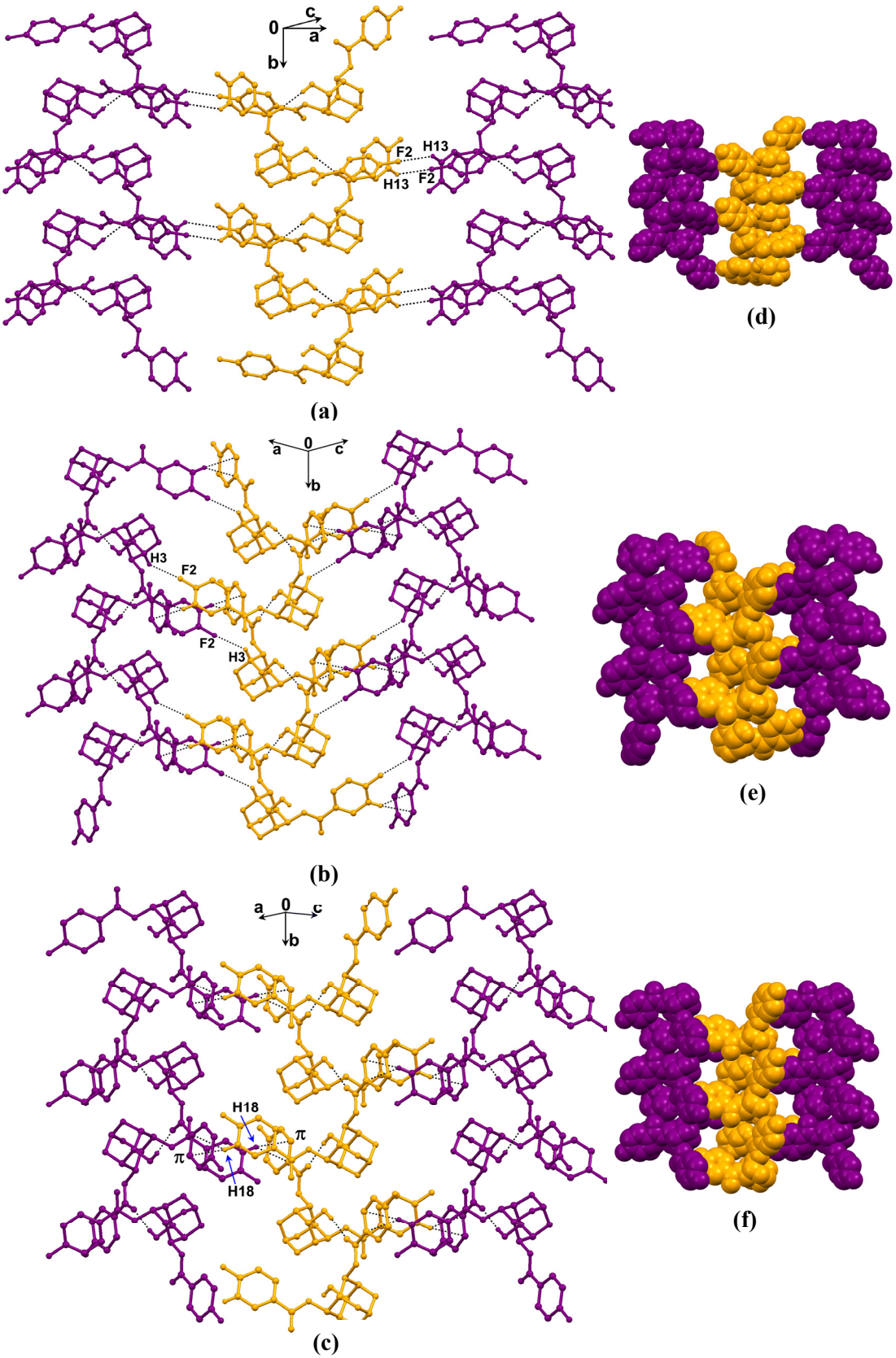

Figure 4A.4.7 Association of helices along *ac*-diagonal in: (a) **2.22•CH_3COCH_3** ($P2_1/c$), (b) **2.22•$ClCH_2CH_2Cl$** ($P2_1/n$) and (c) **2.22•CH_2Cl_2** ($P2_1/n$) solvates; (d)-(f) show CPK view. Guest is omitted for the sake of clarity.

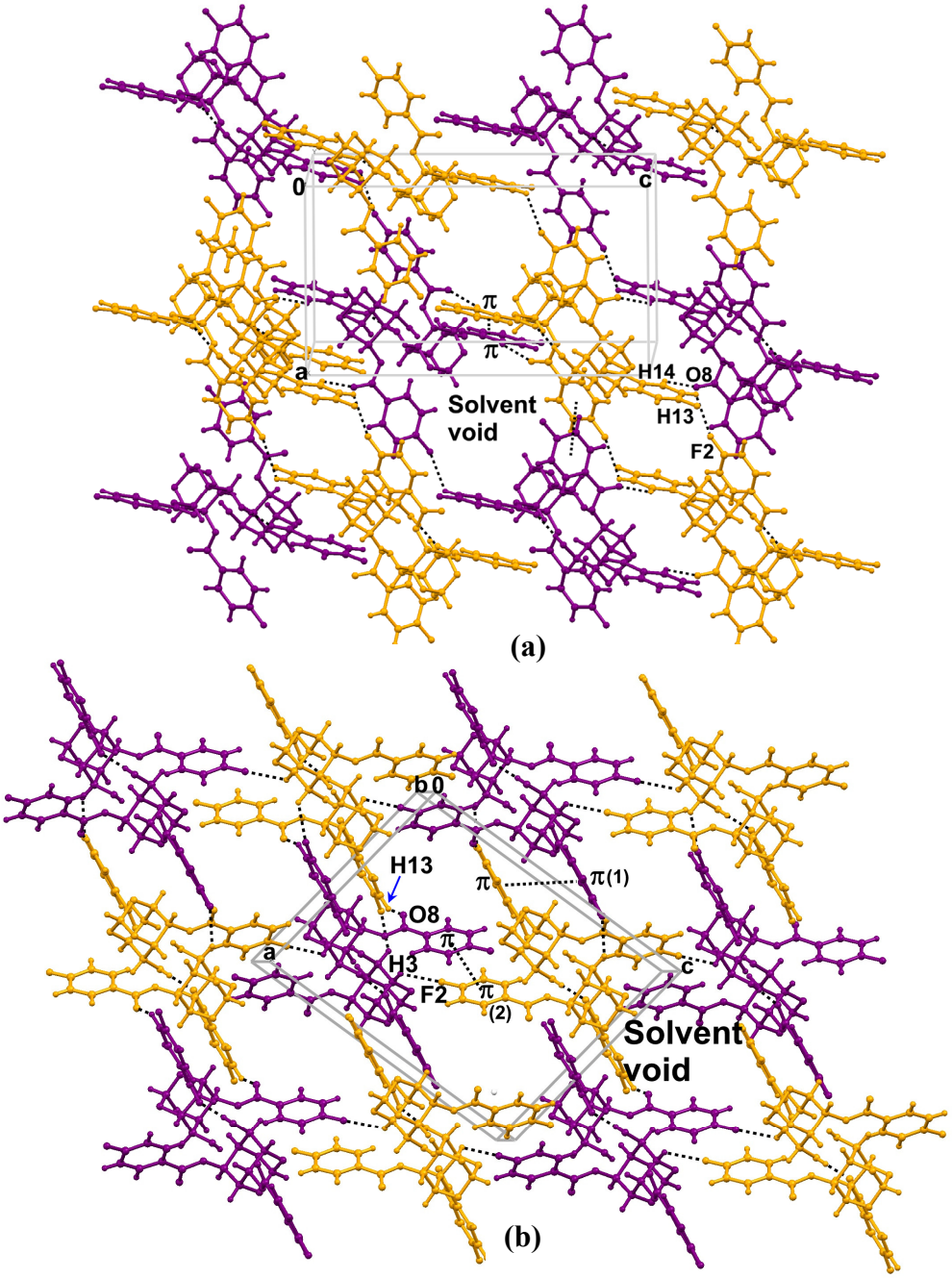

Figure 4A.4.8 Association of dancing pairs in: (a) **2.22•CH_3COCH_3** ($P2_1/c$) and (b) **2.22•$ClCH_2CH_2Cl$** ($P2_1/n$) solvates. Guest is omitted for the sake of clarity.

A view of the molecular organization down the helical axis (*b*-axis) reveals the packing of the helices in the form of molecular 'dancing pairs' (purple/orange, Fig. 4A.4.8). In the $P2_1/c$ solvates of group V, centrosymmetric C14-H14···O8 contacts and π···π interactions connect the neighboring helices (Fig. 4A.4.8a). Weak C13-

H13···O8 and π···π interactions connect helices along the *c*-axis in the $P2_1/n$ solvates, presumably due to the change in orientation of the C6-*O*-*p*-fluorobenzoyl group (Fig. 4A.4.8b). This assembly of helices creates cavities which are occupied by the guest. It is interesting to note that the helical assemblies in the halogenated solvates are held together by mostly weak interactions, as compared to those in the reactive diesters **rac-1.177** and **rac-1.179** which also reveal a much closer packing of helices in their crystals as compared to these solvatomorphs.

The assembly of the host molecules in the triclinic solvates (group V) involves association through hydrogen bonding interactions, forming bilayers and closely mirrors that observed in the solvent less crystals of **2.22** (**2.22FI,** Fig. 4A.4.4c, d, Table 4A.4.1). The bilayers are formed by linkage of O-H···O bonded molecular strings *via* centrosymmetric C-H···O interactions. While bilayers along the *b*-axis (blue-pink) are linked by moderately strong C13-H13···O3 contacts (Fig. 4A.4.9), and C4-H4···π contacts, adjacent bilayers (pink-blue) along the *c*-axis are separated by channels occupied by the guest solvent (toluene/*o*-xylene/benzene).

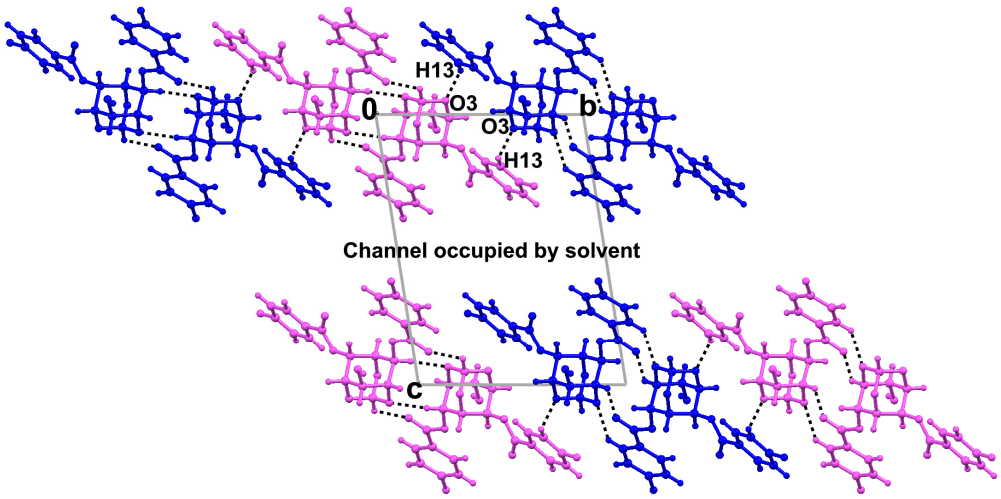

Figure 4A.4.9 Linkage of bilayers in **2.22L** (**2.22•$C_6H_5CH_3$**), belonging to group V (triclinic) solvates.

Table 4A.4.2 Interactions linking molecular helices and bilayers in groups I-V.

Solvates	D-H/X···A (X = Cl, Br)	D-H/X (Å)	H/X···A (Å)	D···A (Å)	D-H/X···A /α (°)
Group I (P2$_1$/n)					
2.5•$CHCl_3$	C19-Br2···O3^{i}	1.901(3)	3.146(2)	5.005(3)	165
	C13-H13···O8^{ii}	0.95	2.53	3.378(4)	149
	π···π^{xix}			3.856(2)	0.00
2.5•CH_3COCH_3	C19-Br2···O3^{iii}	1.900(3)	3.187(2)	5.036(4)	163
	C13-H13···O8^{iv}	0.95	2.54	3.369(4)	146
	π···π^{xx}			3.917(2)	0.02
2.5•CH_2Cl_2	C19-Br2···O3^{iii}	1.886(6)	3.293(3)	4.963(3)	145
	C13-H13···O8^{v}	0.95	2.53	3.195(4)	128
	π···π^{xxi}			3.951(2)	0.02
2.5•CH_3NO_2	C19-Br2···O3^{vi}	1.904(3)	3.105(2)	4.995(3)	171
	C13-H13···O8^{vii}	0.95	2.70	3.593(3)	158
	π···π^{ii}			3.893(2)	0.03
2.5•C_4H_8O	C19-Br2···O3^{iii}	1.965	3.134(4)	5.071(6)	168
	C13-H13···O8^{iv}	0.95	2.45	3.177(6)	134
	π···π^{xx}			3.866(3)	0.03
2.5•$C_4H_8O_2$	C19-Br2···O3^{vi}	1.898(4)	3.440(2)	5.154(5)	148
	π···π^{ii}			3.893(2)	0.03
2.5•CH_3SOCH_3	C19-Br2···O3^{viii}	1.897(4)	3.242(3)	5.029(5)	155
	C13-H13···O8^{ix}	0.95	2.49	3.271(5)	140
	π···π^{xxii}			3.955(2)	0.00
2.7•$CHCl_3$	C19-Cl2···O3^{vi}	1.742(2)	3.290(2)	4.880(3)	150
	C13-H13···O8^{x}	0.95	2.46	3.244(3)	140
	π···π^{ii}			3.828(2)	0.02
2.7•CH_3COCH_3	C19-Cl2···O3^{iii}	1.745(2)	3.257(2)	4.914(3)	157
	C13-H13···O8^{iv}	0.95	2.56	3.373(3)	144
	π···π^{xx}			3.902(2)	0.00
2.7•CH_2Cl_2	C19-Cl2···O3^{vi}	1.737(2)	3.244(2)	4.762(3)	144
	C13-H13···O8^{vii}	0.95	2.49	3.133(3)	125
	π···π^{ii}			3.965(2)	0.04
2.7•CH_3NO_2	C19-Cl2···O3^{vi}	1.742(2)	3.299(2)	4.776(3)	141
	C14-H14···O8^{xi}	0.95	2.60	3.328(3)	134
	π···π^{xiii}			4.032(9)	0.00
2.7•C_4H_8O	C19-Cl2···O3^{iii}	1.734(4)	3.347(3)	4.837(4)	142
	C13-H13···O8^{iv}	0.95	2.51	3.185(4)	128
	π···π^{xx}			3.881(2)	0.00

Table 4A.4.2 Contd…

2.7•$C_4H_8O_2$	C19-Cl2···O3^{iii}	1.736(4)	3.396(2)	4.884(4)	142
	$\pi\cdots\pi^{xx}$			3.889(2)	0.00
2.7•CH_3SOCH_3	C19-Cl2···O3^{iii}	1.743(3)	3.203(2)	4.825(3)	153
	C13-H13···O8^{iv}	0.89(3)	2.56(3)	3.291(3)	141(3)
	$\pi\cdots\pi^{xx}$			3.965(2)	0.03
Group II ($P2_1/c$)					
2.5•$ClCH_2CH_2Cl$	C13-H13···Br2^{xii}	0.95	2.97	3.702(4)	135
	C14-H14···O8^{xiii}	0.95	2.62	3.330(5)	132
	C18-H18···O3^{xxvi}	0.95	2.49	3.422(4)	167
	$\pi\cdots\pi^{xxiii}$			3.835(2)	0.03
2.7•$ClCH_2CH_2Cl$	C13-H13···Cl2^{xiv}	0.95	2.92	3.660(4)	136
	C14-H14···O8^{xv}	0.95	2.59	3.311(5)	133
	C18-H18···O3^{xxvii}	0.95	2.45	3.370(6)	162
	$\pi\cdots\pi^{xxiv}$			3.904(2)	0.00
2.7•CH_3CN	C13-H13···Cl2^{xiv}	0.96(2)	2.82(3)	3.489(9)	128(2)
	C14-H14···O8^{xv}	0.95(3)	2.57(2)	3.281(3)	132(2)
	$\pi\cdots\pi^{xxiv}$			4.152(4)	0.02
2.7•*p*-$C_6H_4(CH_3)_2$	C13-H13···Cl2^{xvi}	0.95	2.86	3.172(2)	101
	C14-H14···O8^{xiii}	0.95	2.63	3.294(2)	127
	$\pi\cdots\pi^{xi}$			3.866(2)	0.02
Group III (C2/c)					
2.7•C_6H_6	C19-Cl2···Cl1^{xvii}	1.730(9)	3.378(5)	5.092(10)	170
	C14-H14···O8^{xviii}	0.93	2.61	3.238(9)	126
	$\pi\cdots\pi^{xxv}$			3.844(7)	0.03
Group IV ($P2_1/c$)					
2.22•CH_3CN	C13-H13···F2^{xiv}	0.95	2.52	3.257(3)	134
	C14-H14···O8^{xiii}	0.95	2.47	3.207(2)	134
	$\pi\cdots\pi^{xxi}$			4.691(2)	0.00
2.22•CH_3COCH_3	C13-H13···F2^{xxix}	0.95	2.64	3.128(3)	112
	C14-H14···O8^{xix}	0.95	2.49	3.190(3)	130
	$\pi\cdots\pi^{ii}$			4.007(2)	0.00
2.22•CH_3NO_2	C13-H13···F2^{xxxvii}	0.95	2.49	3.222(3)	134
	C14-H14···O8^{v}	0.95	2.42	3.133(4)	132
	$\pi\cdots\pi^{v}$			4.466(2)	0.00
2.22•CH_3SOCH_3	C13-H13···F2^{xxx}	0.95	2.68	3.161(4)	112
	C14-H14···O8^{xxi}	0.95	2.58	3.424(4)	127
	$\pi\cdots\pi^{v}$			3.943(2)	0.00

Table 4A.4.2 Contd…

2.22•*p*-$C_6H_4(CH_3)_2$	C13-H13···F2^{xxxii}	0.95	2.56	2.969(2)	106
	C14-H14···O8^{iv}	0.95	2.59	3.269(2)	128
	π···π^{xxxi}			4.058(2)	0.00
Group IV($P2_1/n$)					
2.22•$CHCl_3$	C13-H13···O8^{v}	0.95	2.49	3.286(4)	141
	C18-H18···π^{iii}	0.95	2.96	3.680(3)	134
	π···π(1)^{xxi}			3.836(2)	0
	π···π(2)^{xxxiii}			3.882(2)	0
2.22•CH_2Cl_2	C13-H13···O8^{xxxv}	0.95	2.42	3.162(3)	135
	C18-H18···π^{viii}	0.95	2.85	3.538(2)	130
	π···π(1)^{v}			4.142(2)	0
	π···π(2)^{xxxiv}			3.913(2)	0
2.22•C_4H_8O	C13-H13···O8^{iv}	0.95	2.53	3.208(3)	128
	C18-H18···π^{iii}	0.95	2.64	3.502(3)	150
	π···π(1)^{xx}			3.897(2)	0
	π···π(2)^{xxii}			4.277(2)	0
2.22•$ClCH_2CH_2Cl$	C3-H3···F2^{iii}	1.00	2.53	3.223(3)	126
	C13-H13···O8^{xiii}	0.95	2.48	3.143(4)	127
	C19-F2···π^{xxxiii}	1.356(4)	3.666(2)	3.502(3)	72(2)
	π···π(1)^{xxiii}			3.741(2)	0
	π···π(2)^{xxxiii}			3.846(2)	0
Group V (P-1)					
2.22•C_6H_6	C13-H13···O3^{xv}	0.952(14)	2.495(15)	3.356(2)	150.3(13)
	C4-H4···π^{v}	0.981(15)	2.929(15)	3.895(2)	168.6(12)
2.22•$C_6H_5CH_3$	C13-H13···O3^{xxxvi}	0.95	2.53	3.373(4)	147
	C4-H4···π^{iv}	1.00	2.85	3.827(3)	165
2.22•*o*-$C_6H_4(CH_3)_2$	C13-H13···O3	0.95	2.50	3.358(3)	151
	C4-H4···π	1.00	2.80	3.762(3)	162

α: Dihedral angle between the phenyl rings

Symmetry codes: (i) *x* + 1/2, -*y* + 3/2, *z* – 1/2; (ii) –*x* + 2, -*y* + 1, -*z* + 2; (iii) *x* – 1/2, -*y* + 3/2, *z* + 1/2; (iv) –*x*, -*y* + 1, -*z*; (v) –*x* + 1, -*y* + 1, -*z*; (vi) *x* + 1/2, -*y* + 1/2, *z* – 1/2; (vii) –*x* + 2, -*y*, -*z* + 2; (viii) *x* – 1/2, -*y* + 1/2, *z* + 1/2; (ix) –*x*, -*y*, -*z* + 1; (x) –*x* + 2, -*y*, -*z* + 2; (xi) –*x* + 1, -*y*, -*z* +2; (xii) *x* – 1, -*y* + 3/2, *z* + 1/2; (xiii) –*x* + 1, -*y* + 1, -*z* + 2; (xiv) *x* + 1, -*y* + 3/2, *z* – 1/2; (xv) –*x* + 2, -*y* + 1, -*z*; (xvi) *x* + 1, -*y* + 1/2, *z* + 1/2; (xvii) *x* + 1/2, *y* – 1/2, *z*; (xviii) –*x* + 1/2, -*y* + 1/2, -*z* + 1 ; (xix) –*x* + 2, -*y* + 2, -*z* + 2 ; (xx) –*x*, -*y* + 2, -*z* ; (xxi) –*x* + 1, -*y* + 2, -*z* ; (xxii) –*x*, -*y* + 1, -*z* + 1 ; (xxiii) –*x* + 1, -*y* + 2, -*z* + 2 ; (xxiv) –*x* + 2, -*y* + 2, -*z* ; (xxv) –*x* + 1/2, -*y* + 3/2, -*z* + 1 ; (xxvi) *x* + 1, *y*, *z* ;

(xxvii) $x - 1, y, z$; (xxviii) $-x + 1/2, -y + 1/2, -z + 1$; (xxix) $x + 1, -y + 3/2, z + 1/2$; (xxx) $x - 1, -y + 3/2, z - 1/2$; (xxxi) $-x, -y, -z$; (xxxii) $x - 1, -y + 1/2, z - 1/2$; (xxxiii) $-x + 1, -y + 1, -z + 1$; (xxxiv) $-x + 1, -y, -z + 1$; (xxxv) $-x + 1, -y, -z$; (xxxvi) $-x - 1, -y + 1, -z$; (xxxvii) $x + 1, -y + 1/2, z - 1/2$.

Host-guest interactions in the solvates

The guest molecules interact with the host molecules mainly *via* C-H···O, C-H···X (X = Cl, Br, F) and Cl···Cl interactions. The orthoformate H-atom of the host molecule is involved in C-H···O and C-H···N interactions with the oxygen (acetone, THF, dioxane, nitromethane and DMSO) and nitrogen (CH_3CN) atoms of solvent molecules. Significant interactions made by each guest molecule with the host are discussed below.

Host Guest Interactions in 2.5•$CHCl_3$ (2.5A), 2.7•$CHCl_3$ (2.7A) and 2.22•$CHCl_3$ (2.22A).

The orientation of the guest chloroform molecules in **2.5A** is different from that in **2.7A** and **2.22A**; therefore they associate with the host molecules through different weak interactions. The $CHCl_3$ molecule in **2.5A** (Fig. 4A.4.10a) interacts with the host only *via* a short Cl3···Br2 contact (of type II[39]) whereas in **2.7A**, the included $CHCl_3$ molecule engages in Cl···Cl (Cl4···Cl1, of type II) and long but linear C-Cl···O halogen bonding interaction (C22-Cl5···O3) with the host. The H-atom (H22) of the chloroform molecule in **2.7A** (Fig. 4A.4.10b) and **2.22A** is engaged with the orthoformate bridge oxygen O3 to form a short C22-H22···O3 contact (Table 4A.4.3).

Host-Guest Interactions in 2.5•CH_3COCH_3 (2.5B), 2.7•CH_3COCH_3 (2.7B) and 2.22•CH_3COCH_3 (2.22B)

In **2.5B, 2.7B** and **2.22B** the orientation of the acetone molecules is nearly the same. The carbonyl oxygen O9 of acetone is involved in short and nearly linear C-H···O interactions (C7-H7···O9 contacts) with the orthoformate bridge proton of the host molecules (Fig. 4A.4.10c, d). One of the methyl groups of acetone (C22) in **2.5B** is also involved in weak C-H···Br interactions with the halogen atom of the axial *p*-halobenzoyl group (Table 4A.4.3).

Host-Guest Interactions in 2.5•CH_2Cl_2 (2.5C), 2.7•CH_2Cl_2 (2.7C) and 2.22•CH_2Cl_2 (2.22C).

The included CH_2Cl_2 molecule is disordered over three positions (with occupancy 0.4, 0.4 and 0.2) in **2.5C** and over two positions (0.75 and 0.25 occupancy) in **2.7C**. The major component of CH_2Cl_2 in **2.5C** (two positions) and **2.7C** is involved in halogen···halogen (Cl2···Br1 in **2.5C**; Cl1···Cl3 in **2.7C**) and halogen bonding (C22-Cl1···O3, C23-Cl3···O8 and C23-Cl4···O8 in **2.5C**; C22-Cl4···O3 in **2.7C**, Fig. 4A.4.10e) interactions with the host. In both the solvates the geometries of C-Cl···O contacts are excellent and short halogen···halogen contacts (of type II) are observed between the guest and the host molecules. The methylene proton H22A (of CH_2Cl_2) in **2.5C** is also involved in weak C-H···Br interactions with the host (Table 4A.4.3). On the other hand the DCM molecule in **2.22C** does not form any halogen bonding contacts with the host; instead interacts with the orthoester oxygen atom through C22-H22A···O3 contacts (Fig. 4A.4.10f).

Host-Guest Interactions in 2.5•CH_3NO_2 (2.5D), 2.7•CH_3NO_2 (2.7D) and 2.22•CH_3NO_2 (2.22D).

The included CH_3NO_2 molecule in **2.5D** and **2.7D** showed rotational disorder over two positions with occupancy 0.75 and 0.25 in **2.7D** while in **2.5D**, the occupancies are distributed in major (0.8) and minor (0.2) sites. The CH_3NO_2 molecules in **2.5D** and **2.7D** adopt slightly different orientations and hence engage in different weak interactions with the host molecules. A common interaction however, is the short and almost linear C7-H7···O9 contact between oxygen atom O9 of major component of CH_3NO_2 in **2.5D** and **2.7D** and orthoformate proton H7 of the host molecules (Fig. 4A.4.10g, Table 4A.4.3).The position of the CH_3NO_2 molecule in **2.22D** is slightly altered resulting in C17-H17···O10 interactions with the axial ester of the host (Fig. 4A.4.10h).

Host-Guest Interactions in 2.5•C_4H_8O (2.5E), 2.7• C_4H_8O (2.7E) and 2.22• C_4H_8O (2.22E).

Interestingly, the orientation of the oxygen atom and the two carbon atoms bonded to it in the THF molecule in both the solvates is almost the same but the other two carbons show positional disorder over three positions (0.4, 0.4 and 0.2 occupancy) in **2.5E** and over two positions (0.8 and 0.2 occupancy) in **2.7E**. THF molecules in **2.5E** and **2.7E** inclusion crystals notably interact with the orthoformate group of the host

via short C7-H7···O9 contacts, the geometry being moderately linear (Fig. 4A.4.10i). Additionally in **2.5E**, the carbon atom C25 (not disordered) of the THF molecule engages in short but moderately linear C-H···Br interactions (C25-H25A···Br2, C25-H25···Br2') with the host, the analogous interactions in **2.7E** are longer (Table 4A.4.3). In **2.22E** the orientation of the guest (with one carbon disordered over two positions with equal occupancy) is similar to that in **2.7E**. It interacts with the host orthoformate proton through short C7-H7···O9 contacts and the axial ester *via* C17-H17···O9 interactions (Fig. 4A.4.10j).

Host-Guest Interactions in 2.5•$C_4H_8O_2$ (2.5F) and 2.7• $C_4H_8O_2$ (2.7F).

The included dioxane molecules in both **2.5F** and **2.7F** are disordered over two positions (0.7 and 0.3 in **2.5F** and equal occupancy in **2.7F**). In both solvates oxygen O10 of the major component of the disordered dioxane forms short and somewhat linear C-H···O interactions (C7-H7···O10 contacts) with the host (Fig. 4A.4.10k, l). Additionally in **2.5F**, hydrogen H23B engages in bifurcated hydrogen-bonding interactions (C23-H23B···O3 and C23-H23B···Br2) with oxygen (O3) and bromine (Br2) atoms of the host. In **2.7F**, the guest engages in moderately short C-H···O (C23'-H23D···O3 and C25'-H25C···O8) and C-H···Cl (C24-H24A···Cl2 and C23'-H23D···Cl2) interactions with the host (Table 4A.4.3). Thus, dioxane in **2.7F** makes a total of six interactions with the host (two strong C-H···O; two moderately short C-H···O and two C-H···Cl contacts), which could perhaps be the reason for the preference for dioxane inclusion observed in the mixed solvent crystallization experiments.

Host-Guest Interactions in 2.5•CH_3SOCH_3 (2.5G), 2.7•CH_3SOCH_3 (2.7G) and 2.22•CH_3SOCH_3 (2.22G).

DMSO molecule in **2.22G** is disordered (carbon and sulphur atoms only) over two positions with occupancies 0.4 and 0.6. The guest in all the solvates interacts with host molecules *via* C-H···O=(S) interactions of comparable geometries. The oxygen O9 of the DMSO molecule in **2.5G, 2.7G** and **2.22G** accepts H-atom from the orthoformate group (C7-H7) to form C7-H7···O9 contacts (Fig 4A.4.10m, n). In **2.7G**, O9 of DMSO also interacts with phenyl group (C17-H17) forming C17-H17···O9 hydrogen bonds. The former interaction is short and close to linearity in

both solvates whereas the latter contact in **2.7G** is moderately strong, deviating from linearity (Table 4A.4.3).

Host-Guest Interactions in 2.5•$ClCH_2CH_2Cl$ (2.5H), 2.7• $ClCH_2CH_2Cl$ (2.7H) and 2.22• $ClCH_2CH_2Cl$ (2.22H).

The included dichloroethane molecules in **2.5H**, **2.7H** and **2.22H** (with the exception of one of the Cl atoms) are disordered over two (0.75 and 0.25 occupancy), three (0.4, 0.4, 0.2 occupancy) and two positions (equal occupancy) respectively. The ordered chlorine atom Cl3 (Cl1 in **2.5H**) makes short and linear Cl···π contact[40] with the phenyl ring of the axial C6-*O*-*p*-halo-benzoyl group (Fig. 4A.4.10o, Table 4A.4.3). The disordered chlorine atoms (Cl2 in **2.5H** and Cl4A & Cl4B in **2.7H**) are involved in C-H···Cl interactions with the orthoformate H-atom. In **2.7H** and **2.22H** the methylene carbon (C22A-H23D and C22-H22B) of dichloroethane is engaged in a short and linear C-H···O interaction with the carbonyl oxygen O8 (Fig. 4A.4.10p, Table 4A.4.3), which is not seen in **2.5H**.

Host-Guest Interactions in 2.7•CH_3CN (2.7I) and 2.22•CH_3CN (2.22I)

Acetonitrile molecule in **2.7I** and **2.22I** interacts mainly *via* C-H···N contacts made by the orthoformate H-atom (C7-H7) of the host with N-atom of the acetonitrile having excellent geometry (Fig. 4A.4.10q, Table 4A.4.3).

Host-Guest Interactions in 2.7•p-$C_6H_4(CH_3)_2$ (2.7J) and 2.22•p-$C_6H_4(CH_3)_2$ (2.22J)

The *p*-xylene molecule in **2.7J** and **2.22J** occupies the channel formed by the adjacent helical assemblies along the *b*-axis. The included *p*-xylene molecule has center of symmetry that coincides with the crystallographic inversion center of the space group $P2_1/c$. Therefore only half of the molecule is present in the asymmetric unit and the other half is generated by inversion symmetry by growing the fragment. The *p*-xylene molecule is not involved in any significant interactions with the host molecule. It makes very marginal and long C-H···O interactions (Fig. 4A.4.10r) involving methyl group (C22-H22A) and the orthoester bridge ether oxygen O3.

Host-Guest and Guest-Guest Interactions in 2.7•C_6H_6 (2.7K)

The non-involvement of both the benzene molecules in any significant host-guest

interactions in **2.7K** could be the reason for the instability of the inclusion crystals. The orthoformate H-atom (H7) makes marginal C-H···π interactions with the edge of the disordered benzene molecule. The benzene molecules in **2.7K** interact with each other *via* weak C-H···π contacts forming T-shaped[41] extended polymeric chain in the channel created by the host molecules (Fig. 4A.4.10s).

Host-Guest Interactions in 2.22•C_6H_6 (2.22K), 2.22•$C_6H_5CH_3$ (2.22L) and 2.22•o-$C_6H_4(CH_3)_2$ (2.22M)

In the triclinic solvates **2.22K**, **2.22L** and **2.22M**, the guest occupies the channel between bilayers along the *b*-axis. Benzene, toluene and *o*-xylene molecules interact with the host through weak C-H···π interactions (Fig. 4A.4.10t). In the case of toluene and *o*-xylene, the guest also forms weak C-H···F interactions with the host (Fig. 4A.4.10u, v).

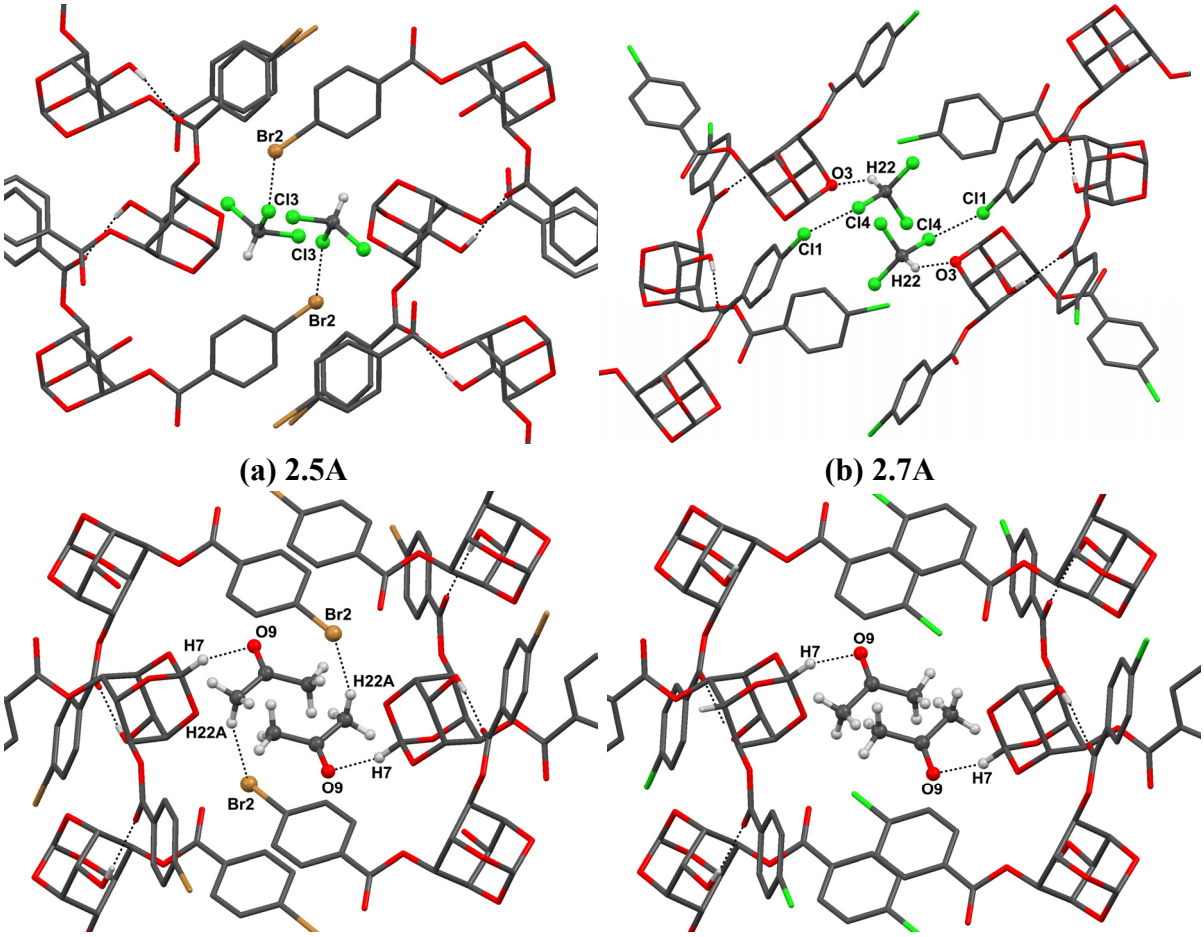

(a) 2.5A **(b) 2.7A**

(c) 2.5B **(d) 2.7B**

Figure 4A.4.10 Host-guest interactions in solvates. Some atoms are omitted for the sake of clarity.

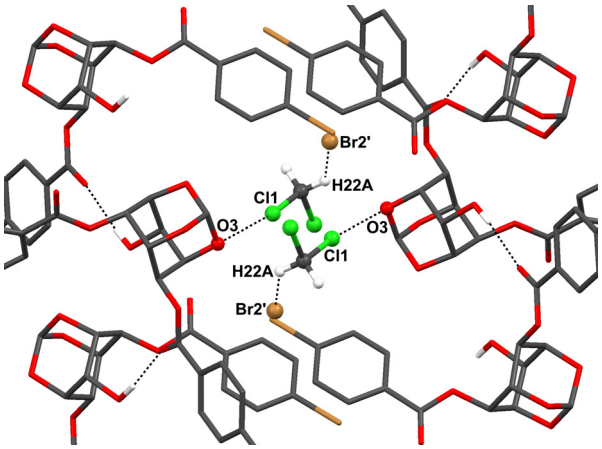

(e) 2.5C

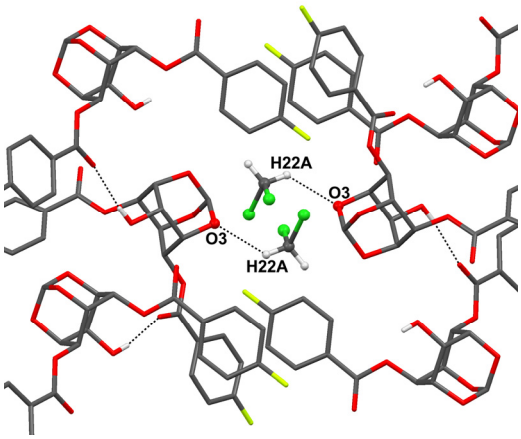

(f) 2.22C

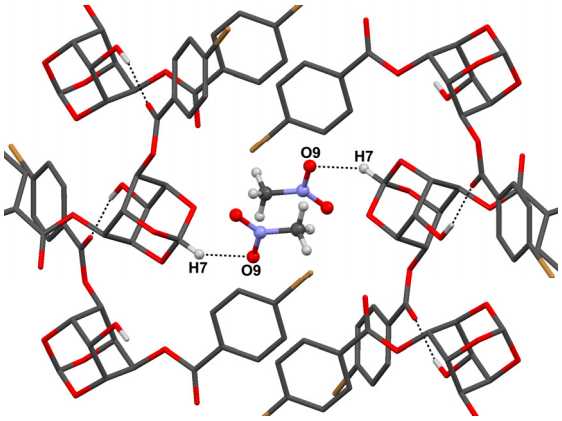

(g) 2.5D

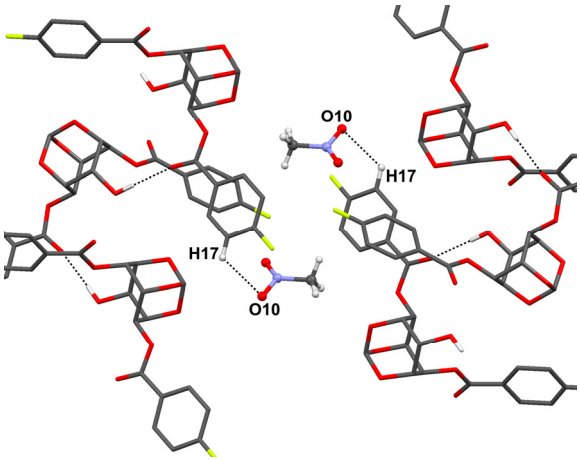

(h) 2.22D

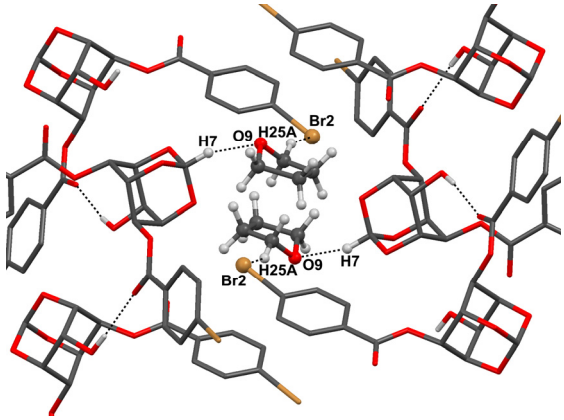

(i) 2.5E

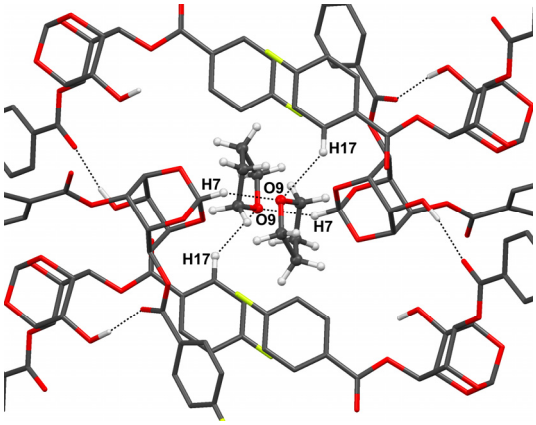

(j) 2.22E

Figure 4A.4.10 Contd….

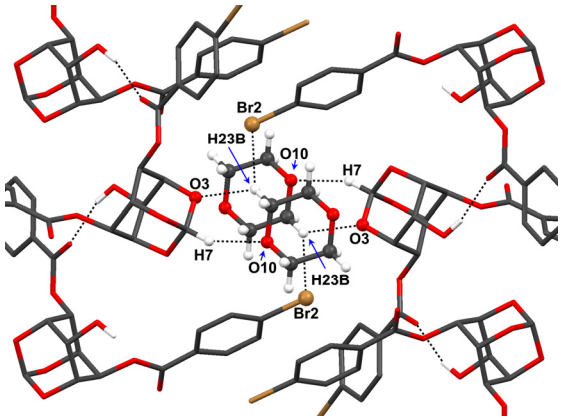

(k) 2.5F

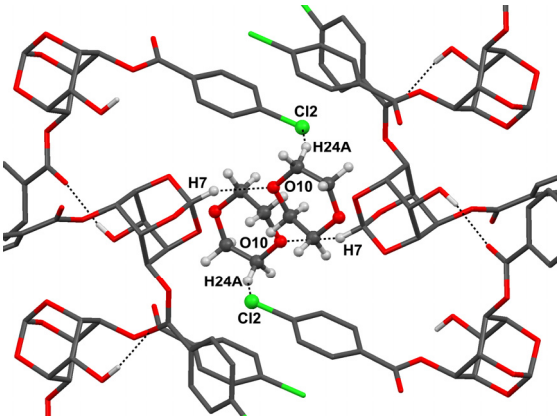

(l) 2.7F

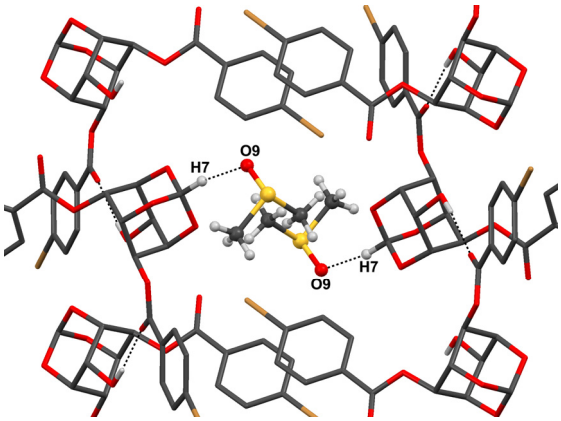

(m) 2.5G

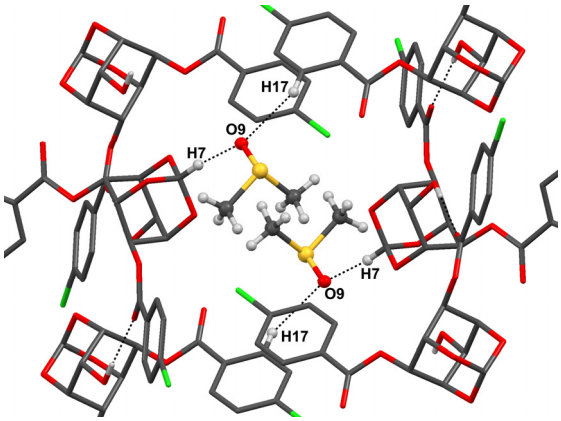

(n) 2.22G

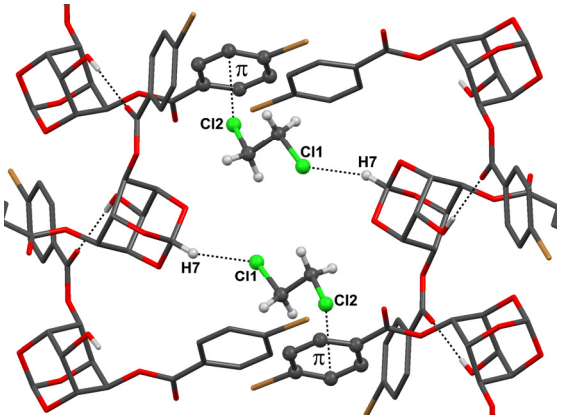

(o) 2.5H

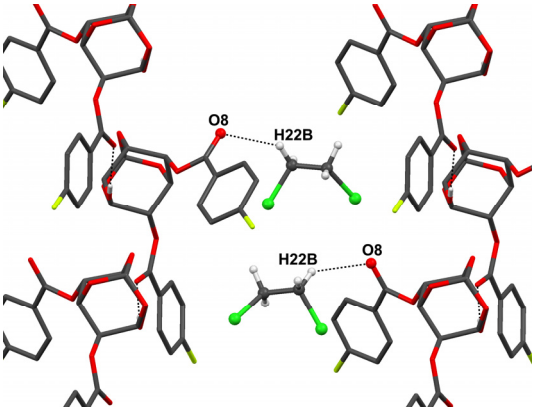

(p) 2.22H

Figure 4A.4.10 Contd….

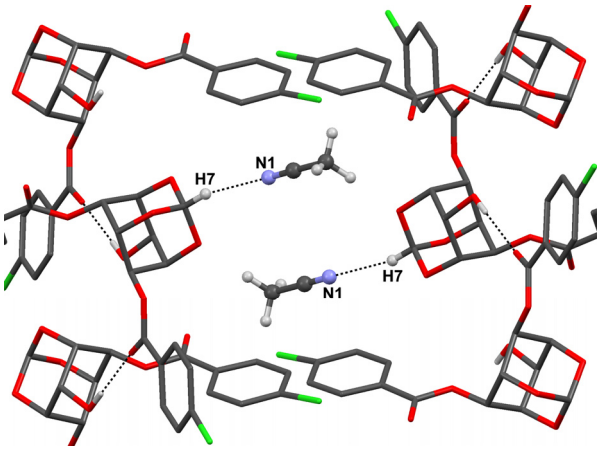

(q) 2.7I

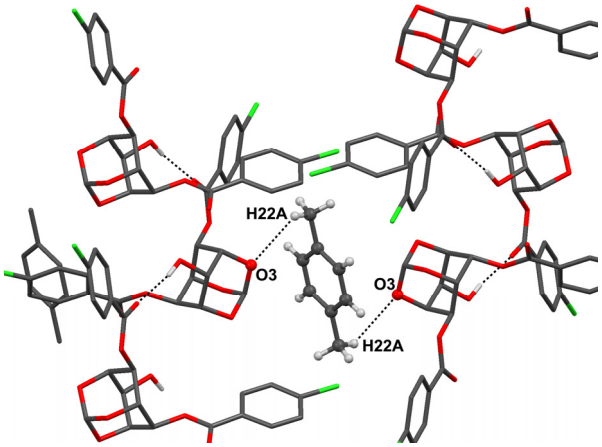

(r) 2.7J

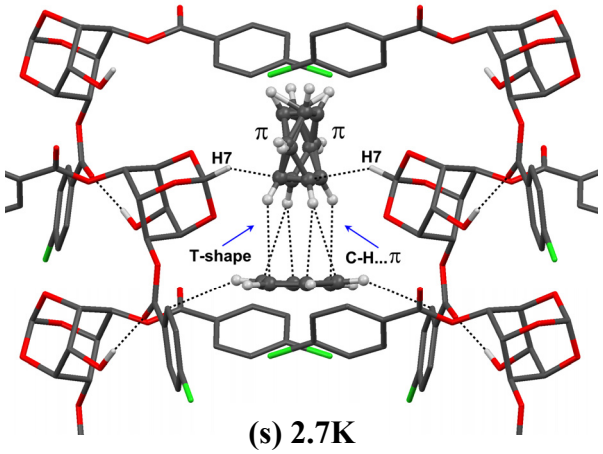

(s) 2.7K

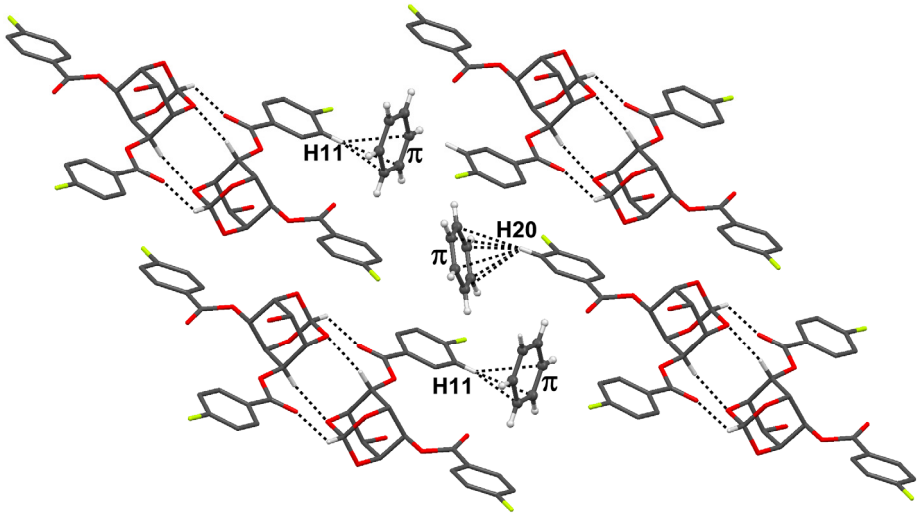

(t) 2.22K

Figure 4A.4.10 Contd….

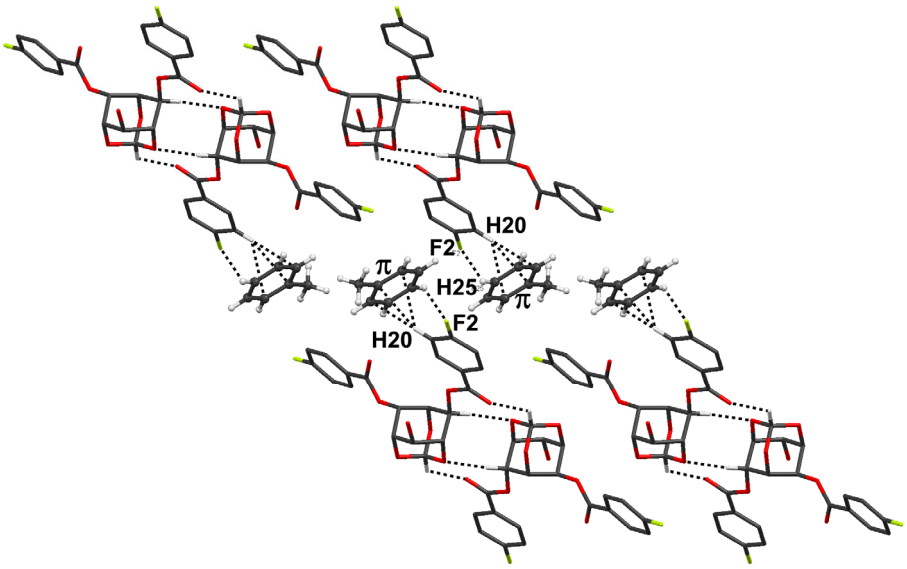

(u) 2.22L

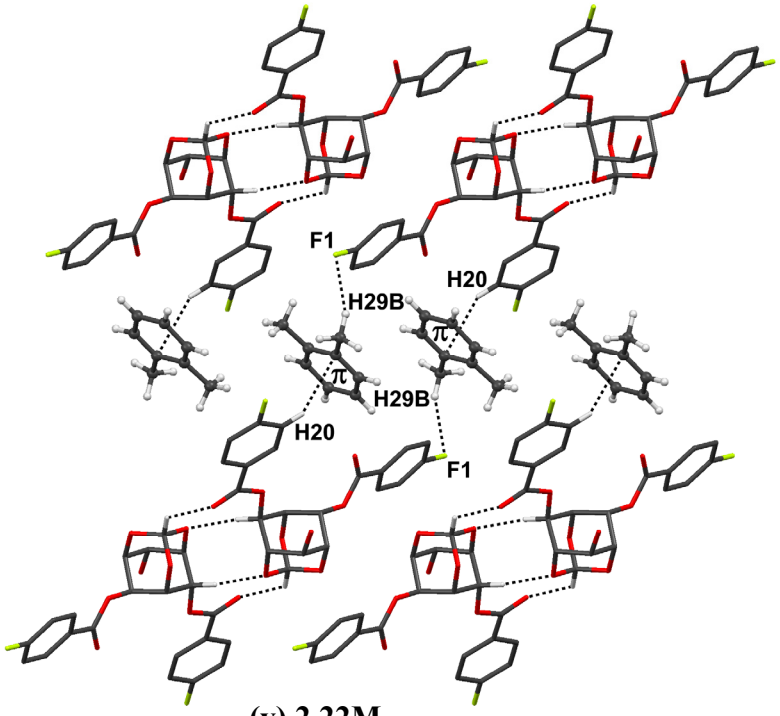

(v) 2.22M

Figure 4A.4.10 Contd….

Table 4A.4.3 Host guest interactions in solvates.

Solvate	D-H···A[a]	D-H /Å	H···A /Å	D···A /Å	D-H···A /°
2.5•$CHCl_3$	Br2···Cl3^{i}			3.571(11)	113
	Cl3···Br2^{ii}			3.571(11)	164
2.7•$CHCl_3$	Cl4···Cl1^{iii}			3.273(10)	175
	Cl1···Cl4^{iii}			3.273(10)	98
	C22-H22···O3^{iv}	1.00	2.53	3.404(3)	145
2.22•$CHCl_3$	C22-H22···O3^{v}	1.00	2.48	3.292(4)	138
2.5•CH_3COCH_3	C7-H7···O9^{v}	1.00	2.27	3.223(4)	159
	C22-H22A···Br2^{vi}	0.98	2.92	3.819(5)	153
2.7•CH_3COCH_3	C7-H7···O9^{v}	1.00	2.30	3.243(3)	157
2.22•CH_3COCH_3	C7-H7···O9^{xxi}	1.00	2.28	3.282(4)	175
2.5•CH_2Cl_2	Cl2···Br1^{vii}			3.269(3)	171
	Br1···Cl2^{vii}			3.269(3)	96
	C22-Cl1···O3^{viii}	1.93	3.036(3)	4.989(15)	173
	C23-Cl3···O8^{ix}	1.74	3.091(5)	4.811(2)	152
	C23-Cl4···O8^{x}	1.76	3.206(6)	4.876(15)	157
	C22-H22A···Br2'^{vi}	0.99	2.26	2.979(12)	128
2.7•CH_2Cl_2	Cl1···Cl3^{xi}			3.285(2)	174
	Cl3···Cl1^{xii}			3.285(2)	97
	C22-Cl4···O3^{xiii}	1.74	3.134(2)	4.838(6)	166
2.22•CH_2Cl_2	C22-H22A···O3^{v}	0.99	2.56	3.302(3)	132
2.5•CH_3NO_2	C7-H7···O9^{xiv}	1.00	2.41	3.307(5)	149
2.7•CH_3NO_2	C7-H7···O9^{xv}	1.00	2.39	3.363(7)	164
2.22•CH_3NO_2	C17-H17···O9	0.95	2.56	3.442(5)	154
2.5•C_4H_8O	C7-H7···O9^{v}	1.00	2.35	3.262(6)	151
	C25-H25A···Br2^{i}	0.99	2.87	3.723(8)	145
	C25-H25A···Br2'^{i}	0.99	2.83	3.768(8)	159
2.7•C_4H_8O	C7-H7···O9^{v}	1.00	2.36	3.299(4)	156
2.22•C_4H_8O	C7-H7···O9^{v}	1.00	2.32	3.264(3)	158
	C17-H17···O9^{vi}	0.95	2.55	3.255(3)	132
2.5•$C_4H_8O_2$	C7-H7···O10^{xiv}	1.00	2.19	3.117(9)	153
	C23-H23B···O3^{xiv}	0.99	2.59	3.371(8)	136
	C23-H23B···Br2^{xvi}	0.99	2.80	3.644(7)	143

Table 4A.4.3 Contd…

2.7•$C_4H_8O_2$	C7-H7···O10^{v}	1.00	2.23	3.135(12)	151
	C7-H7···O10'^{v}	1.00	2.20	3.110(12)	150
	C23'-H23D···O3^{v}	0.99	2.51	3.286(6)	135
	C25'-H25C···O8^{ix}	0.99	2.51	3.481(8)	166
	C24-H24A···Cl2^{i}	0.99	2.79	3.587(12)	138
	C23'-H23D···Cl2^{vi}	0.99	2.76	3.607(7)	144
2.5•CH_3SOCH_3	C7-H7···O9^{xiii}	1.00	2.22	3.199(5)	166
2.7•CH_3SOCH_3	C7-H7···O9^{v}	0.90(3)	2.32(3)	3.204(4)	165(2)
	C17-H17···O9^{vi}	0.91(3)	2.56(3)	3.270(4)	135(2)
2.22•CH_3SOCH_3	C7-H7···O9^{xxii}	1.00	2.18	3.182(4)	176
2.5•$ClCH_2CH_2Cl$	C22-Cl1···Cg*	1.73	3.64	5.301	160
	C7-H7···Cl2^{xvii}	1.00	2.70	3.660(5)	161
2.7•$ClCH_2CH_2Cl$	C22B-Cl3···Cg*	1.69	3.63	5.292	166
	C7-H7···Cl4A^{xviii}	1.00	2.77	3.762(8)	172
	C7-H7···Cl4B^{xviii}	1.00	2.76	3.688(7)	155
	C22A-H23D···O8^{xix}	0.99	2.33	3.29(2)	162
2.22•$ClCH_2CH_2Cl$	C22-H22B···O8^{x}	0.99	2.45	3.236(9)	136
2.7•CH_3CN	C7-H7···N1^{xx}	0.91(2)	2.56(2)	3.451(5)	166
2.22•CH_3CN	C7-H7···N1^{xxiii}	1.00	2.50	3.495(3)	174
2.22•C_6H_6	C11-H11···π^{xxvi}		2.722(17)	3.536(2)	145
	C20-H20···$\pi^{viii, xxvii}$		2.834(16)	3.548(2)	135
2.22•$C_6H_5CH_3$	C25-H25···F2^{viii}	0.95	2.50	3.294(5)	141
	C20-H20···π^{x}		2.70	3.417(4)	132
2.22• *o*-$C_6H_4(CH_3)_2$	C29-H29C···F1^{xxix}	0.98	2.54	3.463(5)	158
	C20-H20···π^{xxx}		2.64	3.389(3)	136

[*] Cg - centroid of the phenyl ring C16-C21

[a] *Symmetry codes:* (i) *x* + 1/2, -*y* + 3/2, *z* – 1/2 ; (ii) *x* – 1/2, *y* + 3/2, *z* + 1/2 ; (iii) –*x* + 1, -*y* + 2, -*z* + 2 ; (iv) –*x* + 1, -*y* + 1, -*z* + 2 ; (v) –*x* + 1, -*y* + 1, -*z* ; (vi) –*x* + 1/2, *y* – 1/2, -*z* + 1/2 ; (vii) –*x* + 1, -*y* + 2, -*z* ; (viii) *x* – 1, *y*, *z* ; (ix) –*x* + 1/2, *y* + 1/2, -*z* + 1/2 ; (x) *x*, *y*, *z* ; (xi) *x*, *y* + 1, *z* + 1 ; (xii) *x*, *y* – 1, *z* – 1 ; (xiii) –*x* + 1, -*y*, -*z* + 1 ; (xiv) –*x* + 1, -*y*, -*z* + 2 ; (xv) *x* – 1/2, -*y* + 1/2, *z* + 1/2 ; (xvi) –*x* + 3/2, *y* – 1/2, -*z* + 3/2 ; (xvii) –*x*, -*y* + 1, -*z* + 2 ; (xviii) *x* + 1, -*y* + 1/2, *z* – 1/2 ; (xix) *x*, -*y* + 1/2, *z* + 1/2 ; (xx) –*x* + 2, -*y* + 1, -*z* ; (xxi) –*x* + 2, -*y* + 2, -*z* + 2 ; (xxii) –*x*, -*y* + 2, -*z* ; (xxiii) –*x* + 2, *y* – 1/2, -*z* + 1/2 ; (xxiv) –*x* + 1, *y* – 1/2, -*z* + 1/2 ; (xxv) –*x*, -*y* + 1, -*z* ; (xxvi) –*x* + 2, -*y*, -*z* + 1;

(xxvii) $-x + 1, -y + 1, -z + 1$; (xxviii) $-x, -y + 1, -z + 1$; (xxix) $x + 1, y, z$; (xxx) $-x + 2, -y + 1, -z + 1$.

Role of solvent in creation of solvates

In the monoclinic solvates of **2.5**, **2.7** and **2.22**, the host molecules assemble helically around the crystallographic 2_1-screw axis through intermolecular O-H···O hydrogen bond employing -OH group and carbonyl oxygen of the C2-*O*-*p*-halobenzoyl group. On the other hand, in the solvent free crystals (obtained from methanol and ethyl acetate) they are linked *via* O4-H4A···O1 contacts to form a one-dimensional molecular string and these strings are associated centrosymmetrically in head-to-head fashion through C-H···O interactions leaving no room for solvent inclusion (Fig. 4A.4.11).[29] However, in the triclinic solvates of **2.22** the host molecules form bilayers (similar to the molecular organisation in the solventless crystal **2.22FI**) and the guest solvent is accommodated in channels between the bilayers.

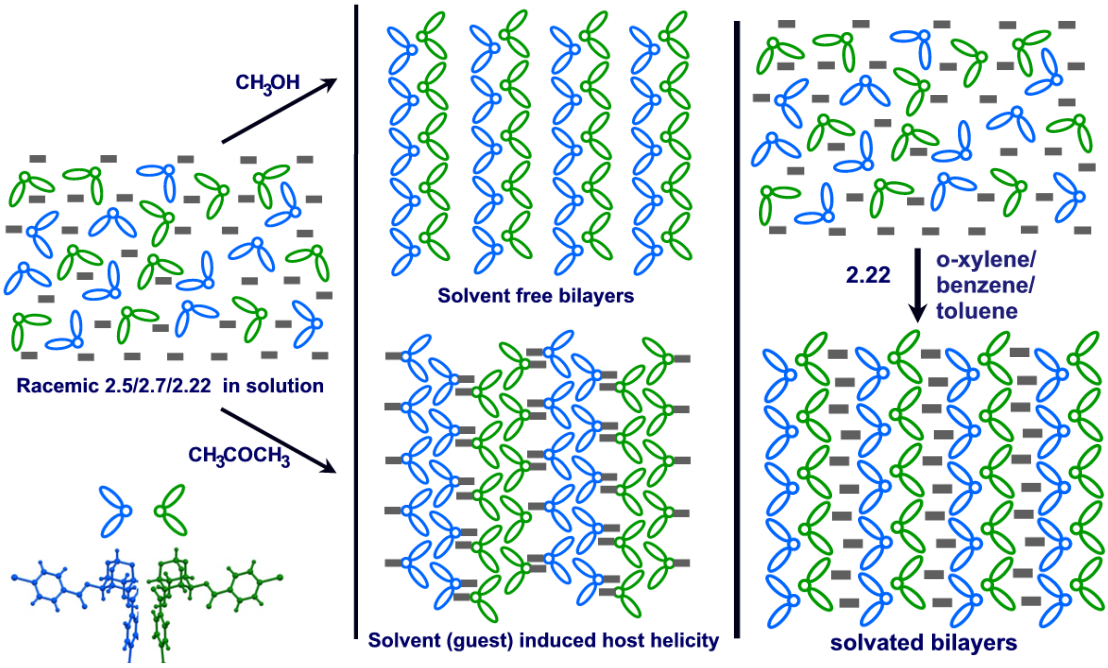

Figure 4A.4.11 Different modes of association of molecules in solvates of **2.5**, **2.7** and **2.22** dependent on the solvent of crystallization.

It is possible that during nucleation of the inclusion complexes, the included solvent molecule chooses to interact with the orthoformate bridge and also engages the axial benzoate through weak intermolecular interactions in solution, thus preventing the host molecules from associating in head-to-head fashion as observed in the solvent free crystals. This leaves the equatorial carbonyl free to interact with the hydroxyl group. Hence, host molecules in pseudopolymorphs associate *via* O-H···O contacts to form helical assemblies similar to those observed in crystals of racemic 2,6-di-*O*-benzoyl-*myo*-inositol 1,3,5-orthoesters.[28,42] Even trace of a solvent, which can interact either with the orthoformate bridge or with benzoyl groups of the host and prevent their association, triggers the helix formation of the host through a different hydrogen bonding pattern and results in the formation of pseudopolymorphs. Moreover, the occupancy of the included solvents, which is full in the freshly grown crystals, reduces with time although the crystals remain intact. This suggests that only a trace of guest solvent is sufficient to hold the host molecules in helical architecture; the excess solvent is expelled from the crystal lattice by the host molecules without destruction of the crystal. In the triclinic solvates, the solvent does not significantly interact with the host (except *via* weak interactions) and perhaps the stronger hydrogen bonding interaction between the host molecules leads them to associate in head-to-head fashion forming bilayers.

4A.4.2 Solid-state reactivity of solvated crystals

The solid-state reactivity of the solvates (of **2.5**, **2.7** and **2.22**) in which the host molecules exhibited a helical assembly in the crystal were studied by heating the freshly grown crystals with activated Na_2CO_3. The reactions were carried out at or below the temperature of escape of solvent from the crystal lattice (as indicated in DSC curves). Heating the reaction mixture at even a slightly higher temperature resulted in complex mixture of products in most cases. Solvates of **rac-2.5** and **rac-2.7** exhibited diverse patterns of solid-state reactivity. The geometry of the nucleophile (Nu) and the electrophile (El) in the five brominated and chlorinated solvates (whose solid-state reactivities were studied) did not approach the values observed in the reactive diesters (Fig. 4A.4.12, d: O4...C15=O8 ~ 3.1 - 3.3 Å; ∠O4...C15=O8 : 84 - 90°) as seen in Table 4A.4.4. The distance of approach in the

brominated solvates was greater than 4 Å and the angle of approach also varied from 44-83°. While **2.5•CH_2Cl_2** and **2.5•CH_3NO_2** did not react in the solid-state, **2.5•$CHCl_3$**, **2.5•CH_3COCH_3** and **2.5•$ClCH_2CH_2Cl$** showed slight reactivity (observed by TLC) yielding the corresponding triester and the diol. However, the reaction proceeded to only a small extent, and most of the diester remained unreacted. In the case of the solvates of **2.7** too, the El-Nu distance was in the range of 3.9-4.3 Å while the angle of approach in only three cases (**2.7•CH_3NO_2**, **2.7•$ClCH_2CH_2Cl$** and **2.7•CH_3CN)** was in the range of 83-84°. **2.7•$ClCH_2CH_2Cl$** showed mild reactivity in the solid-state (with products other than triester **2.8** and diol **2.21** obtained when the reaction temperature was increased) whereas the other solvates yielded a complex mixture of products. In the case of solvates of **rac-2.22,** it was observed that the $P2_1/c$ solvates (**2.22•CH_3COCH_3**, **2.22•CH_3NO_2**, **2.22•CH_3CN** and **2.22•*p*-$C_6H_4(CH_3)_2$**) possessed reasonably good El-Nu geometry. While **2.22•CH_3COCH_3**, **2.22•CH_3NO_2** and **2.22•CH_3CN** reacted to a minor extent in the solid-state yielding the triester and diol, **2.22•*p*-$C_6H_4(CH_3)_2$** gave a mixture of products. This could be perhaps due to the effect of the included solvent *p*-xylene which could interfere in the acyl transfer reaction. The other monoclinic solvates however did not show any acyl transfer reactivity. As a control experiment, the solid-state reactivity of the solvent free crystals **2.22FI** was tested at 115 °C. As expected, the reaction resulted in a mixture of several products, attributed to the unfavourable molecular pre-organization in the crystal.

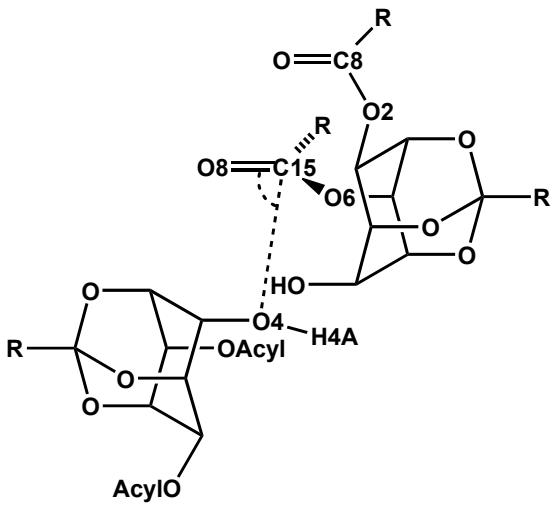

Figure 4A.4.12 Schematic representation of El-Nu geometry in diesters.

Table 4A.4.4 Electrophile-nucleophile geometry in solvates of **2.5**, **2.7** and **2.22**.

Solvate	El-Nu (d Å) (O4...C15=O8)	El-Nu (∠ °) (O4...C15=O8)	O6-C15 (Å) (ax)	O2-C8 (Å) (eq.)
Rac-1.177	3.226, 3.249	88.1, 89.9	1.361(4), 1.354(4)	1.333(4), 1.343(4)
Rac-1.179	3.144(2)	85.6	1.347	1.334
Rac-1.178(B)	3.135(4)	87.6	1.346	1.332
2.5•$CHCl_3$	4.054(4)[i]	44.6	1.351(3)	1.345(4)
2.5•CH_3COCH_3	4.146(4)[ii]	48.5	1.347(4)	1.342(4)
2.5•CH_2Cl_2	4.178(4)[iii]	65.7	1.333(3)	1.345(4)
2.5•CH_3NO_2	4.336(3)[i]	46.0	1.354(3)	1.338(3)
2.5•$ClCH_2CH_2Cl$	4.243(5)[iv]	83.4	1.356(5)	1.339(5)
2.7•$CHCl_3$	4.170(3)[i]	46.5	1.353(3)	1.347(3)
2.7•CH_3COCH_3	4.172(2)[v]	47.5	1.354(2)	1.345(2)
2.7•CH_3NO_2	4.334(2)[v]	83.0	1.350(2)	1.345(2)
2.7•$ClCH_2CH_2Cl$	4.210(5)[vi]	83.9	1.356(4)	1.343(5)
2.7•CH_3CN	3.938(4)[vi]	83.4	1.348(3)	1.347(3)
2.22•CH_3COCH_3	3.568(3)[vii]	86.7	1.357(3)	1.342(2)
2.22•CH_2Cl_2	4.144(2)[iii]	45.9	1.340(2)	1.343(3)
2.22•CH_3NO_2	3.624(3)[viii]	83.0	1.355(3)	1.342(3)
2.22•C_4H_8O	4.068(3)[ii]	57.6	1.347(3)	1.340(2)
2.22•$ClCH_2CH_2Cl$	4.259(3)[vi]	64.8	1.343(3)	1.340(3)
2.22•CH_3CN	3.938(4)[vi]	83.4	1.361(2)	1.350(2)
2.22•*p*-$C_6H_4(CH_3)_2$	3.496(2)[iv]	83.8	1.354(2)	1.339(2)
2.22FI	-	-	1.344(2)	1.347(3)

Symmetry codes: (i) $-x + 3/2, y + 1/2, -z + 3/2$; (ii) $-x + ½, y + ½, -z + ½$; (iii) $-x + 3/2, y + ½, -z + ½$; (iv) $-x + 1, y + ½, -z + 3/2$; (v) $-x + ½, y + ½, -z + ½$; (vi) $-x + 2, y + 1/2 , -z + ½$; (vii) $-x + 2, y – ½, -z + 3/2$; (viii) $-x + 1, y + ½, -z + ½$.

The reason for the poor reactivity of these solvates can be rationalized on the basis of structural features and thermal phenomena. The helices in the solvatomorphs are linked by weak interactions (C-Cl···O, C-H···Cl, C-H···F, π stacking and C-H···π interactions) and are not packed closely in their crystals as compared to **rac-1.177**. Further, the solvates are not stable crystals, loss of solvent from the crystal lattice results in the transformation (*via* melt crystallization) of the solvated crystal to the solvent free forms which do not possess the required geometry for acyl transfer (Table 4A.4.4). The mild reactivity shown by some of the solvates could perhaps be an artifact of the helical assembly of the host molecules (akin to the reactive dibenzoates) with the presence of solvent lending some flexibility in the crystal lattice. A comparison of the O-C bond lengths for the axial and equatorial benzoyl groups of the solvates (Table 4A.4.4) reveals that in most of the solvates the axial bond length (at the migrating group) is longer than the equatorial counterpart, similar to the trend observed in the reactive dibenzoates.[28,42] The C-H···π interactions which hold the migrating axial benzoyl group in proper orientation for the acyl transfer in the reactive dibenzoates are also very weak and marginal in the solvates. The parallel physical and chemical changes i.e. the phase transformation and acyl transfer which occur simultaneously in the reaction mixture, result in the reaction not proceeding to completion, and could perhaps be the reason for the formation of other products apart from the expected triester and the diol.

4A.5 Solvates of racemic 2,6-di-*O*-benzoyl-*myo*-inositol 1,3,5-orthobenzoate

The previous sections 4A.3, 4A.4 dealt with the role of solvent in creating reactive helical molecular assemblies. However, thermally induced changes in the solvated crystal resulted in a loss of the solvent and transformation of a reactive packing into a non-reactive one, limiting the acyl transfer reactivity of the solvated crystal. This section deals with another example of differential solid-state reactivities. The thermal behaviour and the solid-state reactivity of the 2-propanol (form II) and toluene (form III) solvates of **rac-1.179** is discussed; the un-solvated crystals (form I) of **rac-1.179** exhibit clean benzoyl group transfer reaction among its constituent molecules.[28c]

4A.5.1 Synthesis, crystallization and X-ray crystallography

Rac-1.179 was synthesized and crystallized as reported in chapter 2. Quality of form II and form III crystals was poorer than that of form I crystals, but the quality of crystals obtained from 2-propanol (form II) was better than that obtained from toluene (form III). Form II and form III crystals were stable in the open atmosphere for 1-2 days, after which gradual loss of crystallinity was observed. Proton NMR spectra (see chapter 2) of freshly grown crystals of form II indicated the presence of 2-propanol (**rac-1.179**: 2-propanol ~ 1:0.15) and that of form III revealed the presence of toluene in the crystal. The ratio of **rac-1.179**: toluene in form III crystals varied from 1:0.33 to 1:0.45 depending on the method used for drying the sample. Both form II and form III crystals contained traces of water (which was not quantified) as revealed by proton NMR spectra (chapter 2).

The X-ray diffraction measurements for form II crystals of **rac-1.179** were carried out on a MX2 beam line of the Australian Synchrotron at 120 K (λ = 0.71073 Å). Since form II crystals measured less than 5 microns in two of the dimensions, it was difficult to measure diffracted intensities on the laboratory sources routinely used. Even on the brightest of the synchrotron beam line MX2, the percentage of observed reflections was very low. Ultra-thin fibre like crystals were dispersed in paraffin oil; a suitable crystal was selected under polarizing microscope was then mounted on a Hampton Scientific cryoloop and transferred to the cold stream for X-ray data collection. Blu-Ice[43] software was used for data collection. Structure was solved by

direct methods with SHELXS-97 and full-matrix least-squares refinement was carried out using SHELXL.[31] The non-hydrogen atoms were refined anisotropically. We noticed that anisotropic displacement parameters for many of the atoms were Non Positive Definite, a feature observed in structure refinements of other synchrotron data from ultra-thin crystals. Therefore, the anisotropic vibrations were restrained using options DELU and SIMU available in program SHELXL. The hydrogen atoms were fixed using stereochemical criterion and refined isotropically using the riding model option in SHELXL. Two molecules of guest solvent (2-propanol; occupancy 0.25 and 0.125) and two molecules of water (occupancy 0.25 and 0.125), were picked up in the difference Fourier and included in the final cycles of refinement. The geometry of 2-propanol was idealized and restrained during the least-squares procedure. The intensity data from the microcrystals showed somewhat high R_{sym} (~0.12) and the refinement converged to a rather high R value (~0.20) compared to values of normal diffracting crystals. Molecular and packing diagrams were generated using ORTEP-32[32] and Mercury CSD 2.3[33] respectively. Geometrical calculations were performed using PLATON.[34] Crystal data are summarized in Table 4A.5.1.

Table 4A.5.1 Crystal data table for Form II crystals of **rac-1.179**.

	rac-1.179 - form II
Chemical formula	$C_{27}H_{22}O_8$ • [0.25(C_3O); 0.125 (C_3O) • 0.25 (O); 0.125 (O)]
M_r	489.22
Temperature (K)	120
Morphology	Fibres
Crystal size	0.10 × 0.01× 0.01
Crystal system	Triclinic
Space group	*P*-1
a (Å)	6.1780(12)
b (Å)	15.941(3)
c (Å)	28.069(6)
α (°)	84.21(3)
β (°)	87.52(3)
γ (°)	85.76(3)
V (Å^3)	2740.9(9)
Z	4
D_{calc} (g cm^{-3})	1.186
μ (mm^{-1})	0.088
F(000)	1025
T_{min}	0.991
T_{max}	0.999
h, k, l (min, max)	(-6,6), (-18,18), (-32,33)
Reflns collected	10041
Unique reflns	6869
Observed reflns	2306
No. of parameters	673
GoF	0.922
$R_1[I > 2\sigma(I)]$	0.2157
$wR_2[I > 2\sigma(I)]$	0.4424
R_1_all data	0.2992
wR_2_all data	0.5000
$\Delta\rho_{max}$, $\Delta\rho_{min}$(eÅ^{-3})	0.47, -0.42
CCDC dep. No.	787939

4A.5.2 Thermal response of solvates

DSC curves and hot stage microscopy images for both the solvates were recorded as described in Sec. 4A.2. The DSC curve (Fig. 4A.5.2) of form II and form III crystals of **rac-1.179** showed endotherms much before the final melting curve of the crystals, attributed to the escape of solvent molecules from the inclusion crystal lattice. The endothermic peak was immediately followed by an exotherm indicating melt-crystallization of form II crystals to the known form I crystals. The DSC curve of form I crystals of rac-1.179 showed only the melting endotherm.[28c]

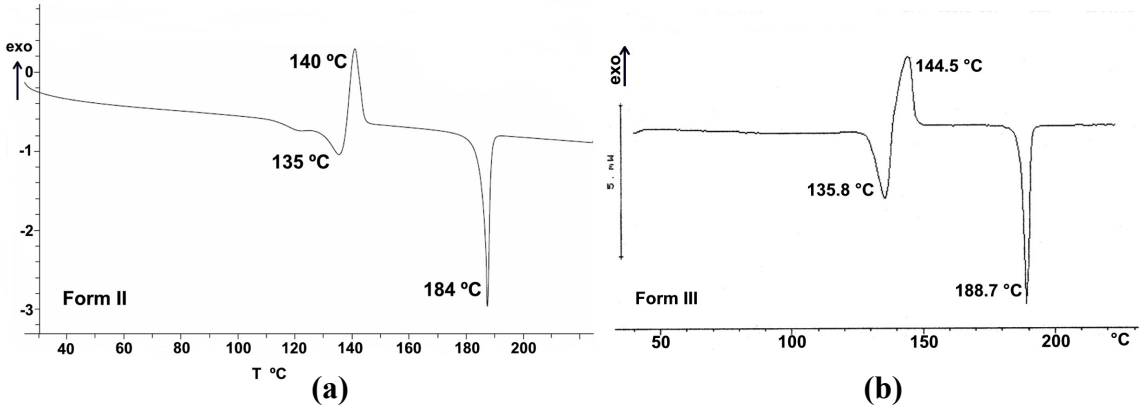

Figure 4A.5.2. DSC curves for crystals of **rac-1.179:** (a) form II and (b) form III.

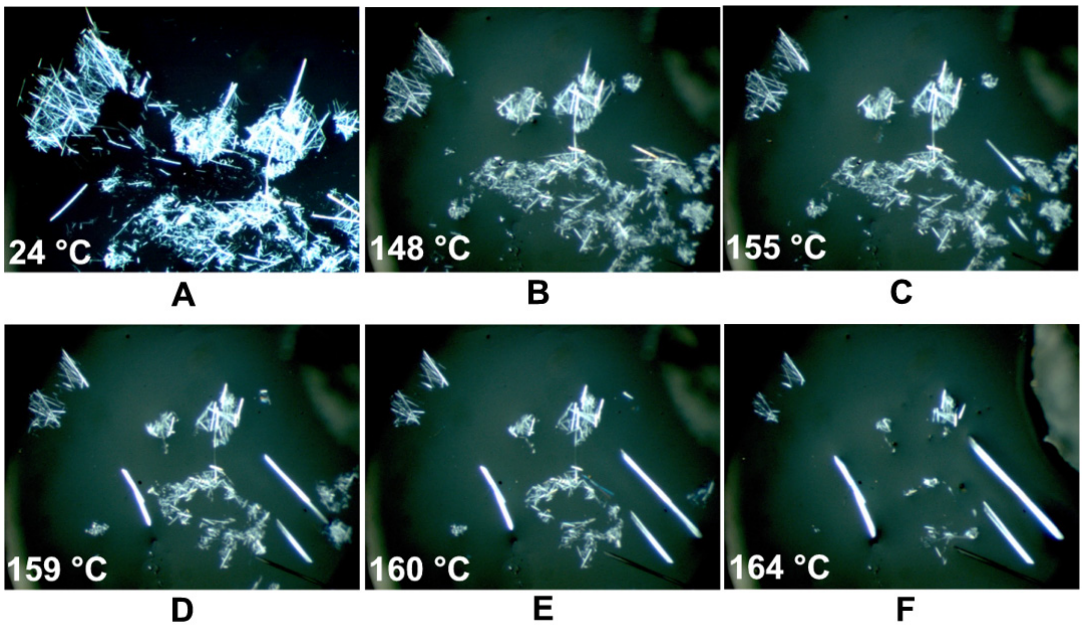

Fig. 4A.5.3 HSM images for Form III crystals of **rac-1.179**. Thin whisker like crystals (A) melt above 130 ºC (B); continued heating initiates formation of crystals (C) which grow (D, E) and eventually give rise to well defined form I crystals.

The thin whisker like form II and form III crystals of **rac-1.179** when heated on a

hot stage polarizing microscope started melting at ~ 130 ºC and with further increase in temperature (Fig. 4A.5.3B - D) slowly recrystallised to yield brittle rectangular plates (Fig. 4A.5.3E). Determination of the unit cell parameters of one such plate (Fig. 4A.5.3F) confirmed it to be the form I crystals of **rac-1.179**. form I crystals of **rac-1.179** when heated on a hot stage microscope did not show any physical change until their melting.[28c]

4A.5.3 Solid-state reactivity

Reactivity of form II crystals of racemic 2,6-di-*O*-benzoyl-*myo*-inositol 1,3,5-orthobenzoate (rac-1.179): Form II crystals of **rac-1.179** (0.025 g, 0.05 mmol) and sodium carbonate (0.045 g, 0.4 mmol) were ground together using mortar and pestle and heated in a sealed tube at 140 °C for 21 h. TLC of the reaction mixture showed the presence of tribenzoate **1.182** and the diol **1.185**, along with *myo*-inositol 1,3,5-orthobenzoate (**2.4**).[36c] The reaction mixture was cooled to room temperature and filtered on a Celite column using ethyl acetate - methanol mixture (6:1) as the solvent. The residue (0.024 g) obtained from this extract when subjected to preparative TLC (eluent: 15% ethyl acetate in light petroleum), yielded 0.006 g (20%) of the tribenzoate **1.182**.

Reactivity of form III crystals of racemic 2,6-di-*O*-benzoyl-*myo*-inositol 1,3,5-orthobenzoate (rac-1.179): Form III crystals of **rac-1.179** (0.059 g, 0.125 mmol) and sodium carbonate (0.106 g, 1.0 mmol) were ground together using mortar and pestle and heated in a sealed tube at 140 °C for 47 h under argon atmosphere. The reaction mixture was cooled to room temperature and extracted with chloroform - methanol mixture (5:1). The residue obtained was column chromatographed (silica gel 230-400 mesh, gradient elution with light petroleum - ethyl acetate) to isolate 0.017 g (23%) of the tribenzoate **1.182**. Although the diol **1.185** was also formed in these experiments (as revealed by TLC) it was not isolated, since determining the yield of one of the products was good enough to get an idea about the extent of conversion of **rac-1.179** to products. Form II and form III crystals did not show detectable acyl transfer reactivity as above, when heated (100 °C, 60 h) with sodium carbonate below the phase transition temperature.

4A.6 Results and discussion

4A.6.1 Structural features

The form I crystals of **rac-1.179**, well-defined square or hexagonal plates (Fig. 4A.6.1a), when heated with solid sodium carbonate, were earlier reported[28c] to undergo facile transesterification in the solid state to yield the tribenzoate **1.182** and diol **1.185** (Scheme 4A.6.1).

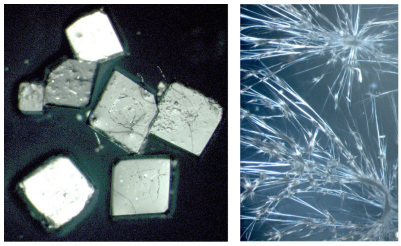

Figure 4A.6.1 Photomicrographs of (a) form I and (b) form II crystals of **rac-1.179**.

Their reactivity was attributed to a helical pre-organization of molecules through O–H···O hydrogen bonding and other weak intermolecular interactions which place the electrophile (C=O of the C6-ester) and the nucleophile (C4–OH) in a favourable geometry for the reaction. The angle of approach of the nucleophile (Nu) towards the electrophile (El) and the distance between them in the reactive form I crystals of **rac-1.179** were 85.6° and 3.14 Å respectively. Furthermore, the helical organization of the molecules provided a reaction channel for the intermolecular acyl transfer in form I crystals, which resulted in high conversion of **rac-1.179** to products **1.182** and **1.185**.

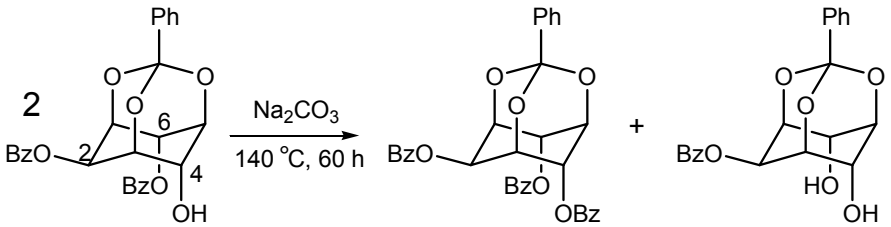

Scheme 4A.6.1 Solid-state benzoyl transfer in form I crystals of **rac-1.179**.

During the course of crystallization experiments it was observed that **rac-1.179** when crystallized from benzene, toluene and 2-propanol yielded thin whisker like crystals (Fig. 4A.6.1b) concomitantly with plates of Form I. Crystal structure solution of the

ultrathin form II crystals indicated that they belonged to the triclinic space group *P*-1 with two independent molecules (an enantiomeric pair) in the asymmetric unit along with two molecules each of 2-propanol and water (Fig. 4A.6.2a). DSC curves and hot stage microscopy suggested a phase transition that was confirmed by X-ray crystallographic studies (by determining the unit cell parameters) as the conversion of these thin crystals (form II) into the form I crystals *via* melt crystallization.Although suitable crystals for single crystal X-ray structural studies could not be obtained from toluene (form III), they showed similar thermal behaviour (to that of form II), i.e. melt crystallization to the form I crystals. The inclusion of toluene in these crystals was inferred from their proton NMR spectra (see chapter 2). The overlap of the constituent molecules in form II crystals with those in form I crystals showed the conformational differences between the molecules (Fig. 4A.6.2b) in the two crystals. There are significant torsional differences in the orientation of the equatorial and the axial benzoyl groups which translate into large variations in the hydrogen bonding patterns and the organization of molecules in the lattice.

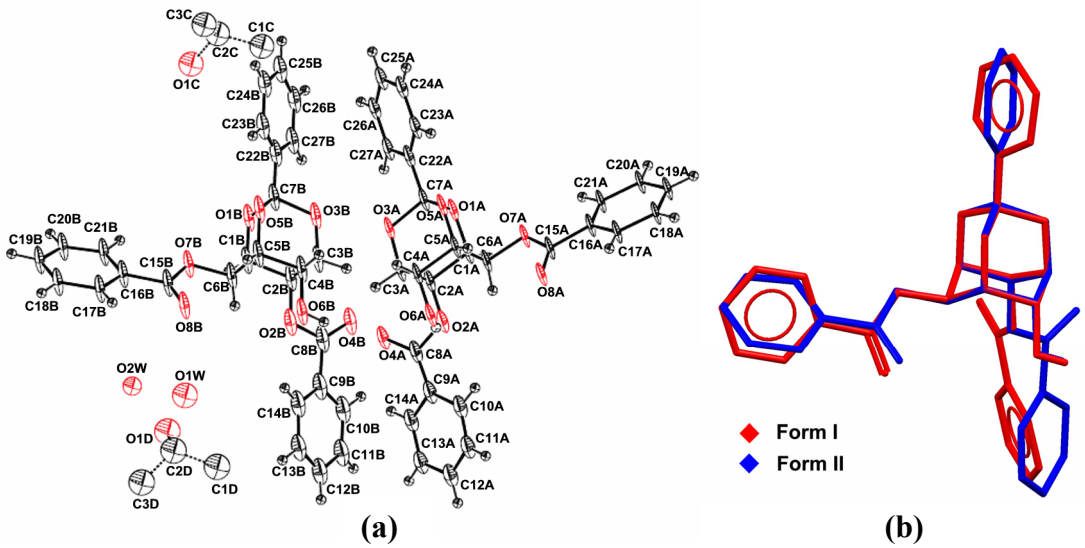

Figure 4A.6.2 (a) ORTEP of molecules in form II crystals of **rac-1.179**. Thermal ellipsoids are drawn at 50% probability and hydrogen atoms are shown as small spheres of arbitrary radii and (b) Molecular overlap of form I and form II crystals showing the conformational differences.

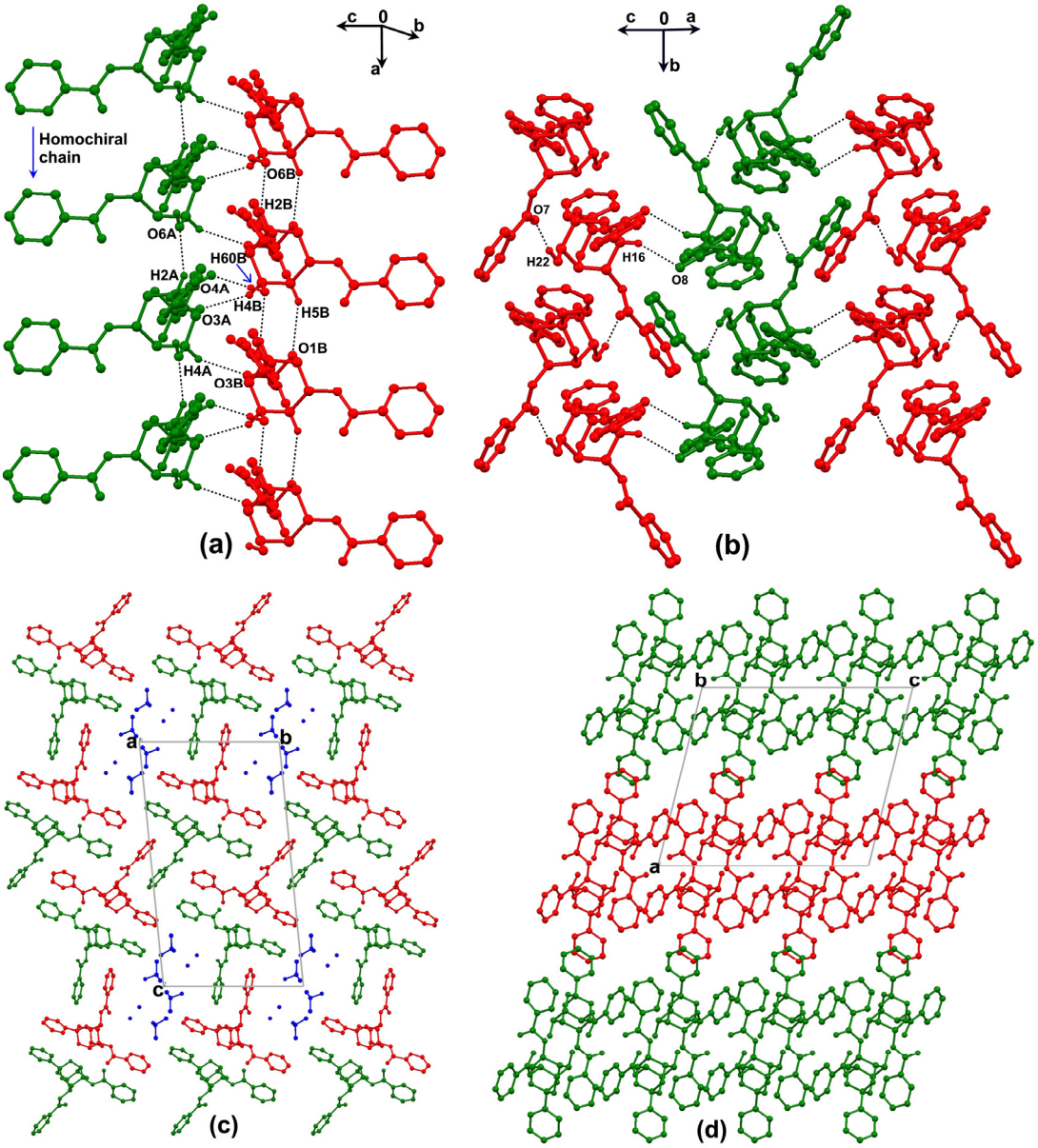

Figure 4A.6.3 Organization of molecules: (a) homochiral molecular chains in form II crystals formed by hydrogen bonding interactions and (b) helices in form I crystals. Packing of molecules: (c) form II - homochiral chains viewed down *a*-axis and (d) form I - closely packed helices. Solvent molecules and hydrogen atoms not involved in hydrogen bonding are omitted for the sake of clarity. Red and green molecules are enantiomers.

Each enantiomer of the host in the asymmetric unit forms a 1D homochiral chain along the *a*-axis through C-H···O interactions (C2A-H2A···O6A, C2B-H2B···O6B and C5B-H5B···O1B contacts, Fig. 4A.6.3a). Adjacent homochiral

chains are linked by O-H···O hydrogen bonding between the heterochiral molecules *via* O6B-H6OB···O4A interactions, supported by a pair of C-H···O contacts (C4B-H4B···O3A and C4A-H4A···O3B). These molecular chains when viewed down the *a*-axis appear as a layer of weakly interconnected dimers (red–green) along the b and c axes, creating channels that are occupied by 2-propanol and water (Fig. 4A.6.3c). It is pertinent to recall here that in the form I crystals, molecules of each enantiomer formed a helical assembly along the *b*-axis through O-H···O hydrogen bonding between the hydroxyl group and the carbonyl oxygen of the 2-O-benzoyl group (Fig. 4A.6.3b), with the adjacent helices linked by C-H···O interactions (Fig. 4A.6.3d).[28c]

Table 4A.6.1 Hydrogen bonding interactions in Form II crystals.

D-H···A	D-H /Å	H···A /Å	D···A /Å	D-H···A /°
O6B-H6OB···H4A^{i}	0.82	2.12	2.934(12)	170
C4A-H4A···O3B^{ii}	0.98	2.51	3.417(14)	153
C4B-H4B···O3A^{i}	0.98	2.54	3.422(16)	149
C2A-H2A···O6A^{iii}	0.98	2.33	3.203(15)	148
C2B-H2B···O6B^{iii}	0.98	2.37	3.233(16)	146
C5B-H5B···O1B^{ii}	0.98	2.57	3.450(16)	150

Symmetry codes: (i) *x*, *y*, *z*; (ii) 1 + *x*, *y*, *z*; (iii) -1 + *x*, *y*, *z*.

4A.6.2 Solid-state reactivity and structure correlation

The 2-propanol (form II) and toluene (form III) solvates of **rac-1.179**, did not show any acyl transfer activity below the phase transition temperature (135 °C), but did show acyl transfer reactivity when heated with sodium carbonate at (or above) the transition temperature. The X-ray diffraction data is good enough to reveal that packing of molecules in form II crystals is not conducive for the benzoyl transfer reaction, since they do not form well defined reaction channels similar to those present in form I crystals (Fig. 4A.6.3d). The pattern of molecular organization in the form II crystals clearly suggests that the electrophile (C=O) and the nucleophile (-OH) are not present in the proper relative orientation for benzoyl transfer reaction (Fig. 4A.6.4). This is because the channels found in reactive form I crystals consist solely of one of the enantiomers of **rac-1.179** (hence the benzoyl transfer occurs between

molecules having the same absolute configuration, green or red molecules in Fig. 4A.6.3b) while in form II crystals neighboring molecules in the channels have the opposite configuration.

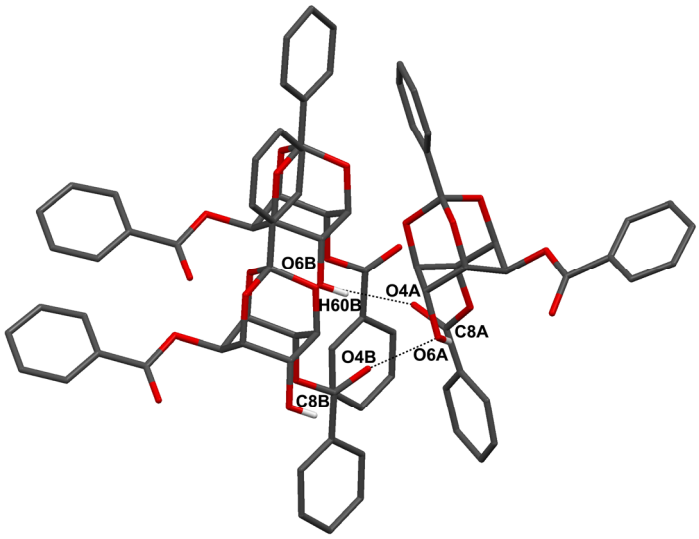

Figure 4A.6.4. Closely interacting molecules in the chain along *a*-axis exhibit El-Nu parameters which are not conducive for acyl transfer reaction in the solid-state.

Table 4A.6.2 Electrophile-nucleophile geometry in form II crystals of **rac-1.179**

O...C=O	d (O...C=O) /Å	∠ (O...C=O) /°
O6A…C8B=O4B^{i}	3.891	34.93
O6B…C8A=O4A^{ii}	3.947	30.24

Symmetry codes: (i) $x + 1, y, z$; (ii) x, y, z.

This is supported by experiment since no benzoyl transfer reactivity was observed on heating the Form II crystals with sodium carbonate, below the phase transition temperature. However, when Form II crystals are heated to the transition temperature of 135 °C in the presence of solid sodium carbonate, *in situ* melt crystallization occurs, and the unreactive Form II crystals are slowly transformed into the reactive Form I crystals which react to give products **1.182** and **1.185** (Scheme 4A.6.1). The extent of conversion of **rac-1.179** to products (about 50%) in this process (*in situ* melt crystallization of Form II crystals to Form I crystals) is not as good (>90%) as that observed in Form I crystals obtained by crystallization from a solvent.

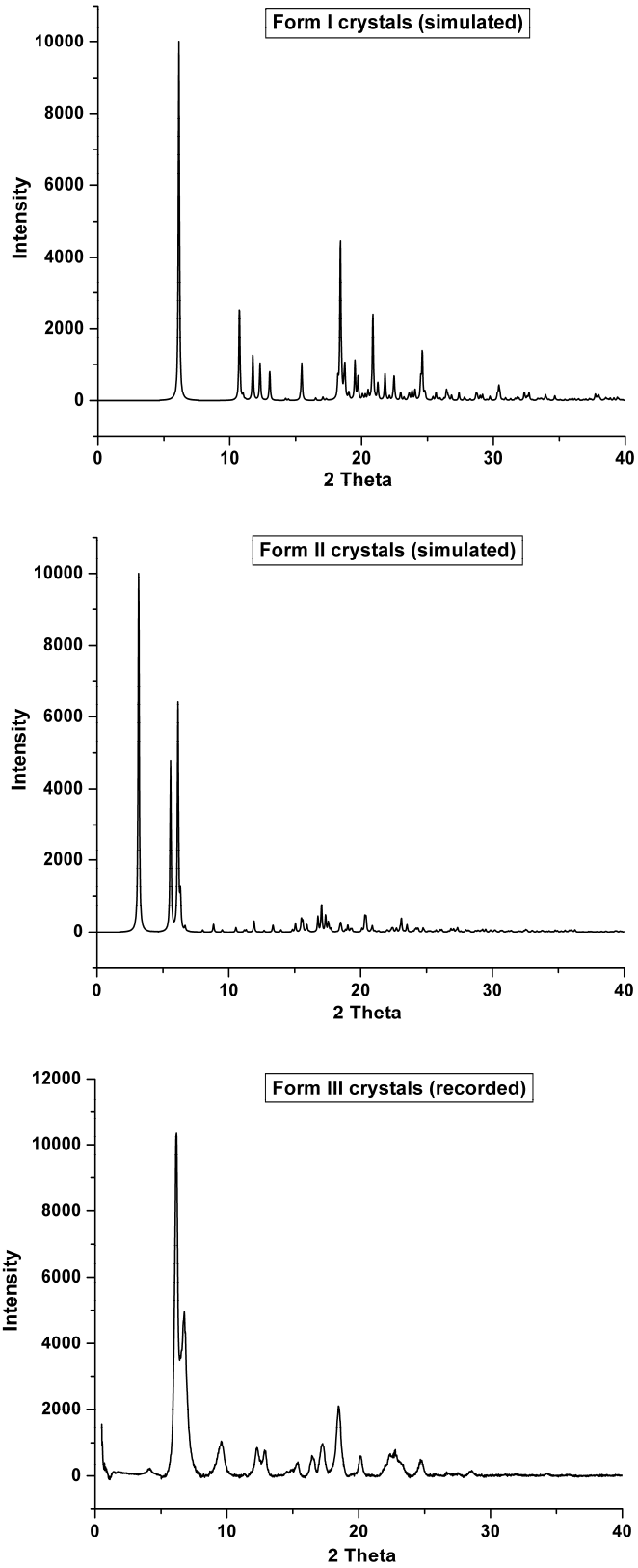

Figure 4A.6.5 Simulated (Form I, Form II) and recorded (Form III) PXRD patterns of crystals of **rac-1.179**.

This difference in reactivity is perhaps because heating the Form I crystals with sodium carbonate brings in only a chemical change, while heating of Form II crystals with sodium carbonate activates parallel phase changes and chemical changes in the solid reaction mixture at the transition temperature. While we could not obtain the crystal structure and examine molecular organization in the Form III crystals, powder diffraction patterns (recorded for Form III and simulated for Form I) reveal structural dissimilarities between Form III (solvated) and Form I (solvent free) crystals (Fig. 4A.6.5). Form III crystals exhibit similar reactivity as well as thermal behaviour as the Form II crystals. The spontaneous transesterification activity of the hitherto unreactive crystals upon change in the molecular organization (*via* desolvation and melt crystallization) to the reactive packing underscores the importance of the proposed topochemical criterion[28] and therein and overall molecular organization responsible for the efficient intermolecular acyl transfer reactions in crystals.

4A.7 Conclusions

Racemic 2,6-di-*O*-(4-halobenzoyl)-*myo*-inositol 1,3,5-orthoformate (halo = bromo (**rac-2.5**), chloro (**rac-2.7**), fluoro (**rac-2.22**)) and racemic 2,6-di-*O*-benzoyl-*myo*-inositol 1,3,5-orthobenzoate (**rac-1.179)** yielded structurally dissimilar solvent-free and solvated crystals depending upon the solvent of crystallization. In the case of the halogenated diesters, the solvent free crystals did not exhibit a favourable helical assembly of molecules essential for solid-state reactivity, while in the solvatomorphs, the solvent was found to induce helical pre-organization of host molecules through interactions with the orthoformate group of the host. In the orthobenzoate **rac-1.179**, the situation was reversed; the solvent-free crystals contained the required molecular geometry for the acyl transfer reaction, but the solvatomorphs did not. The solvates of **rac-2.5**, **rac-2.7** and **rac-1.179**, could be thermally transformed into the solvent-free crystals *via* melt crystallization; the result being the conversion of a helical molecular packing into a non-helical molecular packing in **rac-2.5** and **rac-2.7** and *vice versa* in **rac-1.179**. Accordingly, the solvates of **rac-2.5** and **rac-2.7** showed mild benzoyl transfer reactivity upto the transition temperature, above which reactivity was not observed and a mixture of products was obtained. On the other hand, the hitherto unreactive solvates of **rac-1.179**, displayed benzoyl transfer reactivity above the

transition temperature, indicative of the crossover to the helical molecular pre-organization. Since both the phase transition from the solvated crystal form to the un-solvated crystal form and the chemical reaction occurring in the crystals are thermally motivated, solvation provides a switch to control the reactivity of these molecules. Delineation of the properties of such unusual crystal systems are of relevance in understanding and development of reactive and functional ensemble of molecules in the condensed phases.

Section B: Structures and reactivities of some mono-acylated *myo*-inositol derivatives

4B.1 Introduction

Sodium hydride assisted facile intermolecular acyl migration in racemic 4-*O*-acyl-*myo*-inositol-1,3,5-orthoesters (Scheme 4B.1.1) to the corresponding 2-*O*-acyl derivatives in excellent yields (>90%), in the solution state had earlier been reported from our laboratory.[44] The reaction in solution was irreversible and the 2-*O*-acyl-*myo*-inositol-1,3,5-orthoesters were completely stable in the presence of strong bases (sodium hydride and potassium *t*-butoxide) and at higher temperatures. Therefore, the reactivity of 2-*O*-benzoyl *myo*-inositol orthoesters in the crystalline state in the presence of solid Na_2CO_3 was investigated and attempts were made to correlate it with the crystal structure.

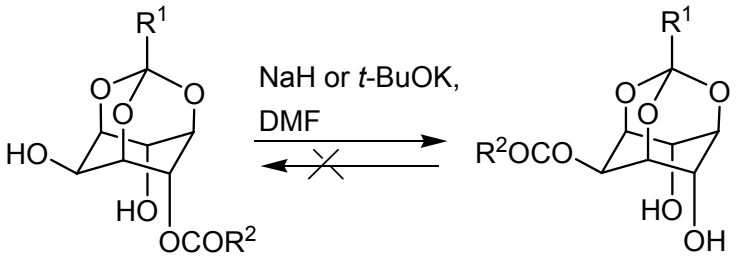

	R^1	R^2
4.1	H	Ph
4.2	H	CH_3
4.3	CH_3	Ph
4.4	CH_3	CH_3

	R^1	R^2
1.183	H	Ph
2.9	H	CH_3
4.5	CH_3	Ph
4.6	CH_3	CH_3

Scheme 4B.1.1 Reactivity of 4-*O*-acyl-*myo*-inositol-1,3,5-orthoesters.

The orthobenzoate **1.185** on crystallization spontaneously yielded chiral crystals (orthorhombic, space group $P2_12_12_1$) irrespective of the solvent used, while the orthoformate diol **1.183** crystallized in the monoclinic space group $P2_1/n$. Analysis of the crystal structures of the diols revealed a relative orientation of molecules that appeared conducive for exhibiting the solid state acyl transfer reactivity, although the El...Nu interaction parameters were not as favourable as those in crystals of corresponding dibenzoates **1.179** and **1.177**. The diols reacted in the solid state giving transesterified products, but it was not a clean reaction; a mixture was obtained and no attempt was made to separate these products (Scheme 4B.1.2). It is fascinating to observe that although these mono-benzoates failed to undergo transesterification in solution, they reacted in the crystalline state due to the relatively rigid assembly of

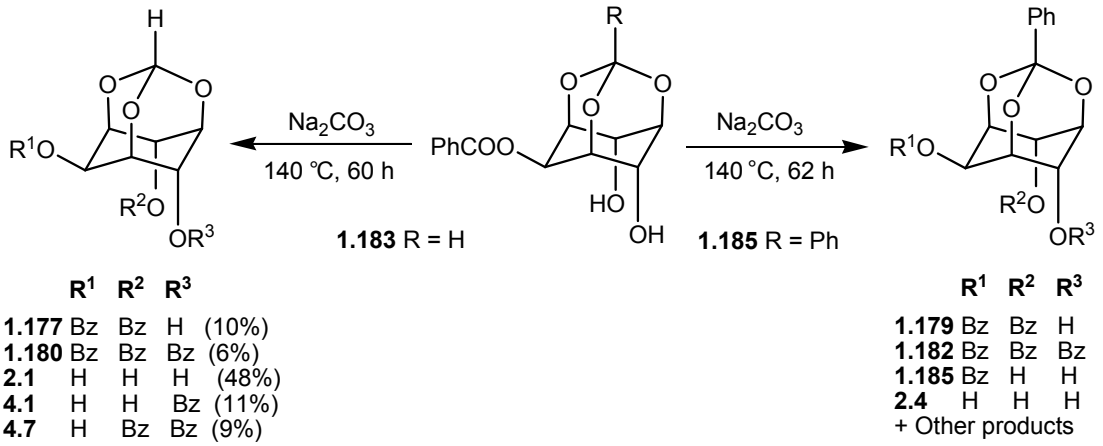

Scheme 4B.1.2 Solid-state reactivity of 2-*O*-benzoylated *myo*-inositol 1,3,5-orthoesters.

molecules in the lattice.[28c] Hence we sought to explore the crystal structures of some mono-acylated *myo*-inositol-1,3,5-orthoesters in our quest for molecules with reactive pre-organization along with structure-reactivity correlations. The esters investigated for acyl transfer reactivity in their crystals are shown in Chart 4B.1.

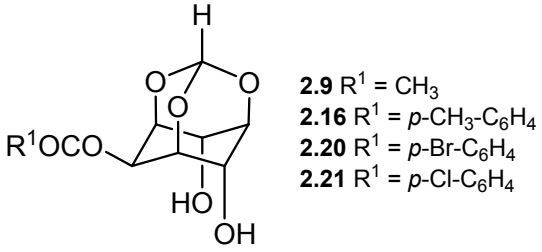

Chart 4B.1 2-*O*-acylated *myo*-inositol 1,3,5-orthoformates.

4B.2 Experimental

4B.2.1 Synthesis, crystallization and X-ray crystallography

The diols under study (Chart 4B.2.1) were synthesised and crystallized as described in chapter 2. X-ray data for the crystals were collected as described in section 4AI.2. The hydroxyl hydrogen atoms in all the structures were located in difference Fourier maps and refined isotropically. The hydroxyl bond lengths in **2.20** (O4-H4A, O6-H6A) were restrained using the DFIX instruction in SHELX. All other hydrogen atoms were placed in geometrically idealized positions and refined isotropically. The crystallographic data are summarized in Table 4B.2.1.

Table 4B.2.1 Crystallographic data for 2-*O*-acylated *myo*-inositol 1,3,5-orthoformates.

	2.9	**2.16**	**2.20**	**2.21**
Chemical formula	$2(C_9H_{12}O_7)\bullet H_2O$	$C_{15}H_{16}O_7$	$C_{14}H_{13}O_7Br$	$C_{14}H_{13}O_7Cl$
M_r	482.39	308.28	373.15	328.69
Temperature (K)	297(2)	297(2)	297(2)	297(2)
Morphology	needle	plate	plate	plate
Crystal size	0.33×0.06×0.03	0.31×0.25×0.09	0.82×0.54×0.17	0.35×0.27×0.12
Crystal system	Orthorhombic	Orthorhombic	Triclinic	Triclinic
Space group	$P2_12_12_1$	$Pna2_1$	P-1	P-1
a (Å)	6.5544(13)	27.213(4)	6.1636(17)	6.1733(7)
b (Å)	17.219(3)	7.7759(12)	6.6939(19)	6.7059(9)
c (Å)	18.111(4)	6.5598(10)	19.234(5)	18.735(2)
α (°)	90	90	89.799(4)	90.489(2)
β (°)	90	90	88.371(5)	92.200(2)
γ (°)	90	90	68.650(4)	111.440(5)
V (Å^3)	2044.1(7)	1388.1(4)	738.8(3)	721.17(15)
Z	4	4	2	2
D_{calc} (g cm^{-3})	1.567	1.475	1.677	1.514
μ (mm^{-1})	0.139	0.118	2.815	0.298
F(000)	1016	648	376	340
T_{min}	0.956	0.964	0.206	0.902
T_{max}	0.996	0.989	0.646	0.965
h, k, l (min, max)	(-7, 7), (-20, 20), (-21, 21)	(-24, 32), (-9, 8), (-7, 7)	(-7, 7), (-7, 7), (-22, 22)	(-7, 7), (-7, 7), (-22, 22)
Reflns collected	19764	6662	7129	6997
Unique reflns	2084	2433	2588	2532
Observed reflns	1847	2338	2201	2294
R_{int}	0.0499	0.0237	0.0296	0.0182
No. of parameters	324	208	207	207
GoF	1.245	1.191	1.049	1.081
$R_1[I > 2\sigma(I)]$	0.0431	0.0297	0.0362	0.0430
$WR_2[I > 2\sigma(I)]$	0.0863	0.0795	0.0967	0.1019
R_1_all data	0.0512	0.0334	0.0430	0.0473
Wr_2_all data	0.0890	0.0921	0.1042	0.1048
$\Delta\rho_{max}$, $\Delta\rho_{min}$(e Å^{-3})	0.15, -0.18	0.25, -0.22	0.50, -0.33	0.24, -0.21

4B.2.2 Solid-state reactivity of 2-*O*-acylated *myo*-inositol 1,3,5-orthoformates

The solid-state reactivities of the diols were carried out as described in the general experimental procedure in section 4AI.1.3, by heating the crystals with Na_2CO_3 below their melting points. The solid-state reactivity of **2.9** was not tested due to the presence of water in the crystal.

2-*O*-(4-methylbenzoyl) *myo*-inositol 1,3,5-orthoformate (2.16): Crystals of **2.16** (0.047 g, 0.152 mmol, mp. 148-150 °C) were heated with sodium carbonate (0.150 g, 1.4 mmol) at 100 °C for 94 h, TLC of the reaction mixture showed the presence of the diester **2.15** and the triester **2.17** along with three other products. The reaction mixture was filtered on a silica column (100-200 mesh) by elution with ethyl acetate (5 x 10 mL) and methanol (2 x 5 mL). The filtrate was concentrated, and the residual mixture was chromatographically separated by gradient elution (on a 230-400 mesh silica column) to obtain the triol **2.1** (0.015 g, 52%), the diester **2.15** (0.010 g, 15%) and the triester **2.17** (0.003 g, 4%) amongst other minor products. When the same reaction was carried out at 126 °C for 20 h, chromatographic separation of the reaction mixture yielded the triol **2.1** (0.012 g, 39%), the diester **2.15** (0.020 g, 29%) and the triester **2.17** (0.007 g, 8%). The products were characterized by comparison of ^{1}H NMR spectra and melting points with literature reports.

2-*O*-(4-bromobenzoyl) *myo*-inositol 1,3,5-orthoformate (2.20): Crystals of **2.20** (0.036 g, 0.1 mmol, mp. 156-157 °C) when heated with sodium carbonate at 128 °C for 65 h, gave a mixture of products which included the diester **2.5**, the triester **2.6** and unreacted **2.20** and two other unidentified products which were not separated.

4B.3 Results and Discussion

4B.3.1 Structural features

(a) *2-O-acetyl myo-inositol 1,3,5-orthoformate (2.9)*

The acetate **2.9** crystallised in the chiral orthorhombic space group $P2_12_12_1$, with two independent molecules of the host and a molecule of water in the asymmetric unit. Crystallization trials from various solvents did not yield any solvent-free crystals. The formation of chiral crystals of a *meso* compound is an interesting phenomenon, which besides aiding in understanding the process of crystallization,[45] also has application in areas of asymmetric autocatalysis[46] and NLO materials.[47]

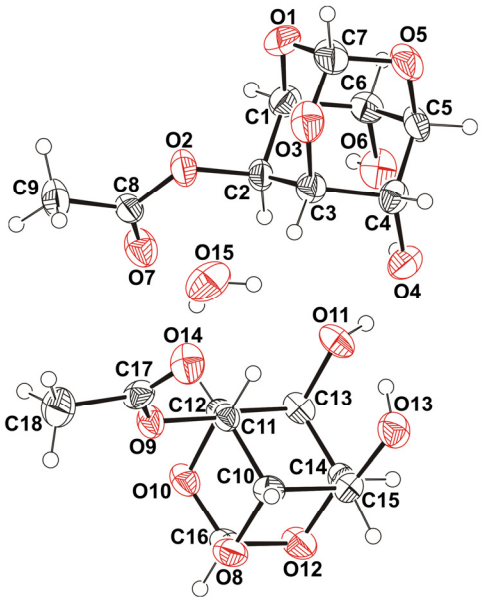

Figure 4B.3.1 ORTEP of **2.9**. Thermal ellipsoids are drawn at 40% probability and hydrogen atoms are shown as small spheres of arbitrary radii.

The structure of the acetate is characterized by the presence of strong hydrogen bonding between the hydroxyl groups of the host and the solvent. The two independent molecules in the asymmetric unit, through O-H···O hydrogen bonding between the hydroxyl groups of adjacent molecules, form a molecular chain along the *a*-axis *via* O6-H6A···O13 and O13-H13A···O4 contacts. The assembly of screw related molecules is supported by short and linear C10-H10···O7 interactions, between the inositol proton H10 of one molecule and the carbonyl oxygen O7 of the neighbour. The guest water molecules occupy the channels between adjacent molecular chains.

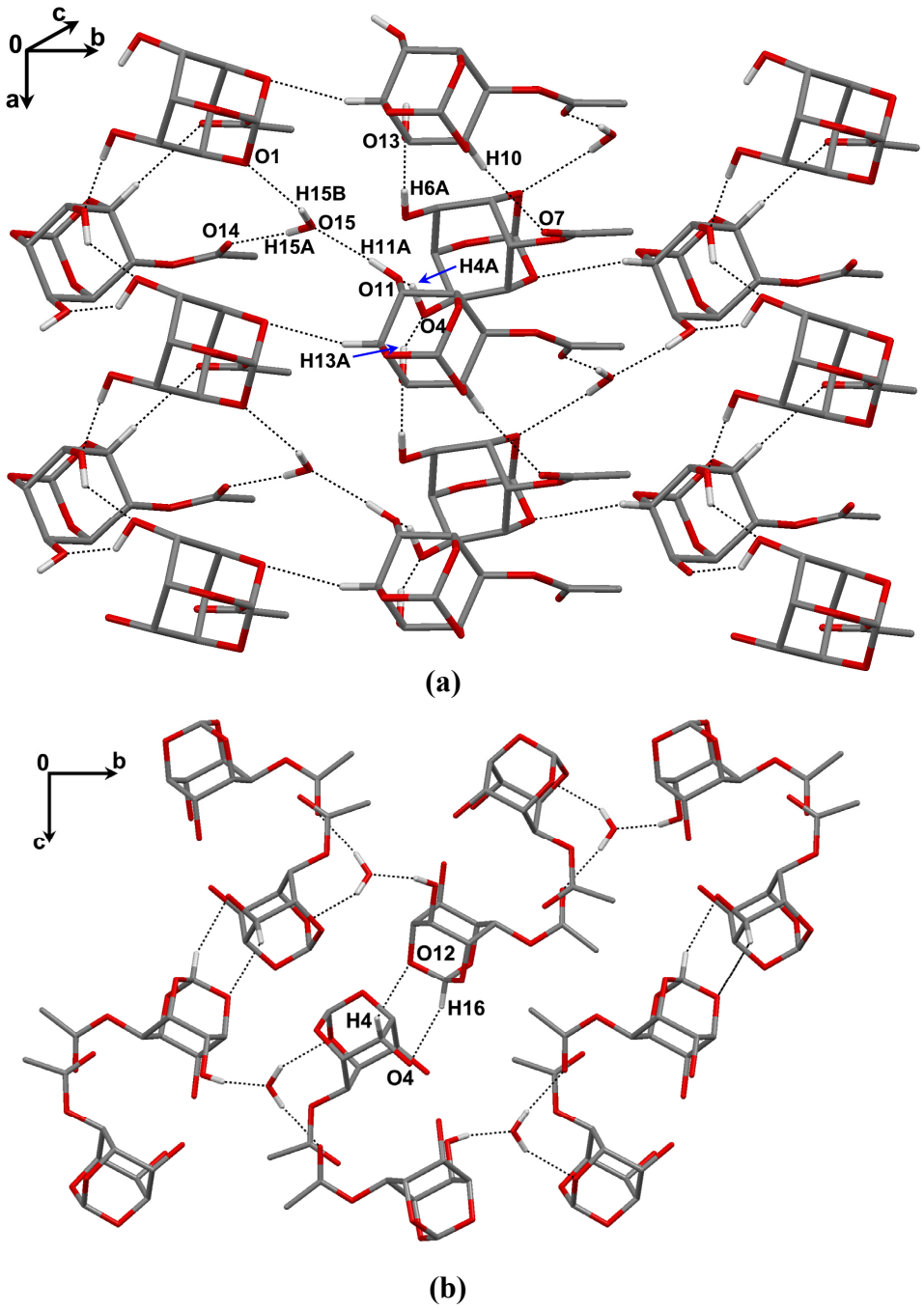

Figure 4B.3.2 Molecular packing in **2.9**: (a) Molecular chains built by hydrogen bonding linked by the guest water molecules along the *b*-axis and (b) Linking of molecular chains along the *c*-axis by C-H···O interactions. Hydrogen atoms not involved in hydrogen bonding are omitted for the sake of clarity.

Each water molecule donates a proton to the orthoester oxygen (O15-H15A···O1) and carbonyl oxygen (O15-H15B···O14) and in turn accepts a hydroxyl proton (O11-

H11A···O15) linking the molecular chains along the *b*-axis *via* short and linear hydrogen bonding contacts. Molecular chains along the *c*-axis are connected by a pair of non-centrosymmetric C-H···O interactions (C16-H16···O4 and C4-H4···O12 contacts, Fig. 4B.3.2b).

(b) *2-O-(4-methylbenzoyl) myo-inositol 1,3,5-orthoformate (2.16)*

The *p*-toluate **2.16** crystallised in the polar orthorhombic space group $Pna2_1$ (Fig. 4B.3.3).

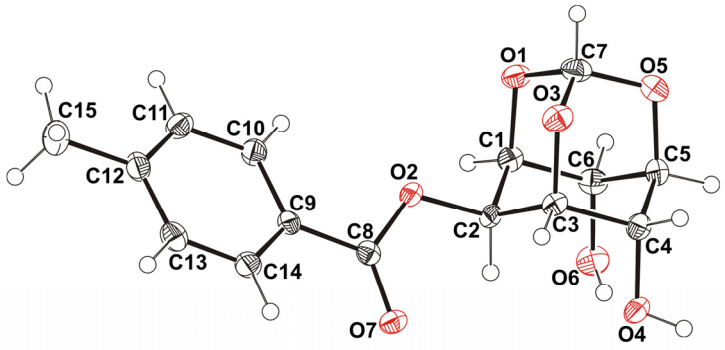

Figure 4B.3.3 ORTEP of **2.16**. Thermal ellipsoids are drawn at 40% probability and hydrogen atoms are shown as small spheres of arbitrary radii.

The hydroxyl group of one molecule is involved in O-H···O hydrogen bonding (O4-H4A···O7) with the carbonyl group of the *p*-toluate ester of a neighbouring glide-related molecule and also makes a weak C-H···O contact (C5-H5···O4), forming a chain of glide related molecules along the *bc*-diagonal (Fig. 4B.3.4a). This is in contrast to the hydrogen bonding observed in the benzoates **1.183** and **1.185** where the hydroxyl group is involved in an O-H···O interaction with the orthoester oxygen atom of the neighboring molecule.[28c] Adjacent chains of glide-related molecules, nearly perpendicular to each other, are linked by C13-H13···O1 contacts across the *a*-axis (Fig. 4B.3.4a). The second hydroxyl group (O6-H6A) plays a role in the linkage of adjacent chains of glide-related molecules through C-H···O interactions (C3-H3···O6), supported by C7-H7···O7 contacts between the orthoformate proton and the carbonyl oxygen. Oxygen O6 also forms short O…C=O contact, an El...Nu interaction (O6…C8=O7: 2.909(3) Å, ∠ O6…C8=O7: 87.1°) with a neighbouring unit-translated molecule along the *c*-axis (Fig. 4B.3.4b, Table 4B.3.1).

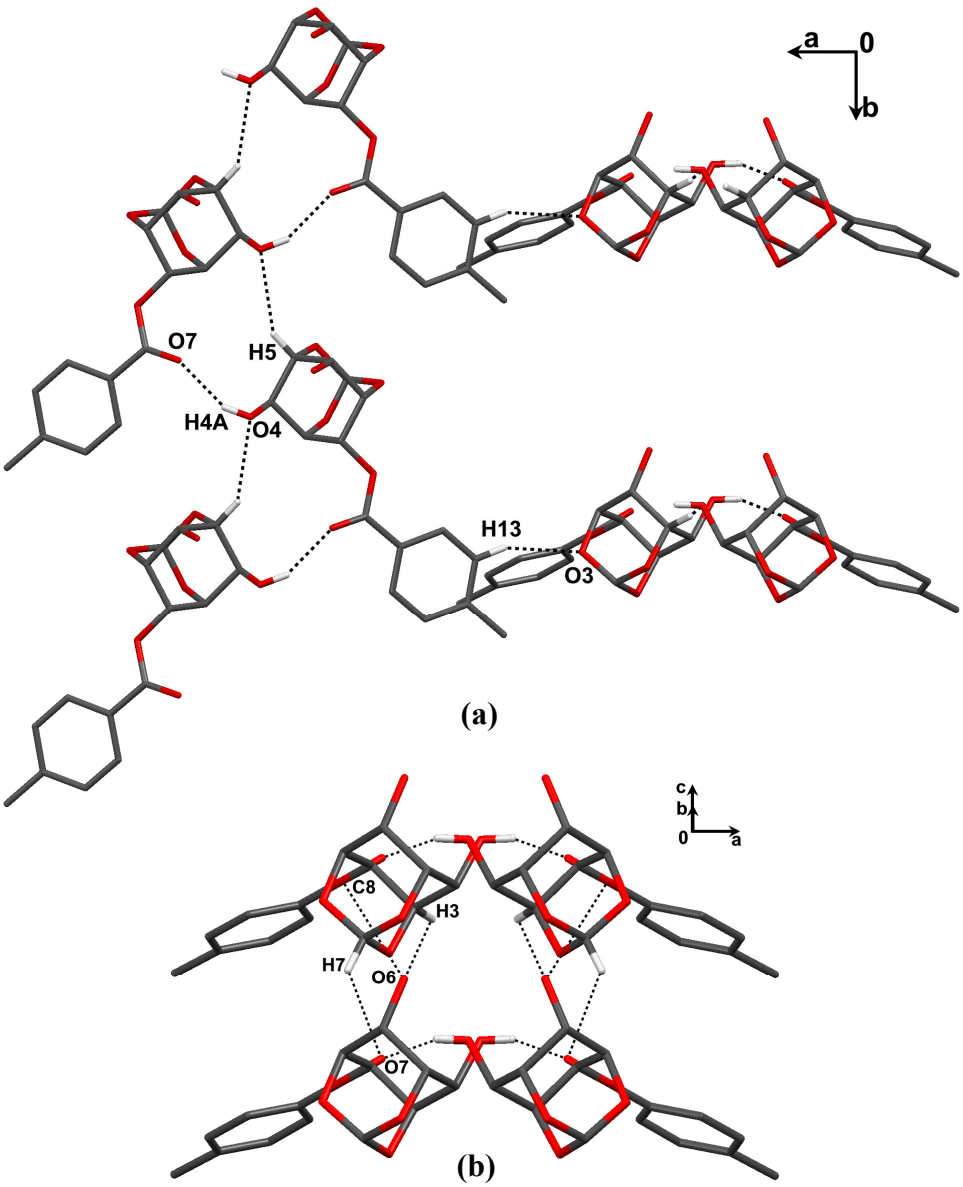

Figure 4B.3.4 Molecular packing in **2.16**: (a) Glide-related molecular chains built by hydrogen bonding linked across the *a*-axis by C-H···O interactions and (b) Linking of molecular chains along the *c*-axis by C-H···O interactions. Hydrogen atoms not involved in hydrogen bonding are omitted for the sake of clarity.

(c) ***2-O-(4-bromobenzoyl) myo-inositol 1,3,5-orthoformate (2.20) and 2-O-(4-chlorobenzoyl) myo-inositol 1,3,5-orthoformate (2.21)***

As observed in the crystalline forms of 2,4,6-tri-*O*-(4-halobenzoyl) *myo*-inositol 1,3,5-orthoformates **2.6** and **2.8**[45] and the corresponding diesters **2.5** and **2.7** (chapter 4AI), the diols **2.20** and **2.21** are also isostructural and isomorphous. Both diols **2.20** and **2.21** crystallize in the triclinic space group *P*-1(Fig. 4B.3.5). Further the hydrogen bonding pattern adopted by the hydroxyl group is similar to that observed in the solvent free crystals of the diesters **2.5** and **2.7**.

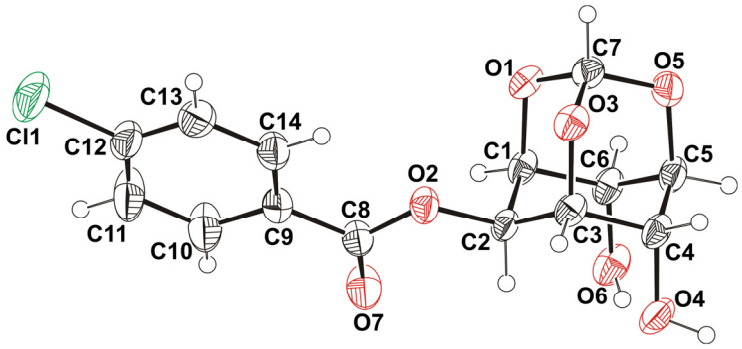

Figure 4B.3.5 ORTEP of **2.21**. Thermal ellipsoids are drawn at 40% probability and hydrogen atoms are shown as small spheres of arbitrary radii.

One of the hydroxyl groups in **2.20** (O6-H6A) and **2.21** (O4-H4A) donates its proton to the orthoester oxygen of a neighbouring molecule (O3, O1) forming a molecular chain along the *b*-axis. Molecular chains along the *c*-axis are linked by centrosymmetric weak C-H···O interactions (C5-H5···O5 and C7-H7···O5) to form bilayers (Fig. 4B.3.6a). These bilayers are interlinked by short halogen···halogen interactions (Br···Br in **2.20** and Cl···Cl in **2.21** of type I[48] (∠Br1 = 172°, ∠Cl1 = 171°, Table 4B.3.1) along the *c*-axis. Along the *a*-axis the bilayers are connected by moderately strong C13-H13···O7, C3-H3···O7 and C7-H7···O6 contacts and short and linear C6-H6···O4 interactions (Fig. 4B.3.6b, Table 4B.3.1).

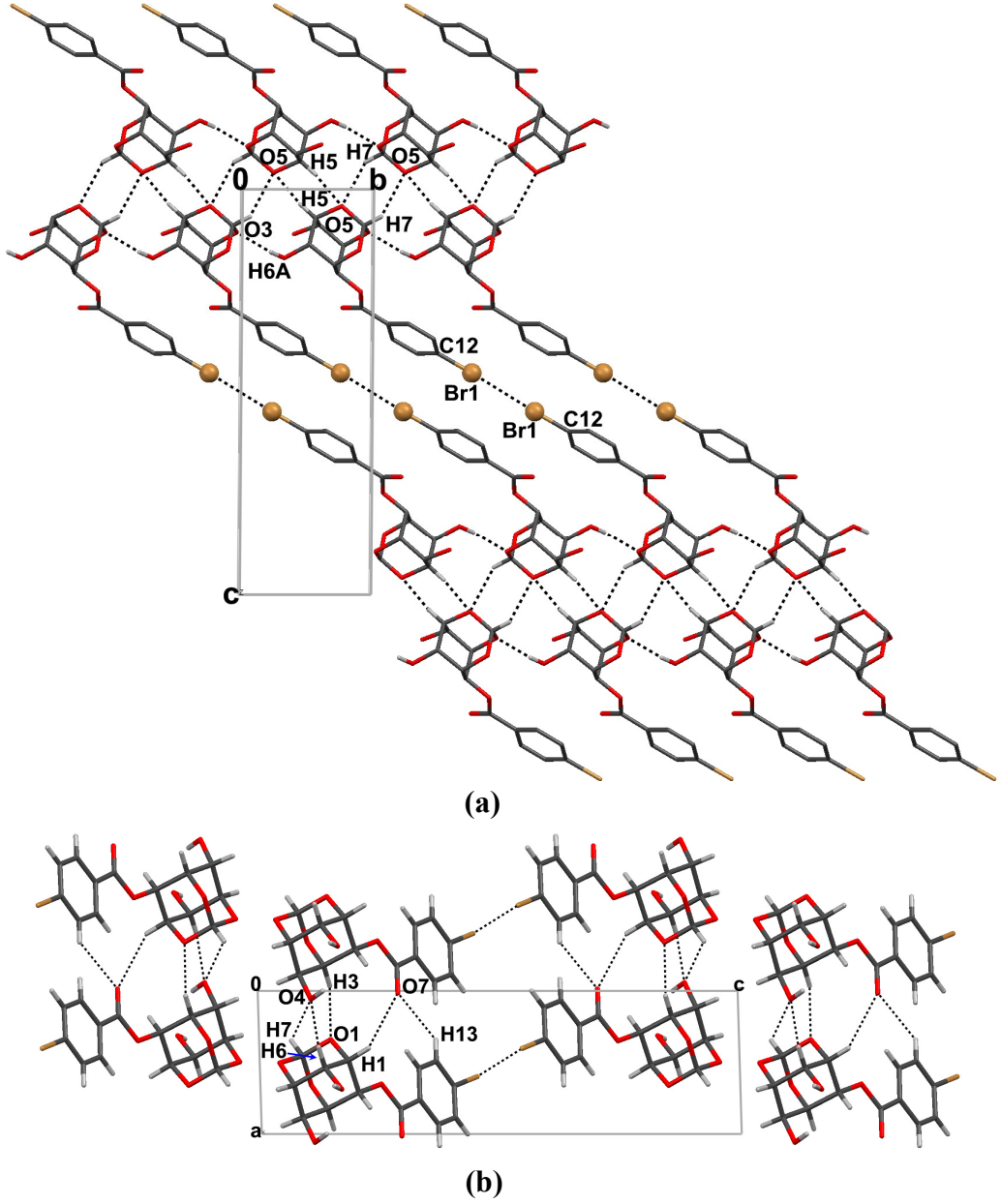

Figure 4B.3.6 Molecular packing in crystals of **2.20**: (a) bilayers linked by halogen-halogen interactions and (b) interlinking of adjacent bilayers by C-H···O interactions. Some hydrogen atoms not involved in hydrogen bonding have been omitted for the sake of clarity.

Table 4B.3.1 Hydrogen bonding interactions in the mono-esters.

Crystal	D-H···A	D-H (Å)	H···A (Å)	D···A (Å)	D-H···A (°)
	O6-H6A···O13^{xiii}	0.83(4)	1.86(4)	2.686(4)	178(6)
	O11-H11A···O15^{iv}	0.89(4)	1.86(4)	2.732(4)	169(3)
	O13-H13A···O4	0.86(5)	2.37(4)	3.011(4)	131(3)
	O15-H15A···O1^{v}	0.83(7)	2.36(7)	3.138(5)	157(7)
	O15-H15B···O14	0.85(5)	2.01(5)	2.860(5)	171(5)
	C4-H4···O12^{xviii}	0.98	2.53	3.345(5)	140
	C10-H10···O7^{v}	0.98	2.46	3.403(4)	161
	C14-H14···O3^{iv}	0.98	2.49	3.281(4)	138
	C16-H16···O4^{xix}	0.98	2.48	3.420(5)	160
2.16	O4-H4A···O7^{x}	0.84(3)	2.10(3)	2.849(2)	149(2)
	C3-H3···O6^{xi}	0.98	2.48	3.229(2)	133
	C5-H5···O4^{x}	0.98	2.59	3.428(2)	144
	C7-H7···O7^{iii}	0.98	2.50	3.270(3)	136
	C13-H13···O1^{xii}	0.93	2.60	3.331(2)	136
2.20	O6-H6A···O3^{iii}	0.81(3)	1.99(3)	2.786(3)	169(3)
	C1-H1···O7^{xiii}	0.98	2.53	3.393(3)	147
	C3-H3···O1^{v}	0.98	2.60	3.560(3)	167
	C6-H6···O4^{xiii}	0.98	2.38	3.351(3)	169
	C7-H7···O4^{xiv}	0.98	2.47	3.238(3)	135
	C13-H13···O7^{xiv}	0.93	2.50	3.300(4)	144
	Br1···Br1^{xvii}			3.492(2)	172
2.21	O4-H4A···O1^{iii}	0.85(3)	1.95(3)	2.788(2)	169(3)
	C3-H3···O7^{xv}	0.98	2.53	3.398(3)	147
	C4-H4···O6^{xv}	0.98	2.39	3.360(2)	169
	C7-H7···O6^{xvi}	0.98	2.47	3.232(2)	135
	C13-H13···O7^{xvi}	0.93	2.50	3.302(3)	144
	Cl1···Cl1^{xvii}			3.315(2)	171

Note: Intra-molecular hydrogen bonding between the hydroxyl groups was observed in the diols but is not included in the present discussion.

Symmetry codes: (i) $-x + 1, y + 1/2, -z + 1/2$; (ii) $-x, y + 1/2, -z + 1/2$; (iii) $x, y - 1, z$; (iv) $-x + 1, y - 1/2, -z + 1/2$; (v) $x + 1, y, z$; (vi) $-x + 1, y + 1/2, -z + 1/2$; (vii) $x + 1/2, -y + 1/2, -z$; (viii) $-x, y - 1/2, -z + 1/2$; (ix) $x - 1/2, -y + 1/2, -z$; (x) $-x + 1/2, y - 1/2, z + 1/2$; (xi) $x, y, z - 1$; (xii) $-x, -y + 1, z - 1/2$; (xiii) $x - 1, y, z$; (xiv) $x - 1, y + 1, z$; (xv) $x + 1, y, z$; (xvi) $x + 1, y + 1, z$; (xvii) $-x + 1, -y + 4, -z + 1$; (xviii) $-x + 3/2, -y + 1, z - 1/2$; (xix) $-x + 3/2, -y + 1, z - 1/2$.

4B.3.2 Solid-state reactivities of 2.16 and 2.20

The *p*-toluate diol **2.16** reacted in the solid-state in the presence of sodium carbonate yielding the diester **2.15**, the triol **2.1** and the triester **2.17** (Scheme 4B.3.1). Scrutiny of its crystal structure reveals that the O6-H6A hydroxyl group makes a short O…C=O contact with the carbonyl carbon C8 of a unit translated molecule along the *c*-axis. The contact is in fact an electrophile (El) - nucleophile (Nu) interaction with the distance separating them 2.909(3) Å and the angle of approach of Nu towards El, O6…C8=O7 is 87.1° (Table 4B.3.2). These values correspond well with those observed for the reactive dibenzoates,[28c] and the distance between the electrophilic and nucleophilic centers is lesser than the sum of their van der Waals radii.

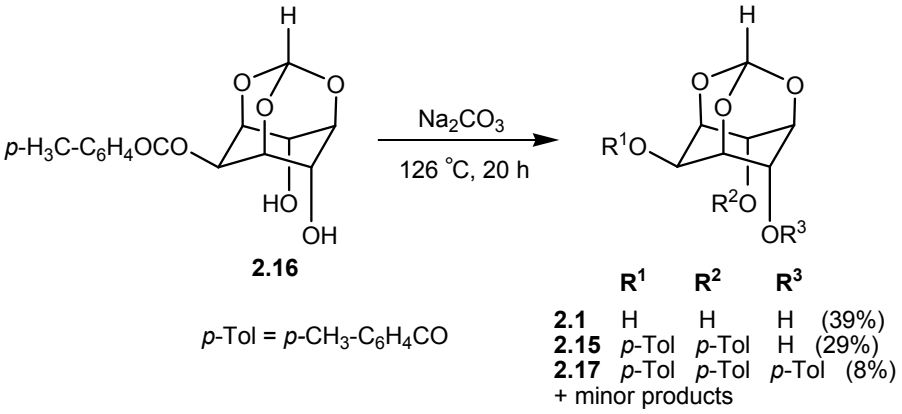

Scheme 4B.3.1 Solid-state reactivity of **2.16**.

p-Toluoyl group transfer is initiated in the presence of the base and the equatorial ester migrates to the axial position of the next molecule, thereby forming the diester **2.15** and the triol **2.1**. Since the acyl transfer is favoured between unit translated molecules due to their El-Nu geometry (Fig. 4B.3.7a), a route for the propagation of the reaction through the crystal cannot be easily visualized. It is possible that the reaction occurs in localized pockets in the crystal between the unit translated molecules, which can account for the formation of the triester and other minor products. While crystals of the diester **2.15** were found to be unreactive in the solid-state (discussed in chapter 3), the crystallinity and reactivity of the diester formed *in situ* in this reaction cannot be easily determined. It is therefore reasonable to conclude that the reactivity observed is a consequence of the excellent El-Nu geometry in the crystals of **2.16** as compared to the analogous geometry in **1.183** and **1.185** (Table 4B.3.2). It was also observed that the reaction when carried out at a lower temperature

for a longer period of time, yielded several products, whereas it was more specific when conducted at a higher temperature.

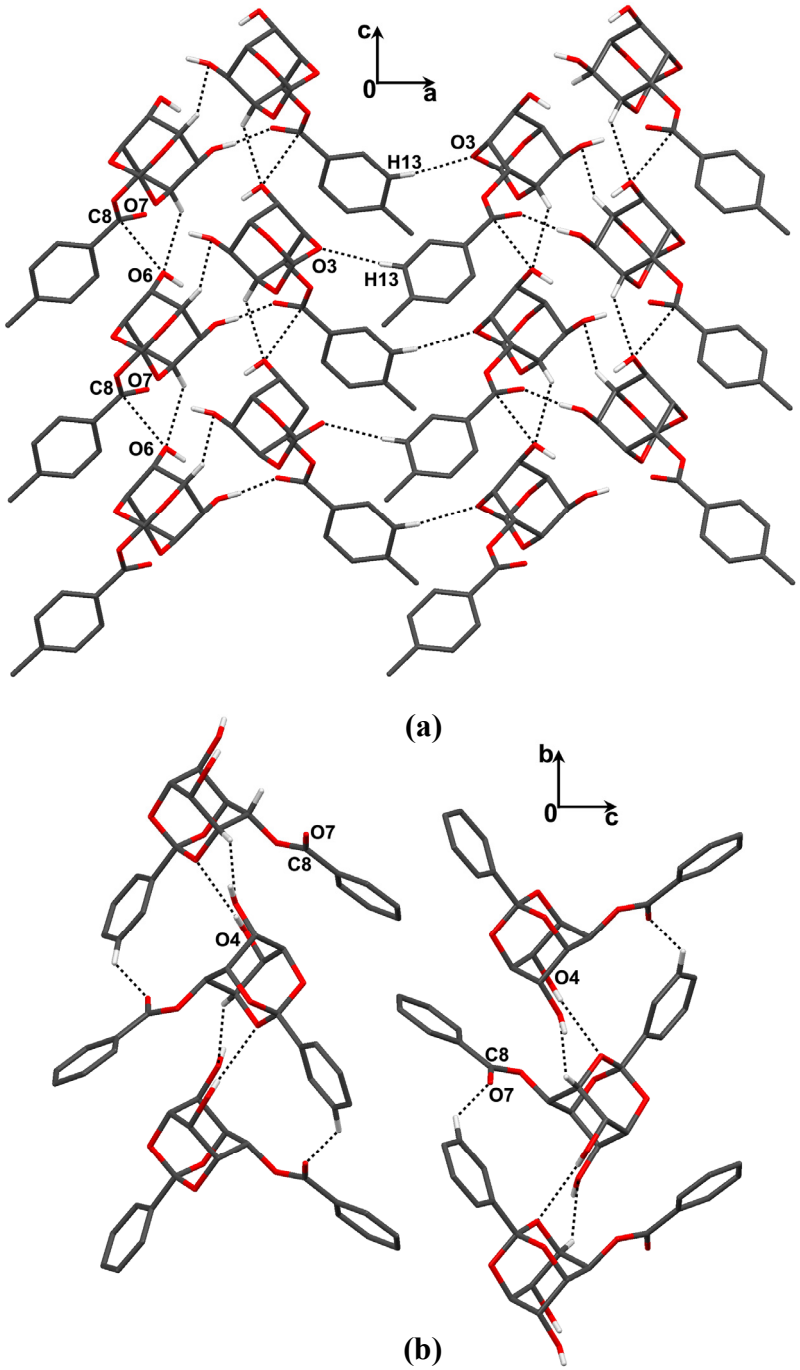

Figure 4B.3.7 El-Nu geometry in crystals of: (a) **2.16**, view of molecular packing down the *b*-axis shows the reactive centres. Chains of screw-related molecules are linked by C-H···O interactions along the *a*-axis. El-Nu geometry in crystals of (b) **1.185** shows hydrogen bonded 2_1-screw related molecules along *b*-axis. Some hydrogen atoms not involved in hydrogen bonding have been omitted for clarity.

Table 4B.3.2 Electrophile-nucleophile geometry in diols **1.183**, **1.185** and **2.16**.

Crystal	N…C=O	N…C=O (Å)	∠ N…C=O (°)	Diester yield (%)
1.183	O4...C15(C8)=O8(O7)^{i}	3.628(2)	105.6	10
1.185	O4...C15(C8)=O8(O7)^{ii}	3.532(3)	106.1	-
2.16	O6…C8=O7^{iii}	2.909(3)	87.1	29

Symmetry codes: (i) $-x + 1, y + 1/2, -z + 1/2$; (ii) $x - 1/2, -y + 1/2, z + 1/2$; (iii) $x, y, z + 1$.

On the other hand, the diol **2.20** upon reaction in the solid-state, yielded a mixture of several products amongst which the diester **2.5**, the triester **2.6** and unreacted **2.20** were identified by TLC analysis. Examination of the crystal structure of diols **2.20** and **2.21** reveals that the bilayer-like packing (Fig. 4B.3.6a) of the molecules is such that it does not bring the hydroxyl group and the carbonyl group of adjacent molecules in the proper orientation for reaction. The distance between potential reactive centres (-OH and C=O) in the nearest neighbouring molecules exceeds 5 Å, which along with a molecular organization that does not help in propagation of the reaction, precludes the possibility of a clean solid-state reaction and results in a mixture of products.

4B.4 Conclusions

The diols **2.16, 2.20, 2.21** and **1.183** have similar molecular structures, differing only in the substitutions at the *para* position in the aromatic ring, but the molecular pre-organization in the crystals vary greatly. The organization of the molecules of these monoesters in their crystals affects their reactivity to different extent.While **1.183** and **1.185** yielded a mixture of products in the solid-state, the reaction in crystals of **2.16** was more specific attributed to better El-Nu geometry in its crystals. Furthermore, increase in the specificity of the reaction with increase in temperature could be due to the lowering of activation energy required for the acyl transfer and the favourable geometry of the reactive centres. However, the extent of conversion of **2.16** to products in not high, perhaps due to the lack of reaction channels that allow domino type of reaction in crystals. In contrast the molecules in **2.20** and **2.21** associate in a fashion which does not bring the El and Nu in the required pre-organization for

reaction, perhaps due to the interplay of other weak interactions in the crystal. The results presented in this section show that compounds that are inert in solution can display reactivity in the solid-state due to the improved relative geometry of the reacting groups and due to the inflexibility of molecular movement enforced by the packing forces in the crystal lattice. A comparison of the crystal structures and reactivity of the mono acylated and di acylated inositol orthoesters reveal the necessity of reaction channels that allow domino type of reaction in crystals, to achieve specificity and high extent of conversion of reactants to products. A study of molecular pre-organization through weak interactions in structurally related compounds containing electrophilic and nucleophilic groups and their reactivities can aid in designing molecules and growing crystals which react to give specific products in good yield.

References

1. (*a*) J. D. Dunitz, *Acta Crystallogr. Sect. B: Struct. Sci.*, **1995**, *51*, 619-631; (*b*) G. R. Desiraju, *Science*, **1996**, *278*, 404-405; (*c*) J. A. R. P. Sarma and G. R. Desiraju, *Crystal Engineering: Polymorphism and Pseudopolymorphism in Organic Crystals: A Cambridge Structural Database Study*, ed. S. R. Seddon and M. Zaworotko, Kluwer, Norwell, MA, USA, 1999; (*d*) T. Threlfall, *Org. Process Res. Dev.*, **2000**, *4*, 384-390; (*e*) J. Bernstein, *Polymorphism in Molecular Crystals*, Oxford University Press, Oxford, UK, 2002; (*f*) R. K. R. Jetti, R. Boese, J. A. R. P. Sarma, L. S. Reddy, P. Vishweshwar and G. R. Desiraju, *Angew. Chem., Int. Ed. Engl.*, **2003**, *42*, 1963-1967; (*g*) A. Kálmán, *Acta Crystallogr. Sect. B: Struct. Sci.*, **2005**, *61*, 536-547; (*h*) K. Manoj, R. G. Gonnade, M. M. Bhadbhade and M. S. Shashidhar, *Cryst. Growth Des.*, **2006**, *6*, 1485-1492; (*i*) A. Kálmán and L. Fábián, *Acta Crystallogr. Sect. B: Struct. Sci.*, **2007**, *63*, 411-417; (*j*) K. Manoj, R. G. Gonnade, M. M. Bhadbhade and M. S. Shashidhar, *CrystEngComm*, **2009**, *11*, 1022-1029; (*k*) R. G. Gonnade, M. M. Bhadbhade and M. S. Shashidhar, *CrystEngComm*, **2010**, *12*, 478-484.
2. (*a*) M. D. Cohen and G. M. J. Schmidt, *J. Chem. Soc.*, **1964**, 1996-2000; (*b*) M. D. Cohen, G. M. J. Schmidt and F. I. Sonntag, *J. Chem. Soc.*, **1964**, 2000-2013; (*c*) I. Abdelmoty, V. Buchholz, L. Di, C. Guo, K. Kowitz, V. Enkelmann, G. Wegner and B. M. Foxman, *Cryst. Growth Des.*, **2005**, *5*, 2210-2217; (*d*) R. C. Nieuwendaal, M. Bertmer and S. E. Hayes, *J. Phys.*

Chem. B, **2008**, *112*, 12920-12926; (*e*) I. Fonseca, S. E. Hayes, B. Blumich and M. Bertmer, *Phys. Chem. Chem. Phys.*, **2008**, *10*, 5898-5907.

3. X. Chen, K. R. Morris, U. J. Griesser, S. R. Byrn and J. G. Stowell, *J. Am. Chem. Soc.*, **2002**, *124*, 15012-15019.
4. D. Braga, M. Cadoni, F. Grepioni, L. Maini and K. Rubini, *CrystEngComm*, **2006**, *8*, 756-763.
5. S. V. Evans, N. Omkaram, J. R. Scheffer and J. Trotter, *Tetrahedron Lett.*, **1986**, *27*, 1419-1422.
6. B. M. Foxman and H. Mazurek, *Inorg. Chim. Acta*, **1982**, *59*, 231-235.
7. (*a*) Q. Yang, M. R. Richardson and J. D. Dunitz, *J. Am. Chem. Soc.*, **1985**, *107*, 5535-5537; (*b*) C. Näther, N. Nagel, H. Bock, W. Seitz and Z. Havlas, *Acta Crystallogr., Sect. B: Struct. Sci.*, **1996**, *52*, 697-706; (*c*) J. Bernstein, R. Davey and O. Henck, *Angew. Chem., Int. Ed. Engl.*, **1999**, *38*, 3440-3461; (*d*) A. W. Newman and S. R. Byrn, *Drug Discovery Today*, **2003**, *8*, 898-905; (*e*) L. X. Yu, M. S. Furness, A. Raw, K. P. Outlaw, N. E. Nashed, E. Ramos, S. P. Miller, R. C. Adams, F. Fang, Jr, R. M. Patel, F. O. Holcombe, Y. Y. Chiu and A. S. Hussain, *Pharmacol. Res.*, **2003**, *20*, 531-536; (*f*) D. Braga and F. Grepioni, *Making Crystals by Design: Methods, Techniques and Applications*, Wiley-VCH, Weinheim, 2007.
8. (*a*) L. Pauling, R. B. Corey and H. R. Branson, *Proc. Natl. Acad. Sci. U. S. A.*, **1951**, *37*, 205-211; (*b*) J. D. Watson and F. H. C. Crick, *Nature*, **1953**, *171*, 737-738; (*c*) A. Rich and F. H. C. Crick, *Nature*, **1955**, *176*, 915-916; (*d*) K. P. Meurer and F. P. Vögtle, *Top. Curr. Chem.*, **1985**, *127*, 1-176.
9. (*a*) I. Sato, R. Yamashima, K. Kadowaki, J. Yamamoto, T. Shibata and K. Soai, *Angew. Chem.*, **2001**, *113*, 1130-1132; (*b*) J. L. Zhou, Y. X. Wang, Y. Wang, Y. L. Song, H. G. Zheng, Y. Z. Li, L. P. Yang and X. Q. Xin, *CrystEngComm*, **2003**, *5*, 62-64; (*c*) M. Reggelin, S. Doerr, M. Klussmann, M. Schultz and M. Holbach, *Proc. Natl. Acad. Sci. U. S. A.*, **2004**, *101*, 5461-5466; (*d*) M. Toda and F. Tanaka, *Macromolecules*, **2005**, *38*, 561-570; (*e*) Y. Okamoto, *J. Polym. Sci., Part A: Polym. Chem.*, **2009**, *47*, 1731-1739.
10. (*a*) M. Albrecht, *Chem. Rev.*, **2001**, *101*, 3457-3498; (*b*) M. J. Hannon and L. Childs, *J. Supramol. Chem.*, **2004**, *16*, 7-22; (*c*) M. Albrecht, *Angew. Chem. Int. Ed.*, **2005**, *44*, 6448-6451; (*d*) C. Piguet, M. Borkovec, J. Hamacek and K. Zeckert, *Coord. Chem. Rev.*, **2005**, *249*, 705-726.

11. (*a*) J. J. L. M. Cornelissen, A. E. Rowan, R. J. M. Nolte and N. A. J. M. Sommerdijk, *Chem. Rev.*, **2001**, *101*, 4039-4070; (*b*) T. Nakano and Y. Okamoto, *Chem. Rev.*, **2001**, *101*, 4013-4038.
12. (*a*) W. E. Allen, C. J. Fowler, V. M. Lynch and J. L. Sessler, *Chem. Eur. J.*, **2001**, *7*, 721-729; (*b*) M. Nayak, R. Koner, H. Stoeckli-Evans and S. Mohanta, *Cryst. Growth Des.*, **2005**, *5*, 1907-1912; (*c*) D. G. Lonnon, S. B. Colbran and D. C. Craig, *Eur. J. Inorg. Chem.*, **2006**, 1190-1197; (*d*) D.-R. Xiao, E.-B. Wang, H.-Y. An, Y.-G. Li and L. Xu, *Cryst. Growth Des.*, **2007**, *7*, 506-512.
13. (*a*) V. K. Praveen, S. S. Babu, C. Vijayakumar, R. Varghese and A. Ajayaghosh, *Bull. Chem. Soc. Jpn.*, **2008**, *81*, 1196-1211; (*b*) J.-C. Xiao, J.-L. Xu, S. Cui, H.-B. Liu, S. Wang and Y.-L. Li, *Org. Lett.*, **2008**, *10*, 645-648; (*c*) F. Dumitru, Y.-M. Legrand, A. V. Lee and M. Barboiu, *Chem. Commun.*, **2009**, 2667-2669.
14. (*a*) S. H. Gellman, *Acc. Chem. Res.*, **1998**, *31*, 173-180; (*b*) P. Dapporto, P. Paoli and S. J. Roelens, *J. Org. Chem.*, **2001**, *66*, 4930-4933; (*c*) Y. Furusho and E. Yashima, *Chem. Rec.*, **2007**, *7*, 1-11.
15. (*a*) J. Sanchez-Quesada, C. Seel, P. Prados and J. Mendoza, *J. Am. Chem. Soc.*, **1996**, *118*, 277-278; (*b*) J. Keegan, P. E. Kruger, M. Nieuwenhuyzen, J. O'Brien and N. Martin, *Chem. Commun.*, **2001**, 2192-2193; (*c*) S. J. Coles, J. G. Frey, P. A. Gale, M. B. Hursthouse, M. E. Light, K. Navakhun and G. L. Thomas, *Chem. Commun.*, **2003**, 568-569; (*d*) K. J. Chang, B. N. Kang, M. H. Lee and K. S. Jeong, *J. Am. Chem. Soc.*, **2005**, *127*, 12214-12215; (*e*) P. Byrne, G. O. Lloyd, K. M. Anderson, N. Clarke and J. W. Steed, *Chem. Commun.*, **2008**, 3720-3722; (*f*) H. Juwarker, J. M. Lenhardt, D. M. Pham and S. L. Craig, *Angew. Chem., Int. Ed.*, **2008**, *47*, 3740-3743.
16. (*a*) E. van der Voort, *J. Cryst. Growth*, **1991**, *110*, 662-668; (*b*) K. J. Roberts, J. N. Sherwood and C. S. Yoon, *Chem. Mater.*, **1994**, *6*, 1099-1102; (*c*) H. A. Garekani, F. Sadeghi, A. Badiee, S. A. Mostafa and A. R. Rajabi-Siahboomi, *Drug Dev. Ind. Pharm.*, **2001**, *27*, 803-809; (*d*) J. Chen, J. Wang, J. Ulrich, Q. Yin and L. Xue, *Cryst. Growth Des.*, **2008**, *8*, 1490-1494; (*e*) S. M. Assaf, M. S. Khanfar, R. Obeidat, M. S. Salem and A. I. Arida, *Jordan J. Pharm. Sci.*, **2009**, *2*, 150-158; (*e*) I. Hod, Y. Mastai and D. D. Medina, *CrystEngComm.*, **2011**, *13*, 502-509.

17. A. Shivanyuk, J. C. Friese, S. Doring and J. Rebek, Jr. *J. Org. Chem.*, **2003**, *68*, 6489-6496.
18. P. O. Brown, G. D. Enright and J. A. Ripmeester, *Cryst. Growth Des.*, **2006**, *6*, 719-725.
19. G. Dyker, M. Mastalerz, I. M. Müller, K. Merz and K. Koppe, *Eur. J. Org. Chem.*, **2005**, 4963-4966.
20. I. M. R. Lande, T. E. Souza, R. S. Correa, F. T. Martins and A. C. Doriguetto, *Acta Crystallogr. Sect. C.*, **2010**, *66*, o463-o465.
21. N. Pérez-Hernández, D. Fort, C. Pérez and J. D. Martín, *Cryst. Growth Des.*, **2011**, dx.doi.org/10.1021/cg101227u.
22. H. Takahagi, S. Fujibe and N. Iwasawa, *Chem. Eur. J.*, **2009**, *15*, 13327-13330.
23. C. Tedesco, L. Erra, I. Immediata, C. Gaeta, M. Brunelli, M. Merlini, C. Meneghini, P. Pattison and P. Neri, *Cryst. Growth Des.*, **2010**, *10*, 1527-1533.
24. (*a*) C. Tan, M. R. Pinto, M. E. Kose, I. Ghiviriga and K. S. Schanze, *Adv. Mater.*, **2004**, *16*, 1208-1212; (*b*) Y. Huang, Q. Fan, X. Liu, N. Fu and W. Huang, *Langmuir*, **2010**, *26*, 19120-19128.
25. Y. Liu, Y. Xin, F. Bai, S. Xu and S. Cao, *Polym. Adv. Technol.*, **2006**, *17*, 199-203.
26. K. Harata, H. Hirayama and K. Uekama, *Carb. Res.*, **2000**, *329*, 597-607.
27. (*a*) D. Blow, *Nature*, **1990**, *343*, 694-695; (*b*) J. A. Brannigan, D. Dodson, H. J. Duggleby, P. C. E. Moody, J. L. Smith, D. R. Tomchick and A. G. Murzin, *Nature*, **1995**, *378*, 416-419.
28. (*a*) T. Praveen, U. Samanta, T. Das, M. S. Shashidhar and P. Chakrabarti, *J. Am. Chem. Soc.*, **1998**, *120*, 3842-3845; (*b*) M. P. Sarmah, R. G. Gonnade, M. S. Shashidhar and M. M. Bhadbhade, *Chem. Eur. J.*, **2005**, *11*, 2103-2110; (*c*) C. Murali, M. S. Shashidhar, R. G. Gonnade and M. M. Bhadbhade, *Eur. J Org. Chem.*, **2007**, 1153-1159.
29. R. G. Gonnade, M. M. Bhadbhade and M. S. Shashidhar, *CrystEngComm*, **2008**, *10*, 288-296.
30. Bruker 2003. SADABS (Version 2.05), SMART (Version 5.631) and SAINT (Version 6.45). Bruker AXS Inc., Madison, Wisconsin, USA.
31. G. M. Sheldrick, *Acta Crystallogr., Sect. A: Found. Crystallogr.*, **2008**, *64*, 112-122.

32. L. J. Farrugia, *J. Appl. Crystallogr.*, **1997**, *30*, 565.
33. C. F. Macrae, P. R. Edgington, P. McCabe, E. Pidcock, G. P. Shields, R. Taylor, M. Towler and J. van de Streek, *J. Appl. Crystallogr.*, **2006**, *39*, 453-457.
34. A. L. Spek, *J. Appl. Crystallogr.*, **2003**, *36*, 7-13.
35. (*a*) S. Chantrapromma, B. Jindawong, H.-K. Fun, S. Anjum and C. Karalai, *Acta Crystallogr., Sect. E: Struct. Rep. Online*, **2005**, *61*, o2096-o2098; (*b*) R. J. Santos-Contreras, F. J. Martinez-Martinez, E. V. Garcia-Baez, I. I. Padilla-Martinez, A. L. Peraza and H. Hopfl, *Acta Crystallogr., Sect. C: Cryst. Struct. Commun.*, **2007**, *63*, o239-o242; (*c*) M. Kubicki, W. Pruka1a and B. Marciniec, *Acta Crystallogr., Sect. C: Cryst. Struct. Commun.*, **2007**, *63*, o754o757; (*d*) W. Pruka1a, D. Pruka1a and M. Kubicki, *Acta Crystallogr., Sect. C: Cryst. Struct. Commun.*, **2008**, *64*, o269-o271.
36. (*a*) L. Fabian, A. Argay, A. Kalman and M. Bathori, *Acta Crystallogr., Sect. B: Struct. Sci.*, **2002**, *58*, 710-720; (*b*) L. Fabian and A. Kalman, *Acta Crystallogr., Sect. B: Struct. Sci.*, **2004**, *60*, 547-558; (*c*) G. V. Bhosekar, C. Murali, R. G. Gonnade, M. S. Shashidhar and M. M. Bhadbhade, *Cryst. Growth Des.*, **2005**, *5*, 1977-1982.
37. (*a*) G. R. Desiraju, *Acc. Chem. Res.* **2002**, *35*, 565-573; (*b*) J. A. van den Berg and K. R. Seddon, *Cryst. Growth Des.* **2003**, *3*, 643-661; (*c*) I. Hyla-Kryspin, G. Haufe and S. Grimme, *Chem. Eur. J.* **2004**, *10*, 3411-3422.
38. P. Metrangolo, G. Resnati, T. Pilati and S. Biella, *Halogen Bonding Fundamentals and Applications*, ed. P. Metrangolo and G. Resnati, Springer, Berlin, 2008.
39. G. R. Desiraju and R. Parthasarathy, *J. Am. Chem. Soc.*, **1989**, *111*, 8725-8726.
40. (*a*) G. R. Desiraju, *Angew. Chem., Int. Ed. Engl.*, **1995**, *34*, 2311-2327; (b) D. S. Reddy, D. C. Craig and G. R. Desiraju, *J. Am. Chem. Soc.*, **1996**, *118*, 4090-4093; (c) M. D. Prasanna and T. N. Guru Row, *CrystEngComm*, **2000**, *2*, 134-140; (d) R. K. R. Jetti, A. Nangia, F. Xue and T. C. W. Mak, *Chem. Commun.*, **2001**, 919-920; (e) I. Saraogi, V. G. Vijay, S. Das, K. Sekar and T. N. Guru Row, *Cryst. Eng.*, **2003**, *6*, 69-77.
41. C. A. Hunter and J. K. M. Sanders, *J. Am. Chem. Soc.*, **1990**, *112*, 5525-5534.

42. C. Murali, M. S. Shashidhar, R. G. Gonnade and M. M. Bhadbhade, *Chem. Eur. J.*, **2009**, *15*, 261-269.
43. T. M . McPhillips, S. E. McPhillips, H. J. Chiu, A. E. Cohen, A. M. Deacon, P. J. Ellis, E. Garman, A. Gonzalez, N. K. Sauter, R. P. Phizackerley, S. M. Soltis, and P. Kuhn, *J. Synchrotron Rad.*, **2002**, *9*, 401-406.
44. K. M. Sureshan and M. S. Shashidhar, *Tetrahedron Lett.* **2000**, *41*, 4185-4188.
45. R. G. Gonnade, M. S. Shashidhar and M. M. Bhadbhade, *Chem. Commun.* **2004**, 2530-2531.
46. (*a*) T. Kawasaki, K. Jo, H. Igarashi, I. Sato, M. Nagano, H. Koshima and K. Soai, *Angew. Chem. Int. Ed*., **2005**, *44*, 2774-2777; (*b*) T. Kawasaki, K. Suzuki, K. Hatase, M. Otsuka, H. Koshima and K. Soai, *Chem. Commun*., **2006**, 1869-1871; (*c*) M. Sakamoto, S. Kobaru, T. Mino and T. Fujita, *Chem. Commun*., **2004**, 1002 -1003.
47. (*a*) R. D. Wampler, N. J. Begue and G. J. Simpson, *Cryst. Growth Des.*, **2008**, *8*, 2589-2594; (*b*) H. Koshima, Y. Wang and T. Matsuura, *Mol. Cryst. Liq. Cryst.*, **1996**, *277*, 63-71.
48. V. R. Pedireddi, D. S. Reddy, B. S. Goud, D. C. Craig. A. D. Rae and G. R. Desiraju, *J. Chem. Soc. Perkin Trans 2*, **1994**, 2353-2360.

Chapter 5

Acyl group migration in crystals: scrutiny of literature reports and conclusions

The important thing in science is not so much to obtain new facts as to discover new ways of thinking about them.

-William Lawrence Bragg

5.1 Introduction

The preceding chapters in this thesis correlated the crystal structures of various acylated *myo*-inositol orthoester derivatives with their solid-state acyl transfer reactivity, including the effect of polymorphism, solvatomorphism and thermally induced phase changes on the course of the reaction. A comprehensive study of the crystal structures and the geometry of the reacting molecules in acylated *myo*-inositol derivatives leads to the conclusion that a facile intermolecular acyl transfer occurs in crystals which have pre-organization of molecules that (a) brings an electrophile (El, C=O) and the nucleophile (Nu, -OH) in favourable geometry, (b) favours supporting weak interactions which stabilize the migrating benzoyl group in proper orientation for the nucleophilic attack, and (c) function as reaction channels and facilitate a domino type of reaction to ensure high convertibility of reactants to products. While crystals which did not possess a helical molecular assembly did not react or yielded a mixture of products in the solid-state, deviation from favourable reactive geometry between the electrophile and nucleophile (solvates of **2.5**, **2.7** and **2.22**) and absence of reaction channels in the crystals (**1.178II**) also resulted in loss of specificity and low conversion of reactant to products.

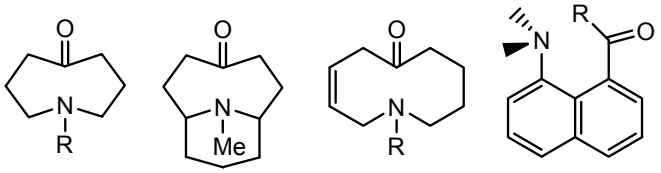

5.1 **5.2** **5.3** **5.4**

Scheme 5.1 Molecules investigated by Burgi and Dunitz to arrive at geometrical parameters for El...Nu interactions in their crystals.

A survey of the literature on structure correlation for reactions involving nucleophilic addition to the carbonyl center reveals the observations of Bürgi and co-workers, who studied the crystal structures of compounds containing an electrophile (C=O) and a nucleophile (NR_3), within the same molecule. On the basis of theoretical calculations and experimental results (in the form of distances obtained from crystal structures) they arrived at the conclusion that a decrease in the N…C=O distance is accompanied by an increase in non-planarity at the carbonyl carbon and a slight lengthening of the C=O bond distance. Molecules of types **5.1** – **5.4** (Scheme 5.1) have N…C=O distances in the range of ~1.5 - ~3.0 Å and the angle of approach of the nucleophile

towards the electrophile is ~105° and not perpendicular to the carbonyl center.[1] Theoretical calculations were carried out for various nuclear arrangements of a model system involving the addition of hydride ion to formaldehyde yielding the methanolate ion[2] (Eqn. 5.1).

$$CH_2O + H^- \longrightarrow CH_3O^- \qquad \textbf{Eqn. 5.1}$$

These along with experimental results (from crystal data) indicated that the N…C=O and O…C=O angles are in the range 105 ± 5° for all distances smaller than 2.5 Å between the electrophile and the nucleophile.[2] Hydroxy acids with intramolecular O...C=O angles of ~98° show the highest rate of intramolecular lactonization[3] and Bender also postulated that a perpendicular approach of the nucleophile to the π-electron system should be preferred over a coplanar approach in order to maximise overlap between the nucleophile and π-electrons of the carboxyl bond in intramolecular lactonization.[4] In the following sections, electrophile-nucleophile geometry in reactive systems involving the carbonyl center and oxygen and nitrogen nucleophiles will be examined along with information gleaned on potential reactive crystals from the CSD.

5.2 Cambridge Structural Database (CSD) Survey on El – Nu geometry

The angle of approach of the nucleophile towards the electrophile and the distance between them in the reactive crystals of inositol orthoester derivatives lies in the range of 84 – 90º and 3.1 – 3.3 Å respectively.[5] It is interesting to note that in the crystals where the distance between the reaction centers is lesser than the sum of their van der Waals radii, the El and Nu are poised for reaction at an angle of ~ 90º. Hence, a survey of the Cambridge Structure Database (v5.31, November 2009) was undertaken for structures containing ester (or carboxylic acid) and hydroxyl functional groups (Fig. 5.2.1a). The distance (defined as a non-bonded contact) between the carbonyl carbon and hydroxyl oxygen was fixed between 2.80 – 3.30 Å (within the sum of van der Waals radii of O and C, 3.22 Å), with no restrictions on the angle between the hydroxyl oxygen and carbonyl carbon (∠O=C···O-H). A similar search was performed for structures containing a carbonyl group and a hydroxyl group (Fig. 5.2.1b). The same searches were performed in the case of nitrogen nucleophiles (Fig. 5.2.1c and 5.2.1d respectively).

The results were analyzed as scatter plots with the angle plotted along the *y*-axis and the distance along the *x*-axis.

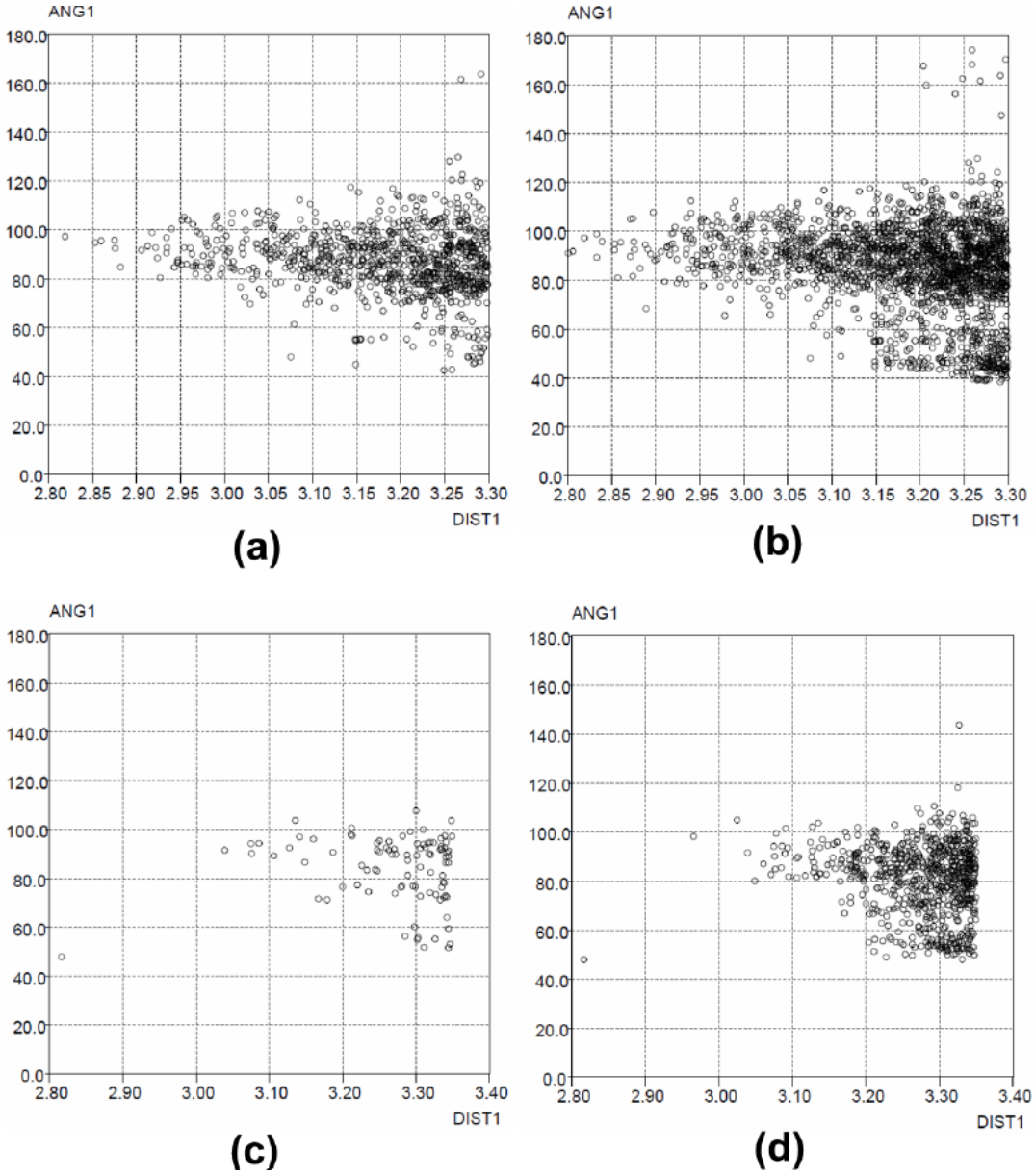

Fig. 5.2.1 Scatter plots of distance Vs. angle for hits obtained in searches of structures containing (a) ester (or acid) and hydroxyl group (b) carbonyl and hydroxyl group (c) ester (or acid) and nitrogen nucleophile (d) carbonyl and nitrogen nucleophile.

It was observed that when the distance between potential pairs of electrophiles and nucleophiles was lesser than the sum of van der Waals radii, the angle between them (O=C···O/N) approaches 90° or is clustered between 80 and 100°. This was predominantly observed in the case of oxygen nucleophiles (Fig. 5.2.1a and 5.2.1b)

and to a lesser extent in the case of nitrogen nucleophiles (Fig. 5.2.1c and 5.2.1d), perhaps due to fewer examples in the latter case. The following section deals with solid-state reactions involving an electrophile and a nucleophilic carbonyl center, and attempts to interpret the reactivity based on the electrophile-nucleophile geometry along with a final example where the reactivity was successfully predicted based on the pre-organization of the El-Nu geometry in the crystals. Molecular structures of all of these systems greatly differ from those which were investigated (in the previous chapters of this thesis) for acyl transfer reactivity and information from which was used to arrive at the necessary conditions for a facile reaction in their crystals.

5.3 Case studies

5.3.1 O → N acyl migration in *O*-acylsalicylamides

Thermally induced O → N acetyl, benzoyl and propionyl group migration in *O*-acylsalicylamides yielding the *N*-acylsalicylamides was briefly described in Chapter 1.

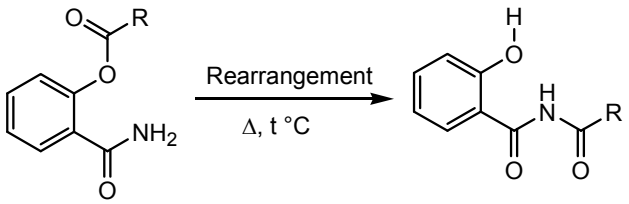

1.142 R = CH_3 t ~ 100 °C **1.145** R = CH_3
1.143 R = C_6H_5 t ~ 100 °C **1.146** R = C_6H_5
1.144 R = C_2H_5 t ~ 85 °C **1.147** R = C_2H_5

Scheme 5.3.1 Acyl migration in *O*-acylsalicylamides.

The rearrangement was earlier studied in solution and the solid-state using spectroscopic and thermoanalytical techniques[6] and later through X-ray crystallographic studies.[7] The reaction involves migration of acyl groups and N-C bond formation. Examination of the El-Nu geometry in the crystals of **1.142-1.144** reveals that the intramolecular N…C=O distance (N1…C8=O3) is shorter than the intermolecular contacts[7] and the angles of approach of the Nu towards the El are >100° in the crystals (Table 5.3.1). Since the acyl transfer in **1.142-1.144** is intramolecular and thermally induced (without the assistance of an external agent), a specific aggregation of molecules that facilitates a domino type of reaction is not required to achieve high conversion of reactant to product.

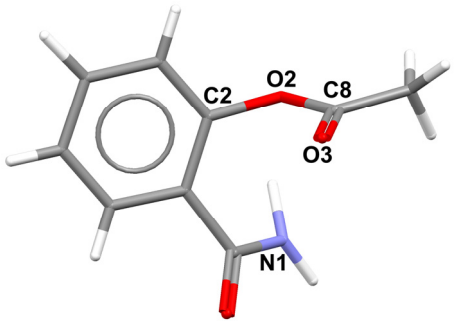

Figure 5.3.1. Electrophile-nucleophile geometry in crystals of **1.142**.

The thermal motion analysis in crystals of acetylsalicylamide indicated large internal motion between C8 and Nl which suggests that the torsional libration about the C2-O2 bond is perhaps responsible for the observed intramolecular acetyl transfer from oxygen to the amide nitrogen.[8] A comparison of the intra- and intermolecular El...Nu parameters (Table 5.3.1) clearly accounts for the non-occurrence of the intermolecular acyl transfer reaction in crystals of *O*-acylsalicylamides.

Table 5.3.1 Electrophile-nucleophile geometry in crystals of *O*-acylsalicylamides.

	1.142	**1.143**	**1.144**
Intramolecular			
N1...C8 (Å)	3.274(6)	3.528(3)	3.34
∠ N1…C8=O3 (°)	101.7	116.1	110.6
Intermolecular			
N1...C8 (Å)	3.875(5), 3.911(5)	>5.0	-
∠ N1…C8=O3 (°)	132.5, 68.4	-	-

5.3.2 Imide formation in co-crystals of amine-anhydride

Zaworotko and co-workers reported attempts towards isolation of co-crystals of carboxylic acid anhydrides and amines, with the hope of converting them to imides.[9] Most of the pairs of anhydrides and amines investigated failed to yield co-crystals but yielded imides, possibly because the rate of the reaction of amines with anhydrides was faster than co-crystal formation.

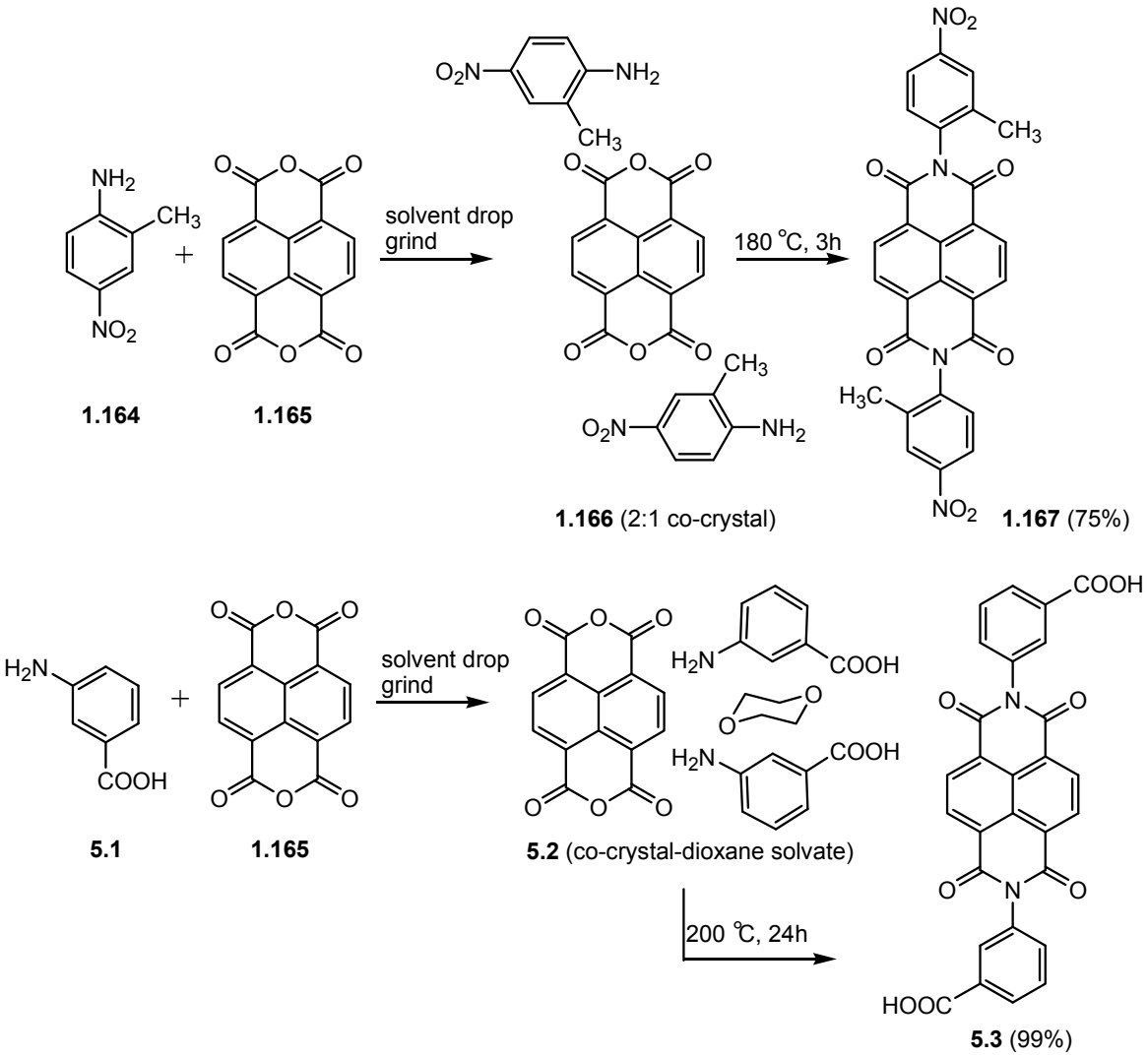

Scheme 5.3.2a Co-crystal mediated di-imide formation.

This view is supported by the fact that weakly basic 2-methyl-4-nitroaniline (**1.164**) and 1,4,5,8-naphthalenetetracarboxylic dianhydride (**1.165**) yielded isolable co-crystals (**1.166**), whose structure was determined by single crystal X-ray diffraction. The reactivity of the co-crystal **1.166** (Scheme 5.3.2a) was justified on the basis of the separation of the carbonyl carbon atom of the dianhydride **1.165** and amino nitrogen atom of the amine by 3.42 Å, which is well within the 4.2 Å limit of the topochemical postulate.[10] On the other hand, 2-amino benzoic acid (**5.1**) and dianhydride **1.165** yielded solvated co-crystals (**5.2**) but solvent-free co-crystals could not be isolated. The solvent-free co-crystals (obtained from **5.1** and **1.165**) were reported to react at ambient temperature, yielding the imide (Scheme 5.3.2a). However, the solvated crystals (**5.2**) on heating expel the solvent and react to form the imide. Since the

reaction involved nucleophilic addition to the carbonyl group, the N…C=O (Nu…El) geometry in these co-crystals was examined. The El-Nu geometry in these co-crystals does not approach closely the values obtained by experimental / theoretical studies (Sec. **5.1** and **5.2**), except in the case of N2…C7=O1 and N1…C13=O4.

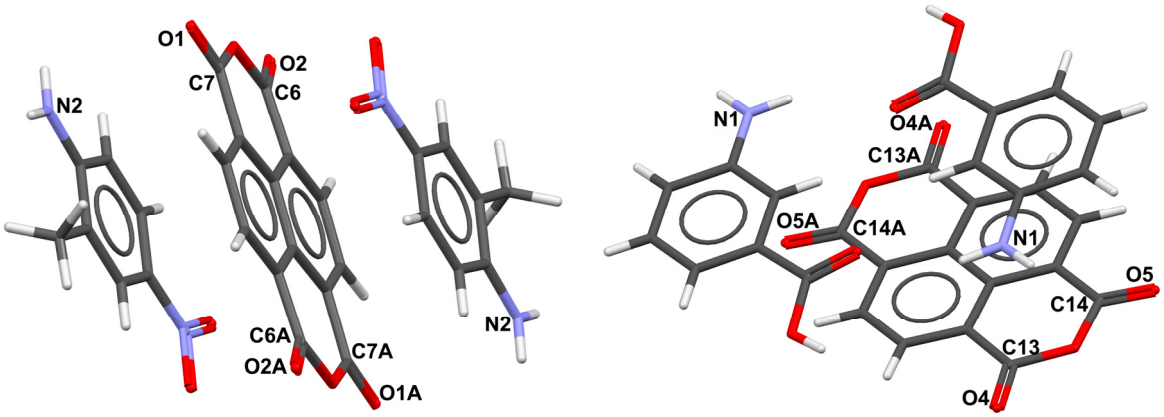

(a) **(b)**

Figure 5.3.2. Electrophile-nucleophile geometry in co-crystals: (a) **1.166** and (b) **5.2**.

Table 5.3.2 Electrophile-nucleophile geometry in dianhydride-amine co-crystals.

Co-crystal	N…C=O	N…C=O (Å)	∠ N…C=O (°)
1.166	N2…C7=O1	3.417	79.1
	N2…C6=O2	4.550	118.4
5.2	N1…C14A=O5A	3.635	70.4
	N1…C14=O5	3.565	114.8
	N1…C13A=O4A	4.752	109.9
	N1…C13=O4	3.135	103.8

The reaction between a cyclic anhydride and primary amine to form an imide is a two step process (Scheme 5.3.2b); and hence interpretation of the experimental results based on the structure of the co-crystal alone may be appropriate only to the formation of the intermediate acid - amide. Since the formation/isolation of the acid-amide is not reported, the El-Nu geometry in the co-crystal or the topochemical postulate alone cannot be used to explain the formation of the imide, in the absence of structural and thermal data of the intermediate.

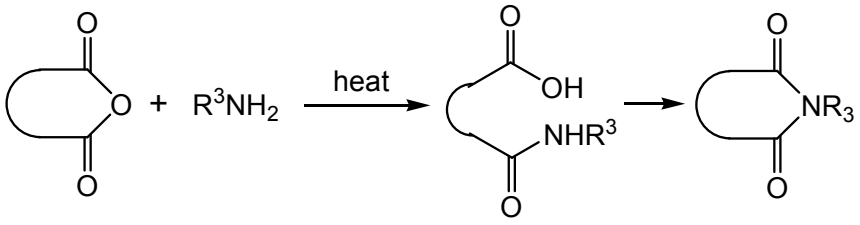

Scheme 5.3.2b Di-imide formation from primary amine and anhydride.

5.3.3 Cyclization of *o*-acetamidobenzamide

o-Acetamidobenzamide was found to crystallize in two distinct solvent-free forms (**1.154α** and **1.154β**) both of which undergo thermal solid-state reaction (Scheme 5.3.3) to give 2-methylquinazol-4-one (**1.156**).[11] The α form could be thermally transformed to the β form at 150 °C. The β form undergoes nucleophilic addition of the amide nitrogen to the acetyl carbonyl group to presumably form a tetrahedral intermediate (**1.155**), which underwent dehydration to give **1.156**. Although the physical data of the intermediate **1.155** isolated suggested it to be the tetrahedral intermediate, its structure could not be established unambiguously.

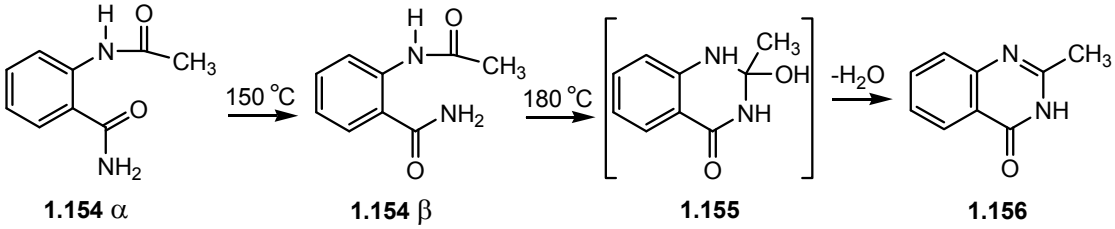

Scheme 5.3.3 Thermal dehydration-cyclization of *o*-acetamidobenzamide in its α and β crystals.

Since this solid state reaction involves the nucleophilic addition of an NH_2 group to a carbonyl group (C=O) the El…Nu parameters in the polymorphs were examined. The molecules in the crystals of **1.154α** associate through N-H...O hydrogen bonding and form dimers where the intramolecular geometry of the electrophile and nucleophile is not favorable for the reaction to occur. In the β form (**1.154β**), due to the change in the conformation of the reactive centers during the phase transition, the molecules show improved intramolecular El-Nu geometry, favorable for cyclization.

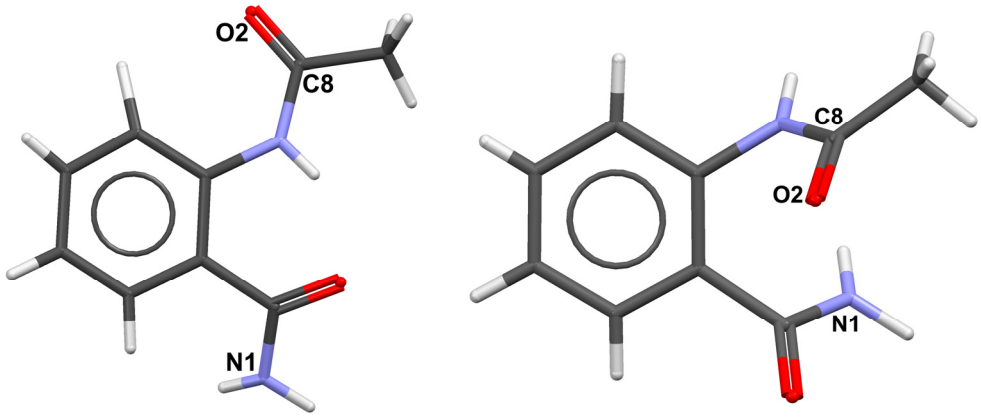

(a) **(b)**

Figure 5.3.3 Intramolecular electrophile-nucleophile geometry in the dimorphs of **1.154:** (a) α form and (b) β form.

Further a slight lengthening of the C=O bond is observed in the reactive β form (Table 5.3.3) which can be correlated with the reactivity observed. These parameters are close to the values observed in the reactive dibenzoates,[5] which correspond very well with the facility of the cyclization reaction. However, the product **1.155** of this reaction is not very stable as it loses a molecule of water fast to yield **1.156**.

Table 5.3.3 Electrophile-nucleophile geometry in polymorphs of **1.154**.

Crystal	N…C=O	N…C=O (Å)	∠ N…C=O (°)	C8=O2 (Å)
1.154α	N1...C8=O2 (intra)	5.370	131.3	1.211
1.154β	N1…C8=O2 (intra)	3.305	89.7	1.230

5.3.4 Acyl transfer in co-crystals of naphthalene diol and its di-*p*-methylbenzoate

The CSD survey (Sec. **5.2**) results yielded the structure of the co-crystal **5.4** which revealed strong O-H···O hydrogen bonding between the two components supported by C-H···O and slipped π···π stacking interactions. Since the co-crystal contains an electrophile (C=O) and a nucleophile (-OH), the geometry between potential reactive centers was examined. The distance of closest approach of a hydroxyl group to the carbonyl carbon of the *p*-toluate ester (Fig. 5.3.4) was found to be 3.166 Å (O1…C16E=O4E and O1…C15=O4) and the angle between them was

85.6° (∠O1…C16E=O4E and ∠O1…C16=O4). Although the co-crystal **5.4** was isolated and its single crystal structure determined, its reactivity in the solid state was not investigated.[12]

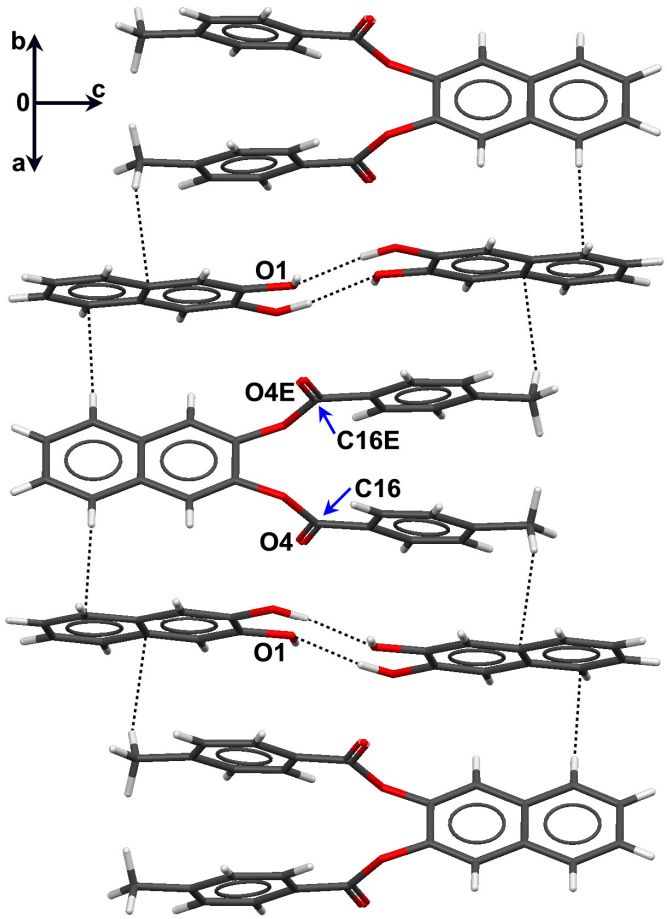

Figure 5.3.4. Electrophile-nucleophile geometry in co-crystals of **5.4**. Dotted lines indicate hydrogen bonding interactions.

Since these co-crystals exhibited good El…Nu parameters it was likely that an acyl transfer reaction could be initiated in the presence of sodium carbonate in the solid-state. The co-crystal was synthesized as reported and characterized by comparison of the unit cell parameters and melting point with that of the reported data. When the co-crystals were ground with anhydrous solid sodium carbonate and heated at 130 °C, *p*-toluoyl group transfer was observed, yielding the mono ester **5.5** and 2,3-naphthalene diol **1.161** (Scheme 5.3.4).[13] The inclusion complex of naphthalene diol and its di-*p*-methylbenzoate (**5.4**) was identified as an intermediate during the solvent-free benzoylation reaction of naphthalene diol.[12] Infrared spectroscopic monitoring of the

reaction mixture supported this possibility.

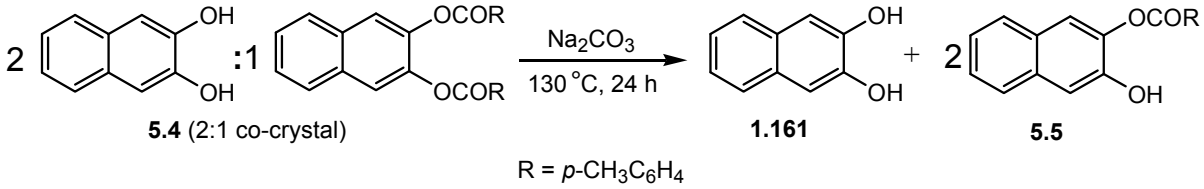

Scheme 5.3.4 Acyl transfer reactivity of co-crystal **5.4** in the presence of sodium carbonate.

As is evident from the above examples as well as the reactive benzoylated *myo*-inositol derivatives, the angle of approach of the nucleophile towards the electrophile in a reactive crystal lies in the range of 80 - 90° for an intermolecular reaction involving attack on the carbonyl centre and 100 - 116° for an intramolecular reaction. While the exact mechanism and transition state of these reactions cannot be clearly decoded at present, it appears that the El-Nu geometry in a crystal can be used as a criterion to predict the acyl transfer reactivity of the crystal. Crystals that possess a favorable rigid pre-organization of the reaction centres score over the molecular organization in dispersed phase, thereby leading to differential reactivities in the condensed and dispersed phases.

5.4 Conclusion

The experimental results, database surveys and analysis of solid-state reactions reported in literature involving the carbonyl group and an electrophile indicates that the presence of favorable electrophile-nucleophile geometry is a prerequisite for a facile reaction. Additionally in an intermolecular reaction, the presence of a reaction tunnel for propagation of the reaction through the crystals is also essential for a clean reaction and to achieve complete conversion of reactants to products. An understanding of polymorphism, solvatomorphism and phase changes in a system can be utilized to control the reactivity in the solid-state. It appears that prior assessment of the electrophile-nucleophile geometry in crystals can be used as a criterion for the prediction and explanation of their solid state reactivity and as corollary, reactions that are facile in the crystalline state can often be explained based on the geometry of the reactive centers. Solid-state reactions have not been utilized to a large extent in synthetic organic chemistry with the exception being photochemical reactions in

organic crystals. The reason for this could be the difficulty associated in predicting crystal structures and obtaining crystals that contain the reactive centers in the right orientation and the existence of polymorphic modifications and their phase transitions. Even with such limitations, it is still meaningful to explore reactions in the condensed phases as an alternative to solution state reactions, for the unique product selectivity, high yield, and more often than not simplicity in workup and handling that a facile solid-state reaction can exhibit.

5.5 References

1. H. B. Bürgi and J. D. Dunitz, *Acc. Chem. Res.* **1983**, *16*, 153-161.
2. H. B. Bürgi, J. D. Dunitz, J. M. Lehn and G. J. Wipff, *Tetrahedron*, **1974**, *30*, 1563-1572.
3. D. R. Storm and D. E. Koshland, *J. Am. Chem. Soc.*, **1972**, *94*, 5815-5825.
4. M. L. Bender, *Chem. Rev.,* **1960**, 60, 53-113.
5. (*a*) T. Praveen, U. Samanta, T. Das, M. S. Shashidhar and P. Chakrabarti, *J. Am. Chem. Soc.*, **1998**, *120*, 3842-3845; (*b*) M. P. Sarmah, R. G. Gonnade, M. S. Shashidhar and M. M. Bhadbhade, *Chem. Eur. J.*, **2005**, *11*, 2103-2110; (*c*) C. Murali, M. S. Shashidhar, R. G. Gonnade and M. M. Bhadbhade, *Chem. Eur. J.*, **2009**, *15*, 261-269; (*d*) C. Murali, M. S. Shashidhar, R. G. Gonnade and M. M. Bhadbhade, *Eur. J Org. Chem.*, **2007**, 1153-1159.
6. A. J. Gordon, *Tetrahedron*, **1967**, *23*, 863-870.
7. (*a*) K. Vyas, V. M. Rao and H. Manohar, *Acta Cryst. Sect. C*, **1987**, *43*, 1197-1200; (*b*) K. Vyas and H. Manohar, *Mol. Cryst. Liq. Cryst.,* **1986**, *137*, 37-43.
8. K. Vyas, H. Manohar and K. Venkatesan, *J. Phys. Chem.* **1990**, *94,* 6069-6073.
9. M. L. Cheney, G. J. McManus, J. A. Perman, Z. Wang and M. J. Zaworotko, *Cryst. Growth Des.*, **2007**, *7*, 616-617.
10. G. M. J. Schmidt, *J. Pure Appl. Chem*, **1971**, *27*, 647-678.
11. (*a*) L. A. Errede, M. C. Etter, R. C. Williams and S. M. Darnauer, *J. Chem. Soc., Perkin Trans. 2*, **1980**, 233-238. (*b*) M. C. Etter, *J. Chem. Soc., Perkin Trans. 2* **1983**, 115-121.
12. S. Nakamatsu, K. Yoshizawa, S. Toyota, F. Toda and I. Matijasic, *Org. Biomol. Chem.* **2003**, 2231-2234.
13. M. I. Tamboli, S. Krishnaswamy and M. S. Shashidhar, Unpublished results.